ISSN (online): 3059-9725

Journal of Nepal Hydrogeological Association (JNHA)

Volume 1 September 2024

Published by
Nepal Hydrogeological Association
Babarmahal, Kathmandu, Nepal
Estd. 2011 A.D. (2067 B.S.)
Email : info@nha.org.np
Website : www.nha.org.np

EDITORIAL BOARD OF JOURNAL-NEPAL HYDROGEOLOGICAL ASSOCIATION
(2023-2025)

Editor-in-Chief
Dr. Kabi Raj Paudyal
Central Department of Geology, Tribhuvan University, Kathmandu, Nepal

Editor
Dr. Christoff Andermann
Prof. Geosciences Rennes, Université de Rennes, CNRS, UMR 6118, Rennes, France

Editor
Dr. Daniel D. Clark-Lowes FGS
Nubian Consulting, Oak Court, Silver Street, Wiveliscombe, Somerset, TA4 2PA U.K.

Editor
Dr. Maria Rastvorova
Associate Professor of the Department of Tourism, University "KROK", Kyiv, Ukraine

Editor
Dr. Tej Prasad Gautam
Associate Professor and Associate Chair of the Department Institution-Department of Petroleum Engineering and Geology, Marietta College, Marietta, OH, USA

Editor
Dr. Robert V. Schneider
Lecturer, Geology and Geophysics University of Houston, USA

Editor
Dr Jaishri Sanwal Bhatt
Jawaharlal Nehru Centre for Advanced Scientific Research Geodynamics Unit, Bangalore, India

Editor
Dr. Dilli Ram Thapa
Department of Geology, Birendra Multiple Campus, Tribhuvan University, Nepal

Editor
Dr. Ramita Bajracharya
Lecturer, Central Department of Geology, Tribhuvan University, Kathmandu, Nepal

Editor
Dr. Bijay Man Shakya
Hydrogeologist-Freelancer/Nepal

Editor
Mr. Bala Ram Upadhyaya
Hydrogeologist. Department of Irrigation, Government of Nepal

SEVENTH EXECUTIVE COMMITTEE
(2023-2025)

Prof. Dr. Dinesh Pathak
President
Central Department of Geology, Tribhuvan University
Email: dpathaktu@gmail.com

Mr. Khila Nath Dahal
Vice President
Department of Water Resources and Irrigation
Email: kndahal@gmail.com

Mr. Anil Khatri
General Secretary
Department of Water Resources and Irrigation
Email: khatrianil01@yahoo.com

Mr. Bala Ram Upadhyaya
Secretary
Water Resources Research and Development Centre,
Pulchowk, Lalitpur, Nepal
Email: brupadhyaya1@gmail.com

Mr. Om Kumar Khadka
Treasurer
Nir Drilling and Construction P.Ltd.
Email: geologist.omk@gmail.com

Mr. Moti Bahadur Kuwar
Immediate Past President
Former Joint Secretary, Ministry of Energy, GON
Email: motikunwar2018@gmail.com

Mr. Pushpa Raj Dahal
Executive Member
Prosperous Terai Madhesh Irrigation Special Program
Email: pushpardahal@gmail.com

Mr. Subash Acharya
Executive Member
Tri-Chnadra College, TU
Email: subashacharya045@gmail.com

Ms. Manjari Acharya
Executive Member
Central Department of Geology, TU
Email: acharya11.manjari@gmail.com

Mr. Govinda Ojha
Executive Member
Freelancer
Email: geo.ojha05@gmail.com

Mr. Nabin Parajuli
Executive Member
KUKL
Email: icenabin@gmail.com

Journal of Nepal Hydrogeological Association (JNHA), Vol (1), 1-15 (2024)
ISSN: 3059-9725 (Online)

RESEARCH ARTICLE

Mountain hydrogeology and influence of active fault: A study of the Bhimgethi-Devisthan section in Western Nepal

Asmita Sapkota[1], Sunil Lamsal[1] and *Kabi Raj Paudyal[1]
[1]Central Department of Geology, Tribhuvan University, Kirtipur, Nepal
**Corresponding author: paudyalkabi1976@gmail.com*
***(Submission Date**: 29 May 2024; **Accepted Date:** 26 July, 2024)*

ABSTRACT

Mountain springs are the sole dependable water sources in the hilly region for peoples' daily needs. The current study examines the hydro-geological scenario in the area of the active fault zone. Through fieldwork and questionnaire survey, the study analyzes the characteristics of natural mountain springs in relation to geology, slope, aspect, type of deposit, spring type, discharge rate, and electrical conductivity. All the springs surveyed are perennial. About 71 % of springs are fracture and fault-dominated, indicating that the fractured and deformed rock plays a significant role in controlling the groundwater occurrence. Current study has shown that discharge of springs near the fault zone has decreased considerably over the last decade, with some springs shifting to lower elevation due to landslides triggered by shearing. Fault zones can act as either a conduit or a barrier to groundwater flow. The numerical analysis of fault zone architecture and permeability structure reveals a conduit-barrier fluid flow system. The damage zone, constituting of fractures, facilitates for rainwater recharge, while the core functions as a barrier, particularly in the southern half of the study area. Additionally, the findings related to electrical conductivity further support the presence of a barrier-type fluid flow system in the southern part along the fault core. However, the springs associated with silicified breccia indicate a conduit flow system in the northern section. Overall, the fault zone significantly influences the origin, discharge rate, and flow direction of spring sources across the study area.

Keywords: ***Mountain Hydrogeology, Natural Springs, Active Fault, Fracture Aquifer***

INTRODUCTION

The Mountain aquifer system in the hilly region of Nepal is essential to understanding the water resources of the region to overcome the ever-increasing water demand. Spring is the major source of water supply in the hills and mountains of Nepal generally used for domestic and agricultural purposes. It is the precious access to safe drinking water that occurs when groundwater naturally flows from geo-materials onto the Earth's surface or into a body of surface water. It has dynamic movement that varies considerably concerning variations in the condition of climate, topography, geology, and geomorphology (Pitts and Alfaro, 2001; Todd and Mays, 2005). Spring sources in the Mid-hill region of Nepal have been depleted and even dried due to the combination of bio-physical (e.g. climate changeability, changes in land use pattern) and socioeconomic (e.g. spring maintenance) variables (ICIMOD, 2015).

Bari Gad Fault is a strike-slip active fault in Lower Himalaya which trends approximately northwest-southeast, parallel to Badi Gad Khola and Nisi Khola (Nakata, 1882; Nakata, 1889). Landform present in the area shows 15 m and 240 m of vertical and horizontal slip respectively. Arita et al. (1984) and Sakai (1985) have defined this fault as Barigad Kaligandaki Fault (BKF) after observing its extension along Kaligadaki River in southeast. The active nature of the fault triggers numbers of large landslides along the fault zone (Timilsina and Paudyal, 2018). Lamsal et al. (2023) reviewed the stratigraphy of the Jajarkot thrust sheet and mentioned the fact that the actual boundary of the thrust sheet is not well defined. Bhusal and Gyawali (2017) have worked on springs within the catchment of the Badi Gad Khola focused on water quality of those springs. However, there is a lack of research on how active fault impacts mountain springs. To fulfill this gap, this study examines the hydro-geological scenario within the active fault zone.

It is well known that structural features do affect groundwater movement. An active or potentially active fault largely governs the majority of groundwater in bedrock as this zone can act as either a conduit or barrier to groundwater flow (Barton et al., 1995; Gudmundsson, 2000; Gudmundsson et al., 2001; Mayer and Sharp, 1998). Since springs are widespread along fault zones, active fault zones collect and transmit large amounts of groundwater, typically under considerable fluid pressure (Curewitz and Karson, 1997; Léonardi et al., 1998; Muir-Wood and King, 1993). Additionally, the trends of faults in the local hydraulic gradients can greatly affect groundwater flow (Phillips, 1991). The fault pattern and associated stress concentration, the trend of the fault plane zone about that of the groundwater flow, and the changing permeability and size of the resulting fault slip plane are the considerable parameters that affect the flow of groundwater (Gudmundsson, 2000).

Study area

The study area lies in the Gulmi and Baglung district of western Nepal about 350 km west of Kathmandu Valley (Fig. 1). It belongs to the hilly region experiencing sub-tropical to alpine climatic conditions with altitudes extends from 820 meters to 2425 meters above sea level. The overall drainage system is dendritic and makes deep V-shaped valleys. Major river systems include Badigad Khola, Darlin Khola, Kut Khola and Nisi Khola.

Fig. 1: Political map of Nepal showing location area (white polygon) within the Gulmi and Baglung district.

OBJECTIVES

The research work focuses on the scenario of the hydro-geological condition along the Badi Gad fault, an active fault of the Lesser Himalayan region. The specific objectives are as follows:

- To characterize the springs from various aspects.
- To access the interrelation between fault zone and mountain springs.

METHODOLOGY

The methods that were adopted to achieve the objectives of the research can be broadly classified into three sections: desk study, fieldwork, data interpretation and analysis. Firstly, relevant literature, research journals, and maps from different sources were reviewed. During the field traverse the geological data were collected and the fault zone was thoroughly investigated throughout the study area to prepare the geological map and evaluate the architecture and permeability condition of the rocks of the region. The evidence of active fault was gathered through a detailed field investigation. Special efforts were focused on clarifying the nature of active faulting and its impact on various aspects of groundwater resources. Satellite images were used to determine well exposed localities of the fault zone and eight localities were verified from the field study for measuring the fault core and damage zone width. For this measurement, a vertical traverse of about 700 m was made in each location to cover the well exposed region of the fault zone.

Spring inventory was a fundamental part of the research as it provides data on groundwater sources and their distribution (Fig. 2 a and b). The spring sources and their distribution were evaluated from the questionnaire survey. With the cooperation of local people, the spring sources were visited and the source data were collected, recording the information using a designed inventory sheet which includes the name of the spring, an attitude of bedrock (if present), soil types, types of spring, water discharge, land use of a surrounding area, the shifting case of springs and variation in water volume within the last decade. The discharge rate of springs was measured by the volumetric method with the help of a bucket and stopwatch during the field.

Fig. 2: Photographs of spring sources a) Fault/shear zone spring at Bhimgethi (GPS: 00420437E, 03127705N). b) Measuring the electrical conductivity of spring water at the Huldi/Chhis village (GPS: 00413611E, 03134816N).

RESULTS

Geological Setting

Geologically, the study area is dominantly characterized by low-grade meta-sedimentary units of the Nawakot Group and this succession is overlain by the metamorphic crystalline rocks separated by the Mahabharat Thrust as described in central Nepal (Stöcklin and Bhattarai, 1977; Stöcklin, 1980). These crystalline rocks are equivalent to the rocks of the Kahun Klippe (Paudyal and Paudel, 2013) (Fig. 3).

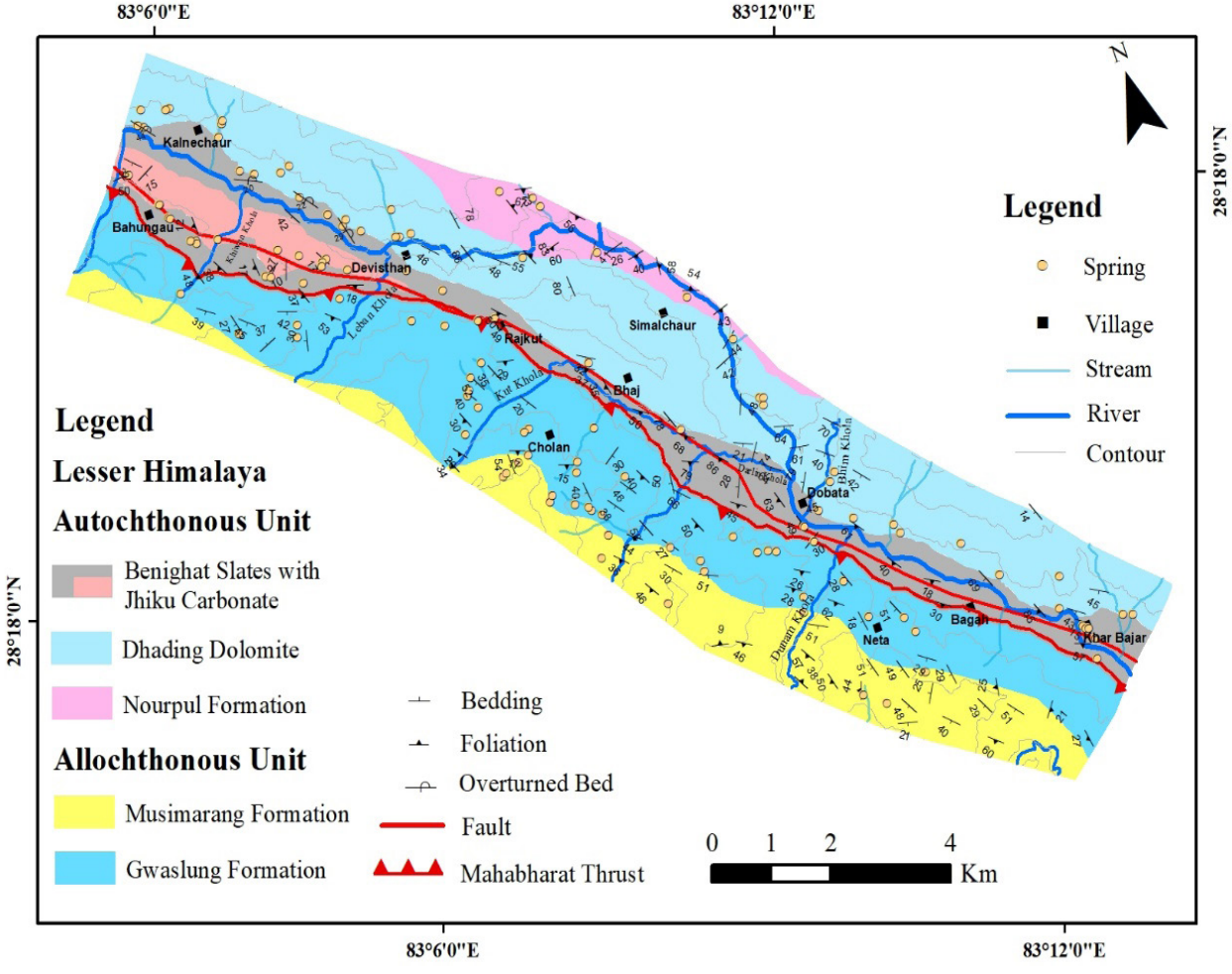

Fig. 3: Geological map of the study area with distribution of springs.

The Nawakot Group in the mapped region include the Nourpul Formation, Dhading Dolomite, and Benighat Slates (DMG, 2003). The stratigraphy of this group is a extension of the rock strata defined by Timilsina and Paudyal (2018), and Gaire and Paudyal (2021) from adjacent area in the east. The Nourpul Formation is exposed to the northeast section of the study area by making assorted succession comprising fine- to medium-grained, thin- to thick-bedded metasandstone, white to grey quartzites inter-bedded with thinly laminated phyllites and slates (Fig. 4a). The ridge forming Dhading Dolomite consists of monotonous, massive to highly fractured and folded, dense to fine crystalline stromatolitic, siliceous and cherty dolomite with grey phyllite partings, occasionally found in its basal portion (Fig. 4b). The Benighat Slates comprise the thinly bedded, black ferruginous slates with occasional beds of dolomites and limestones (Fig. 4c). The Jhiku beds are also exposed in the northwest section of the study area within this unit and are characterized by thin-bedded, siliceous dolomite inter-bedded with slates and some siliceous limestone.

The transported thrust sheet sharply overlain on rocks of the Nawakot Group by the Mahabharat Thrust. This rock succession is lithologically divided into two different units in the study area which are correlable with the Gwaslung Formation and the Musimarang Formation from the Kahun Klippe, eastern part of the present study area (Paudyal and Paudel, 2013). Fine-to-medium-grained, platy to thin-bedded, grey to bluish-colored, siliceous, dolomitic marble represents the Gwaslung Formation (Fig. 4d). This unit is transitionally underlain by the younger Musimarang Formation which is distributed in the southern section of the study area. This younger Musimarang Formation consists of white to dirty-white, platy-to-medium-bedded quartzite intercalated with well-foliated, quartz and mica schist (Fig. 4e).

The black ferruginous slates of the Benighat Slates appear to be heavily crushed and converted to fault gauges/breccia because of the movement of fault within this unit (Fig. 5a and b). Additionally, the shear sense indicating features and outcrop scale faults shows the movement along the strike which defines fault plane propagation as strike-slip fault. Number of asymmetrical boudinage and multiple folds are frequently developed within the fault zone due to the fault movement (Fig. 5c and d).

Fig. 4. (a) The mixed lithology of the Nourpul Formation along road section towards Devisthan from Burtibang (GPS: 00416803E, 03134916N). (b) The monotonous sequence of the Dhading Dolomite along the left bank of Nisi Khola section at Kalnechaur (GPS: 00411148E, 03138050N). (c) Dark ferruginous slate of the Benighat Slates exposed at Bhimgethi (GPS: 00419414E, 03128502N). (d) The outcrop of dolomitic marble with schist partings of the Gwaslung Formation at the Cholan village. (GPS: 00416156E, 03130578N). (e) The alternating quartzite and schist succession of the Musimarang Formation at the Darlin Deurali village (GPS: 00419510E, 03125704N).

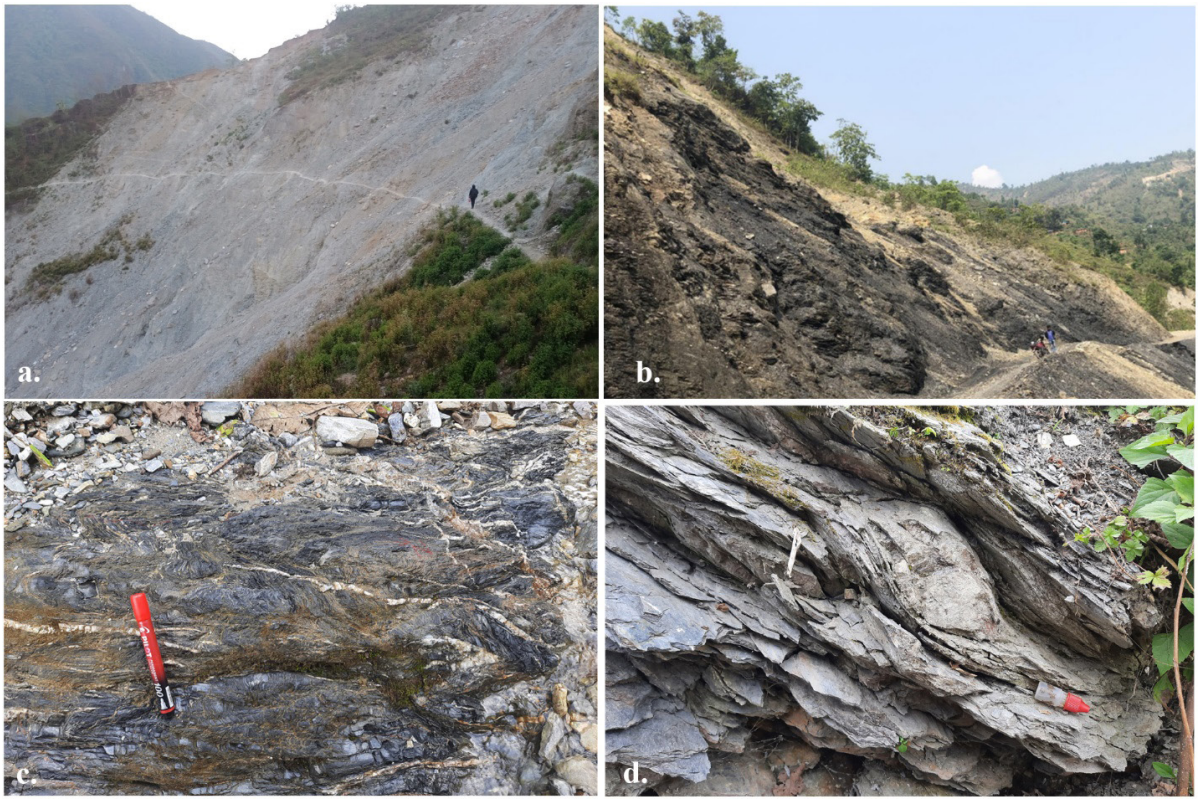

Fig. 5: (a) Outcrop of shear zone induced landslide at the Huldi village (GPS: 00412704E, 03134772N). (b) Outcrop of shear zone in the Benighat Slates at Bhimgethi on the right bank of Badi Gad Khola (GPS: 00420437E, 03127705N). (c) Multiple folding observed in slate of the Benighat Slates at Balghas village (GPS: 00420447E, 03127789N). s(d) Asymmetrical boudinage of quartz vein observed in the Benighat Slates at the Bahungau village (GPS: 00410988E, 03136844N).

Distribution of springs

There was a total of 122 springs identified in the study area, all of which are perennial, and their distribution is presented in Fig. 3. These springs are the major source of water supply for drinking, domestic use and agricultural needs in the area. However, only in some areas, the river water is lifted to a higher altitude for irrigation purposes. Especially during the dry season, the population suffers from severe water shortage since water discharge of existing springs has been significantly reduced than in past years and some perennial springs are going to become seasonal. In some communities, the water shortage has become so bad that residents have had to bring drinking water from about 5 – 10 km away to fulfil their basic water demands.

Generally, the recharge system of a particular area is highly influenced by the rainfall pattern and its variation and ultimately affects the discharge rate of spring in that area. Moreover, the discharge rate also depends on the other factors which can control the topography of the area. The discharge of 122 springs was measured in the pre-monsoon season and categorized based on Meinzer's (1923) classification system. As

a result, there are 67 springs of seventh magnitude, 53 springs of sixth magnitude and 1 spring of fifth magnitude (Table 1). Fig. 6a shows the variation of discharge in the study area which ranges from 0.2 lpm to 60 lpm. The discharge of springs on the left bank of Nisi Khola is higher than on the right bank. The landslides and shear zones, frequently observed along the fault line, have a greater effect on the groundwater resource since the discharge of the spring is found to be lower along the fault zone area than in other sections. Also, from the discussion with people, they claim that the spring sources have been relocated downslope owing to landslides and discharge of springs has decreased greatly since the last ten years (Fig. 6b). Thus, water scarcity is worse along the fault zone than elsewhere in the region.

Table 1: Types of spring of the study area based on discharge rate.

Discharge Rate (lps)	Magnitude	No. of springs
1-10	Fifth	1
0.1-1	Sixth	53
0.01-0.1	Seventh	67

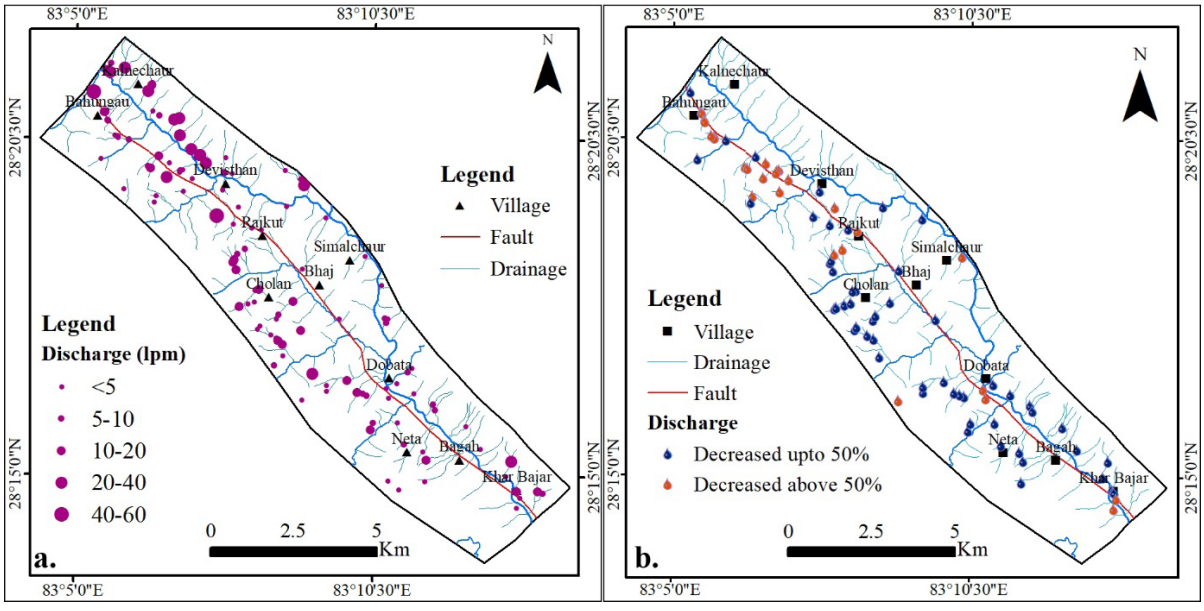

Fig. 6: (a) Distribution of springs by discharge rate. (b) Water volume situation in last ten years.

By inventory of springs, most of the springs are of fracture and fault types, making up 49 % and 22 % respectively; only 12 % are contact springs and 17 % are depression springs (Fig. 7a). But sometimes, a single spring includes two types of spring mechanisms. In terms of slope, 74 % of springs are located on moderate slopes 18 % are on steep slopes and only 8 % are on gentle slopes (Fig. 7b).

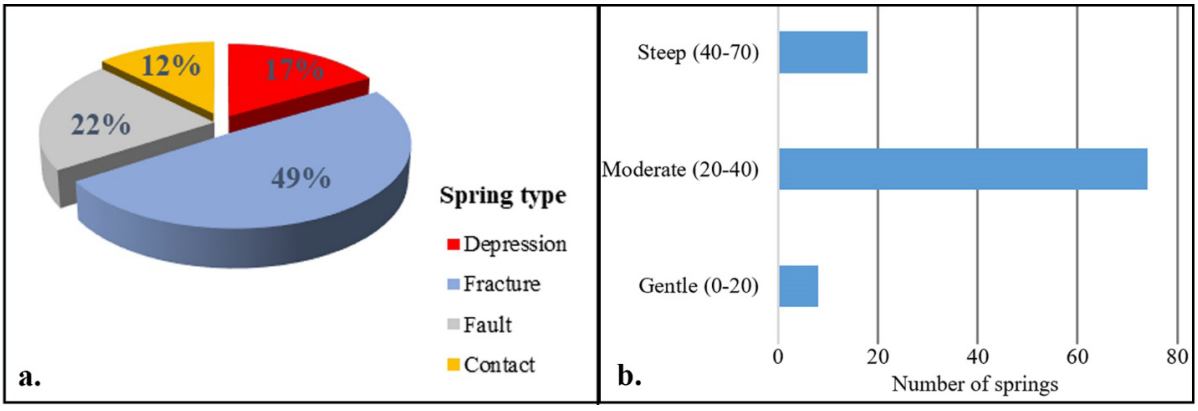

Fig. 7: Distribution of springs based on (a) Spring type (b) Slope.

There are more springs facing southwest than in any other direction (Fig. 8a). In terms of land use around the source of springs, the maximum area is covered by forest region followed by cultivation, barren land, and others. Forest areas make up 55 %; 25 % are in cultivation areas and 20 % are in bushes (Fig. 8b). Mainly three types of deposits have been identified around the spring sources, namely colluvium, residual and rock deposits in which 54 % of springs belong to rock deposits while 25 % are colluvium deposits and 21 % are residual deposits (Fig. 8c). The study shows that the electrical conductivity of springs ranges from 42 µS/cm to 489 µS/cm which was measured in pre-monsoon season (Fig. 2b). The highest value of EC is observed around in southern section whereas it is lowest in the northern section of the study area (Fig. 9a).

Daily precipitation records of three stations were manually checked, compared with surrounding nearby stations, and analyzed to examine the trend of rainfall patterns in the study area over these recent periods. The arithmetic mean method is used to calculate the average annual rainfall of the study area and is found to be 2182 mm. The graph shows a slightly increasing trend of rainfall in the study area (Fig. 9b).

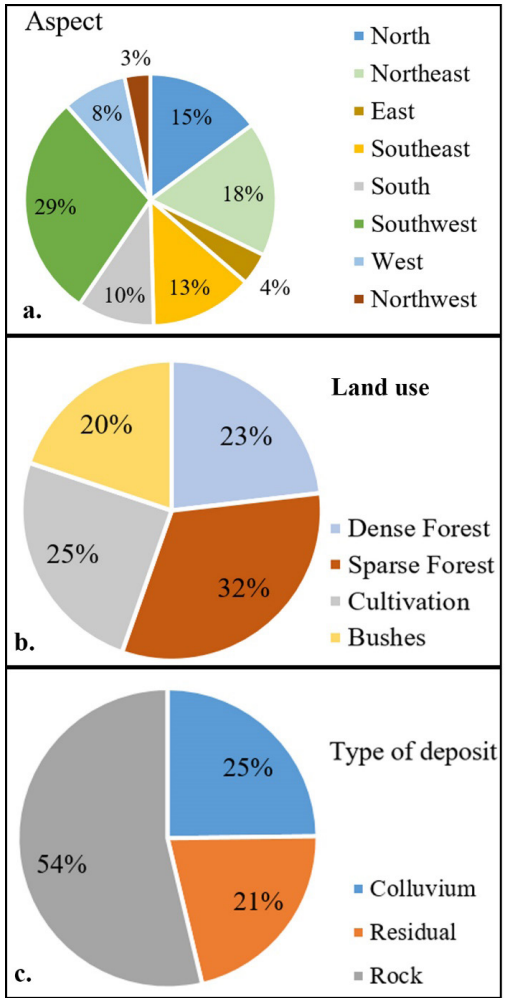

Fig. 8: Distribution of springs based on (a) Aspect (b) Land use and (c) Type of deposit.

Numerical measures of fault zone architecture and permeability structure

Basically, two major components of fault zone include the fault core and damage zone, which are surrounded by the host rock, have different geometrics and structures (Bruhn et al., 1994; Caine et al., 1996; Evans et al., 1997; Gudmundsson et al., 2001). The fault core comprises the fault gauge and breccia with intense deformations based on the host rock composition while damage zone is characterized by the numerous fractures of various sizes, highly folded/crushed bedrock. The width between the fault core and damage zone, which significantly regulates groundwater flow as a barrier or conduit, is revealed by (Caine et al., 1996).

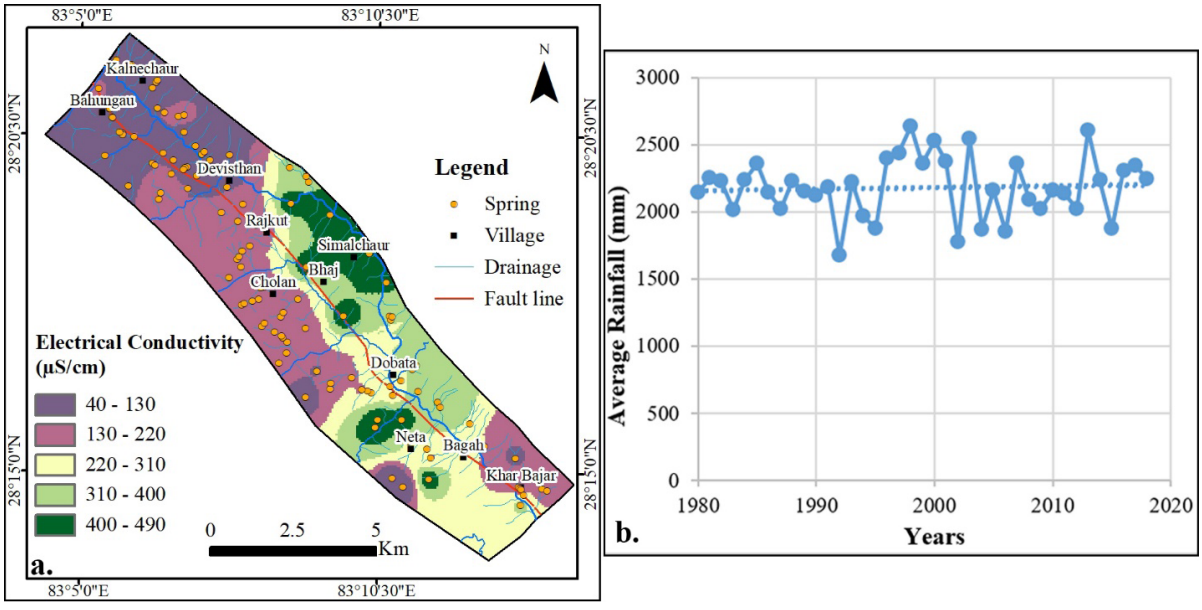

Fig. 9: a) Distribution of electrical conductivity of spring water. b) The average rainfall of the study area (source: Department of the Hydrology and Meteorology, 2022).

Three numerical indices- Fa, Fm, and Fs are used to describe the architecture and permeability structure of fault zones (Caine et al., 1996) and calculated by the given formula:

$$F_a = \frac{damage\ zone\ width}{total\ fault\ zone\ width} = \frac{damage\ zone\ width}{core\ width + damage\ zone\ width} \quad (1)$$

$$F_m = mean\ of\ F_a\ values\ for\ a\ single\ fault\ zone \quad (2)$$

$$F_s = (F_a)_{max} - (F_a)_{min} \quad (3)$$

The relative width of the fault core and damage zone at a chosen area is expressed by the value of Fa, a fault zone architectural index, whose value ranges from 0 to 1. The value near 1 ideally tells that the fault core is absent whereas near 0 tells the damage zone is absent. Fm is the mean value of Fa while Fs gives the spatial variability index.

In the study area, the fault core comprises the fault breccia and fault gauge with extensive deformations whose exposed width ranges from around 20 m to 120 m. Likewise, the damage zone thickness is found to be several hundred meters, thicker along ridge section than river section, and characterized by numerous fractures of various sizes, highly folded and crushed bedrock (Fig. 5a and b). The width of the fault core and damage zone is calculated from eight locations using the equation (1) mentioned above, and found the value of architectural index as Fa = 0.80. The value of Fs = 0.17 is obtained from the maximum and minimum value of Fa using the equation (3) and this obtained small value tells about the uniform homogeneity of fault zone.

DISCUSSION

In the hilly region, groundwater existence and their movement, that is spring distribution in a particular area is closely connected to the topography, rainfall, land use/ land cover type (Agarwal et al., 2012; Negi and Joshi, 2004; Tambe et al., 2012; Todd and Mays, 2005), geomorphology, lithology, slope and lineaments (Sitender and Rajeshwari, 2011). Regarding slope, 74 % of springs emerge through moderate slopes ranging from 200 to 400 while 18 % of springs are from the steep slope (400 - 700). However, only 8 % are from a gentle slope (00 - 200). In comparison with gentle slopes, the residual hills and structural hills have excellent potential for groundwater only if they have high lineament density (Sitender and Rajeshwari, 2011). In addition, the local geology, bedding and joint orientation, water table located above the ground surface and nature of the fracture significantly define the surfacing of springs (Pacheco and Alencoao, 2002; Valdiya and Bartarya, 1989). In the study area, most of the springs (about 71 %) are fracture and fault-dominated because of highly fractured and deformed bedrock, with contact springs and depression springs being less common. Consequently, the fractured and deformed rock plays a significant role in controlling groundwater occurrence.

Spring discharge is highly influenced by changes in rainfall and human activities in the recharge area (Negi and Joshi, 2004; Pant and Rawat, 2015). In the research area, from Fig. 3A, the discharge rate of the spring is varied from place to place. Of the total 122 springs surveyed, 36 % have a consistent water discharge volume, 20 % have experienced a reduction of more than 50 % inn their water volume, and 42 % have seen a decrease within a certain limit over the last decade (Fig. 6b). The carbonate rock shows the highest discharge rate (up to 40 lpm) even on the southwest slope as contact and fracture spring around the Kalnechaur section (GPS: 00411148E, 03138050N) of the study area. However, the middle study section has only fewer spring sources with less discharge (0.2 lpm to 9 lpm) (Fig. 2b). More specifically, spring discharge in the fault zone has considerably declined over the years (Fig. 2), with some springs are shifting to lower elevations due to landslides triggered by shearing. This shows that the springs originated near the fault zone are more vulnerable. Hence, besides the factors like rainfall and human activities, the active fault might have a significant role in decreasing the water discharge of springs.

An active or potentially active fault largely governs the majority of groundwater in bedrock (Barton et al., 1995; Gudmundsson, 2000; Gudmundsson et al., 2001; Mayer and Sharp, 1998). The fault zone behaves either as a conduit, barrier, or conduit-barrier flow system depending on the proportion of the fault core and damage zone structure as well as grain size and fracture permeability (Caine et al., 1996). Furthermore, deformational conditions and chemistry of the fault zone fluid make critical understanding of fault zone architecture and permeability structure. Laboratory permeability examination on oriented samples taken from the field reveals that the core is a low permeability barrier parallel and perpendicular to the fault plane whereas the damage zone is often a high permeability conduit parallel to the fault plane (Chester and Logan, 1986; Caine et al., 1996). Taking eight locations' data from

the study area, the architectural index is found to be 0.80. From the field observations, the damage zone appears to be fracture-dominated while the fault core section has clay-rich gauge. However, in the northern section, the fault core lithology is dominated by silicified breccia. As mentioned above, when the width of the fault core is significantly greater than that of the damage zone, the fault zone acts as a barrier to flow. In the study area, the damage zone is highly developed, and the lower permeability of the fault core causes the fault zone to partially impede groundwater flow. Hence, the result from the calculated value of the architectural index and field observations with present lithology, the fault zone architecture is a conduit-barrier fluid flow system. The value of Fs = 0.17, obtained small value suggests about the uniform homogeneity of the fault zone.

Taking into consideration the finding of fault zone architecture and the orientation of bedding, the damage zone allows the recharge of rainwater but the core functions as a barrier in the southern half of the study area which is also valid from the spring sources. Due to this reason, the residents of the Simalchaur, Malarani have faced a water deficit so significantly that they have had to bring drinking water from about 8 – 10 km away. Meanwhile, the spring sources with the silicified breccia suggest the conduit flow system in the northern section. Hence, the geological distribution has greater control over the fault zone characteristics and ultimately spring sources. Besides this, the movement of the fault zone is a major concerning factor which has a considerable effect on spring sources throughout the study area in terms of their origin and discharge rate. Even being a slightly increasing trend of rainfall (Fig. 9b) with a fractured zone, the discharge of the springs has been reduced significantly year after year and this may experience a serious issue in future.

CONCLUSION

Geologically, the study area comprises the units of the Nourpul Formation, Dhading Dolomite and Benighat Slates of the Nawakot Group. And, the crystalline rocks of thrust sheets are classified as the Gwaslung Formation and the Musimarang Formation. The Mahabharat Thrust and Badi Gad Fault are the major regional geological structures observed in the study area. Among the identified springs in the study area, 74 % of springs emerge through moderate slopes ranging from 200 to 400. Most of the springs (about 71 %) are fracture and fault-dominated because of highly fractured and deformed bedrock. The carbonate rock shows the highest discharge rate even on the southwest slope. The result from the calculated value of architectural index and field observations with present lithology, the fault zone architecture is a conduit-barrier fluid flow system. The damage zone, consisting of fractures, facilitates for rainwater recharge, while the core functions as a barrier, particularly in the southern half of the study area. Additionally, the findings related to electrical conductivity (300 μS/cm to 489 μS/cm) further support the presence of a barrier fluid flow system in the southern section which is because of more time for water in rock contact, also suggest the more depth of water with slower movement. There is a high variability of spring discharge between around the fault zone and another region, indicating that the fault zone has many influences on groundwater. The flow rate of springs has been decreasing considerably along the fault zone over the years, with some springs shifting to lower elevation due to shear-induced landslides. The increased mass movement could pose a serious issue for deficiency of spring resources or possibly dried-up springs in future.

ACKNOWLEDGEMENT

Authors' would like to acknowledge the Central Department of Geology, Tribhuvan University, Nepal for their technical guidance and for providing the necessary facilities to carry out this research. First author would like to acknowledge the Water Resources Research and Development Centre (WRRDC) for allowing such a great opportunity as research/thesis interns under the research program. We are grateful to Durga Bolakhe and Rajan Mahat for their support during the field work.

AUTHOR CONTRIBUTIONS

All the authors have made significant contributions to preparing this research article. Asmita Sapkota and Sunil Lamsal have equal contribution for data collection, data analysis and interpretation and final manuscript preparation. Dr. Kabi Raj Paudyal took verification traverses in the field and has the role of manuscript review, data analysis and interpretation. The first draft of the manuscript was written by Asmita Sapkota and all authors contributed to making the final version.

CONFLICT OF INTEREST

The authors declare that the paper has not previously published in another journal/bulletin.

DATA AVAILABILITY STATEMENT

The data that support the findings of this study are available from the first author, upon reasonable request.

REFERENCES

Agarwal, A., Bhatnagar, N.K., Nema, R.K. and Agrawal, N.K., 2012. Rainfall dependence of springs in the midwestern Himalayan hills of Uttarakhand. International Mountain Society, 32(4), 446–455. doi:10.1659/MRD-JOURNAL-D-12-00054.1.

Arita, K., Shiraishi, K. and Hayashi, D., 1984. Geology of Western Nepal and a comparison with Kumaun, India, 21(1), 21.

Barton, C.A., Zoback, M.D. and Moos, D., 1995. Fluid flows along potentially active faults in crystalline rock. Geology, 23(8), 683–686. doi:10.1130/0091-7613(1995)023<0683:FFAPAF>2.3.CO;2.

Bhusal, J. and Gyawali, P., 2015. Water quality of springs in Badigad Catchment, Western Nepal. Bulletin of the Department of Geology, 18, 67-74. doi:10.3126/bdg.v18i0.16458.

Bruhn, R.L., Parry, W.T., Yonkee, W.A. and Thompson, T., 1994. Fracturing and hydrothermal alteration in normal fault zones. Pure and Applied Geophysics, 142, 609-644. doi:10.1007/BF00876057.

Caine, J.S., Evans, J.P. and Forster, C.B., 1996. Fault zone architecture and permeability structure. Geology, 24(11), 1025–1028. doi:10.1130/0091-7613(1996)024<1025:FZAAPS>2.3.CO;2.

Chester, F.M. and Logan, J.M., 1986. Implications for mechanical properties of brittle faults from observations of the Punchbowl fault zone, California. Pure and Applied Geophysics PAGEOPH, 124(1-2), 79-106.

Curewitz, D. and Karson, J.A., 1997. Structural settings of hydrothermal outflow: Fracture permeability maintained by fault propagation and interaction. Journal of Volcanology and Geothermal Research, 79, 149–168. doi:10.1016/S0377-0273(97)00027-9.

DMG, 2003. Geological map of Baglung, Gulmi and Puythan districts in 1:50000 scale. Department of Mines and Geology, Kathmandu.

Evans, J.P., Forster, C.B. and Goddard, J.V., 1997. Permeability of fault-related rocks, and implications for hydraulic structure of fault zones. Journal of Structural Geology, 19, 1393-1404. doi:10.1016/S0191-8141(97)00057-6.

Gaire, P. and Paudyal, K.R., 2021. Geological mapping and structural analysis in Shantipur-Wami Taksar area of Gulmi-Baglung district, western Nepal to assess the Badi Gad Fault and related features. Himalayan Geology, 42(1), 1-8.

Gudmundsson, A., 2000. Active fault zones and groundwater flow. Geophysical Research Letters, 27(18), 2993–2996. doi:10.1029/1999GL011266.

Gudmundsson, A., Berg, S.S., Lyslo, K.B. and Skurtveit, E., 2001. Fracture networks and fluid transport in active fault zones. Journal of Structural Geology, 23(2), 343–353. doi:10.1016/S0191-8141(00)00100-0.

ICIMOD, 2015. Reviving the Drying Springs Reinforcing Social Development and Economic Growth in the Midhills of Nepal. Kathmandu, Nepal: ICIMOD.

Lamsal, S., Sah, R.B. and Paudyal, K.R., 2023. Discrepancies and Research Gaps on the Lithostratigraphy of the Jajarkot Thrust Sheet, Western Nepal Himalaya. Journal of Institute of Science and Technology, 28(2), 53-62. doi:10.3126/jist.v28i2.61172.

Léonardi, V., Arthaud, F., Tovmassian, A. and Karakhanian, A., 1998. Tectonic and seismic conditions for changes in spring discharge along the garni right lateral strike slip fault (armenian upland). Geodinamica Acta, 11(2–3), 85–103. doi:10.1080/09853111.1998.11105312.

Mayer, J.R. and Sharp, J.M., 1998. Fracture control of regional ground-water flow in a carbonate aquifer in a semi-arid region. Geological Society of America Bulletin, 110(2), 269–283. doi:10.1130/0016-7606(1998)110<0269:FCORGW>2.3.CO;2.

Meinzer, O.E., 1923. Outline of ground-water hydrology: with definitions. U.S. Government Printing Office.

Muir-Wood, R. and King, G.C.P., 1993. Hydrological signatures of earthquake strain. Journal of Geophysical Research, 982(B12), 22035–22068. doi:10.1029/93jb02219.

Nakata, T., 1982. A photogrametric study of active faults in the Nepal Himalayas. Journal of Nepal Geological Society, 2, 67-80.

Nakata, T., 1989. Active faults of the Himalaya of India and Nepal. Geological Society of America, 232, 243–264. doi:10.1130/SPE232-p243.

Negi, G.C.S. and Joshi, V., 2004. Rainfall and spring discharge patterns in two small drainage catchments in the western Himalayan Mountains, India. The Environmentalist, 24(1), 19–28. doi:10.1023/B:ENVR.0000046343.45118.78.

Pacheco, F. and Alencoao, A., 2002. Occurrence of springs in massifs of crystalline rocks, northern Portugal. Hydrogeology Journal, 10(2), 239–253. doi:10.1007/s10040-001-0186-0.

Pant, C.C. and Rawat, P.K., 2015. Declining changes in spring hydrology of non-glacial river basins in Himalaya: A case study of Dabka catchment. In Joshi R. (Ed.), Dynamics of Climate Change and Water Resources of Northwestern Himalaya, (151-179), Springer.

Paudyal, K.R. and Paudel, L.P., 2013. Geological study and root zone interpretation of the Kahun Klippe, Tanahu, Central Nepal. Himalayan Geology, 34(2), 93–106.

Phillips, O.M., 1991. Flow and Reactions in Permeable Rocks. Cambridge Univeristy Press, New York.

Pitts, M. and Alfaro, C., 2001. Geologic/ Hydrogeologic Setting and Classification of Springs. In LaMoreaux, P.E. and Tanner, J.T. (Eds.), Springs and Bottled Waters of the World, (33–71), Springer.

Sakai, H., 1985. Geology of the Kali Gandaki Supergroup of the Lesser Himalaya in Nepal. Memoirs of the Faculty of Science, Kyushu University (Japan), 25(3), 337-397.

Sitender, R. and Rajeshwari, S., 2011. Delineation of groundwater potential zones in Mewat District, Haryana, India. International Journal of Geomatics and Geosciences, 2(1), 270–281.

Stöcklin, J., 1980. Geology of Nepal and its regional frame. Journal of the Geological Society of London, 137(1), 1–34. doi:10.1144/ gsjgs.137.1.0001.

Stöcklin, J. and Bhattarai, K.D., 1977. Geology of Kathmandu Area and Central Mahabharat Range Nepal, Department of Mines and Geology Kathmandu, Nepal, p. 86.

Tambe, S., Kharel, G., Arrawatia, M. L., Kulkarni, H., Mahamuni, K. and Ganeriwala, A. K., 2012. Reviving dying springs: Climate change adaptation experiments from the Sikkim Himalaya. Mountain Research and Development, 32(1), 62–72. doi:10.1659/ MRD-JOURNAL-D-11-00079.1.

Timalsina, K. and Paudyal, K.R., 2018. Fault-controlled geomorphic features in Ridi-Shantipur area of Gulmi District and their implications for active tectonics. Journal of Nepal Geological Society, 55(1), 157-165.

Todd, D. and Mays, L., (Ed). 2005. Groundwater Hydrology (3rd ed.). John Wiley and Sons, p. 636.

Valdiya, K.S. and Bartarya S.K., 1989. Diminishing discharges of mountain springs in a part of Kumaun Himalaya. Current Science, 58(08), 417–426.

Journal of Nepal Hydrogeological Association (JNHA), Vol (1), 16-42 (2024)
ISSN: 3059-9725 (Online)

RESEARCH ARTICLE

Geomorphic assessment of morphology of Siwalik origin rivers in Far-west Nepal

***Motilal Ghimire[1] and Puspa Sharma[1]**
[1]Central Department of Geography, Tribhuvan University[1]
**Corresponding author: motighimire@gmail.com*
***(Submission Date**: 6 August 2024; **Accepted Date:** 27 August 2024)*

ABSTRACT

Geology, tectonics, topography, climate, land use, and human activity impact river morphology significantly, affecting downstream morphology and hydrology. In Nepal, rivers traversing complex geology and active tectonics are subjected to intense weathering and erosion, resulting in a high sediment yield and substantial impacts on river morphology. Despite the importance of understanding river morphology, studies on Himalayan rivers remain limited. This study investigates the characteristics of basin and river morphonology of the Siwalik origin river in far-west Nepal using GIS, remote sensing, field surveys, and hydrodynamic modeling. The basin, spanning 702 km2, features distinct land use patterns, with the upper catchment predominantly forested and the lower catchment heavily agricultural. Geologically, the upper catchment is underlain by Siwalik Group rocks, while the lower reach consists of quaternary deposits. An examination of the catchment characteristics, change in plan and cross-sectional form at various channel reaches was conducted using time series optical satellite imagery and InSAR data from ALOS PALSAR and Sentinel-1. The study revealed that steep and rugged topography, high uplift rates, and intense monsoons contribute to frequent and extensive landslides, which lead to high sediment yield in the basin's upper part and impact channel morphology downstream. The study also exposed the correlation between channel slope, sediment type, and river morphology. The river processes such as erosion (bank and avulsion), deposition, and channel abandonment during the last decade have evidenced changes in the planform of river morphology. The hydrodynamic model indicates that changing hydraulic variables influence the river's processes and morphology. Cross-sectional analysis of the rivers also shows significant variability in sediment aggradation and degradation, impacting bed-level and flow patterns, indicating dynamic river processes. Notable sediment gains at certain cross-sections and losses at others indicate dynamic river processes, impacting bed-level rise, erosion, and flow patterns. A decrease in the annual rates of all river processes (erosion, avulsion, deposition, and channel abandonment) suggests stabilization in riverbanks. Comparatively, deposition remains the most extensive process, which indicates an excessive sediment load from upstream. This research provides a conceptual frame where the independent landscape factors (geology, climate, human activities) and dependent variables (sediment supply, stream discharge) shape river morphology.

Keywords: ***River morphology, geomorphology, Remote Sensing, InSAR, Siwalik Hills, Tarai***

INTRODUCTION

River basins and morphologic characteristics are intricate components shaped by geology, tectonics, topography, climate, land use, and human activity (Horton, 1932). These factors influence the basin's geomorphic and hydrologic features, impacting downstream river morphology and hydrological response. The shape and pattern of rivers are the culmination of historical changes in climate, tectonic activities, land use, and human interference,

highlighting the complex interplay of natural and anthropogenic factors (Van Appledorn, Baker and Miller, 2019).

Understanding river morphology and its linkages to catchment conditions provide a holistic view of river systems, aiding in the comprehension of channel morphology, floods, stability, and ecology (Hey et el., 1997). This knowledge is crucial for soil conservation, watershed management, flood control, and addressing issues like bank erosion and channel avulsion(Benda et al., 2003, Dietrich and Dunne, 1978). In Nepal, where rivers traverse complex geology and active tectonics, intense weathering and erosion processes lead to high sediment yields and significant impacts on river morphology and downstream disasters (Shrestha et al., 2008; Ghimire, 2020; Ghimire and Higaki, 2015; Shrestha and Tamrakar, 2012; Kale, 2002).

Despite its importance, studies on the river morphology of Himalayan rivers are limited and often focused on hazards rather than morphology. Few studies on the upper catchment processes in the Siwaliks exist, providing valuable insights (Khanal et al., 2007; Chalise and Khanal, 2002; Dhital et al., 1993; Ghimire, 2020). In this context, investigating the basin and morphologic features of the Mohana-Khutiya Rivers in far west Nepal, originating from the Siwalik Range and flowing traversing Tarai, presents an opportunity to enhance understanding in this field. Hence, this study aims to examine the characteristics of the basin and river morphology of the Siwalik origin river.

CONCEPTUAL FRAMEWORK

Rivers function as open systems, influenced by a multitude of factors both upstream and downstream (Piégay and Schumm, 2003; Schumm, 1981). Channel morphology, a significant aspect of river systems, is shaped by these factors and is categorized as an independent and dependent type (Hogan and Luzi, 2010). Independent landscape factors, including geology (including tectonics), climate, and human activities, exert a direct influence on watershed conditions. Geology, affected by processes like volcanism and tectonics, determines bedrock distribution and topography (Montgomery and Buffington, 1993). Climate, driven by atmospheric circulation and modified by topography, influences soil and vegetation. Human activities also alter watershed conditions significantly (Ghimire et al., 2023).

These enforced conditions determine dependent landscape variables such as sediment supply, stream discharge, and bed and bank material (Buffington and Montgomery, 2013). The combination of these variables shapes channel characteristics, with the channel adjusting in response to changes. Additionally, time plays a crucial role as an independent variable since the landscape's origin. Understanding these interactions is essential for comprehending river dynamics. Studies by Buffington and Montgomery (2013), Montgomery and Buffington (1993), and Schumm (1981) provide valuable insights into these relationships. A conceptual framework of the study is presented in Fig. 1.

METHODOLOGY

We employed parameters encompassing basin geomorphology, geology, land use, and morphometric analysis to evaluate the river basin and morphologic characteristics. We used GIS and remote sensing data alongside data obtained from field surveys conducted in 2015 and 2018 to generate terrain parameters and assess morphological and hydrodynamic characteristics of the Mohan-Khutiya River basin—part of the data derived from the studies done by (Mott-Macdonald and TMS, 2018) were reviewed, updated, and used. The current lead author was involved as a river morphologist for the project.

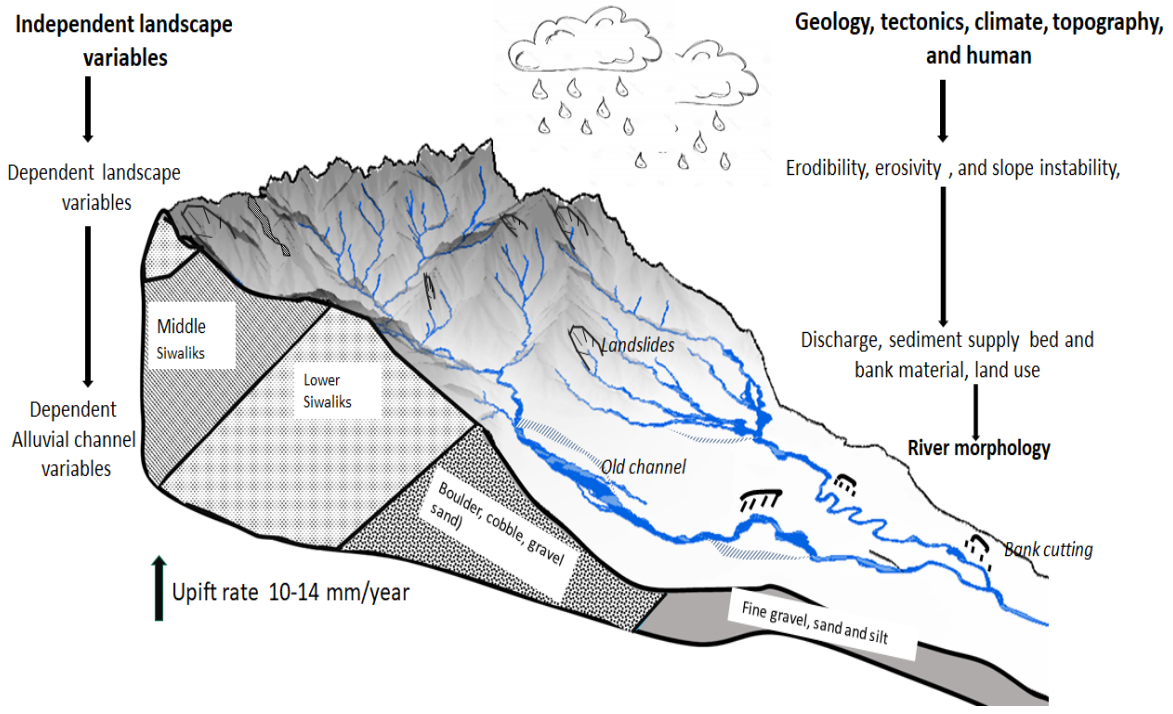

Fig. 1: Conceptual model showing the relation between basin characteristics and river morphology (e.g. Khutiya – Shiva Ganga River), modified from Ghimire (2021).

Methodologically, we analyzed basin features, established geomorphic characteristics of hill and alluvial sections, assessed river processes, and examined morphological changes, including channel avulsion, abandonment, aggradation and degradation of the Mohana-Khutiya River.

Data sources and techniques

Data on geology were obtained from the maps published by the Department of Mines and Geology (DMG), focusing on rock type and structure. Morphometric parameters, including drainage network and basin and river slope, were derived from a 12.5-meter resolution Digital Elevation Model (DEM) obtained from ALOS 2007, using hydrological tools in ArcGIS.

Data on geomorphology and river morphology, such as topography, geomorphic units, changes in river planform morphology and sediment characteristics, were gathered from high-resolution imagery provided by Google Earth representing 2013, 2018, and 2024. We analyzed DEM and multi-spectral imageries of Landsat 8 to complement the data interpretation. Hydraulic data such as discharge, water level and water depth, velocities and Froude number, and flood extent (one in 50 years) were produced by Mott-MacDonald and TMS in 2018 by analyzing the HEC-RAS hydrodynamic model. Cross-section surveys and field observations conducted in 2018 by Mott-MacDonald and TMS were used to run the hydrodynamic model and estimate sediment transport capacity. Information on

landslides was obtained from visual interpretations of Google Earth images and Landsat imagery from 2018-2024. The landslides were data extracted from the inventory made by (Ghimire *et al.* (2020).

Application of InSAR

DEMs derived from Interferometric Synthetic Aperture Radar (InSAR) and from ALOS PALSAR and Sentinel-1 were used to examine the changes in cross-section form in the exact location at various channel reaches. InSAR provides high-resolution radar imagery suitable for interferometric applications. It accurately measures surface deformations or elevation by analyzing phase differences in radar signals acquired from two or more satellite passes. The generation of DEM from SAR-based interferometric techniques has been widely used in various studies (Braun, 2021; Marchetti, 2023; Nagler et al., 2015; Solari et al., 2019). We used ALOS PALSAR DEM (Resolution 12.5) data from 2010, retrieved from https://search.asf.alaska.edu/#/, accessed on 2022-11-05.

We also derived DEM covering the study area from the pair of Sentinel-1A imageries (IW, Descending mode, VV polarization) (ESA, 2023) taken on 2024-07-08, 2024-07-20 and 2018-03-30; 2018-04-23). These imageries were retrieved from https://search.asf.alaska.edu/#/, accessed on 2024-05-05. We reconstructed DEM of 13.5 m resolution using interferometric techniques available in the ESA-developed open-source software Sentinel Application Platform (SNAP). To obtain good coherence and micro-topographic variations, we considered the temporal baseline not exceeding 30 days and the perpendicular baseline above 100-150m(Braun, 2021; Ferretti et al., 2007). InSAR DEM representing riverbed and adjacent bare or small grass-covered floodplain sites were selected to create cross-section profiles. Various operations available in the Sentinel Application Platform (SNAP), such as Geocoding, enhanced spectral diversity, interferogram generation, filtering, phase wrapping and unwrapping, and finally creating DEM, were applied.

STUDY AREA

Location and land use

The catchment of the Mohana Khutiya river basin lies between latitude 28°38'1.76"N to 28°58'59.15"N), and longitude 80°31'36.73"E and 80°45'24.74"E in WGS 84, UTM Zone 44 N (see Fig. 1). The basin extends from Chure Hills (Siwalik Hills, also known as sub-Himalayan hills, at low altitude) in the north and in Tarai (meaning low flat land) up to the Indo-Nepal border in the south. The catchment covers an area of 702.4 km2 in the far west of Nepal (Fig. 2). The Mohana-Khutiya river system lies in the district of Kailali in Sudurpaschim Province. This river system has 359 settlements, with over 300,000 distributed over six rural and urban municipalities (NSO, 2021). Dhangadi and Attrariya are the two major towns located in this catchment.

The basin has two distinct land use patterns. The upper catchment is predominantly forest, shrub, and grassland (90%), with minimal agricultural disturbance. In contrast, the lower catchment is heavily agricultural and built-up (55%), with significant deforestation. The Mohana River's lower catchment has 69.5% agricultural and built-up areas. The Khutiya River's lower catchment has 51.3% forest cover. Agricultural lands are mainly in the flood plain zone, south of the Bhabar region, exposed to high flood, siltation, and erosion hazards due to minimal forest along riverbanks.

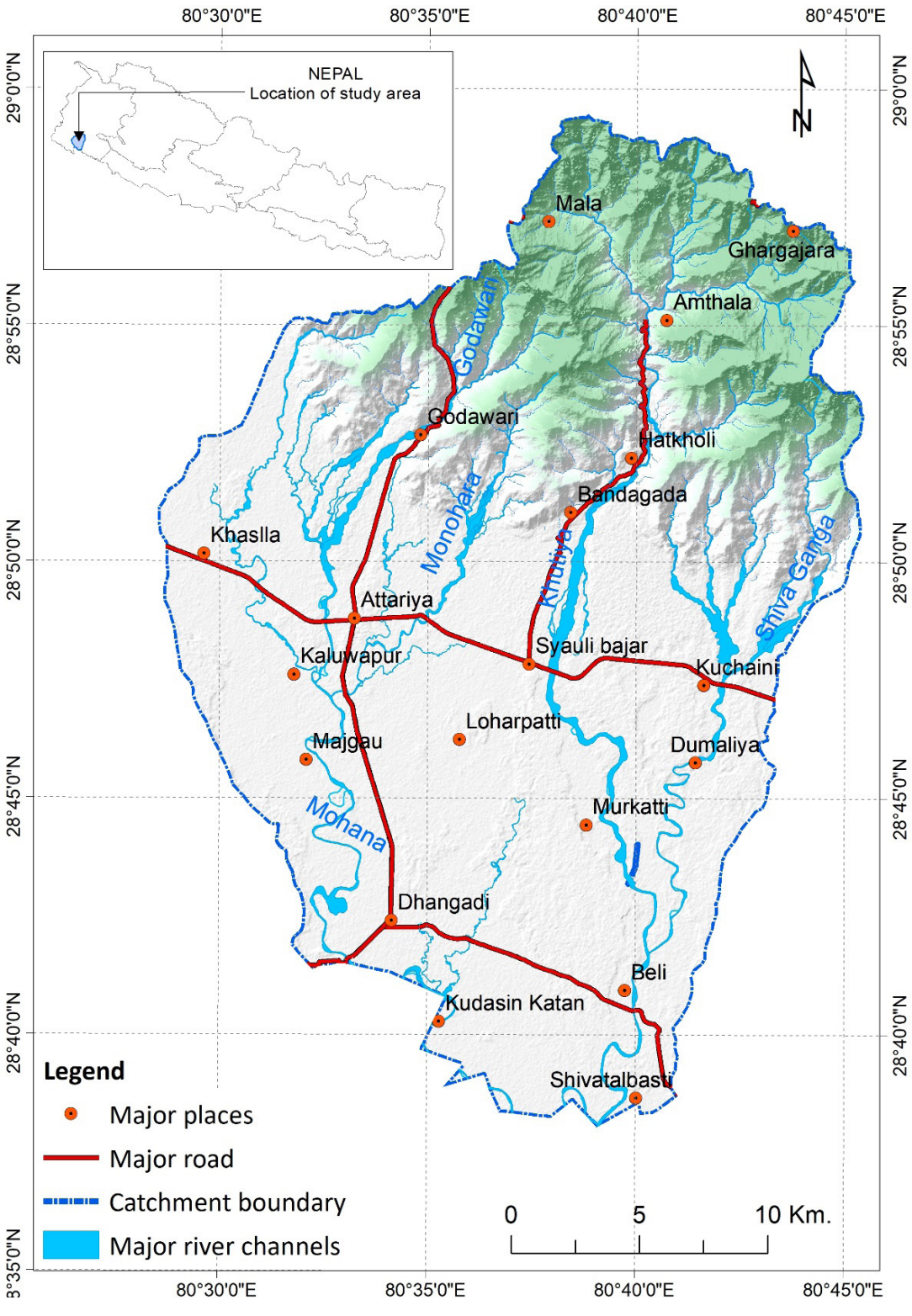

Fg. 2: Study Area, Mohana-Khutiya River Basin

Geology, topography, and drainage

The Mohana-Khutiya basin is underlain by the rocks of the Siwalik Group in the upper reach and recent quaternary deposits in the lower reach. The Siwalik Ranges, the youngest Himalayan belt, are tectonically active, leading to rock deformation and an unstable landscape. The Siwaliks are divided into Lower Siwaliks (LS) and Middle Siwaliks (MS) (Fig. 3). The LS, primarily mudstone with sandstone, occupies the southern part of the catchment. In this group, the proportion of mudstone is greater than that of sandstone in aggregate. The MS contains more sandstone, with coarser grains in the upper formations and thicker sandstone beds than mudstone beds. The sandstone beds range in thickness from 1 to 30 m, while the mudstone ranges from 0.5 to 4 m (DMG, 2007; Ghimire et al., 2024).

The Siwaliks are delineated as the Main Frontal Fault, the most active fault, thrust over the alluvium in the Piedmont zone (Nakata, 1989). Similarly, Jogbudha Thrust runs South East-North West in the northern part of the Khutiya catchment. Both thrusts dip 25°–30° North East to North East. Bedrocks generally dip towards the northeast, with an amount of 30°-70° (DMG 2007; Dhital 2015).

The upper catchment's drainage is influenced by bed structure and faults, forming trellis-to-rectangular patterns with a high drainage density of 5.82 km/km^2. The stream's average slope is 22.8%, capable of transporting large sediments during monsoon rainstorms. Of 3890 streams with a total length of 1,479 km, 93 percent of streams (first- to second-order steams) have slopes above 25%. These streams are colluvial types that couple with hillslope processes, which deliver a huge amount of debris to the river system (Fig. 4).

.

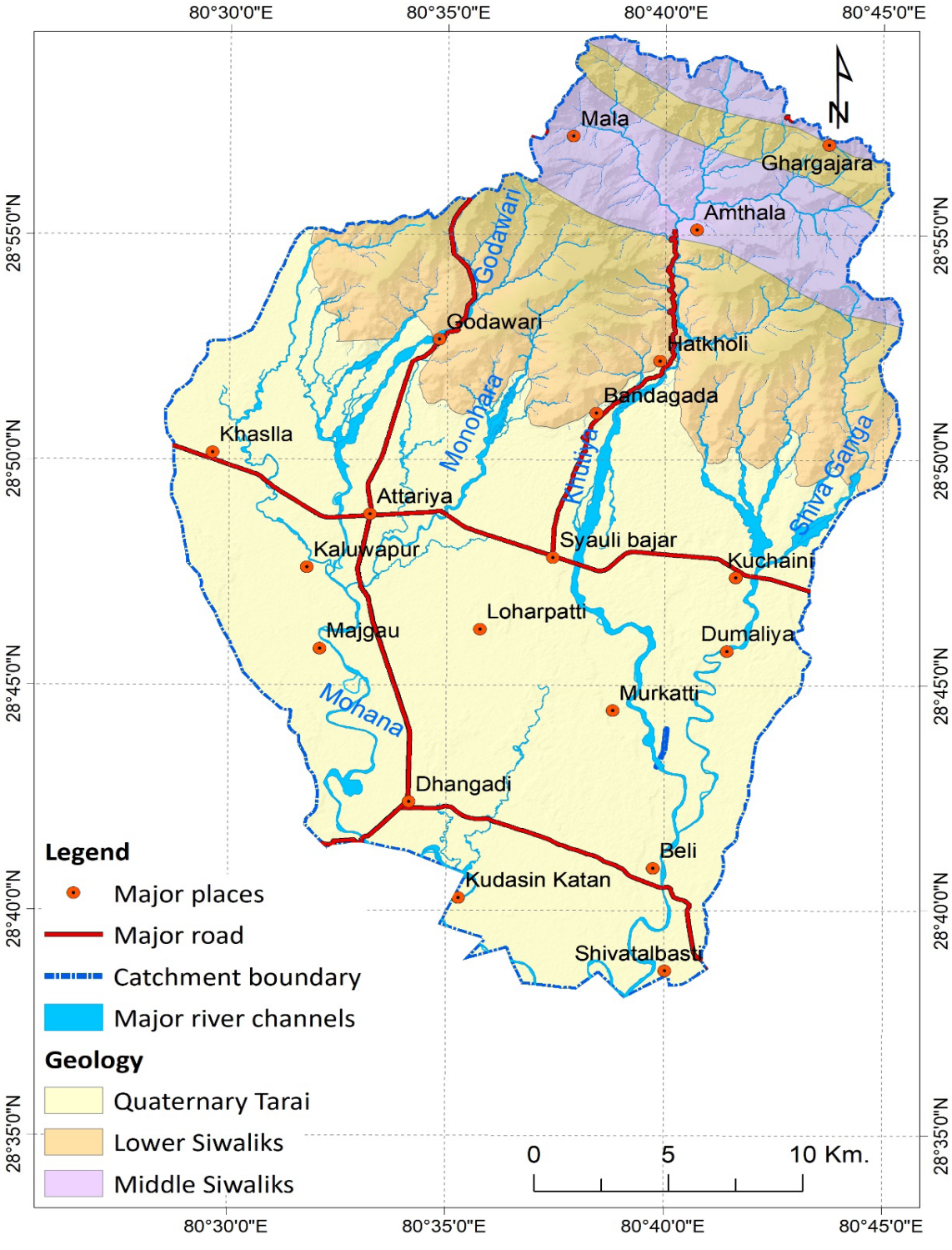

Fig. 3: Geological map of the Mohana-Khutiya River basin

RESULT AND DISCUSSION

Hillslope processes of the upper catchment and rainfall events

The upper catchment area, characterized by strong relief (160-1940 masl), steep topography (mean slopes ~ 25±10o), active tectonics, and complex geology, exhibits numerous old, active, recurring, and expanding landslides. Factors such as topography, bedding structure, fractures, tectonic uplift, and differential weathering of mudstone and sandstone influence these landslides, contributing significant sediment loads to rivers and streams during monsoons. About 1563 mm of precipitation falls annually, of which the summer monsoon contributes more than 80%. Since the last 70 years, about a maximum 24 hours maximum rainfall events above 150 mm were 30, i.e., one in 2.3 years, and have shown increasing trend (Fig. 4). Such events can trigger landslides and debris flow in hillslopes. Nine rainfall events with intensity above 200m/24 hours were recorded, capable of initiating widespread and devastating landslides and debris flow (Fig. 4). In July 7-8 ever recorded (DHM, 2024) extreme rainfall was recorded, i.e., 573.6 mm/24 hour at Hanmannagar. Apart from the rainfall, tectonic upliftment and incision rate are pronounced in creating landslides and erosion. Lavé and Avouac (2000) estimated the uplift rates in the Siwaliks of central Nepal to range between 1-4 mm/year based on the deformation of fluvial terraces. Similarly, erosion rates in the Siwaliks are estimated to be around 2-6 mm/year, varying significantly with monsoon intensity and river dynamics (Bookhagen and Burbank, 2010).

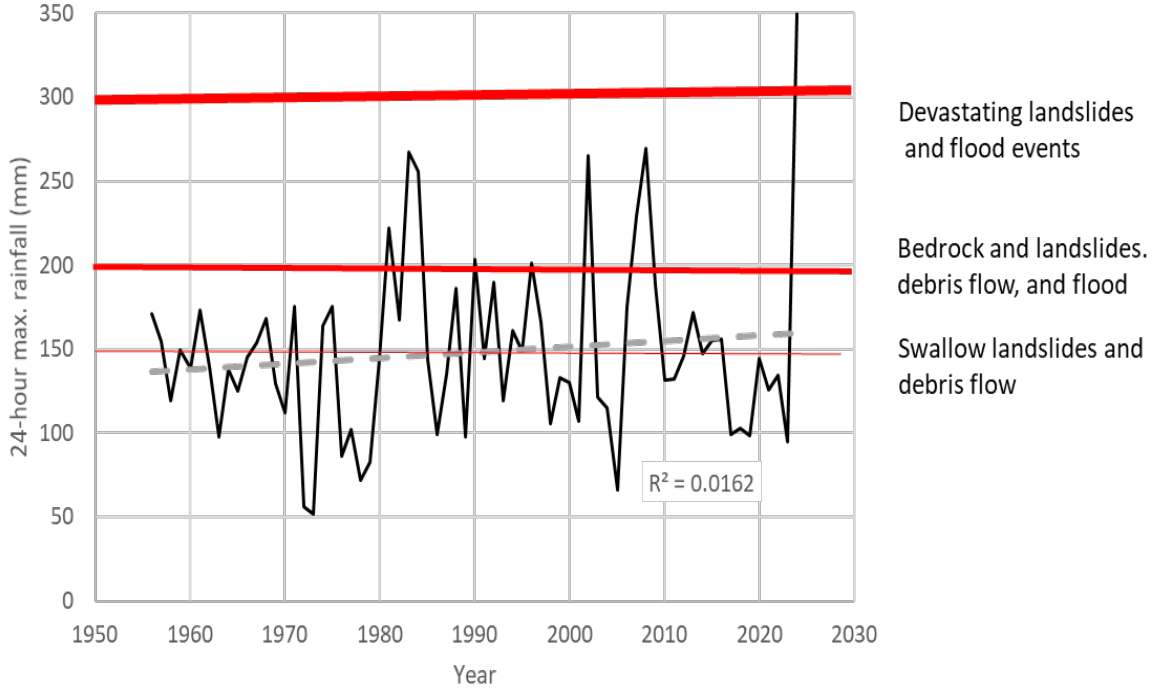

Fig. 4: Historical observation of the 24-hour extreme rainfall events in Dhangadi (DHM, 2020, 2024).

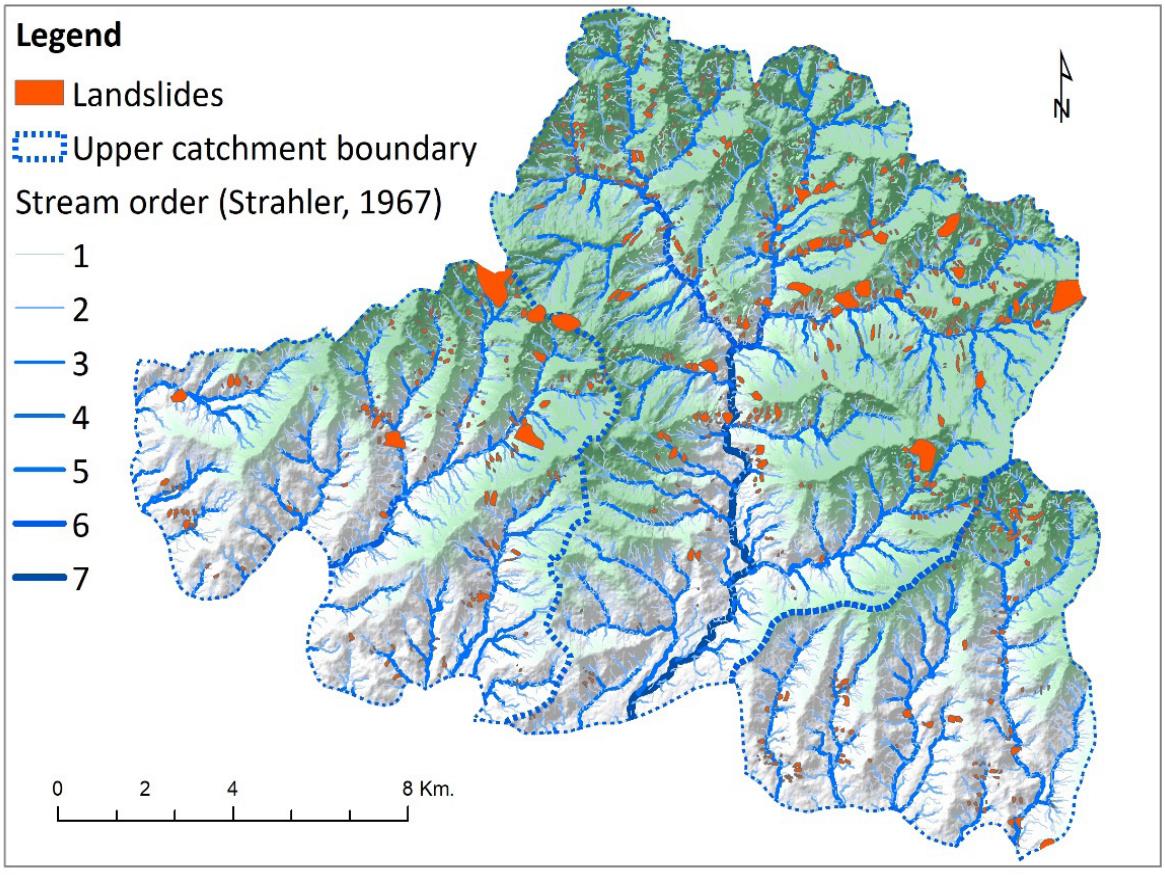

Fig. 5: River order and landslide distribution in the Upper Mohana-Khutiya catchment.

Numerous complex slides are seen on the stream and gully head, from where the hillslope materials are released into colluvial streams and further transported downstream. The sediment, ranging from fine clay to large boulders, is transported through narrow valleys and deposited in foothill riverbeds.

Based on Google Earth images (2020), landslides in the Mohana and Khutiya River catchment are classified as rockfall, slides, debris fall, and swallow scar failures (Fig. 5). Rockfalls and slides are prevalent on steep anti-dip slopes, while rotational failures occur on gentler, weathered slopes. Additionally, erosion scars, exposed rocks, and land degradation were recognized due to bare steep slopes, overgrazing, and deforestation. River undercutting causes foot slope failures, indicating active river incision. An inventory of 6040 landslides and erosional scars with a total area of 3484 hectares was made. Using the empirical formula, i.e., $D=0.05\times A0.45$, where D=Depth, A =area (Hovius et al., 1997), a total volume of 4,315.75 million m3 of sediment is estimated from the currently active landslides.

Geomorphic characteristics

The Mohana Khutiya River system is classified into five geomorphic units based on topography, river morphology, geology, and sediments (Fig. 6):

Steep river gradient, bedrock, and coarse sediments. This zone features the Chure (Siwalik Hill) underlain by sandstone and mudstone. It has a seventh-order drainage network with strong gradients, receiving sediments from landslides, debris flows, and erosion. The riverbed consists largely of boulders, cobbles, and gravels, with exposed and incised bedrock in steep channels. Uplifted terraces indicate former floodplains. Managing landslides and erosion is crucial to reduce sediment delivery to the lower catchment. The river morphology is controlled by bedrock and geological structure. Reducing human disturbances like cultivation, grazing, and deforestation is recommended, while expensive structural measures to control erosion are often questionable.

Alluvial fan deposits: This zone comprises alluvial fan deposits, which feature decreasing sediment size from boulders to sand towards south. Riverbeds are wide, shallow, and braided, with unstable island bars. Flashy discharge causes sediment transport during high water levels. The Khutiya River has a significant fan base, while others, like Mohana and Manohara, have smaller fans. Embankment construction requires site assessment due to the risk of channel avulsion (Fig. 6 and 7).

Upper alluvial plain deposits. A transitional zone dominated by gravel and sand deposits, with braided and meandering channel patterns. Evidence of channel avulsions and lateral migration is present. The channel width is intermediate between zones 2 and 4/5 (Fig. 8).

Middle alluvial plain deposits: This floodplain area features meandering rivers with pool formation at bends. Bank erosion is a major sediment supply source. Abrupt reductions in sediment supply can cause the river to erode its bed. Gradual sediment supply reduction through riparian vegetation restoration is recommended (Fig. 6).

Lower alluvial plain deposits: A floodplain with gentle slopes featuring fine sand and silt deposits. Channels are narrow, deep, and meandering with alternate bar deposits. Overbank flooding, bank erosion, avulsion, and siltation are common. Bank erosion at meander bends significantly affects agriculture and livelihoods.

Fifty-year flood plain: The Flood plain is a belt along a river that can be affected by flood events of the magnitude that may recur once in 50–years, i.e., a 2% chance of being inundated by a flood in any given year (Fig 5). These floodplains are critical for flood control, as they act as natural buffers, absorbing excess water and reducing flood damage. However, these floodplains have been heavily encroached by human activity.

These classifications highlight the need for specific management strategies to address sediment transport, erosion control, and flood risk mitigation.

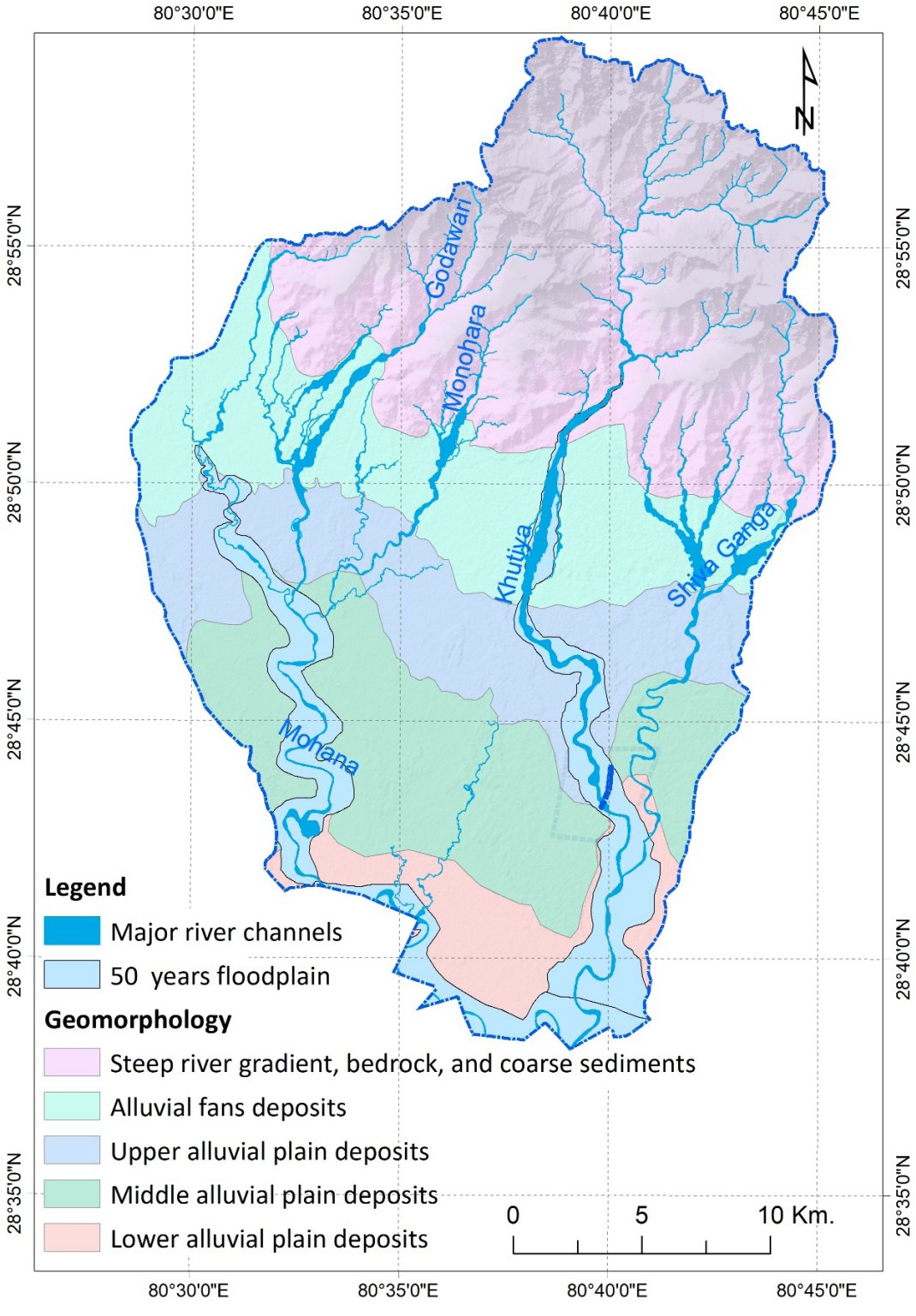

Fig. 6: Geomorphological unit

Fig. 7: Boulder, cobble, and gravels near the apex of the fan of Godawari River.

Fig. 8: At 15km downstream from the fan apex. Unlike upstream, the river bed consists mainly of sand, gravel, and silt. Photos on the left show the upstream and right downstream of the Godavari River bridge.

Morphological characteristics of the river

The morphological characteristics of the channel reaches are defined by the morphological characteristics of the channel pattern, such as sinuosity, braidedness, and meandering characteristics of the channel (Table 1). Sinuosity is the ratio of the curvilinear length of the river to the straight-line distance between its endpoints. The braidedness of a river is determined by the network of sub-channels separated by small, often temporary islands, called braided bars. Meandering refers to a series of sinuous curves, bends, or loops of a river typical in flood plains comprising sand and silts with gravel fractions.

The Mohana, Godawari, and Manohara rivers in the hilly region share similar geomorphological features. The Mohana River spans 70 km straight (13 km) and meandering reaches (57 km) (Table 1). The straight reaches have steep slopes and braided and broader channels with boulders, gravel, and sand sediments. The meandering reaches have gentler slopes and are narrow, and sediments are mainly of sand and silt, with some fine gravel.

The Godawari River, a 23 km tributary of the Mohana, generally has straight reaches. Towards the south, it tends to meandering (sinuosity of 1.4). It indicates the Mohana's sediment distribution, with braided channels and steep slopes in the first two reaches and milder slopes in the third, comprising sand and gravel.

The Monohara River, another tributary of the Mohana, extends 20 km and has similar characteristics: steep, straight reaches transitioning to a meandering third reach (sinuosity of 1.46) and a sediment composition of boulders, gravels, sands, and silt.

The Khutiya and Shivaganga rivers, key Mohana tributaries exhibit diverse geomorphological features (Fig. 6 and Table 1). The Khutiya River spans 52 km, comprising 20 km straight (39% of total length) from the fan apex depicting a broad (507 m wide braided pattern). Such an extensive fan and braided-ness indicate the massive sediment transport supplied from the hilly catchment and fan. The remaining reaches towards the south witness wandering to the meandering pattern. The straight reaches have steep slopes with boulders, gravel, and sand, while the wandering to meandering reach has mild slopes comprising sand, fine gravel, and silt.

The Shivaganga River is a 35-km tributary of the Khutiya, with five braided tributaries that meet at the fan zone. The straight and braided segment features steep slopes and similar sediments as the Khutiya's straight reaches, while the meandering segment (20 km) downstream has mild slopes and finer sediments of sand and silt.

The geomorphological features of these rivers indicate a correlation between channel slope, sediment type, and river morphology, which aligns with findings by Leopold et al., (2020), Schumm (2007), studies by Bridge and Lunt (2006), Knighton (2014), and Ghimire (2020)

.

Table 1: Channel characteristics of the Mohana-Khutiya River System

River	Reach ID	Reach Characteristics	Channel length	Sinuosity index	Slope %	Channel area (km^2)	Average width (m)	Maximum Depth at bankful discharge (m)	Width depth ratio	Sediment characteristic
Mohana, Godawari, Monohara	1	Hill	5.0-9.3	1.12-1.2	14.1	0.34-0.62	25-79			Sand, gravel and boulder
	2	Fan	4.8- 8.4	1.1-1.14	1.1	12.1 0.26	164-507	0.75-1.5	99-135	Sand, gravel, boulder
	3	Peripheral fan (Godawari Confluence)	6.5- 13.9	1.5-2-0	0.1	4.24-1.97	109	1.5	87	Sand
	4	Flood plain, meander (India border)	8.6-21.3	1.4-2.1	0.1	9.38-3.68	92-168	2	25-46	Sand and silt
	5	Flood plain, meander (India border-Khutiya)	8.6. 21.3	1.79	0.1	4.42-0.62	144-173	2	25- 86	Sand and silt
Khutiya-Shivganga	1	Hill	10.9-19.91	1.3-1.3	8.3-14.7	3.5	60-74	NA	-	Sand, gravel and boulder (upper segment
	2	Braided	3.78-6.51	1.0-1.1	1.1-1.4	6.23-33	164-507	1.5-2	109-253	Sand, gravel and boulder (upper segment
	3	Flood plain, Meander (Shivaganga confluence)	15.46-19.55	1.6 -1.4	0.2	11.5-26.1	59-169	2-2.3	29-75	Sand and silt
	4	Meander (Mohana confluence (Nepal-India border)	9.77	1.45	0.1	13.4	137.3	2.25	61.0	Sand and silt

Sediment load transport capacity and river processes

Flow gauging stations are unavailable, so depth, velocity and water surface gradient (energy gradient) were taken from the HEC-RAS 1d hydrodynamic model (2018 model) for a 1 in 50-year return period produced by Mott-Macdonald and TMS (2018) (Table 2). Historical extreme rainfall data (1980-2016) from DHM was used as input for the model. Discharge increases over twelve times downstream from Mohana at foothill to Khutiya Mohana confluence, indicating significant tributary contribution. The contribution from the Khutiya is highest. Sediment transport capacity was estimated using the Van Rijn (1984) method (Table 2), with HEC-RAS 1D hydrodynamic model outputs for a 50-year return period discharge. The median sediment grain sizes (D10, D50, D90) were used for predictions. Compared to other methods, Van Rijn's (1984) method is better predictable.

Sediment load varies significantly downstream, from 4316 to 5.85 tons/day, depending on discharge, depth, velocity, sediment characteristics, flow and environment (Van Rijn, 1984). Table 2 shows that the first 7 km (approximately) of the rivers have a high capacity for transporting sediment. A straight channel with steep gradient characterizes the first two river reaches. But it has to be noted that, here, only point transport was estimated, the total load downstream over the cross-section in the straight reaches may be relatively smaller than in the meandering ones because of less discharge and less flow area in the upstream reach (Mott-Macdonald and TMS, 2018). There will be gravel and cobble deposition in these reaches but no sand deposition on the bed. However, bed erosion is not likely to happen as these reaches of the river is dominated by gravels and boulders.

The sediment load carrying capacity of river at downstream reaches (the sand and silt zone, with fractions of gravel) at 12, 17, and 47 km is low. The low sediment transport capacity indicates aggradation of sediments on riverbed. However, at 31 km, after the Godawari and Manohara confluence (3 km downstream) and at confluence of Mohana and Khutiya, the sediment load capacity is 2324 and 45213 tons /day, respectively. In these reaches, the net effect will be degradation as aggradation decreases.

Changing hydraulic variables along the channel show dynamic morphology, influencing aggradation and degradation. If water cannot transport sediment, deposition raises channel height (aggradation). Conversely, increased velocity or slope erodes the channel (degradation), altering river morphology.

Table 2: Hydraulic parameters and sediment load at distances along Mohana River

Distance from Foot hill at fan apex (km)	Geomorphic Unit	Discharge (cu m/s)	Depth (m)	Energy Grade Slope (m/m)	Average velocity (m/s)	Velocity at Deepest (m/s)	Froude #	Sediment load (tons/ day)
Mohana River								
0.0	Sand and gravel	209	2.51	0.002696	1.94	3.07	0.56	3024
2.5	Sand and gravel	225	2.93	0.002116	1.76	3.01	0.5	2812
7.3	Sand and gravel	269.05	3.53	0.002093	1.73	3.4	0.5	4316
12.4	Sand and silt	717.77	3.6	0.000307	1.15	1.32	0.22	110
17.2	Sand and silt	1014.86	3.76	0.000726	1.52	2.08	0.33	693
31.1	Sand and silt	1221.82	4.77	0.001008	2.18	2.88	0.4	2324

Distance from Foot hill at fan apex (km)	Geomorphic Unit	Discharge (cu m/s)	Depth (m)	Energy Grade Slope (m/m)	Average velocity (m/s)	Velocity at Deepest (m/s)	Froude #	Sediment load (tons/ day)
46.6	Fine sand and silt	1512.81	4.74	0.000243	1.07	1.41	0.2	141
57.6	Fine sand and gravel	2557.7	4.58	0.002804	3.81	4.67	0.68	13627
Khutiya River								
0.0	Sand and gravel	1045.68	4.28	0.000844	1.88	2.45	0.36	1276
20.6	Fine sand and silt	1493.31	4.48	0.000536	1.45	2.01	0.29	599
35.5	Fine sand and silt	2557.7	4.58	0.002804	3.81	4.67	0.68	13627

River erosion and aggradation processes

The planform and cross-sectional morphology of the Mohana-Khutiya River reveal various river processes contributing to different forms of erosion and providing sediments to the river. Notable processes include bank erosion, river bend scouring, confluence erosion, and deposition. These processes change channel migration, avulsion, and bed level, altering the river's planform and cross-sectional morphology.

Bank Erosion: The Mohana-Khutiya River's upper catchment and the river's floodplains downstream (Tarai plain) are significant sediment sources, comprising coarse sediments in Fan deposits and Upper alluvial plain deposits and fine sediments in zones in the Lower alluvial plain. In the first two zones, non-cohesive sediments (silt, sand, gravel, cobbles) restrict bank slopes to 30-45° and erode through shallow slides. In the lower reaches, cohesive sediments are prone to undercutting and collapse due to toe erosion or reduced bank strength due to saturation during floods, leading to liquefaction. Similarly, water flow within the bank sediments causes sediment rearrangement and internal erosion (piping or sapping), destabilizing layers and leading to large-scale backslides.

River Bend Scours: River bend scour potential is high in the Mohana-Khutiya River system, particularly in the sand and silt zone. About 60, 22, 18, 37, and 49 bends were observed in Mohana, Godavari, Monohara, Khutiya, and Shivganga. The catchment of the Mohana has Lower Siwalik rocks where mudstone dominates over sandstones; therefore, in the foothill, the riverbed comprises sand and silt, which favors the development of meanders. Towards downstream, the meanders are highly pronounced, comprising sharp bends with smaller radii and non-less cohesive bank materials such as sand and silt; the bend scouring has higher rates at higher flow velocity. Bank and bend erosion contribute to increased sediment load downstream, which impacts channel alignments and causes channel shifts.

Confluence Scours: Key confluences, such as where the Godawari River and Manohara join Mohana and the meeting points of the Khutiya and Shivganga Rivers, experience increased discharge and sediment load, affecting downstream morphology. This can induce sand bar development and scour in nearby areas to maintain flow conveyance.

Protrusion Scours: Scours develop where natural hard banks or erosion-resistant structures, similar to Bridge abutment scours, obstruct flow. Topographical surveys indicate structures like embankments and bridges along the rivers induce channel scouring.

Channel Avulsion: Time series imagery and paleo-channels show rapid shifts in the Moahana and

Khutiya Rivers and the tributaries' location on the floodplain, often triggered by floods. This process significantly influences channel location and floodplain dynamics.

Change in river morphology: Planform and Cross-sectional form

Planform river morphology refers to the shape and pattern of a river as seen from an aerial view or map. It encompasses the horizontal layout and patterns of river channels, including their bends, meanders, straight segments, and network configurations (Fuller *et al.*, 2013). Cross-section river morphology refers to the vertical profile of a river channel, taken perpendicular to the direction of flow (Fuller *et al.*, 2013). Understanding planform and cross-sectional morphology is essential for analyzing river dynamics, sediment transport, hydraulic characteristics, and the impact of human activities (Fuller and Smart, 2007). River processes, revealed in planform and cross-section form, are important geomorphological processes that attract a great deal of attention from river engineering scientists in many parts of the world (Best and Rhoads, 2008; Ibitoye, 2021).

Erosion (bank and avulsion), deposition and channel abandonment between 2014, 2018, and 2024 evidence changes in river morphology (Fig. 9 and Table 3). Total bank erosion over both periods is significant at 710.7 hectares. The total area affected by avulsion is relatively small (39.4 ha) compared to other processes. Bank erosion decreased from 82.7 ha/year (2014-2018) to 66.7 ha/year (2018-2024). Similarly, erosion from avulsion decreased dramatically from 8.0 ha/year to 1.3 ha/year.

Deposition remains the most extensive process compared to erosion, covering 1171.5 hectares between 2014 and 2024. This is indicative of an excessive sediment load from the upper catchment. Deposition also decreased from 141.3 ha/year to 106.4 ha/year. The total area affected (113.9 ha) by channel abandonment indicates that this process is less dominant than direct deposition. A significant decline in the deposition rate due to channel abandonment was observed, from 18.8 ha/year (2014-2018) to 6.8 ha/year (2018-2024).

A decrease in the annual rates of all river processes (erosion, avulsion, deposition, and channel abandonment) suggests an overall stabilization in riverbanks or effective erosion control measures, including successful intervention in preventing rapid channel changes or a natural decrease in avulsion events after 2018. The decreasing trends in river dynamic processes suggest that existing management practices may be effective. Studies by Fuller *et al.* (2013) and Hooke (1984) also support that effective river management can reduce erosion and avulsion rates.

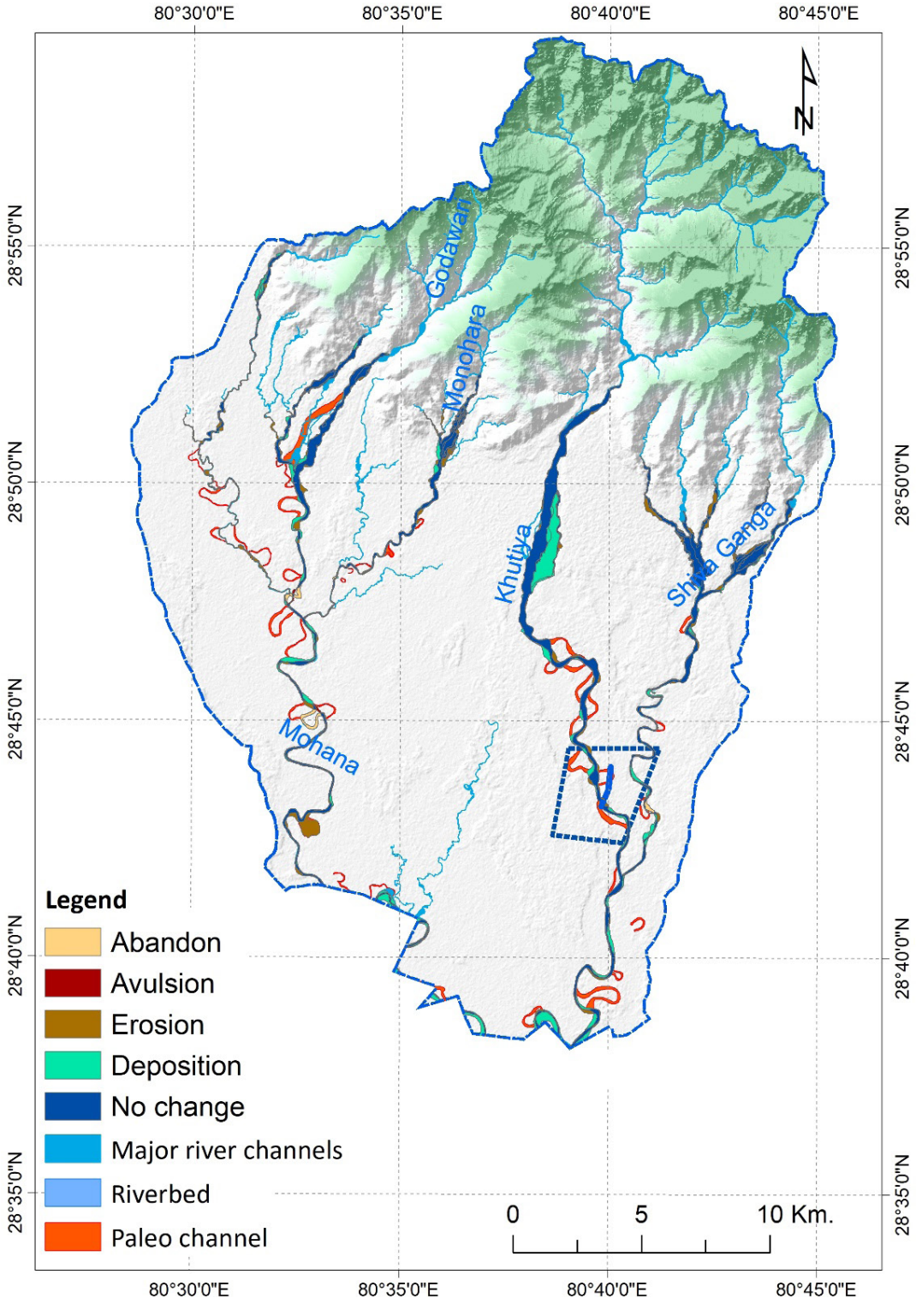

Fig. 9: Planform change in river morphology between 2018-2024.

Table 3: River processes in planform of channel morphology.

River Processes	2014-2018		2018-2024		Total	
	Area (ha)	Ha/year	Area (ha)	Ha/year	Area (ha)	Ha/year
Bank erosion	330.8	82.7	379.9	66.7	710.7	73.3
Avulsion and erosion	32.2	8.0	7.2	1.3	39.4	4.1
Deposition	565	141.3	606.5	106.4	1171.5	120.8
Channel abandonment and deposition	75.3	18.8	38.6	6.8	113.9	11.7
No change	1764.6	441.2	1667.6	292.6	3432.2	353.8

Cross-section morphology was examined using DEM derived from the Interferometric synthetic aperture radar (INSAR) data taken by Sentinel-1A in April 2018 and July 2024. The ALOS PALSAR DEM representing 2010 was also used to examine the change in the cross-sectional form of the river morphology (Kryniecka, *et al.*, 2022; Marchetti, 2023). Sentinel-1 images and ALOS PALSAR DEM were also obtained from the Alaska Satellite Facility. The cross-sectional profile at different locations of the Mohana, Godavari and Khutiya Rivers reveals that aggradations and degradation processes are significant in all cross-sections (Table 4 and Fig. 9). However, there is substantial variability in sediment aggradation and degradation across different geomorphic zones (Table 4). Within the river, with the same cross-section, there is also remarkable variability in the river processes (Fig. 9). There was a significant net gain of sediment in m3/m at CS1 (fan zone), CS4 (Sand, silt and gravel) and CS8 (sand and silt zone). At this location, the net gain of sediments was 93, 1209.9, and 253 m3/m, respectively. CS2 witnessed the highest net gain (1209.9 m^3/m) in a fan zone, followed by CS10, i.e., 722.6 m3/m in a fine sand and silt zone. Huge deposition in these areas (although sediment characteristics differ) could potentially lead to bed-level rise and impact flow patterns.

Significant to substantial sediment loss was observed at CS3 (fan), CS6 (sand, silt, and fine gravel), CS9 (fine sand and silt), and CS12, CS13, and CS14 (fan). CS6, CS9, and CS13 indicate significant sediment loss, which could imply an increase in erosion and sediment transport downstream.

The decline in bank erosion and avulsion rates suggests stabilization of riverbanks or effective erosion control measures. Several river training programs, such as constructing levees, embankments, spurs, or other structures to ensure the river flows safely within its banks, especially in areas prone to erosion or flooding, have been constructed in the Mohana-Khutiya basin by the Government of Nepal. This aligns with studies by Fuller *et al.* (2013) Hooke (1984), and Thorne *et al.* (1997) emphasizing that effective river management can reduce erosion and avulsion rates.

Table 4: River processes observed in cross-sectional channel morphology

Cross-section	Degradation				Aggradation				Annual Balance (m3/m)	Zone
	Total depth (m)	Yearly average	Length (m)	Vol/m/ year	Total rise (m)	Yearly average	Length (m)	Vol/m/ year		
CS1	-5.55	-0.97	140	-136.2	7.69	1.35	170	229.2	93.0	Fan (SCGB)
CS2	-13.67	-2.40	300	-719.7	24.44	4.29	450	1929.5	1209.9	Fan (SCGB)
CS3	-12.94	-2.27	290	-658.6	7.05	1.24	360	445.4	-213.2	Fan (SCGB)
CS4	-7.05	-1.24	250	-309.3	10.92	1.92	250	479.0	169.7	Sand, silt, fine gravel
CS6	-15.83	-2.78	280	-777.5	6.22	1.09	280	305.3	-472.2	Sand, silt, fine gravel
CS8	-9.63	-1.69	360	-608.5	10.43	1.83	470	860.0	251.5	Sand and silt
CS9	-10.91	-1.91	350	-670.2	5.91	1.04	240	249.0	-421.2	Fine sand and silt
CS10	-5.61	-0.98	370	-364.2	10.16	1.78	610	1086.8	722.6	Fine sand and silt
CS11	-5.62	-0.99	120	-118.4	3.61	0.63	80	50.7	-67.7	Sand and silt
CS12	-17.27	-3.03	200	-606.0	8.81	1.55	160	247.3	-358.7	Fan (BCG)
CS13	-23.75	-4.17	210	-874.9	7.67	1.35	210	282.6	-592.3	Fan (BCG)
CS14	-14.15	-2.48	130	-322.7	1.00	0.18	30	5.3	-317.5	Fan (SG)

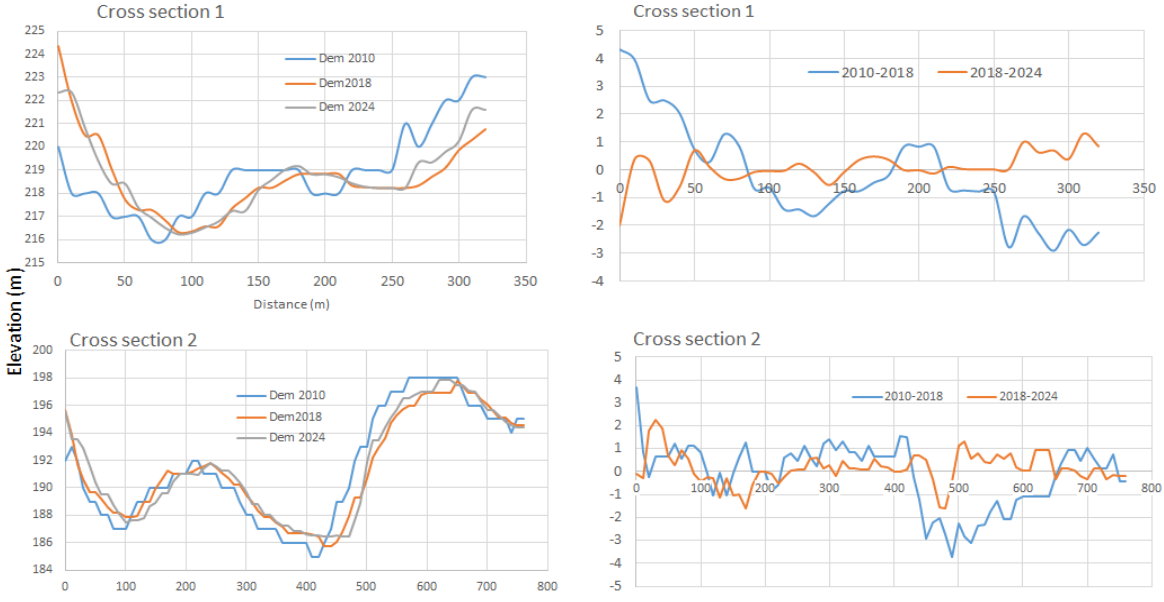

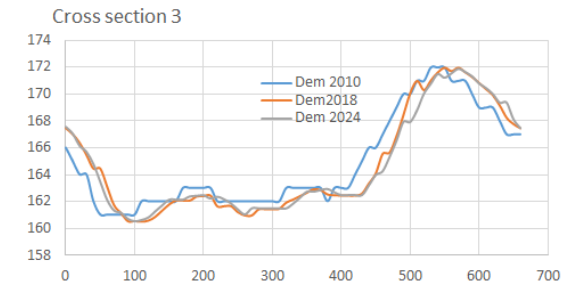
Cross section 3
Dem 2010
Dem2018
Dem 2024

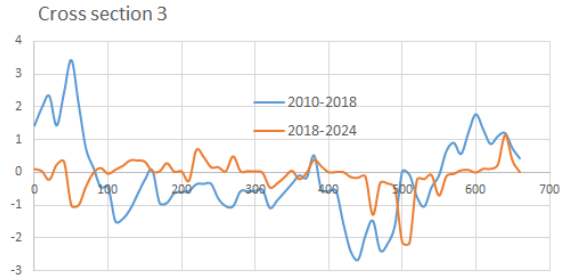
Cross section 3
2010-2018
2018-2024

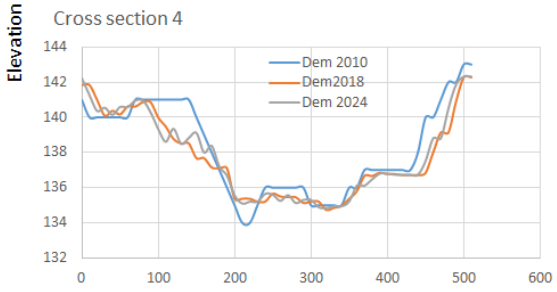
Cross section 4
Dem 2010
Dem2018
Dem 2024

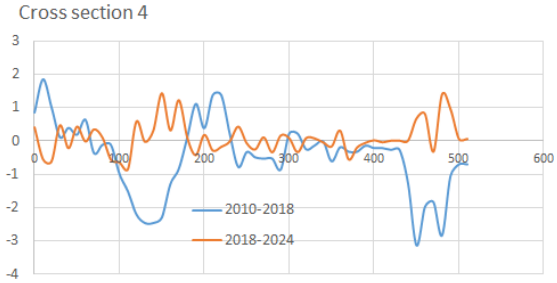
Cross section 4
2010-2018
2018-2024

Elevation (m)

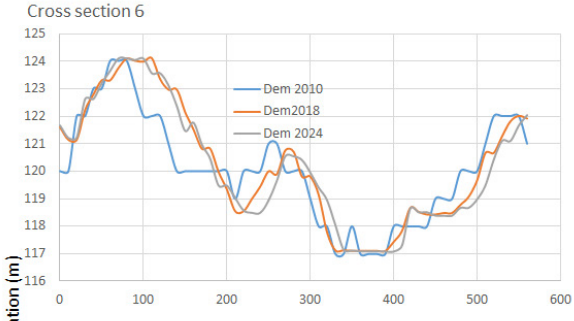
Cross section 6
Dem 2010
Dem2018
Dem 2024

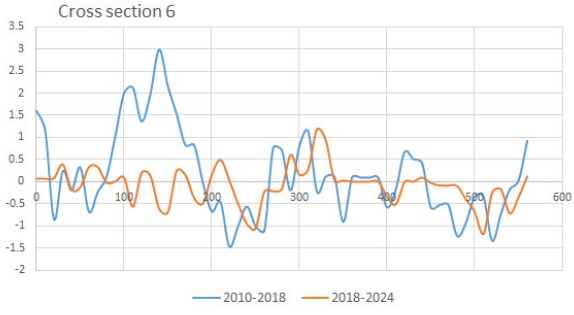
Cross section 6
2010-2018
2018-2024

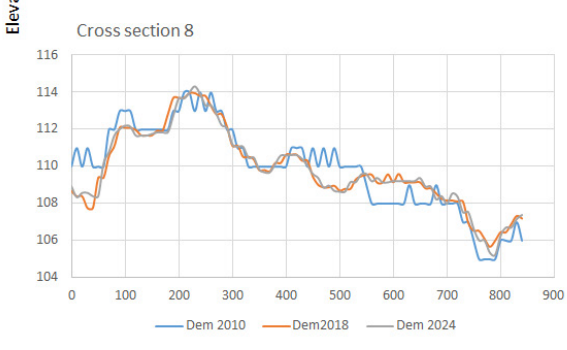
Cross section 8
Dem 2010
Dem2018
Dem 2024

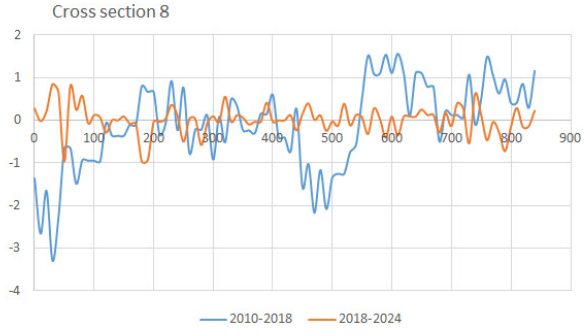
Cross section 8
2010-2018
2018-2024

Fig. 10: Cross section forms the river morphology measured at various locations.

CONCLUSIONS

This study employed a comprehensive approach to investigate the basin and morphologic features of the Mohana-Khutiya Rivers in far-west Nepal, employing GIS, remote sensing, field surveys, and hydrodynamic modeling. These methods enabled a detailed analysis of the river morphology and its influencing factors across a basin of 702.4 km², characterized by distinct land use patterns in upper and lower catchment and complex geological settings. Geologically, the upper catchment is underlain by Siwalik Group rocks, while the lower reach consists of quaternary deposits. The study revealed that steep and rugged topography, high uplift rates, and intense monsoons contribute to frequent and extensive landslides, which lead to high sediment yield in the basin's upper part and impact channel morphology downstream. The study also exposed the correlation between channel slope, sediment type, and river morphology. During the last decade, river processes such as erosion (bank and avulsion), deposition, and channel abandonment have evidenced changes in the planform of river morphology. The hydrodynamic model indicates that changing hydraulic variables influence the river's processes and morphology. Cross-sectional analysis of the rivers also shows significant variability in sediment aggradation and degradation, impacting bed-level and flow patterns, indicating dynamic river processes. Notable sediment gains at certain cross-sections and losses at others indicate dynamic river processes, impacting bed-level rise, erosion, and flow patterns. A decrease in the annual rates of all river processes (erosion, avulsion, deposition, and channel abandonment) suggests stabilization in riverbanks. Comparatively, deposition remains the most extensive process, which indicates an excessive sediment load from upstream.

Lastly, this research provides valuable insights into the complex interplay of factors shaping river morphology in the Mohana-Khutiya basin. The findings can inform better management practices and policies to mitigate risks and enhance the sustainability of riverine systems in the region through effective soil conservation, watershed management, and flood control strategies.

ACKNOWLEDGMENTS

I, as lead author, acknowledge Mott-MacDonald and Total Management System (TMS), Nepal, for providing me the opportunity to work as a River Morphologist on the Asian Development Bank-funded project "Preparation of Priority River Basin Flood Risk Management Project in Nepal," undertaken by the Government of Nepal, Department of Irrigation. A significant portion of the data used in this paper was incorporated with updates from this project. I also thank Dr. Kaji Iqbal Hassan, a senior hydrologist from Mott MacDonald, for his guidance and support. We also acknowledge the USGS, European Space Agency, and Alaska Data Facility for providing the remote sensing data, which were crucial for this study.

AUTHOR CONTRIBUTIONS

Dr. Motilal Ghimire prepared the study concept and research design. He conducted fieldwork and generated spatial data from satellite images, including InSAR data, Digital Elevation Models, and published maps. His specific contributions were to the study of basin characteristics and the morphology of the river under investigation. Dr. Puspa Sharma contributed to data generation and updating using remote sensing sources. She also assisted with data analysis, cartography, writing, and manuscript formatting.

CONFLICT OF INTEREST

The authors declare no competing interests.

DATA AVAILABILITY STATEMENT

The data supporting this study's findings are available from the corresponding author upon reasonable request.

REFERENCES

Alaska Data Facility, 2022. ALOS DEM, PALSAR. Alaska Data Facility. Retrived from https://search.asf.alaska.edu/#/, accessed on 2022-11-05.

Benda, L., Veldhuisen, C. and Black, J., 2003. Debris flows as agents of morphological heterogeneity at low-order confluences, Olympic Mountains, Washington. Geological Society of America Bulletin, 115, 1110-1121. https://doi.org/10.1130/B25265.1

Best, J.L., and Rhoads, B.L., (Eds.). 2008. Sediment transport, bed morphology and the sedimentology of river channel confluences. In River Confluences, Tributaries and the Fluvial Network (45-72). John Wiley and Sons, Ltd. DOI: 10.1002/9780470760383.ch4

Bookhagen, B. and Burbank, D.W., 2010. Toward a complete Himalayan hydrological budget: Spatiotemporal distribution of snowmelt and rainfall and their impact on river discharge. Journal of Geophysical Research: Earth Surface, 115(F3). https://doi.org/10.1029/2009JF001426

Braun, A., 2021. Retrieval of digital elevation models from Sentinel-1 radar data–open applications, techniques, and limitations. Open Geosciences, 13, 532-569. https://doi.org/10.1515/geo-2020-0246

Bridge, J.S. and Lunt, I.A., 2006. Depositional models of braided rivers. Blackwell Publishing Oxford, UK. https://doi.org/10.1002/9781444304374.ch2

Buffington, J.M. and Montgomery, D.R., 2013. Geomorphic classification of rivers. In: J. Shroder and E. Wohl, (Eds). Treatise on Geomorphology; Fluvial Geomorphology, 9 (730-767). San Diego, CA: Academic Press. DOI: 10.1016/B978-0-12-374739-6.00263-3

Chalise, S.R. and Khanal, N.R., 2002. Recent extreme weather events in the Nepal Himalayas. The extremes of the extremes: extraordinary floods, 271 (141-146). IAHS-AISH Publication. https://api.semanticscholar.org/CorpusID:133391210

Dhital, M.R., 2015. Geology of the Nepal Himalaya: regional perspective of the classic collided orogen. Springer, Switzerland. https://doi.org/10.1007/978-3-319-02496-7

Dhital, M.R., Khanal, N. and Thapa, K.B., 1993. The role of extreme weather events, mass movements, and land use changes in increasing natural hazards: a report of the preliminary field assessment and workshop on causes of the recent damages incurred in South-central Nepal during (July 19-20, 1993). ICIMOD.

Dietrich, W. and Dunne, T., 1978. Sediment budget for a small catchment in a mountainous terrain. Z. Geomorphol. Suppl. 29 (191-206). 10.1130/0091-7613(2001)029.

DMG, 2007. Geological maps of exploration block 1-10. Department of Mines and Geology (DoMaG), Government of Nepal. Kathmnadu.

ESA, 2023. European Space Agency (ESA) 202122023- sentinial 1 syenthetic aperture radar (SAR) data [Data sets] Retrieved from https://search.asf.alaska.edu/#/, accessed from 2021 to 2024-05-05

Ferretti, A., Monti-Guarnieri, A., Prati, C., Rocca, F. and Massonet, D., 2007. InSAR principles-guidelines for SAR interferometry processing and interpretation.

Fuller, I. and Smart, G.M., 2007. River and Channel Morphology: Technical Report Prepared for Horizons Regional Council: Measuring and Monitoring Channel Morphology. Horizons Regional Council.

Fuller, I., Reid, H. and Brierley, G., 2013. Methods in geomorphology: investigating river channel form. In Treatise on geomorphology: methods in geomorphology, 73-91. Elsevier. https://doi.org/10.1016/B978-0-12-374739-6.00374-2

Ghimire, M.L., Timalsina, N. and Zhao, W., 2023. A Geographical approach of watershed prioritization in the Himalayas: a case study in the middle mountain district of Nepal. Environment, Development and Sustainability, 1-34. https://doi.org/10.1007/s10668-23-03610-5

Ghimire, M.L., 2020. Basin characteristics, river morphology, and process in the Chure-Terai landscape: A case study of the Bakraha river, East Nepal. Geographical Journal of Nepal, 13, 107-142. https://doi.org/10.3126/gjn.v13i0.28155

Ghimire, M.L., Watanabe, T. and Evans, I. S., 2024. Geomorphological significance of the morphometric characteristics of first-order basins in the Siwalik Hills in the Himalayas, Nepal. Physical Geography, 45(3), 231-266. Doi: 10.1080/02723646.2023.2216954

Ghimire, S. and Higaki, D., 2015. Dynamic river morphology due to land use change and erosion mitigation measures in a degrading catchment in the Siwalik Hills, Nepal. International Journal of River Basin Management, 13, 27-39. https://doi.org/10.1080/15715124.2014.963860

Google, 2024. Mohana Khutiya River basin, Far west Nepal [Image]. Retrieved from https://earth.google.com/... 2022 May - 2024 August.

Hey, R.D., Newson, M.D. and Thorne, C.R., 1997. Applied fluvial geomorphology for river engineering and management. John Wiley.

Hogan, D.L. and Luzi, D.S., 2010. Channel geomorphology: fluvial forms, processes, and forest management effects. In R.G. Pike, T.E. Redding, R.D. Moore, R.D. Winkler, and K.D. Bladon (Eds.), Compendium of forest hydrology and geomorphology in British Columbia, 1(331-372). British Columbia Government.

Hooke, J.M., 1984. Changes in river meanders: a review of techniques and results of analyses. Progress in Physical Geography, 8(4), 473-508.

Horton, R.E., 1932. Drainage-basin characteristics. Transactions, American geophysical union, 13, 350-361. https://doi.org/10.1029/TR013i001p00350

Hovius, N., Stark, C.P. and Allen, P.A., 1997. Sediment flux from a mountain belt derived by landslide mapping. Geology, 25, 231-234.

Ibitoye, M., 2021. A remote sensing-based evaluation of channel morphological characteristics of part of lower river Niger, Nigeria. SN Applied Sciences, 3, 340. https://doi.org/10.1007/s42452-021-04215-1

Kale, V.S., 2002. Fluvial geomorphology of Indian rivers: an overview. Progress in Physical Geography, 26, 400-433.

Khanal, N.R., Shrestha, M. and Ghimire, M.L., 2007. Preparing for flood disaster: mapping and assessing hazard in the Ratu Watershed, Nepal. International Centre for Integrated Mountain Development (ICIMOD). https://doi.org/10.1191/0309133302pp343ra

Knighton, D., 2014. Fluvial forms and processes: a new perspective. Routledge. https://doi.org/10.4324/9780203784662

Kryniecka, K., Magnuszewski, A. and Radecki-Pawlik, A., 2022. Sentinel-1 Satellite Radar Images: A New Source of Information for Study of River Channel Dynamics on the Lower Vistula River, Poland. Remote Sensing, 14, 1056.

Lavé, J. and Avouac, J.P., 2000. Active folding of fluvial terraces across the Siwaliks Hills, Himalayas of central Nepal. Journal of Geophysical Research: Solid Earth, 105, 5735-5770. https://doi.org/10.1029/1999JB900292

Leopold, L.B., Wolman, M.G., Miller, J.P. and Wohl, E.E., 2020. Fluvial processes in geomorphology. Courier Dover Publications.

Marchetti, G., 2023. Riverbed sediment size and morphological changes from sentinel-1-2 satellite data [Doctoral dissertation, Free University of Bozen-Bolzano]. https://bia.

unibz.it/esploro/outputs/doctoral/Riverbed-sediment-size-and-morphological-changes/9910065681960012 41#file-0

Montgomery, D.R. and Buffington, J.M., 1993. Channel classification, prediction of channel response, and assessment of channel condition (13-42). Springer-Verlag, New York.

Mott-Macdonald and TMS, 2018. Preparation of priority river basins flood risk management project, Nepal. Kathmandu.

Nagler, T., Rott, H., Hetzenecker, M., Wuite, J. and Potin, P., 2015. The Sentinel-1 mission: New opportunities for ice sheet observations. Remote Sensing, 7(7), 9371-9389. https://doi.org/10.3390/rs70709371

Nakata, T., 1989. Active faults of the Himalaya of India and Nepal. In L. Lawrence, Jr. Malinconico, and R.J. Lillie (Eds.), Tectonics of the western Himalayas. Geological Society of America. https://doi.org/10.1130/SPE232-p243

NSO, 2021. National population and housing census 2021 (National Report) 1. National Planning commission, National statistics office(NSO), GoN, Nepal.

Piégay, H. and Schumm, S.A., 2003. System approaches in fluvial geomorphology. Tools in fluvial geomorphology, 103-134. https://doi.org/10.1002/0470868333.ch5

Schumm, S.A., 1981. Evolution and response of the fluvial system, sedimentologic implications. In Frank G. Ethridge; Romeo M. Flores (Eds.), Recent and Ancient Nonmarine Depositional Environments, 31 (19-29). SEPM, Society for Sedimentary Geology (Special Publication). https://doi.org/10.2110/pec.81.31.0019

Schumm, S.A., 2007. River variability and complexity. Cambridge University Press.

Shrestha, M.B., Tamrakar, N.K. and Miyazaki, T., 2008. Morphometry and sediment dynamics of the Churiya River area, Siwalik Range in Nepal. Boletin de geologia, 30, 35-48.

Shrestha, P. and Tamrakar, N.K., 2012. Morphology and classification of the main stem Bagmati River, Central Nepal. Bulletin of the Department of Geology, 15, 23-34. https://doi.org/10.3126/bdg.v15i0.7415

Solari, L., Del Soldato, M., Montalti, R., Bianchini, S., Raspini, F., Thuegaz, P. and Casagli, N., 2019. A Sentinel-1 based hot-spot analysis: landslide mapping in north-western Italy. International Journal of Remote Sensing, 40(20), 7898-7921.

Thorne, C.R., Hey, R.D. and Newson, M.D., (Eds.) 1997. Application of applied fluvial geomorphology: problems and potential. In Applied fluvial geomorphology for river engineering and management, (365-370). John Wiley and Sons Ltd.

Van Appledorn, M., Baker, M.E. and Miller, A.J., 2019. River-valley morphology, basin size, and flow-event magnitude interact to produce wide variation in flooding dynamics. Ecosphere, 10 (1), e02546. https://doi.org/10.1002/ecs2.2546

Van Rijn, L. C., 1984. Sediment transport, part I: bed load transport. Journal of Hydraulic Engineering, 110(10), 1431-1456.

Journal of Nepal Hydrogeological Association (JNHA), Vol (1), 43-56 (2024)
ISSN: 3059-9725 (Online)

RESEARCH ARTICLE

Hydrogeological studies in the Western part of Banke District, Nepal (Province 5)

***Dipika Shah[1], Dinesh Pathak[1], Nir Shakya[1], Ramesh Gautam[1] and Surrendra Raj Shrestha[1]**

[1]Central Department of Geology, Tribhuvan University, Kathmandu, Nepal

**Corresponding author: id.dipikashah@gmail.com*

(Submission Date: 29 July 2024; Accepted Date: 5 September 2024)

ABSTRACT

Study of subsurface geology, aquifer system, thickness of hydro stratigraphic units, potential area based on transmissivity and yield, flow direction of groundwater of the western part of Banke District was carried out covering the area of 616.15 km². Lithological, hydrogeological and meteorological data maps, lithologs, static water level, precipitation, transmissivity, yield, springs etc. were carried out during desk study and field work. The study area consists of alluvial deposits of Pleistocene to Recent age derived from the Siwalik Hills and the mountains to the north and deposited by the Rapti River. Lithologically, the study area consists of clay, silt, sand and gravel. The cobbles, pebbles and somewhat boulders are also present. Geologically, the study area is located in Indo Gangetic Plain. The Indo Gangetic Plain is divided into Bhabar Zone and Terai Plain. Further the Terai Plain is divided into Middle Terai and Southern Terai. The Bhabar Zone is estimated of an area 68.83 km². Aquifers in the study area are confined types. The springs were found in the northern flat of the study area. Where the observed springs formed a line called spring line which is the southern boundary of Bhabar Zone and the base of Siwalik is northern boundary. The flow direction of ground water over the study area is towards the north.

Key word: ***Hydrogeology, Hydro stratigraphy, Transmissivity, Yield, Springs***

INTRODUCTION

Banke District, a part of Province No. 5, is one of the seventy seven districts of Nepal. It is located in Mid-western, Nepal with Nepalgunj as its district headquarter and lies between Longitude 81° 30' 0" to 81° 48' 30" and Latitude 28° 19' 0" and 27° 57' 0". There are three main cities in the Banke District: Nepalgunj, Kohalpur and Khajura Bajaar. The Hydrogeological study of western part of Banke District was carried out to know about the area of Bhabar Zone, Sub surface geology, Aquifer system, flow direction and potential area. The Rapti Nadi is the major river and its tributaries Amarai Khola, Amila Nala, Beha Nala, Chyama Khola, Dudawa Khola, Dondra Nala, Itahawa Nala, Jethan Nala, Jethi Nala, Kiran Nala, Man Khola, Murgiha Nala, Pendari Nala and Rohini Nala. The Stream network formed by these streams has an average density of one stream every 10 Km² in Banke (Gautam, 2005). The study area covers 616.15km² area and the population is 3,52,816 (CBS, 2017). Geologically, the study area is Indo Gangetic Plain. The Indo Gangetic Plain is divided into Bhabar Zone and Terai Zone. Further the Terai Zone is divided into Middle Terai and Southern Terai. The Bhabar Zone consists of coarser deposits such as gravel, cobble, and pebble. The Terai Zone consists of sand, gravel and high proportion of silt and clay. The study area is underlain by Churia group, Terrace deposits and Alluvium. The Alluvium

can be subdivided into three groups, Northern Alluium in the Bhabar Zone, Central Alluvium in the undulating plain and Gangetic Alluvium Plain in the southern strip (JICA, 1995). A spring line is usually seen to separate the northern Bhabar Zone from the southern Terai plain (Dhital, 2015). The outcrop area of Bhabar Zone is estimated at 120 km² in Banke area (Tillson, 1985), and is a principal recharge area for the ground water reservoir of the Banke Terai. The location map of the study area is shown in Fig. 1.

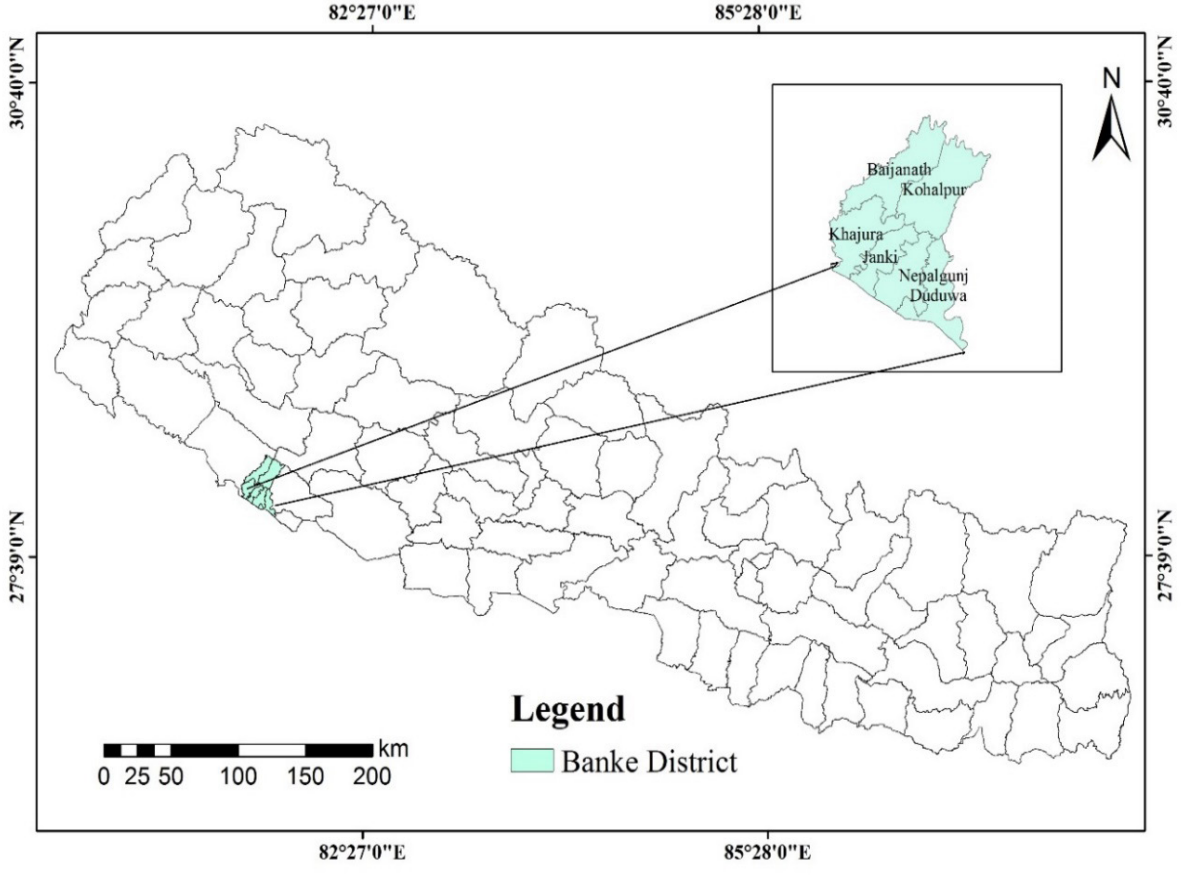

Fig. 1: Location map of Banke District of the study area.

Altogether seventy-four deep tube wells are located in the study area. The well at Chisapani is flowing. The well drilled up to depth 64 to 195.12 m which were constructed at Karkado, Nepalgunj, and K-Gaun, Sitapur-3 of Banke District. The location of deep tube well is shown in Fig. 2.

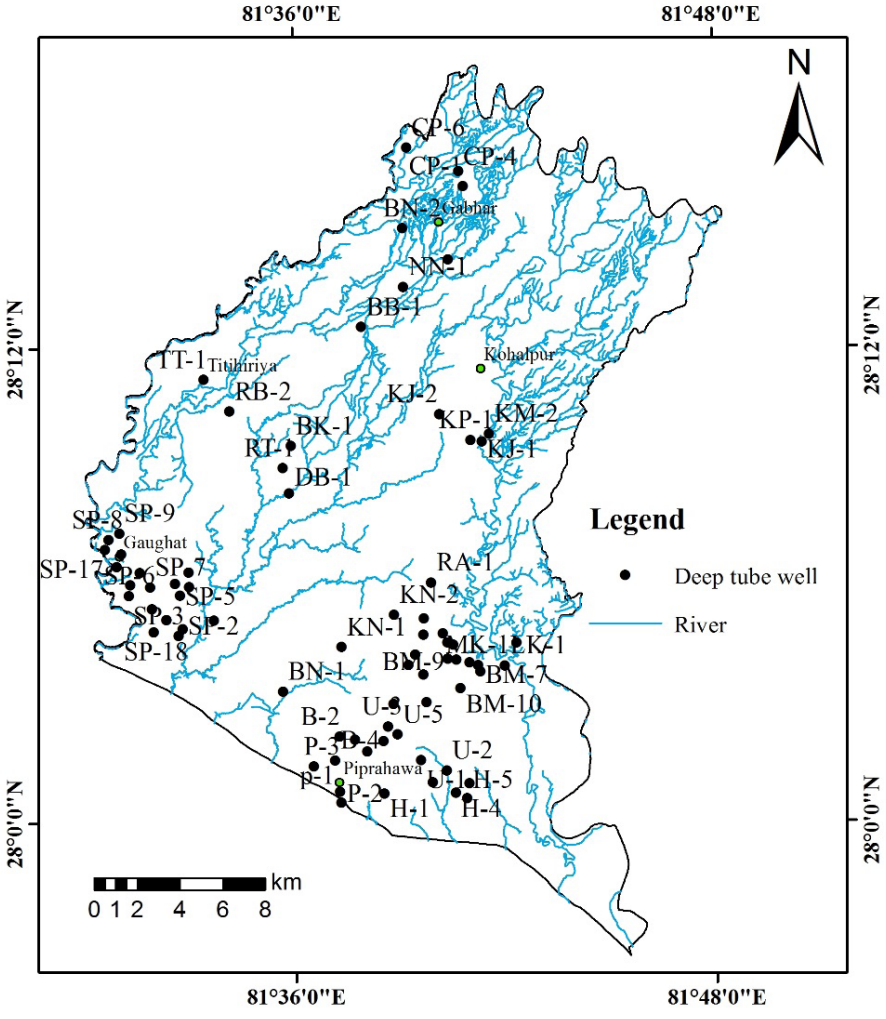

Fig. 2: Location of Deep Tube Well of the study area.

METHODOLOGY

The research is based partly on primary data and partly on secondary data. Collection of previous literature, topographical maps, geological maps, lithological data hydrogeological and meteorological data related to the study area was carried out during desk study. Hydrogeological database of the study area has been prepared in GIS and potential zones for groundwater exploitation have been delineated. Field investigation was carried out for collecting the detailed information on hydrogeological condition of the area. The GPS was used to obtain the coordinates of the observation points and topographical maps (1:25,000) were used as base map in the field. Altogether eight springs was observed during the field study. The observed springs are S1, S2, S3, S4, S5, S6, S7 and S8. The springs are contact spring. After joining all the spring, there observed a line called spring line in ArcGIS and finally the Bhabar Zone is delineated from the spring line. Total Seventy-four deep tube wells are located in the study area. The data obtained from the

pumping test was analyzed and different thematic layers of transmissivity and yield was prepared in the ArcGIS in order to delineate potential zones, flow movement of groundwater using static water level above mean sea level, geological map from observed lithological data and springs. Again, six section lines were drawn in ArcGIS and cross sections were plotted in Rockwork software in order to know hydrogeological conditions and hydro stratigraphical units with confined aquifers and confining layers. And finally, the fence diagram was drawn in order to know 3-D distribution of hydro stratigraphic units in the study area. The thickness maps of aquifer horizons are prepared in ArcGIS.

RESULTS AND DISCUSSION

Delineation of Bhabar Zone (Spring Inventory)

The springs are located at the elevation of 174 meter to 194 meter. Mostly the springs are found in forest area. Based on the deposits, the springs are located in alluvium deposits of rivers. The observed springs are tabulated below (Table 1).

Table 1: Location of springs in the study area.

S.N	Spring	Location	Elevation (m)	Deposit type	Spring type
1	S1	Geruwa khola ,Mehadewa Village	182	Alluvial deposit	Contact spring
2	S2	Rohini khola, Pipaltakur Village	191	Alluvial deposit	Contact spring
3	S3	Duduwa khola, Nayabasti Village	174	Alluvial deposit	Contact spring
4	S4	Duduwa khola, Ranighat Village	190	Alluvial deposit	Contact spring
5	S5	Itahawa Nala, Jumalibasti Village	194	Alluvial deposit	Contact spring
6	S6	Jethi Nala, Thakuritol Village	208	Alluvial deposit	Contact spring
7	S7	Jethi Nala, Daillichar Village	211	Alluvial deposit	Contact spring
8	S8	ManKhola, Jumalibasti Village	200	Alluvial deposit	Contact spring

All the spring observed in field (Table 1), formed a line called spring line which separates the Babar Zone from Terai Plain. The northern part consists of very coarse grain materials and southern part consists of fine grain materials. There exist lateral facies variation changes in the succession. Due to this lateral change of facies, there exist back pressuring of groundwater because of low permeability in southern part (Sah, 2015) and the spring is formed. The spring line also arises due to topographic gradient. Most of the river coming from the hills pass through the permeable zone of north and are found recharging aquifer in the northern part. Rivers which have few cusecs of water mostly vanish in summer while passing through the permeable zone and usually appear after the spring line (Sharma, 1981). The springs observed during field are contact spring. The map is prepared below (Fig. 3) on the basis of observed spring. For the Bhabar Zone delineation, the southern boundary is represented by spring line where as the southern boundary of Siwalik is considered as northern boundary. The area of Bhabar Zone is estimated at nearly 68.83 km^2.

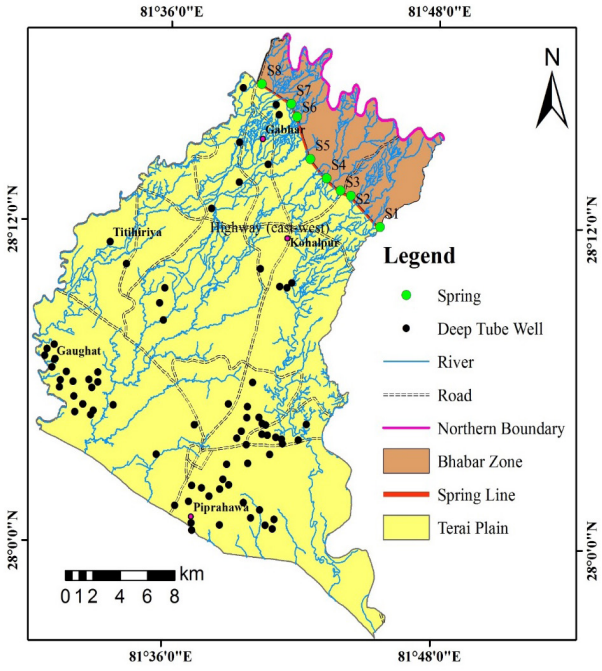

Fig. 3: Delineation of Bhabar Zone on the basis of spring line of the study area.

Groundwater movement and direction

The map (Fig. 4) based upon water level from msl that shows that general flow is towards southern part of the study area. There are two divides, one flow from the upper region north to south-west and another to south-east to the nearby river. It is due to controlled by topography.

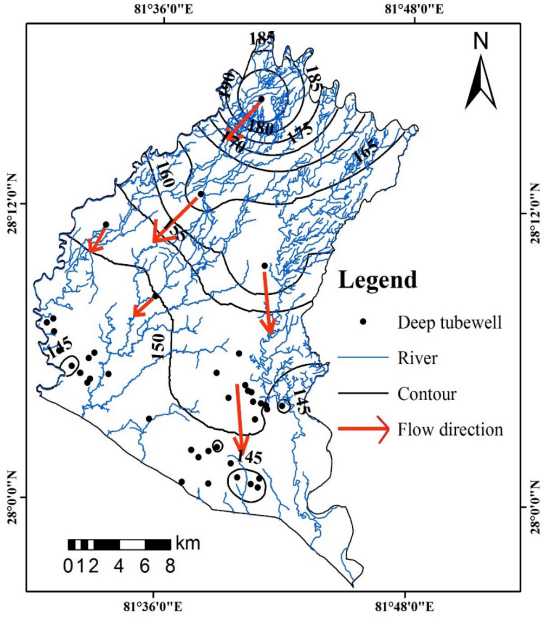

Fig. 4: Water level map above msl with flow direction (contour interval 5 m).

Hydrogeology and hydro stratigraphy of the study area

Sub-surface study was explained on the basis of lithologs of deep tube wells carried out in the study area. The lithologs up to depth 130 were taken for the study. These lithologs vividly gives the picture of sub surface hydrogeology. In modeling regional flow systems, aquifers and confining beds are defined using the concept of the hydro stratigraphic units (Maxey, 1964). Hydro stratigraphic units comprise geologic units of similar hydro geologic properties. Based on the lithologic descriptions contained in the water well records, a hydro stratigraphic model of the aquifer system was developed (Pathak, 2002). Altogether six lithological cross section were drawn (Fig. 5). The cross section is used to describe the subsurface hydrogeology, lithological variations and hydro stratigraphic units. It determines rather changing trend of sub surface sedimentation and flow region of ground water. The top soil is clay.

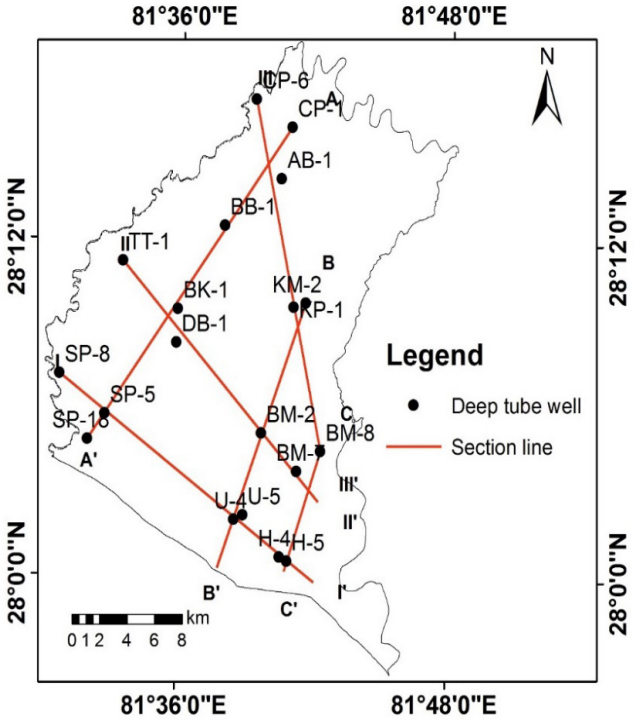

Fig. 5: Cross section lines in the study area.

Cross section A - A' along N-S direction

Cross section A-A' (Fig. 6) runs along north to south direction and includes the well located at Chisapani, Bankatwa, Budhanipur, Sitapur. Surface elevation of well varies from 193 to 144 m above mean sea level. This area consists of four confined aquifer which consists of gravel and some portion of sand in northern part as aquifer materials and in southern parts sand and some portion of gravel as aquifer materials. The aquifer are bounded both side by confining layer making confined. The fining southward succession is seen along the profile. The hydro stratigraphic units along this section are shown in Fig. 7.

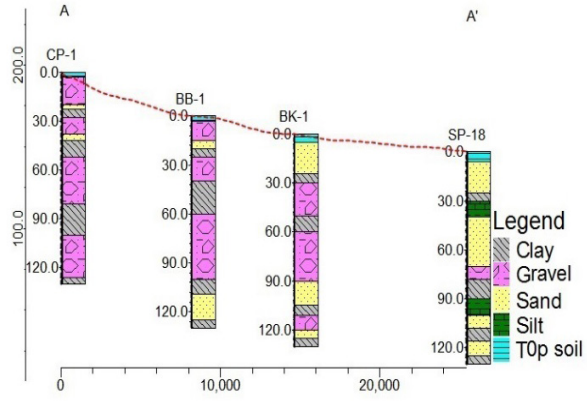

Fig. 6: Cross section along A-A' profile.

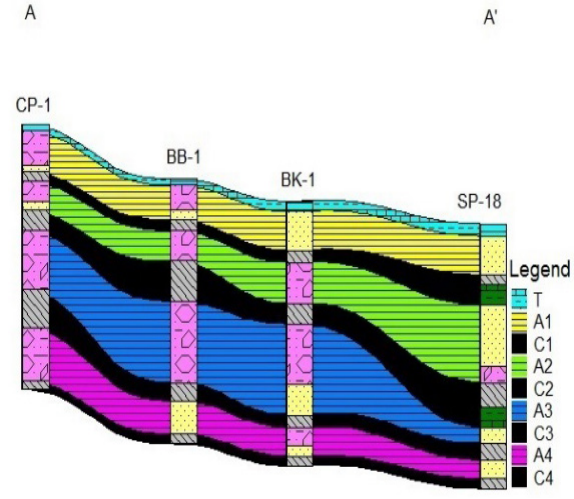

Fig. 7: Hydro stratigraphic units along A-A' profile.

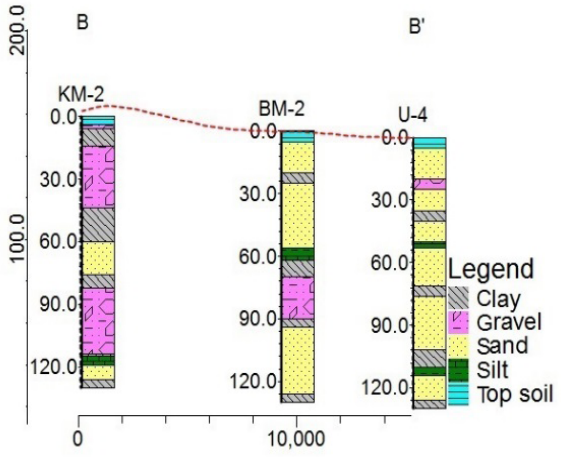

Fig. 8: Cross section along B-B' profile.

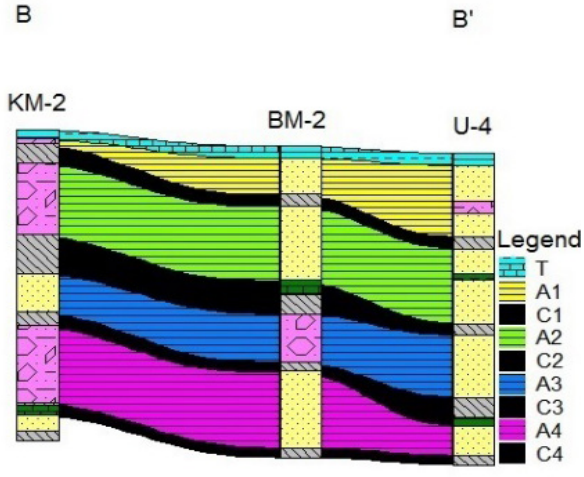

Fig. 9: Hydro stratigraphic units along B-B' profile.

Cross section B - B' along N-S direction

Cross section B-B' (Fig. 8) runs along north to south direction and includes the well located at Kohalpur, Mannpur, Banghusara, Basudevpur, Lodhegaon, Udaypur. Surface elevation of well varies from 159 to 149 m above mean sea level. The gravel and sand are the aquifer materials. More or less fining southward succession is seen along this section. The aerially extension of hydro stratigraphic unit were shown in Fig. 9.

Cross section C - C' along N-S direction

Cross section C-C' (Fig. 10) runs along north to south direction and includes the well located at Padampur, Kamdi, Dhittapurwa-111, Hirminya. Surface elevation of well varies from 151 to 145 m above mean sea level. The northern part consists of coarse sand and gravel whereas the southern part consists of fine sand and some gravels. Lenses of clay and silt are dominant at along this section. The aerial distribution of hydro stratigraphic units was shown in Fig. 11.

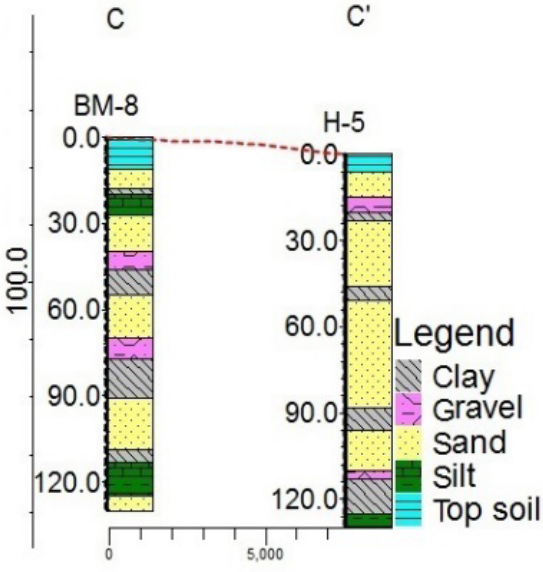

Fig. 10: Cross section along C-C' profile.

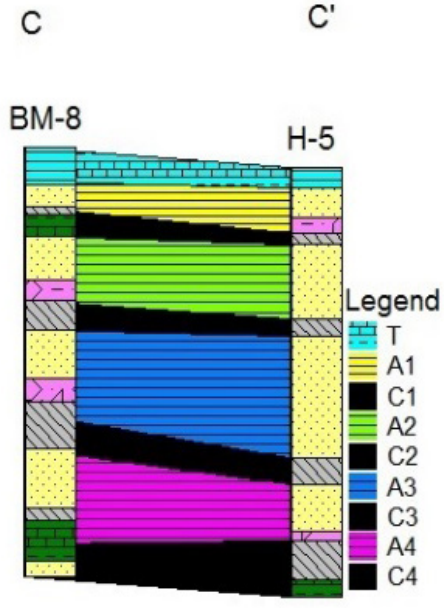

Fig. 11: Hydro stratigraphic units along C-C' profile.

Cross section I - I' along W-E direction

Cross section I-I' (Fig. 12) runs along west to east direction and includes the well located at Sitapur, Udaypur and Hirminya VDC. Surface elevation of wells ranges from 147 to 149 m above mean sea level. The section comprises of fine sand, silt and clay beds and also some amount of gravel. The silt and clay beds are dominant along this section line. The grain size distribution of aquifer material is almost same. The aerial distribution of hydro stratigraphic units is shown in Fig. 13.

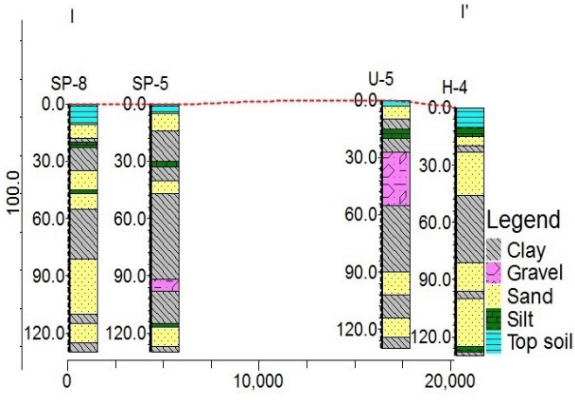

Fig. 12: Cross section along I-I' profile.

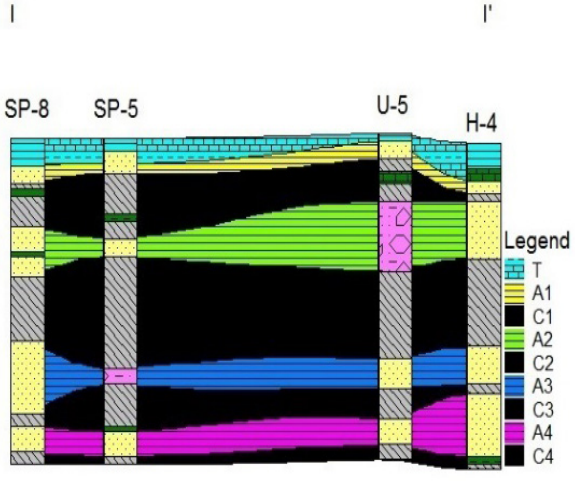

Fig. 13: Hydro stratigraphic units along I-I' profile.

Cross section II - II' along W-E direction

Cross section II-II' (Fig. 14) runs along west to east direction and includes the well located at Titaraiya, D-gaun, Sahapurwa and Basudevpur. Surface elevation of wells ranges from 149 to 154 m above mean sea level. The section comprises of fine sand, silt and Coarse sand and gravel. The silt and clay beds are dominant along this section line. The grain

size distribution of aquifer material is more or less same. The aerial distribution of hydro stratigraphic units was shown in Fig. 15.

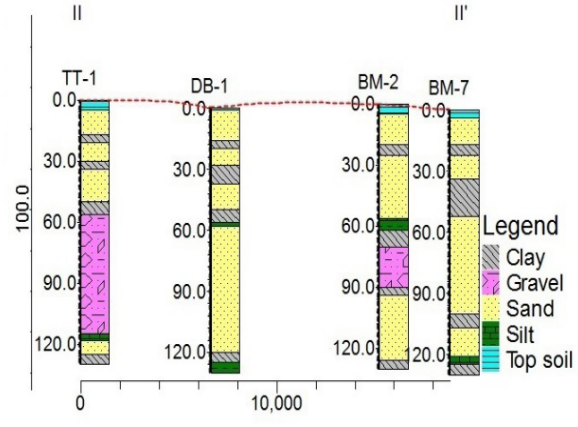

Fig. 14: Cross section along II-II' profile.

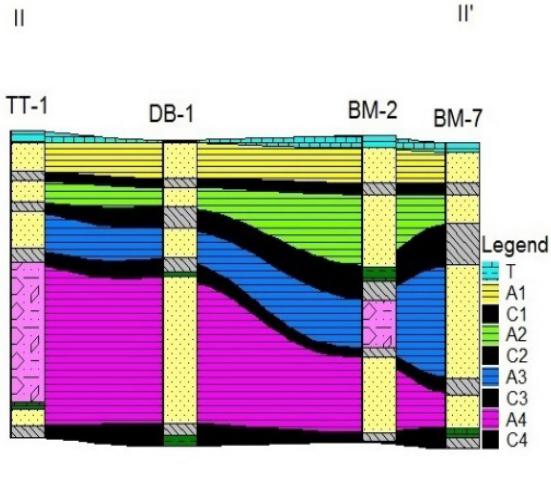

Fig. 15: Hydrostratigraphic units along II-II' profile.

Cross section III - III' along N-S direction

Cross section III-III' (Fig. 16) runs along north to south direction and includes the well located at Chisapani, Baniyabhar, Kohalpur Pipari, Basudevpur. Surface elevation of well varies from 184 to 151 m above mean sea level. Southward gradually fining of material is seen in the section. The section line is continued from almost northern part to middle of Southern part. The northern part consists of coarse sand and gravel whereas the southern part consists of finer sand little amount of coarser sand and gravel. Lenses of clay and silt were dominant at Southern part. The aerial distribution of hydro stratigraphic units was shown in Fig. 17.

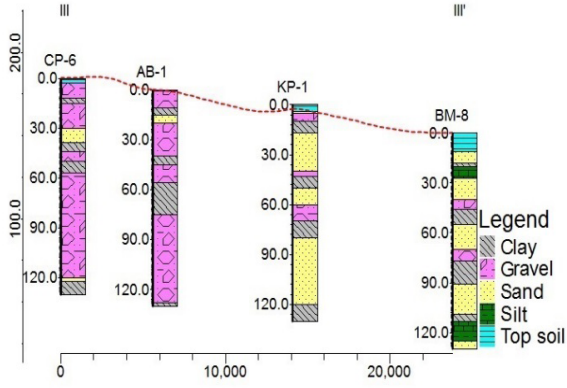

Fig. 16: Cross section along III-III' profile.

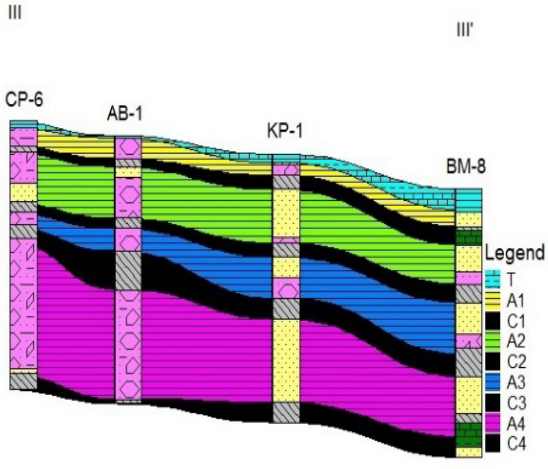

Fig. 17: : Hydro stratigraphic units along III-III' profile.

Fence diagram

It is 3- dimensional representation of lithology of selected area from lithologs of deep tube wells. It defines the hydro stratigraphy of the area. Around 16 wells with depth 130 occupying the study area were taken and the hydro-stratigraphic units were defined as 'C' confining layer and 'A' as aquifer. The different aquifers were given the name A1, A2, A3 and A4– confined aquifer. The

study area exists of four aquifers up to depth 130 m. The confined and unconfined aquifer exists all over the area. There was no well drilled in the Bhabar Zone so no well was taken during the section. The section lines (Fig. 18) and the distribution of hydro stratigraphic units overall study area is shown on the fence diagram (Fig. 19). The stratigraphic units give the information of flow system and distribution of aquifer all over the area. The confining layer (C) separates the aquifers. In these ways the different aquifers are distributed in the study area. The thickness of hydro stratigraphic units (A1, A2, A3 and A4) ranges from 2 to 30 m, 7 to 32 m, 6 to 48 m and 9 to 69 m. The thickness varies because sediments of fluviatile origin and with shifting nature of stream channels.

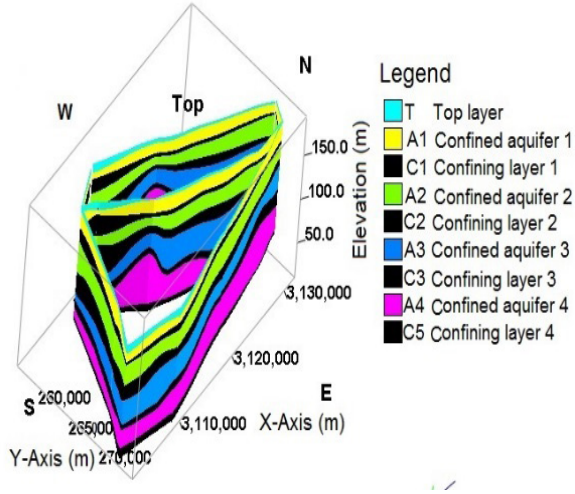

Fig. 19: Fence diagram showing various hydro stratigraphic units in the study area.

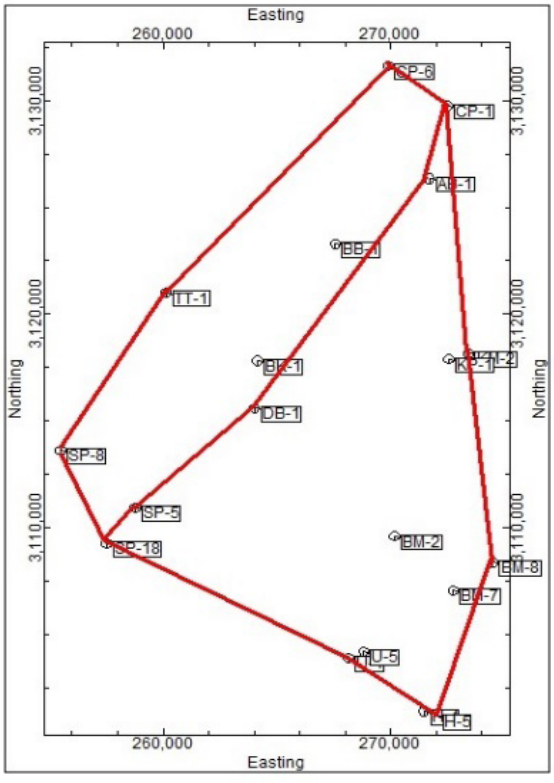

Fig. 18: Section lines to prepare the fence diagram.

Aquifer thickness of hydrostratigraphic units (A1, A2, A3 and A4)

a. Confined aquifer (A1): The aquifer thickness ranges between the 2-11.3 m (Fig. 20).

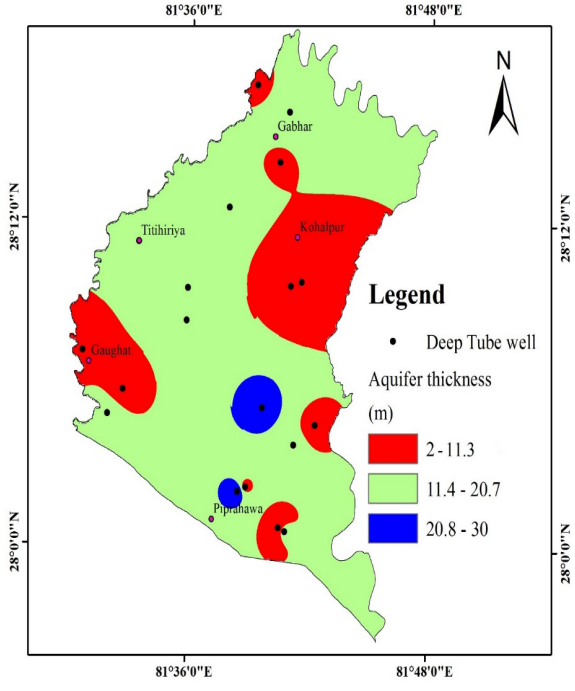

Fig. 20: Thickness map representing confined aquifer A1 of the study area.

b. Confined aquifer (A2): The aquifer thickness range between the 7-15.3 m (Fig. 21).

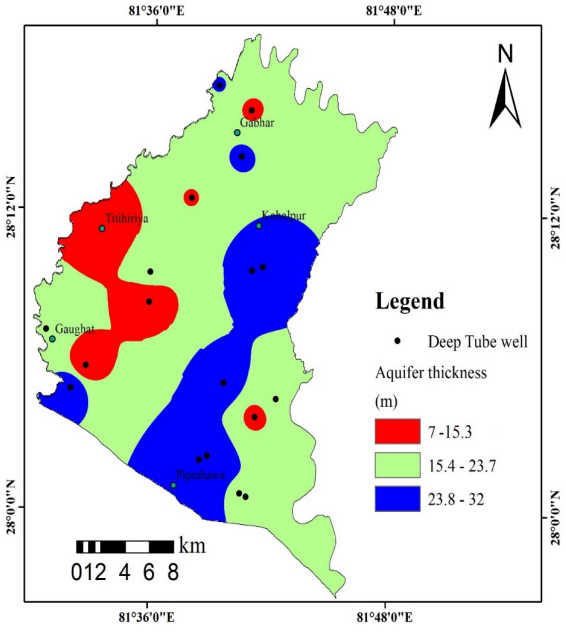

Fig. 21: Thickness map representing confined aquifer A2 of the study area.

c. Confined aquifer (A3): The aquifer thickness ranges between the 6-20 m (Fig. 22).

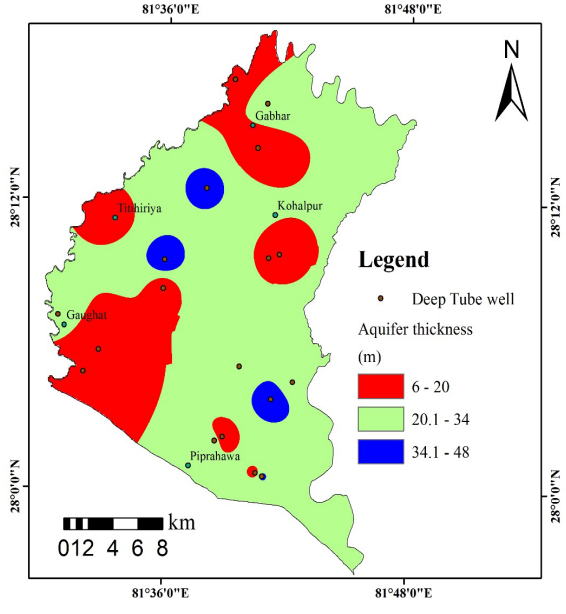

Fig. 22: Thickness map representing confined aquifer A3 of the study area.

d. d. Confined aquifer (A4): The aquifer thickness range between the 9-29 m (Fig. 23).

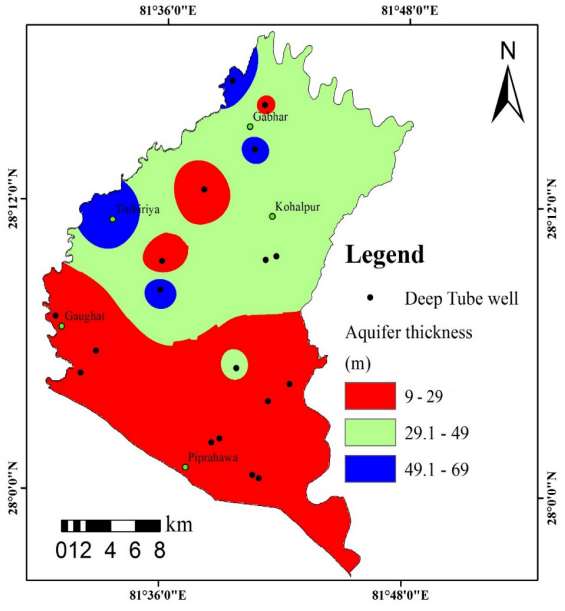

Fig. 23: Thickness map representing confined aquifer A4 of the study area.

Ground water potentiality

Quantitative interpretation of groundwater reservoirs is possible only when the values of hydraulic constants of aquifers are known. (Kumar, 2009) described that to access groundwater potential in any area, it is essential to know the aquifer parameters. They are influence by porosity, grain size, sorting and packing of aquifer materials. The transmissivity and yield data were available so that the analysis was done through these data.

The potential zone of the study area is prepared on the basis of transmissivity (Fig. 24) and yield (Fig. 25). Firstly, the raster map of transmissivity and yield were prepared and reclassify it and given a rank and weight (Table 2) and then the weighted sum were done and finally the potential map was prepared and the potential area were classified as low, medium and high (Fig. 26). Overall, the study area is potential for ground water exploration. Areas of fine-grained sediments have poor water

production like silt and coarse-grained sediments have higher potential like sand and gravel. It is because of coarser aquifer materials with high permeability and porosity. Overall, the study shows the ground water condition of deep aquifer meets to fulfill the water demand.

Table 2: Rank and weight given to transmissivity and yield.

Parameter	Rank	Weight
Transmissivity	1	50 %
	2	
	3	
Yield	1	50 %
	2	
	3	

Potential Zone on the basis of transmissivity and yield

Zone A (Low potential zone): The area covers L-Gaon, Phutaha, Kataliya, Banghusara, Amarahawa, Molahpurwa, Lolinpurwa, Sahapurwa, Jodhapurwa, Puraini, Birta, Hirminya, Parsanpur, Lodhegaon, Lalapurwa, Tankapaseri, Bhawaniyapur, Balegaon, Khajura and Ranjha.

Zone B (Medium potential zone): The area covers K-Gaon, L-Gaon, A-Gaon, Gaughat, Phutaha, Padampur, Naharpurwa, Loharanpurwa, Suryapur, Udaypur, Piparhawa, Babugaon, Kariyatipurwa, Bankatwa, Mahalpurwa, Belvhar, Baniyabhar, Lalapurwa, Jharkatti, Thakurpur, Gautambasti, Tithariya, Karkado, Karelokhola, Naubasta and Pitamari.

Zone C (High potential zone): The area covers Gaughat, L-Gaon, Dhittapur-1, Dhittapur-11, Dhittapur-111, Piparhawa, D-gaon, Raniyapur, Pipari, Mannapur, Gabar, Baniyabhar, Jhandahawa and Budhanipur.

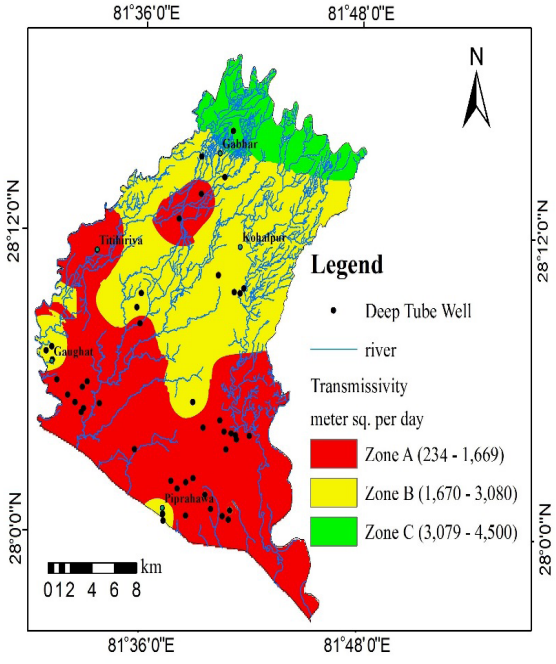

Fig. 24: Ground Water Potentiality Zone on the basis of Transmissivity (m²/day).

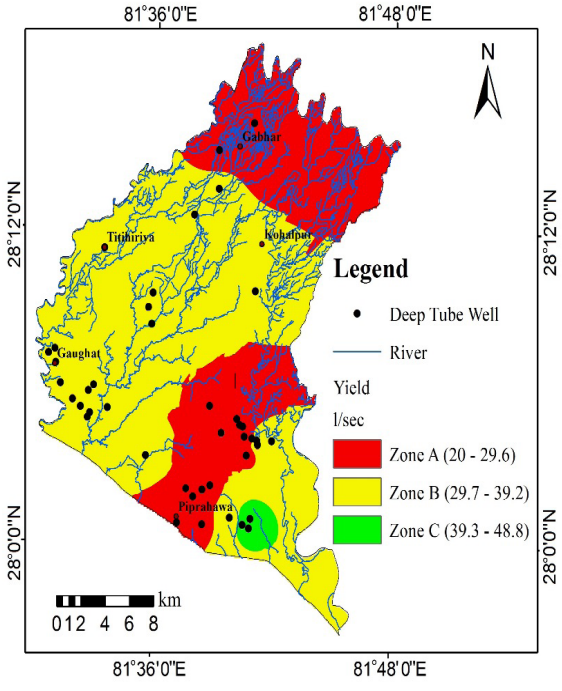

Fig. 25: Ground Water Potentiality Zone on the basis of yield (l/sec).

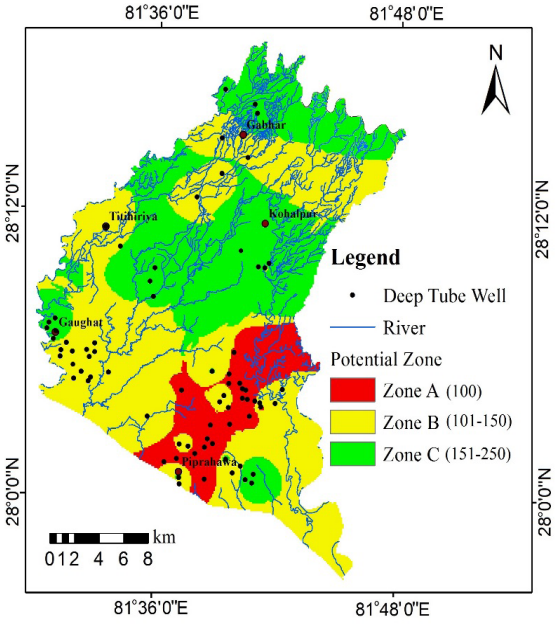

Fig. 26: Final potential zone of the study area on the basis of transmissivity and yield.

CONCLUSION

The Indo-Gangetic plain is divided into Bhabar Zone and Terai Plain. The Terai Plain is divided into Middle Terai and Southern Terai. The Bhabar Zone consists of coarser sediments like pebble, cobble, boulder, gravel whereas the Terai Plain consists of finer sediments like clay, silt, sand and some amount of gravel.

The Bhabar Zone is estimated of an area 68.83 km^2. The northern boundary of Bhabar Zone is base of Siwalik Range and southern boundary is spring line. The springs are contact type.

The ground water flows from north to south direction. There are two flow divides from north to south-east and north to south-west. Aquifers (Hydro stratigraphic units – A1, A2, A3 and A4) in the study area are confined types. The well of Chisapani is flowing well.

The three potential zones were divided on the basis of results obtained by yield and Transmissivity, Zone A as a low potential area, Zone B yield as a medium potential area and Zone C as a high potential area. The Zone A covers the area at covers L-gaon, Phutaha, Kataliya, Banghusara, Amarahawa, Molahpurwa, Lolinpurwa, Sahapurwa, Jodhapurwa, Puraini, Birta, Hirminya, Parsanpur, Lodhegaon, Lalapurwa, Tankapaseri, Bhawaniyapur, Balegaon, Khajura and Ranjha, Zone B covers at K-gaon, L-gaon, A-gaon, Gaughat, Phutaha, Padampur, Naharpurwa, Loharanpurwa, Suryapur, Udaypur, Piparhawa, Babugaon, Kariyatipurwa, Banktwa, Mahalpurwa, Belvhar, Baniyabhar, Lalapurwa, Jharkatti, Thakurpur, Gautambasti, Tithariya, Karkado, Karelokhola, Naubasta and Pitamari. Similarly, the Zone C covers at Gaughat, L-gaon, Dhittapur-1, Dhittapur-11, Dhittapur-111, Piparhawa, D-gaon, Raniyapur, Pipari, Mannapur, Gabar, Baniyabhar, Jhandahawa and Budhanipur.

RECOMMENDATION

a. At the periphery of study area, due to lack of enough data the result obtained may not be reliable to use for practical purpose. But it will serve for academic purposes. Detail study is recommended in this area.

b. The more detail study is needed for delineation of Bhabar Zone. The Bhabar Zone should be preserved because ground water recharge is high in this zone.

AUTHOR CONTRIBUTION

First, all the authors have made the study concept and design. Miss Rosni BC and Miss Dipika Shah started field works around four weeks to collect field data. Dr. Dinesh Pathak, Mr. Surrendra Raj Shrestha, Mr. Nir Shakya and Mr. Ramesh Gautam have analyzed, interpreted and finalize the data to bring the conclusion. The first draft was written by Dipika Shah and finally, all authors contributed to making final version of manuscript.

CONFLICT OF INTEREST

The authors declare no conflict of interests.

DATA AVAILABILITY STATEMENT

The data that supports the findings of this study are available from the corresponding authors, upon reasonable request.

REFERENCES

Central Bureau of Statistics (CBS), 2017. National Population and Housing Census 2011, Nepal. Government of Nepal, National Planning Commission Secretariat, (200-203).

Dhital, M.R., 2015. Geology of Nepal Himalaya: Regional perspective of the classical collided orogen. Springer International publishing, Switzerland. p. 498.

Gautam, B., 2005. Hydrogeological study in south-western part of the Banke District, Western Nepal. M.Sc Thesis, Central Department of Geology, Institute of Science and Technology, Tribhuvan University, Nepal.

JICA, 1995. The Master Plan on the Terai Groundwater Resources. Repot of Sanyu Consultants Incorporation, 2, (9-12).

Kumar, C.P., 2009. Aquifer Parameter Estimation, National Institute of Hydrology,

Roorkee, India, Education, Technology, Business. p. 2.

Maxey, G.B., 1964. Hydro stratigraphic units. Journal of Hydrogeology, 2, (124-129).

Pathak, D., 2002. Basement structure, hydrogeology and groundwater: flow model of Nara Basin, southwest Japan. PhD thesis, Osaka City University, Japan.p.129.

Sah, R.B., 2015. Stratigraphy of Nepal. Stratigraphic Association of Nepal (SAN), 10, (6-8).

Sharma, C.K., 1981. Ground Water Resources of Nepal. Published by Mani Ram Sharma, Bishalnagar, Nepal. (62-64).

Tillson, D., 1985. Hydrogeological Technical Assistance to the Agricultural Development Bank of Nepal. ADP-UNDP report.

Journal of Nepal Hydrogeological Association (JNHA), Vol (1), 57-66 (2024)
ISSN: 3059-9725 (Online)

RESEARCH ARTICLE

Temporal variability of seasonal and annual rainfall in Nepal

***Damodar Bagale**

Central Department of Hydrology and Meteorology, Tribhuvan University, Kathmandu, Nepal

**Correspondence author: damu.bagale@gmail.com*

***(Submission Date**: 20 July 2024; **Accepted Date:** 6 September 2024)*

ABSTRACT

This study analyzed 107 weather stations' 42-year rainfall data (1977-2018), using the normal ratio method to estimate missing rainfall from nearby stations. This study identified the mean winter, monsoon, and annual rainfall as 69.7 mm, 1433.2 mm, and 1791.5 mm respectively. The winter, monsoon, and annual rainfall have large temporal variability. Nepal received high rainfall from Jun to September (monsoon) and the rest of the eight months received low rainfall causing water scarcity in Nepal. This study examined the increase of rainfall with heights up to mid-mountain then the rainfall decreases with height in monsoon season. But in winter generally, the rainfall amount increases with height. However, rainfall totals both seasonal and annual have been decreasing since 2000 both nationally and regional-wise.

Keywords: ***Temporal, Variability, dry and wet episodes, Seasonal, Nepal***

INTRODUCTION

In South Asia, the monsoon is the major rainfall period. There is large-scale variability of rainfall such as; intra-seasonal, and inter-annual. According to Wang et al. (2020), interactions between the various Asian monsoon subsystems, mid-latitude processes, and tropical cyclones have a greater impact on the South Asian nation. Specifically, a large portion of the inter-annual variability of the Asian monsoon in the tropics is explained by the El Nino Southern Oscillation (ENSO) (Webster et al., 1998). However, such a relationship is nonstationary (Kumar et al., 1999). In India, monsoon rainfall fluctuation has depended on the ENSO conditions (Varikoiden et al., 2015). Numerous previous researchers (Varikoiden et al., 2015; Kumar et al., 2013; Krishnamurthy, and Gowashmi, 2000; Balme and Jadhav, 1984; Ramanadham et al., 1973) have examined the seasonal rainfall study in India. South Asian region receives relatively less rainfall during ENSO monsoon years (Kumar et al., 2013; Sein et al., 2015; Bagale et al., 2021).

In Nepal, rainfall is the primary water source, influenced by both local and large-scale climatic factors. The monsoon, which brings the majority of rainfall, occurs between June and September due to the southwest Indian monsoon (Bagale et al., 2023a). This monsoon approaches Nepal through southeasterly circulation, drawing moisture from the Bay of Bengal and sometimes the Arabian Sea (Bohlinger et al., 2017). Numerous studies have examined rainfall variability by previous researchers (Bagale et al., 2023a; Shrestha et al., 2019; Karki et al., 2017; Sigdel and Ikeda, 2012; Ichiyanagi et al., 2007; Kanskar et al., 2004).

Bagale et al. (2023a) analyzed data from 107 stations across Nepal from 1977 to 2018, highlighting significant variability in monsoonal rainfall and identifying both deficit and wet episodes. Ichiyanagi et al. (2007) examined seasonal and annual rainfall variability, noting an altitudinal dependency, with enhanced monsoon rainfall up to 2000 m, and a decline at higher altitudes. Karki et al. (2017) found that the eastern region of Nepal experiences more frequent decreases in seasonal and annual rainfall trends compared to the western region. Shrestha et al. (2019) analyzed rainfall data from 43 stations between 1981 and 2015, revealing a declining annual rainfall trend in the Kaligandaki and Koshi river basins. Panthi et al. (2015) observed a reduction in pre-monsoon, post-monsoon, and winter rainfall in most zones, although the Gandaki River basin in central Nepal saw an increase in monsoon rainfall. These findings provide crucial insights into Nepal's shifting rainfall patterns. Most of the previous studies have examined the east-to-west variability; there is still lacking gradient-wise (Terai, mountain, and Himalayas) rainfall studies in recent decades. The main objective of this study is an identify lowland, midland, and highland-wise rainfall variability in Nepal.

Study Area

Nepal is a landlocked, mountainous nation. China's Highland Tibet is located on the side facing north, and India is on the side south. Its latitude ranges from 26° 22' to 30° 27' N and its longitude ranges from 80° 04' to 88° 12'E (Fig. 1).

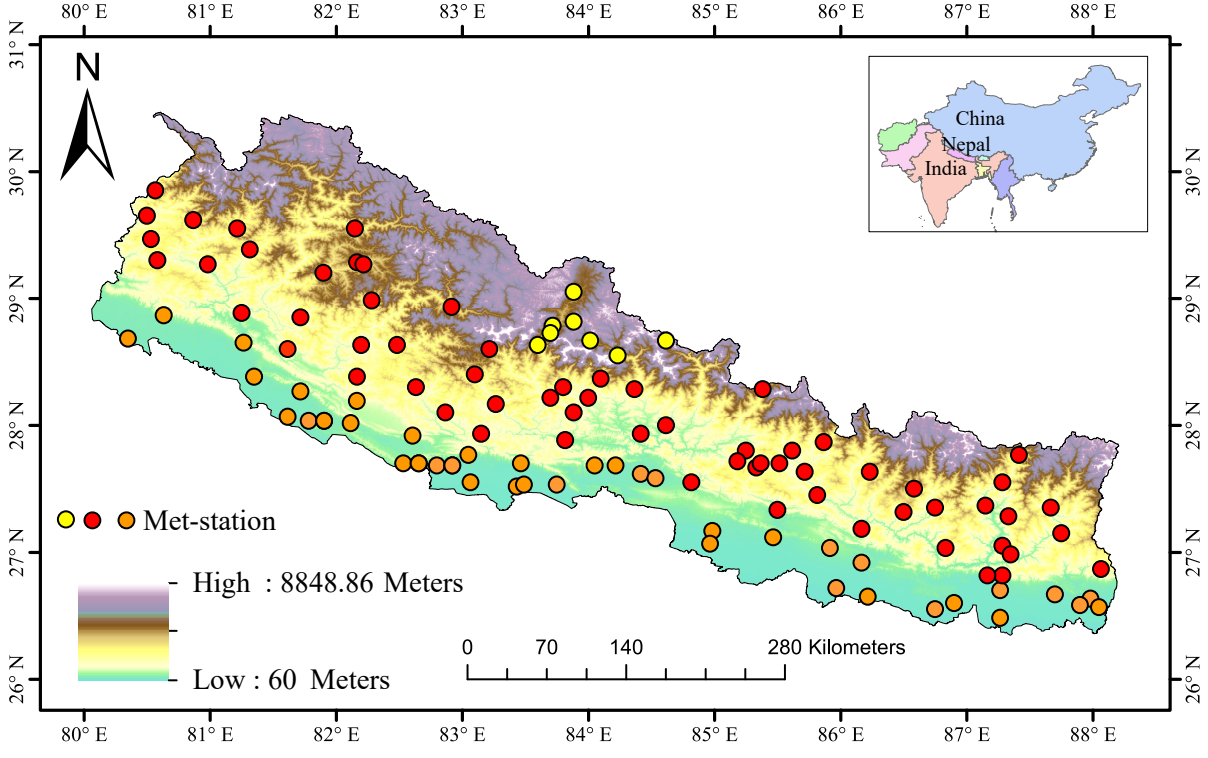

Fig. 1: Spatial distributions of stations over the Himalayas (yellow), midlands (red), and lowlands (orange) in Nepal.

Nepal has a varied terrain that runs from the low Terai area in the south, which is only 60 meters above sea level, to the high Mount Everest region in the north, which is 8848.86 meters above sea level. The nation has an area of 147516 km2 (Fig. 1). We have used 40, 59, and 8 stations for the Terai, Mountain, and Himalayas [lowland (L), midland (M), and highland (H)] of Nepal.

METHODOLOGY

Data (methods of data collection)

The Department of Hydrology and Meteorology, Government of Nepal, provided daily rainfall data from 107 meteorological stations covering 1977–2018. Monthly total rainfall was calculated by summing daily rainfall, and annual totals were obtained by summing monthly data. Seasonal rainfall was also computed for the summer monsoon (June–September) and winter (December–February). The arithmetic mean method was applied to calculate the annual, seasonal, and monthly averages for each station. Furthermore, rainfall data selection and management detail procedures are followed (Bagale et al., 2023a). Missing rainfall values were estimated using the Normal ratio method (Myrondis, D and Nikolaos, T., 2021; Bagale et al., 2023b).

RESULTS

Rainfall statics

Using time series data from 107 stations, the annual profile of monthly and seasonal total rainfall has been computed, located in the Terai, Mountain, and Himalayas [lowland (L), midland (M), and highland (H)] of Nepal (Fig. 2b). We have used 40, 59, and 8 stations for LMH-wise study (Fig. 2a). There is high amplitude variation of intra-annual rainfall. In December, January, and February, highlands and midlands observed higher rainfall than lowlands. In April, May, June, July, September, and October low land received more rainfall than midland and highland in Nepal. In March highlands observed more rainfall than mid and lowlands. In August and November, midlands received more rainfall than highlands and lowlands. The rainfall of Nepal is observed to increase from January up to July maximum and decrease toward November minimum (Fig. 2a).

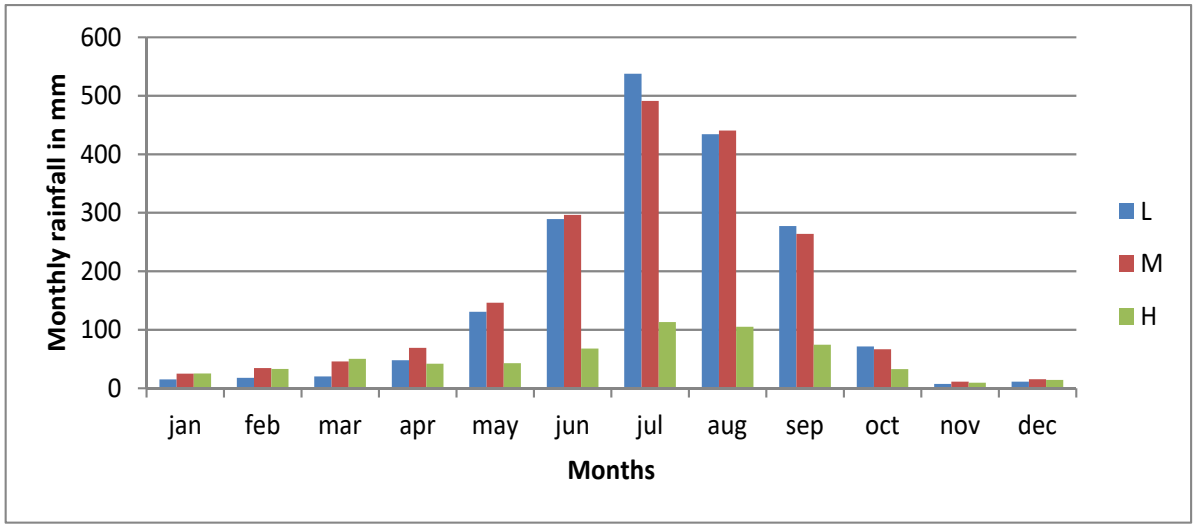

Fig. 2a: The average monthly rainfall figures showed fluctuation from 1977 to 2018.

Midland observed more rainfall than the lowlands and highlands annually (Fig.2b). In pre-monsoon and post-monsoon show similar rainfall patterns only the amount is different. Generally, the midland of Nepal received heavier rainfall than the lowland and highlands. Compared to mountainous and lowland areas, the Himalayan region received little rainfall during the pre-monsoon, monsoon, and post-monsoon seasons but received high rainfall in the winter season..

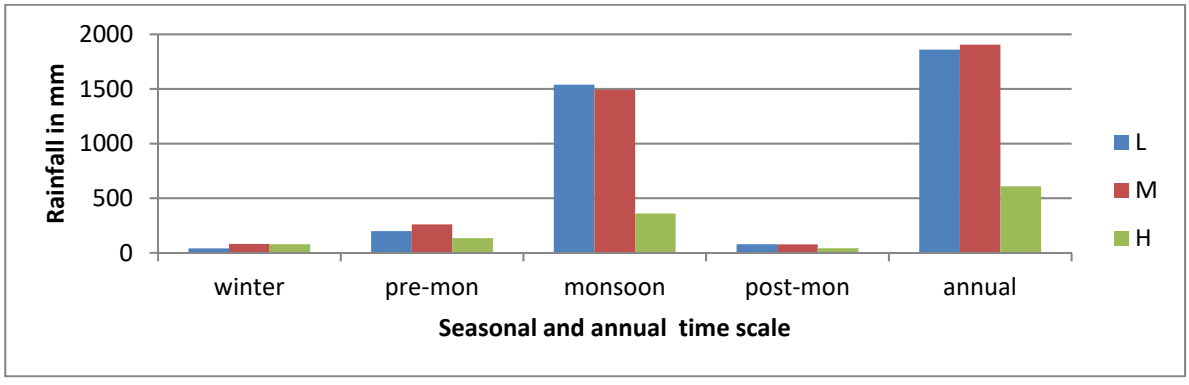

Fig. 2b: The average seasonal and annual rainfall figures from 1977 to 2018 in different regions lowland, midland, and highland (LMH) of Nepal.

Table 1: Regional and national rainfall statistics

Time scales	National	Lowlands	Midlands	Highlands
Winter	70.34	40.83	81.53	79.13
Pre-monsoon	228.36	198.64	260.66	134.69
Monsoon	1425.16	1538.32	1491.74	359.94
Post-monsoon	75.24	78.41	77.59	41.72
Annual	1791.52	1858.89	1904.34	608.49

Table 1 shows that the highlands had less total annual rainfall, it received more rainfall in the winter than other regions. From the lowlands to the midlands, there is an annual rise in rainfall. However, midlands regions in the central region had pockets of heavy rainfall. Pre- and post-monsoon rainfall levels in Nepal rise from the lowlands to the midlands but are negligible in the high-mountain regions.

Spatial distribution of annual rainfall

Annual rainfall in Nepal shows significant spatial variation, with rainfall decreasing from the eastern-central to the western regions (Fig. 3b). However, high mountainous areas of central Nepal receive more rainfall than other regions. Rainfall ranges from less than 200 mm in the lower Himalayan areas to over 4000 mm in central Nepal, highlighting the strong influence of topography on rainfall patterns across the country. Rainfall is somewhat heavy on the windward side of the region and very light on the leeward side. Because orographic forces predominate, the country's highest rainfall was recorded up to the midlands, after which it gradually dropped. The annual cycle of monthly rainfall is lowest in November and highest in July (Fig. 3a).

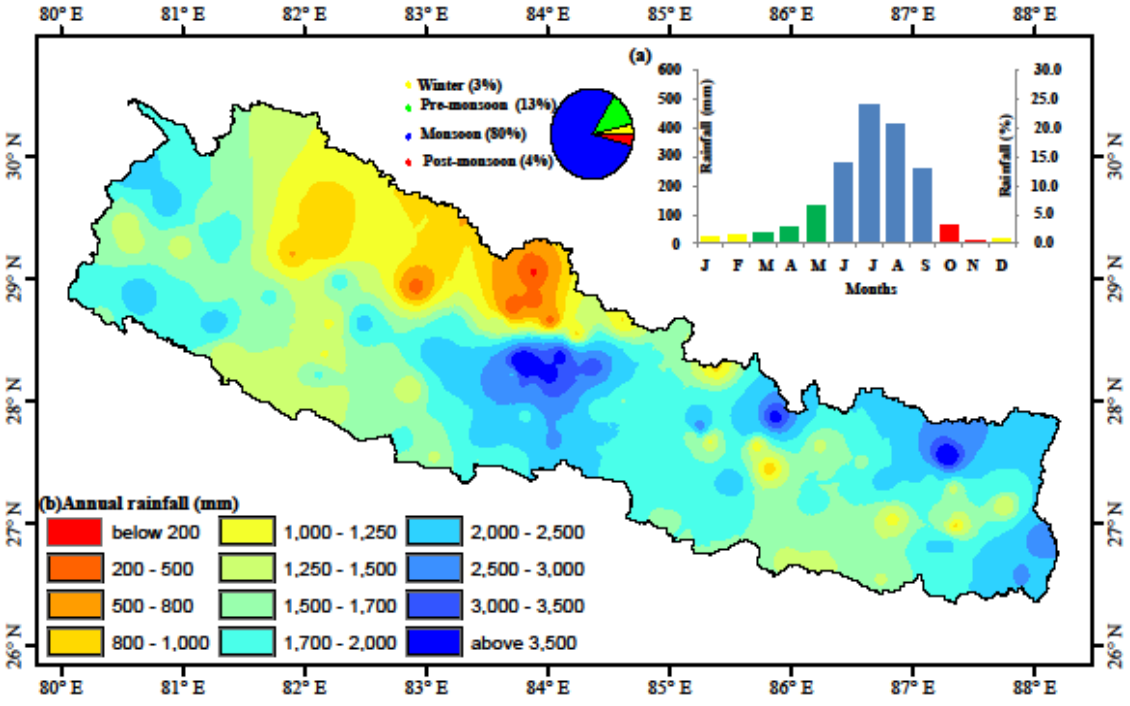

Fig. 3: Spatial variability of the average annual rainfall over Nepal from 1977 to 2018, along with the variability of the average monthly rainfall cycle from 1977 to 2018, and represented as a pie chart with the seasonal quantity of rainfall (%).

The monsoon season, from June to September, brings the majority of rainfall, with around 80% falling during this period of intense rainfall. The rest is distributed as follows: 3% during the pre-monsoon, 13% in the post-monsoon, and 3% in the winter (Fig 3a).

Temporal Rainfall Variability in Nepal

This study used rainfall data from 107 stations to analyze the temporal variation in rainfall. According to long-term climatology, Nepal receives 1791.52 mm of rain on average annually between 1977 and 2018. A significant inter-annual fluctuation occurs across the research periods. The statistical study indicates that during annual intervals, there is a temporal variability between the minimum rainfall in 1992 and the maximum in 1986.

The average rainfall data from 107 sites was used in this study to generate the temporal variability of seasonal rainfall. The long-term climatology from 1977 to 2018 showed that Nepal's average seasonal rainfall was 1433.42 mm for the monsoon season and 69.67 mm for the winter season. Similarly, long-term climatology indicates that Nepal receives 1791.52 mm of rainfall on average annually. The summer and winter seasons differ greatly from one another. According to the statistical analysis, there are 19 seasons with monsoon rainfall below the mean and 23 seasons with above-average rainfall (Fig. 4a). Similarly, Fig. 4b shows the variability of winter rainfall.

`

The temporal variability of rainfall throughout the monsoon season ranges from minimums in 1992 to maximums in 1986. Since the monsoon rains predominate in Nepal each year, a similar pattern of

rainfall was seen there as well. Comparably, it was shown that the variability of winter rainfall peaked in 1989 and decreased to a minimum in 2006. This study identified a significant rainfall deficit/excess during the monsoon and winter seasons over the last 42 years, as seen in Fig. 4(a, b)

.

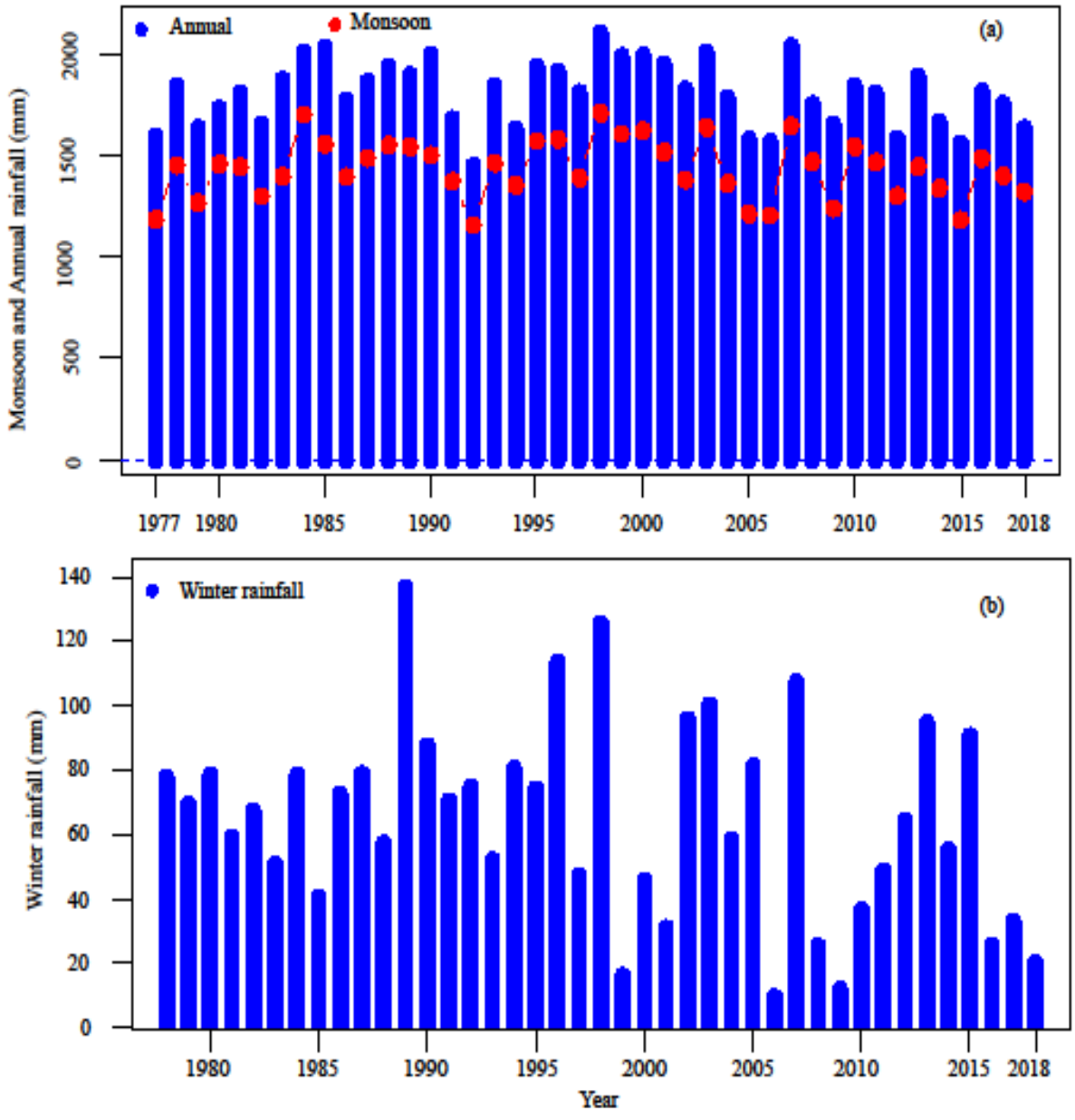

Fig. 4 Temporal variability of seasonal (winter and summer) and annual rainfall over Nepal averaged from 107 stations. The time series of seasonal and annual rainfall averaged over different regions from 1977 to 2018

During the seasonal and annual time scales there was a large variability of rainfall in deficit to excess episodes is clearly shown in Fig. 4a, and b.

LMH-wise temporal variations of winter, summer, and annual rainfall

Time series of seasonal and annual rainfall averaged over Nepal from 1977 to 2018 from monthly precipitation data of 107 stations in different regions. Out of 107 stations; we used 8, 59, and 40 stations for the Himalayas, Mountainous, and Terai regions for seasonal and annual rainfall analysis. The temporal variability of rainfall of different regions; winter, summer, and annual rainfall depicted in [Fig. 5 (a, b, c)]. Similarly, during the study period, the average seasonal and annual rainfall received in different regions are tabulated in Table 2.

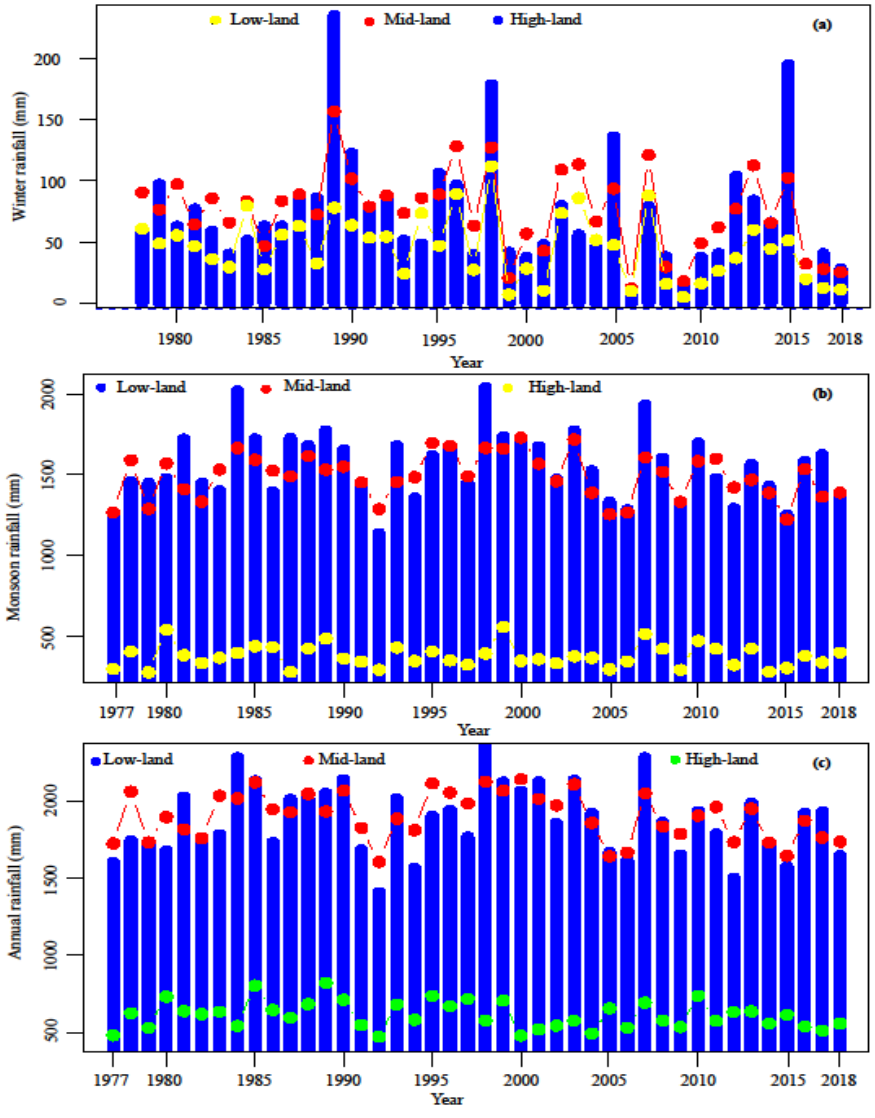

Fig. 5: Temporal variability of seasonal (winter, summer) and annual rainfall over the Himalayas, midlands, and lowlands of Nepal averaged from 8, 59, and 40 stations. The time series of seasonal and annual rainfall averaged over different regions from 1977 to 2018.

Table 3: Average rainfall of 1977-2018 for different regions and different time scales.

Regions	Winter	Summer	Annual
High-lands	79.12	359.94	608.49
Mid-lands	81.53	1491.74	1904.34
Low-lands	40.83	1538.32	1958.90

During the winter, summer, and annual seasons, there was a large variability of rainfall in deficit to excess episodes for the different regions only the magnitude is different in Fig. (5a, b, and c). The average winter, summer, and annual time steps season rainfall observed in highlands, midlands, and lowlands (Table 2). The temporal variability of low-lands, mid-lands, and high-lands rainfall was observed in (Fig. 4) and Table 3.

The highlands received a lower amount of total rainfall than the midlands and lowlands. The lowlands and midlands of Nepal observed neck-to-neck rainfall in comparisons between them. On average between them a little bit more in the lowlands. There is more rainfall fluctuation in the lowlands of Nepal. Lowlands received the maximum rainfall in 1999 and the minimum in 1992. Highlands received maximum precipitation in 1986 and minimum received in 1997. The midland observed more rainfall in 1986 followed by 1996. During the winter and summer seasons there was a large variability of rainfall in deficit episodes to excess episodes for the different regions only the magnitude is different Fig. (5a, b, c). During the winter and summer seasons, there was a large variability of rainfall in deficit episodes to excess episodes for the different regions only the magnitude is different in Fig. (5a, b)
.

Discussion

The monsoon is the primary source of rainfall, accounting for approximately 80% of total rainfall during the monsoon season. Pre-monsoon rainfall is 13%, post-monsoon rainfall is 4%, and winter rainfall is 3%, as illustrated in Fig. 2(a). This study's findings are similar to previous research results (Karki et al., 2015; Kansakar et al., 2004) identified monsoons accumulate around 80% of annual rainfall totals.
Ichiyanagi et al. (2007) have noticed that rainfall increased from low land to high land up to 2000 m and normally rainfall totals decrease at higher elevations > 2000 m (especially in lesser Himalayas). The present study's findings resembled with above-mentioned researchers' findings decrease in rainfall in higher altitudes.

Total annual rainfall is very low in the Himalayas (Ichiyanagi et al., 2007; Bagale et al., 2023a). The region is dominated Indian monsoon system only the magnitude is variable. Compared to the Terai and Mountainous regions, the Himalayan region experienced greater rainfall during the winter months but less during other periods.

Rainfall variability in Nepal is highly unpredictable across different time scales, from intra-seasonal to decadal (Karki et al., 2017; Ichiyanagi et al., 2007; Bagale et al., 2023a). This study identified low and high rainfall patterns (Fig. 4a, b, c), with findings aligning with previous research. The results also match studies in India (Vorikoedal et al., 2015) and Bangladesh (Ahasan et al., 2010), supporting similar results.

The rainfall analysis identified that the monsoon rainfall decreased more than the winter rainfall in Nepal after 2000 the decreasing monsoon is more than winter. Similar results were presented by previous researchers in neighboring countries in India (Kumar et al., 2013). Similarly, Choudhary et al. (2003) noticed monsoon rainfall observed decreasing in Bangladesh
.

Conclusion

This study analyzed rainfall data from 107 stations in Nepal between 1977 and 2018. It focused on the temporal variability of rainfall, examining variations across different time scales, including intra-seasonal, intra-annual, and inter-annual periods. The study has focused on the past four decades' overall rainfall patterns, dry and wet rainfall, and rainfall characteristics. Nepal has received high rainfall in the June to September months and the rest of the months received low rainfall causing water scarcity in Nepal. The highlands of Nepal have received low rainfall. The monsoon precipitation dominates the annual rainfall due to heavy monsoon rainfall. The monsoon and winter rainfall have large temporal variability during the study periods. However, rainfall totals both seasonal and annual have been decreasing since 2000. Furthermore, the average seasonal and annual rainfall received in Nepal was 63.97 mm/winter, 1422.42 mm/monsoon, and 1791.52 mm/annual respectively during the periods 1977-2018.

Acknowledgments

The Department of Hydrology and Meteorology (DHM) of Nepal is acknowledged for providing data from rain gauge observations.

References

Ahasan, M. N., Chowdhary, M. A. and Quadir, D. A., 2010. Variability and Trends of Summer Monsoon Rainfall Over Bangladesh. Journal of Hydrology and Meteorology, 7(1): 1-17. https://doi.org/10.3126/jhm.v7i1.5612

Bagale, D., Sigdel, M. and Aryal, D., 2021. Drought Monitoring Over Nepal for the Last Four Decades and its Connection With Southern Oscillation Index. Water, 13: 3411. https://doi.org/10.3390/w13233411

Bagale, D., Sigdel, M. and Aryal, D., 2023. Influence of Southern Oscillation Index on Rainfall Variability in Nepal During Large Deficient Monsoon Years. Journal of Institute of Science and Technology, 28(1): 11-24. https://doi.org/10.3126/jist.v28i1.43452

Bagale, D., Devkota, L., Adhikari, T. and Aryal, D., 2023. Spatio-Temporal Variability of Rainfall over Kathmandu Valley of Nepal. Journal of Hydrology and Meteorology, 11(2): https://doi.org/10.3126/jhm.v11i1.59661

Bohlinger, P., Sorteberg, A. and Sodemann, H., 2017. Synoptic Conditions and Moisture Sources Actuating Extreme Precipitation in Nepal. Journal of Geophysical Research: Atmospheres, 122: 12,653-12,671. https://doi.org/10.1002/1017JDO27543

Bhalme, H. and Jadhav, S., 1984. The Southern Oscillation and its relation to the monsoon rainfall. Journal of Climatology, 4, 509-520.

Chowdhury, M. R., 2003. The El Niño-southern oscillation (ENSO) and Seasonal Flooding–Bangladesh. Theoretical and Applied Climatology, 76: 105-124. https://doi.org/10.1007/s00704-003-0001-z

Ichiyanagi, K., Yamanaka, M. D., Muraji, Y. and Vaidya, B. K., 2007. Precipitation in Nepal Between 1987 and 1996. Int. J. Climatol., 27: 1753-1762. doi:10 :1002/joc.1492

Karki, R., Hasson, S. U., Schickhoff, U., Scholten, T. and Böhner, J., 2017. Rising Precipitation Extremes Across Nepal. Climate, 5: 4. https://doi.org/10.3390/cli5010004

Kumar, K. K., Rajagopalan, B. and Cane, M. A., 1999. On the Weakening Relationship Between the Indian Monsoon and ENSO. Science, 284: 2156-2159. https://doi.org/10.1126/science.284.5423.2156

Kumar, K. N., Rajeevan, M., Pai, D., Srivastava, A. and Preethi, B., 2013. On the Observed Variability of Monsoon Droughts Over India. Weather and Climate Extremes, 1: 42-50. https://doi.org/10.1016/j.wace.2013.07.006

Kansakar, S. R., Hannah, D. M., Gerrard, J. and Rees, G., 2004. Spatial Pattern in the

Precipitation Regime of Nepal. International Journal of Climatology: A Journal of the Royal Meteorological Society, 24: 1645-1659. https://doi.org/10.1002/joc.1098

Krishnamurthy, V. and Goswami, B. N., 2000. Indian monsoon-ENSO relationship on interdecadal timescale. Journal of Climate, 13(3), 579–595. https://doi.org/10.1175/1520-0442(2000)013<0579:IMEROI>2.0.CO;2

Myronidis, D. and Nikolaos, T., 2021. Changes in Climatic Patterns and Tourism and Their Concomitant Effect on Drinking Water Transfers into the Region of South Aegean, Greece. Stochastic Environmental Research and Risk Assessment, 35(9): 1725-1739. https://doi.org/10.1007/s00477-021-02015-y

Panthi, J., Dahal, P., Shrestha, M. L., Aryal, S., Krakauer, N. Y., Pradhanang, S. M., Lakhankar, T., Jha, A. K., Sharma, M. and Karki, R., 2015. Spatial and Temporal Variability of Rainfall in the Gandaki River Basin of Nepal Himalaya. Climate, 3: 210-226. https://doi.org/10.3390/cli3010210

Ramanadham, R., Visweswara Rao, P. and Patnaik, J. K., 1973. Break in the Indian summer monsoon. Pure and Applied Geophysics PAGEOPH, 104(1), 635–647. https://doi.org/10.1007/BF00875908

Shrestha, S., Yao, T., Kattel, D. B. and Devkota, L. P., 2019. Precipitation Characteristics of Two Complex Mountain River Basins on the Southern Slopes of the Central Himalayas. Theoretical and Applied Climatology, 138(1-2): 1159-1178. https://doi.org/10.1007/s00704-019-02897-7

Sigdel, M. and Ikeda, M., 2012. Summer Monsoon Rainfall Over Nepal Related With Large-Scale Atmospheric Circulations. J Earth Sci Clim Change, 3: 112. https://doi.org/10.4172/2157-7617.1000112

Sein, Z. M. M., Ogwang, B., Ongoma, V., Ogou, F. K. and Batebana, K., 2015. Inter-Annual Variability of May-October Rainfall Over Myanmar in Relation to IOD and ENSO. Journal of Environmental and Agricultural Sciences, 4: 28-36.

Varikoden, H., Revadekar, J., Choudhary, Y. and Preethi, B., 2015. Droughts of Indian Summer Monsoon Associated with El Niño and NonEl Niño years. International Journal of Climatology, 35: 1916-1925. https://doi.org/10.1002/joc.4097

Wang, B., Luo, X. and Liu, J., 2020. How robust is the Asian precipitation-ENSO relationship during the industrial warming period (1901-2017)? Journal of Climate, 33(7), 2779–2792. https://doi.org/10.1175/JCLI-D-19-0630.1

Webster, P. J., Magaña, V. O., Palmer, T. N., Shukla, J., Tomas, R. A., Yanai, M. and Yasunari, T., 1998. Monsoons: processes, predictability, and the prospects for prediction. Journal of Geophysical Research: Oceans, 103(C7), 14451–14510. https://doi.org/10.1029/97jc02719

Journal of Nepal Hydrogeological Association (JNHA), Vol (1), 67-78 (2024)
ISSN: 3059-9725 (Online)

RESEARCH ARTICLE

Hydrological influences of the landslide mechanisms: insight into the Aakhu Khola Watershed, Dhading District, Nepal

Achyut Timalsina[1] and *Bharat Prasad Bhandari[1,2]

[1]College of Applied Science, Tribhuvan University, Kathmandu, Nepal

[2]Central Department of Environmental Science, Tribhuvan University, Kathmandu, Nepal

[*]Corresponding author: bbhandari@cdes.edu.np

***(Submission Date**: 3 July 2024; **Accepted Date:** 6 August 2024)*

ABSTRACT

This study aims to determine the role of hydrological factors that influence landslides in the Aakhu Khola watershed in Dhading District, Nepal. The effort commenced by using satellite imagery and ArcGIS to create a spatial and temporal landslide inventory map. The four hydrological factors map was created using a 12.5 m digital elevation model, and a rainfall map was prepared using IDW interpolation of ten years of rainfall. The pixel size of the factors' subclasses and the pixel size of landslides within the subclasses were determined. The activity state landslide inventory map was used to ascertain the influence of rainfall on the occurrence of landslides. A regression study was performed to determine the significant relation between rainfall and landslides. The frequency ratio value was used to evaluate the correlation between landslides and the corresponding components. There is a significant positive correlation between the total annual rainfall and the total annual landslide from 2010 to 2023. The active and recent landslides exhibit a significant correlation with yearly precipitation. The linear regression analysis reveals a strong correlation between activity stages and rainfall, indicating a close relationship between the two variables. The frequency ratio value is greater at a distance of 100 meters from the drainage. The occurrence of landslides is inversely connected to the topographical wetness index but directly related to the stream power index. There is a positive association between the drainage density and landslides. All the results indicate hydrological control over the landslide mechanism in the study area.

Key words: ***Hydrological control, Landslide, stream power index, topographical wetness index***

INTRODUCTION

The rainfall-induced landslide is very common in the entire Himalayan region. Because most landslides in Nepal occur during the monsoon season, heavy rainfall is regarded as the primary cause of landslides (Dahal et al., 2009). The hills near drainage have more landslide events in Nepal (Regmi et al., 2014; Pokharel and Bhandari, 2019; Thapa and Bhandari, 2019). Toe cut and head erosion are major landslide-initiating factors in the Himalayas, ultimately caused by hydrological activities (Bhandari and Dhakal, 2020). Rainfall is the major cause to occur landslide and the long term rainfall in the Monsoon period play significant role to cause landslide in the Himalaya (Bhandari and Dhakal, 2021, Dahal et al., 2008). Rainfall pattern, geology, and geomorphology determine a rainfall-induced landslide's characteristics. According to Chen et al. (2019), rainfall-induced landslides tended to occur on a dip slope rather than a windward slope. The authors concluded that geological settings were a more effective control of the mass wasting processes on a hill slope scale than the rainfall condition. Chigira (2011) studied Japan's

geological and geomorphological characteristics of rain and earthquake-induced landslides. According to that study, the responses of various geological materials to rain and ground shaking differ. The trigger of a landslide depends on material strength loss, precipitation through pore pressure, and water table height (Larsen et al., 2010; Guzzetti et al., 2008). The occurrence of landslides can be attributed to a combination of natural factors such as steep slopes, weak geology, and high rainfall, as well as human activities such as deforestation and unplanned human settlements. Human activities, such as inappropriate land use, encroachment on hazardous slopes, and unplanned development like road construction and irrigation canals without proper protective measures, worsen the danger of landslides in hilly places. The pore water pressure and hydrostatic pressure on the soil slope as well as rock-soil slope cause shallow to massive landslide. This study aims to access the hydrological action on the slope which ultimately trigger for landslide occurrence in the Aakhu Khola watershed of Dhading District Nepal. The study will also explain the combined role of flowing water, rain water and topographical wetness for landslide occurrence in the study area.

MATERIALS AND METHODS

Study Area

Aakhu Khola watershed has been proposed for this study. This area lies in the Dhading District of Bagmati province, Nepal (Fig.1). This consist of ward no 10 and 11 of Nilkantha municipality, and wards 1-6 of Ruby valley rural municipality, ward no.1-5 of Khaniyabas rural municipality, ward no. 1-5 of Gangajamuna Rural Municipality, ward no. 1-5 of Netrawati Rural Municipality, ward no 1, 2, 4, 5, 6, 7 of Tripurasundari Rural Municipality, and ward no.6 and 7 of Jwalamukhi Rural Municipality. It covers all the local level of north Dhading. This is one of the major Tributary of Budi Gandaki River.

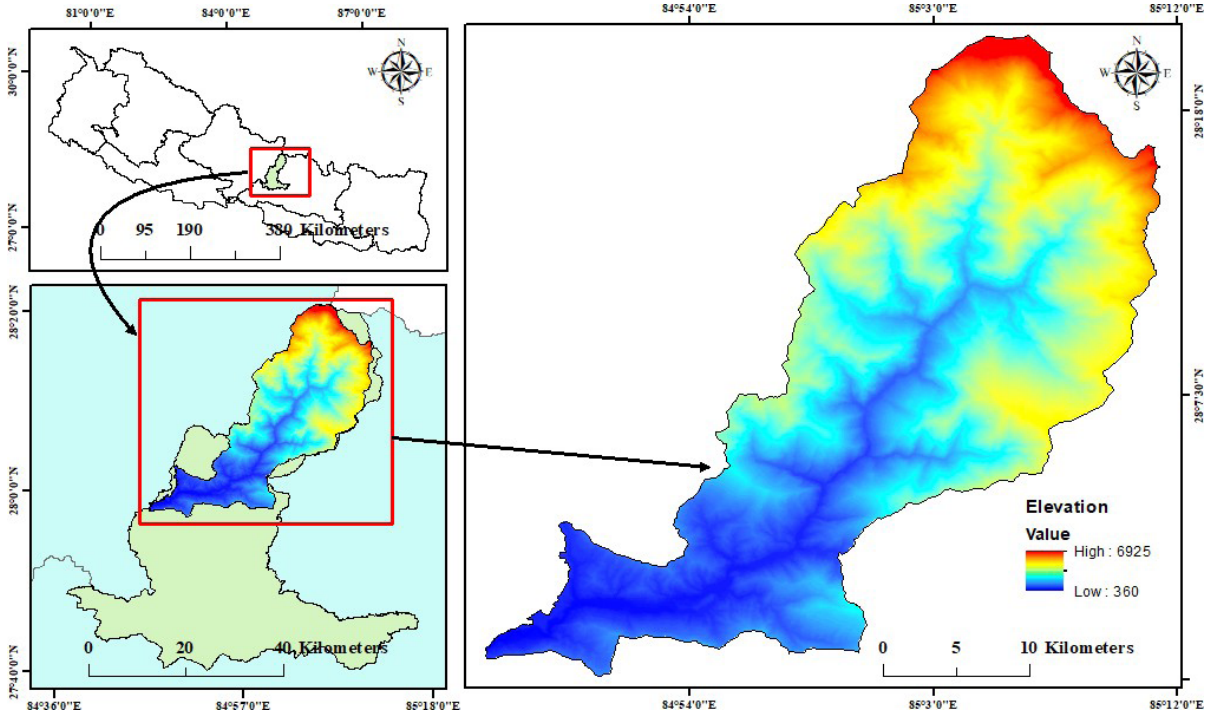

Fig. 1: Location map of the study area

The catchment area starts in GPS location (27°58'6.74"N ,84°46'19.57"E) near Budi Gandaki River and Northen most GPS location (28°20'38.86"N, 85° 4'52.17"E). The catchment area of the river is 701.04 km2. The watershed ranges from a Sub tropical climate in south to Alpine region in north with elevation range 6950 m north in Higher Himalaya range to 425m southern reaches. The study area starts from the alpine region to hilly and then to mountain. Average annual rainfall in the watershed is about 2213.22 mm.

METHODS OF DATA COLLECTION

This study focused on the spatial and temporal distribution of landslides and evaluated their probability using several methodologies. A combination of primary and secondary data sources, such as literature, satellite pictures, Google Earth, and field trips, are used to construct a landslide inventory map (LIM). To analyze the hydrological impacts for landslide, the landslide inventory map was prepared by using Landsat, Sentinel-2 and Google earth imageries from 2000 to 2023.

Primary data collection

The main data gathering method consisted of conducting field observations, which were supplemented by the use of tools such as GPS and a checklist. On field visits, certain landslide locations were chosen, and detailed images were taken for understanding landslides. After the first visit, a detailed inventory map of the landslides was created. Following that, a second phase of on-site verification was carried out, during which supplementary checklists were filled out. During the second field visit, Key Informant Interviews (KIIs) were performed regarding water resources and rainfall pattern in the study area. Similarly, the spring survey was conducted during field visit.

Secondary data collection

A variety of methodologies and data sources were used in the comprehensive assessment of landslide in the study area. The assessment process utilized ArcGIS 10.8, Google Earth, USGS data, meteorological data, and geological information. The field verification of landslide locations was crucial in ensuring accuracy and generating a detailed inventory map. In order to create a map that identifies the factors that contribute to landslides, a digital elevation model (DEM) with a resolution of 12.5 meters was obtained from the ALOSPALSAR website. The thematic maps related to water and playing role to cause landslide were prepared with the help of DEM. The geological map was obtained from the Department of Mines and Geology, Nepal. The rainfall data of twenty-three years was obtained from four different stations and the rainfall map was created.

HYDROLOGICAL FACTORS

Stream power index (SPI)

SPI map is prepared by using the DEM and determined using GIS software. ALOSPALSAR DEM with (12.5*12.5 m) resolution is used as data for the preparation of SPI map. The SPI is grouped into five categories (-45.696 to -9.5668, -9.5668 to -5.243619, -5.243619 to -1.53811, -1.53811 to 1.5498, 1.5498 to 33.0472) using the natural perk classification method (Fig.2a).

Rainfall

Rainfall map is prepared by using interpolation, IDW in Arc GIS. For this process, the rainfall data of twenty year was obtained from the department of hydrology and meteorology (DHM) of Nepal. Rainfall is sorted into five groups based on the obtained values. These categories include rainfall ranges from 1574.119141 to 1990.4233, 1990.4233 to 2255.344, 2255.344 to 2507.6497, 2507.6497 to 2772.570, and 2772.570 to 3182.56 (Fig. 2b).

Distance to drainage

Distance to river map is prepared by using GIS software. ALOSPALSAR DEM (12.5*12.5 m) resolution is used as data for the preparation of distance to river map. The distance to the river is

divided into five groups, each representing a specific range. These classes are 400-800, 800-1200, 1200-1600, 1600-2000 and >2000 (Fig.2c).

Topographic wetness index (TWI)

TWI map is prepared by using the DEM and determined using GIS software and formula TWI= ln (α/tanβ). Where α is the local upslope area draining through a certain point per unit contour length and tanβ is the local slope in radians. ALOSPALSAR DEM with (12.5*12.5 m) resolution is used as data for the preparation of TWI map. The TWI is separated into five groups (0.9242-4.2873, 4.2873-5.9688, 5.9688-8.2109, 8.2109-11.9476, 11.9476-24.74) using the natural break classification method (Fig.2d).

DATA ANALYSIS

Simple linear regression

A simple linear regression model consists of a single independent variable and a single dependent variable. The model calculates the gradient and y-intercept of the regression line, which symbolizes the correlation between the variables. The slope of a line in a regression model indicates the rate of change in the dependent variable for each unit increase in the independent variable. On the other hand, the intercept shows the estimated value of the dependent variable when the independent variable is zero.

Linear regression is a statistical method that demonstrates the linear association between the independent variable (also known as the predictor variable) on the X-axis and the dependent variable (also known as the output variable) on the Y-axis. In this research, simple linear regression is used to find the relation between the total annual landslides and total annual rainfall from 2000 to 2023. So, landslide is taken as dependent variable and rainfall is taken as predictive variable.

Frequency ratio

The frequency ratio is a quantitative tool for evaluating the landslide possibility in the particular region based on the correlation between landslides and causative factors using the spatial analyst tool of Arc GIS (Thapa and Bhandari, 2019). The Frequency Ratio indicates the correlation between several factors that influence landslides and the specific places where landslides occur.

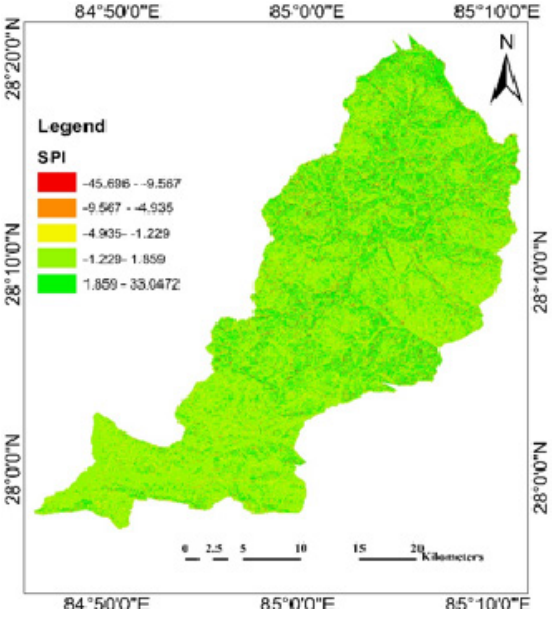

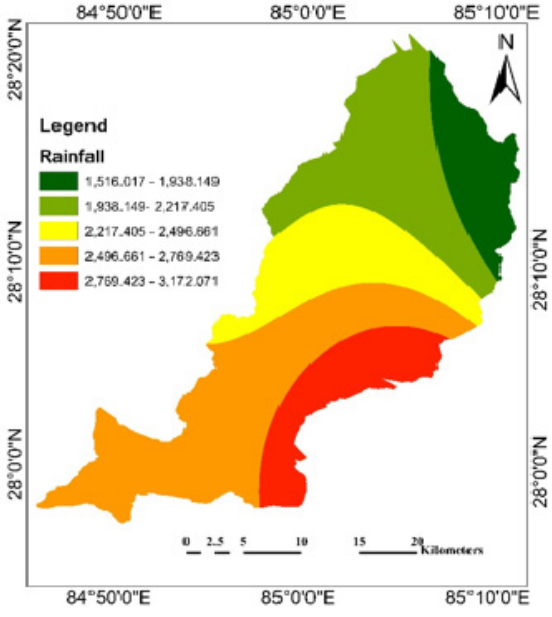

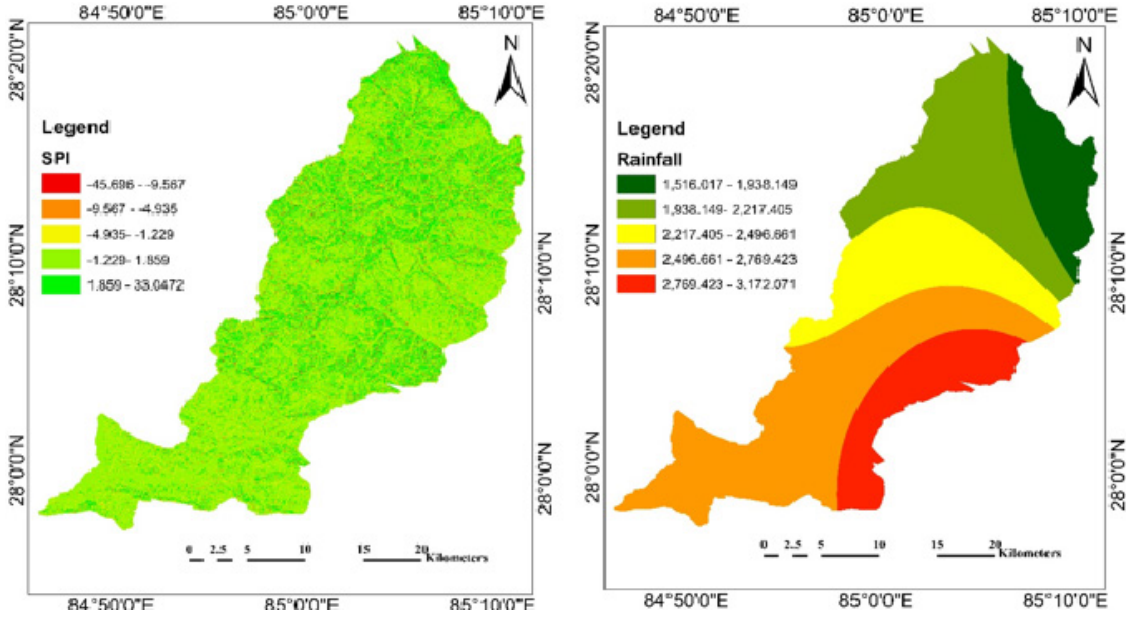

Fig. 2: Hydrological factors map a) Stream power index b) Rainfall c) Distance to stream d) Topographical wetness index.

Due to its mathematical simplicity and quick evaluation time, it is chosen for this study as the fundamental analysis for an initial probabilistic assessment. It is reasonable to expect that the factors that caused past landslides will probably result in future landslides as well. According to this assumption, a correlation can be identified between the occurrence of landslides and the lack of landslides in a region where landslides are influenced by specific causes (Gyawali et al. 2021). The following relation provides the frequency ratio value.

$$FR = \frac{N_a / N}{N_b / N^l}$$

Where,

N_a = number of pixels in each landslide conditioning factor class

N = number of all pixels in total the study area

N_b = number of landslide pixels in each landslide conditioning factor class

N^l= number of all landslide pixels in total the study area

RESULTS

Landslide inventory

The research focused on studying landslides in a specific area using satellite images and on-site visits, identifying a total of 807 landslides. These landslides varied in size, with the smallest being 55.31 square meters, the largest measuring 1,551,345 square meters, and an average size of 10864.96 square meters. The combined area of all the landslides was calculated to be 8749795.8638 square meters. This area represents 1.24% of the total study area. The Darcha landslide and Jharlang landslides are the largest landslide in the study area. Similarly, the Dhunigaun landslide is also a remarkable landslide in the study area. The Dapcha landslide killed 16 people and destroy seven houses in the year 2019.

Rainfall induced landslides

The temporal inventory map from 2000 to 2023 was prepared using satellite imagery and real-ground surveys. We verified some of the landslides through community surveys and focus

group discussions. The total annual rainfall was obtained after synthesizing the raw daily rainfall data obtained from the Department of Hydrology and Meteorology, Nepal. The Figure 3 displays the distribution of total annual landslides and rainfall. Similarly, the regression between temporal landslide inventory data and temporal rainfall distribution data was obtained (Fig.4). The result shows that the coefficient of determination between rainfall and landslides is 0.8196, which indicates that the model is close to the prediction. In the Figure 4, the majority of the points are close to the best fit line. The model predicts a proportion of variance in the landslides that is close to one simple mean high value. This implies that the amount of rainfall can predict the landslides. The significant test results confirm the significance of the result, demonstrating a p value of 0.00015 and F value of 54.32. This implies that the amount of rainfall significantly influences the occurrence of landslides.

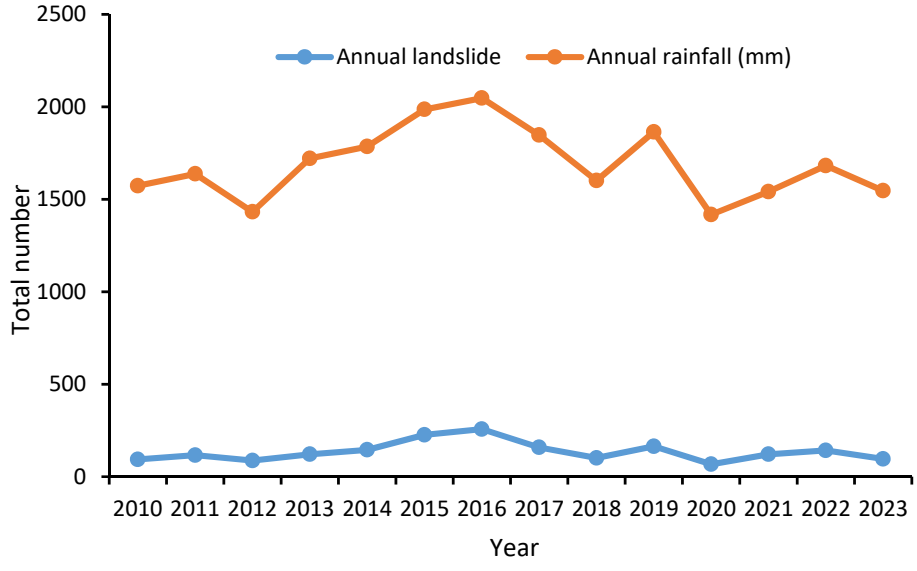

Fig. 3: Distribution of annual rainfall and annual landslide in the study area

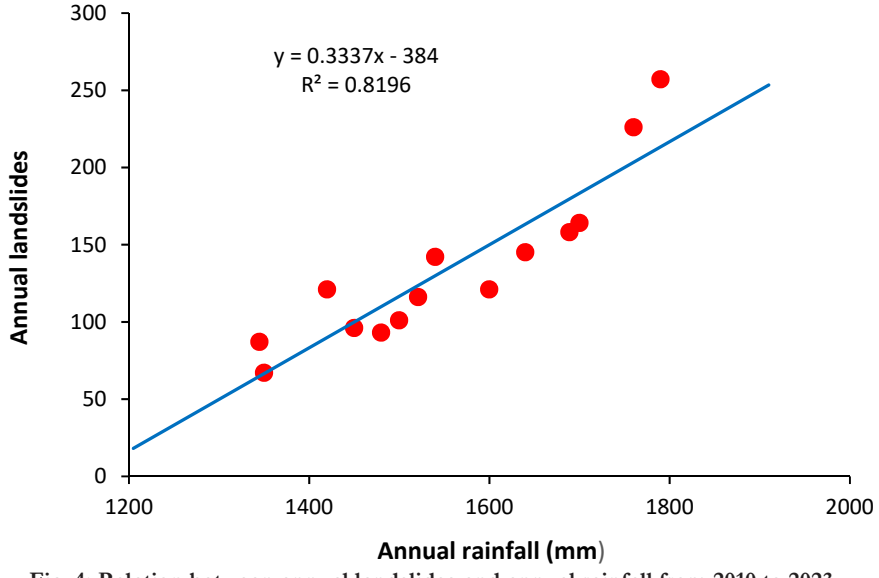

Fig. 4: Relation between annual landslides and annual rainfall from 2010 to 2023.

State of activity

The activity state of landslide was studied based on the five major classes namely active, new, inactive, reactivated and stabilized. The relationship between activity state of landslides and total annual rainfall is obtained. The regression between rainfall and activity state of landslides (reactivated, inactive, active and new) is shown in the Figure 5 a, b, c, d) respectively. The points are closer with the fit line and coefficient of determinations in each curve is greater than 80%. The result indicates that there is strong association between annual rainfall and activity of state. The new, active and reactivated landslide increased with increasing rainfall amount whereas the inactive landslides increased with decreasing rainfall amount. The result shows that the activity state of landslide depends on the total rainfall of the area.

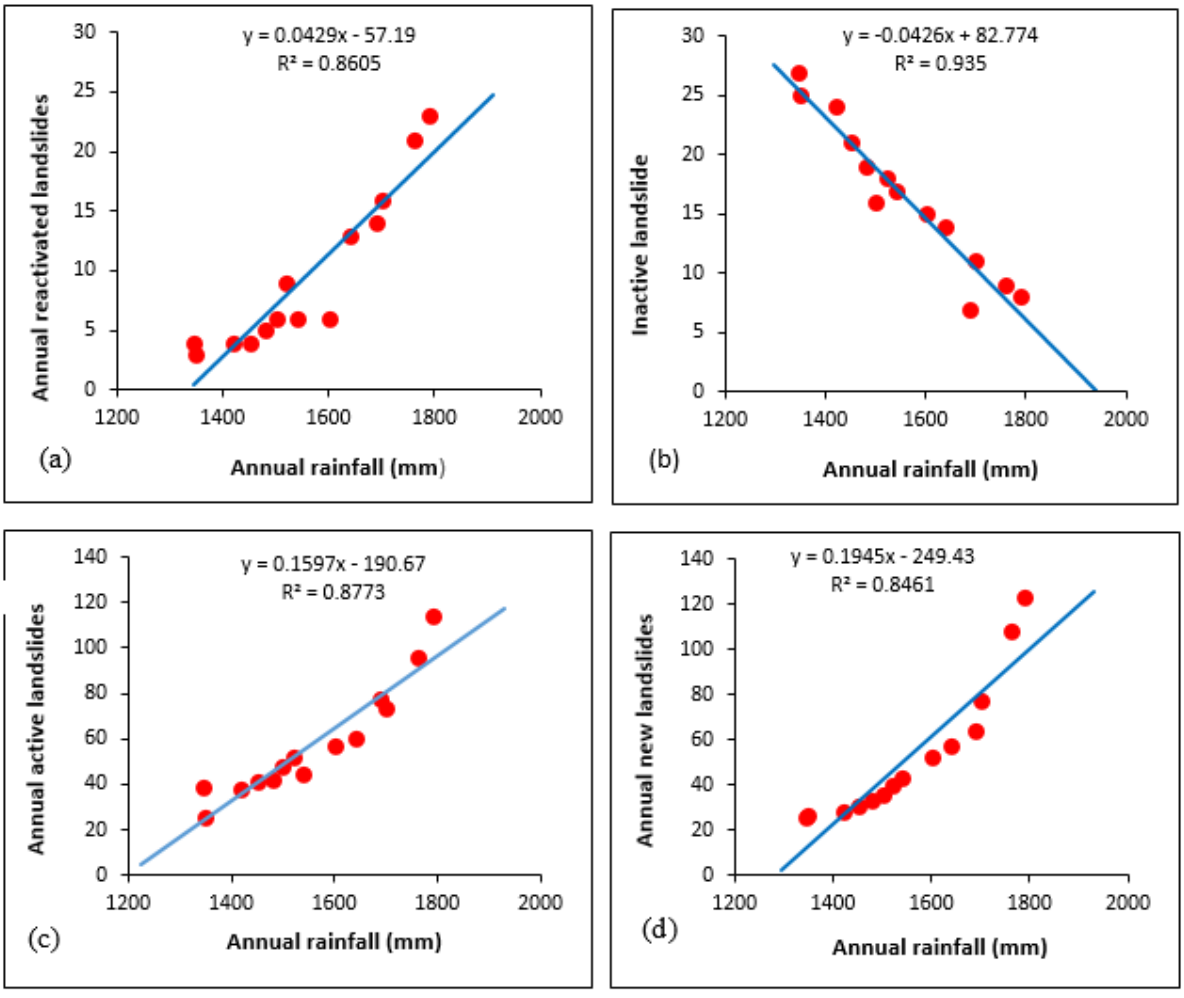

Fig. 5: The regression between annual rainfall and a) annual reactivated landslide b) inactive landslide c) annual active landslide d) annual new landslide.

Landslide size distribution

The size of the landslides (very small, small, medium, large and very large) based on Bhandari and Dhakal (2019) was obtained from 2010 to 2023. The landslide size distribution was correlated with the total annual rainfall. Year wise landslide distribution and total rainfall is shown in the table 1. Total annual rainfall is maximum in 2016. In the same year small and medium landslide is higher in number. Similarly, very large landslide was also occurred during the heavy rain time. The number of very large landslides increased in 2015, 2016 and 2019. The total annual rainfall exceeded more than 1700 mm. The small sized and shallow landslides are mostly controlled by rainfall amount. The medium sized landslides are dominant in the year having rainfall maximum. The size of landslide and rainfall amount also show that landslides are mostly controlled by rainfall in the study region.

Table 1: Annual rainfall and size distribution of landslide.

		Size of landslide				
Year	**Annual rainfall (mm)**	**Very small**	**Small**	**Medium**	**Large**	**Very large**
2010	1480	12	20	38	5	5
2011	1521	18	40	52	9	3
2012	1345	26	27	39	4	3
2013	1600	52	57	15	6	2
2014	1640	57	60	14	13	5
2015	1760	32	96	108	21	8
2016	1790	32	123	114	23	9
2017	1689	7	64	78	14	2
2018	1500	16	36	48	6	3
2019	1700	11	74	77	16	8
2020	1350	21	26	27	6	5
2021	1420	18	24	38	9	3
2022	1540	17	43	45	9	6
2023	1450	31	41	21	4	6

Frequency ratio analysis

The frequency ratio value of each subclass was obtained by using pixel number of landslide, class and sub-class. The frequency ratio value increased with increasing stream power index. The erosive capacity of River increases with increasing stream power index and cause toe cut and foothill erosion so that the number of landslides increases. Similarly, the frequency ratio (FR) value is higher in the area having higher drainage density. Drainage density has positive correlation with landslide. The FR value increased with increasing rainfall amount as shown in the table 2. Similarly, distance to drainage has positive association with landslide because, the FR value increased with decreasing distance to drainage. The topographical wetness index and landslide has negative association. The FR value decreased with increasing topographical wetness index.

Table 2: Frequency ratio distribution of five hydrological factors

Factors	Sub class	FR
Stream Power Index(SPI	-45.69 to -9.56	1.071
	-9.56 to -5.24	1.045
	-5.24 to -1.53	1.019
	-1.53 to 1.54	1.137
	1.54 to 33.047	2.676
Drainage Density(DD)	0 - 0.6461	0.36705
	0.646199 - 1.06	0.755855
	1.0650 - 1.44	1.17229
	1.4479 - 1.87	1.269799
	1.878 - 3.051	1.628132
Rainfall	1574.11 - 1990.42	0.599933
	1990.42-2255.344	0.670908
	2255.344 - 2507.649	0.725309
	2507.649 - 2772.570	1.070411
	2772.570 - 3182.56	1.197803
Distance to River	0 - 100	1.314859
	100 - 200	0.936945
	200 - 300	0.776706
	300 - 400	0.690032
	>400	1.129667
Topographic Witness Index	0.9242 - 4.2873	1.037844
	4.2873 - 5.9688	0.982469
	5.9688 - 8.2109	0.646215
	8.2109 - 11.9476	0.428743
	11.9476 - 24.74	0.156439

DISCUSSION

This study examined the hydrological control of landslides at a catchment scale. We correlated various hydrological factors with the landslide data. The work began with landslide spatial and temporal inventory mapping. We prepared the temporal inventory annually from 2010 to 2023 using Google Earth, Sentinel, and Landsat images of various years. Similarly, the size-based landslide inventory, ranging from tiny to very large was prepared by following the classification guidelines provided by Bhandari and Dhakal (2020). The activity-state-based landslide inventory was also prepared and classified into five classes: new, active, reactivated, inactive, and stabilized. The Nepal Government's Department of Hydrology and Meteorology provided rainfall data from 2010 to 2023. Using the ArcGIS spatial analyst tool, we prepared the rainfall map and other related factors. The regression analysis between the number of annual landslides and the amount of rainfall was conducted. The correlation between the activity state and the amount of rainfall was also obtained. The frequency ratio value for each class also obtained to determine the correlation between landslides and hydrological factors such as drainage distance, topographical wetness index, stream power index, and drainage density. The higher FR value indicates a better correlation between the class and landslides.

The regression of annual landslides and annual rainfall shows that the landslides and rainfall are positively significant. The coefficient of determination shows that there is a closer relationship between landslides and rainfall amounts. Many researchers studied rainfall-induced landslides in the Nepal Himalaya (Dahal and Hasewaga, 2008; Dhakal, 2014; Bhandari and Dhakal, 2020) and around the world (Iverson, 2000; Guzzetti et al., 2008). Similarly, the FR value increased with increasing annual rainfall, indicating that there is a good relationship between landslides and rainfall. As drainage density increased, the FR value increased. A higher number of drainages makes the slope unstable, either due to increasing hydraulic pressure or continuous erosion. We observe landslides near drainages in the study area. Numerous drainages in the Kanniyabas area contribute to the distribution of small to large landslides. Similarly, water flows at high speed into several dry streams during the rainy season, causing Meghan landslides, Galche landslides, and Seuri landslides. These three landslides are active and move every year in the monsoon period, so people have been facing challenges for a long time. The Jharlang landslide is the study area's mega (very large) landslide, which has been active for 20 years and is still creating problems in the rainy season. The Jharlang landslide consists of three major natural drainages and several gullies. The landslide becomes active from the early to late monsoon period but remains inactive for the rest of the time. The 24-hour maximum rainfall recorded in the Khaniyabas area is 350 mm, and the maximum total rainfall only in the monsoon period is 1600 mm from 2010 to 2023, indicating that the rainfall occurs mostly in the monsoon period and the winter rain is negligible. The topographic wetness index is the function of both the slope and the upstream contributing area per unit width orthogonal to the flow direction. We primarily design and use the index for hillside soil conditions. Soil thickness, soil composition, and organic matter content correlate with the topographical index. We have used the TWI to study spatial-scale effects on hydrological processes and to identify hydrological flow paths for geochemical modeling. It also provides information on the hydrological flow's impact on the unit area. The topographic wetness index is a tool to indicate areas accumulating water flow, often with seasonally and permanently waterlogged ground. As such, it is very useful to show the geomorphic complexity of a landslide terrain, including the pattern of dry areas and wet areas. On a steep slope, the TWI value decreases, whereas on a gentle slope, it increases. The results show that the FR value decreased as TWI increased. Previous researchers used the TWI value to correlate with landslides (Schmidt et al., 2008; Wang et al., 2020; Bhandari et al., 2024) and found that the landslide has a negative correlation with TWI. The stream power index represents the erosive power of flowing water. The higher the stream power index, the more erosion capacity there is. There is a positive correlation between the stream power index and landslides. Erosion and bank cutting are the primary causes of landslides in weak geological areas.

CONCLUSION

The main objective of this study was to evaluate the hydrological control on the landslide in the Aakhu Khola watershed of Dhading District, Nepal. The study begun from the preparation of the landslide inventory map of the study area by using Landsat and Google Earth imageries. The hydrological factors map such as precipitation, drainage to distance, topographical wetness index and drainage density were prepared by using Arc. GIS. Landslides events are correlated with the selected hydrological factors. The results indicate that rainfall is primarily responsible for landslides, and the total number of landslides closely matches the total annual rainfall. As drainage density values rose, landslide events increased. Similarly, near the drainage, the number of landslides is higher. The topographical wetness index and landslides are highly correlated. The number of landslides decreased in the area with a higher topographical wetness index. The landslides

show a positive relationship with the stream power index. The number of new and active landslides are increasing every year also signifies that the landslides are hydrologically controlled in the study area.

REFERENCES

Bhandari, B. P. and Dhakal, S., 2020. Spatio-temporal dynamics of landslides in the sedimentary terrain: a case of Siwalik zone of Babai watershed, Nepal. SN Applied Sciences, 2(5), 1-17. https://doi.org/10.1007/s42452-020-2628-0.

Bhandari, B. P. and Dhakal, S., 2021. A multidisciplinary approach of landslide characterization: A case of the Siwalik zone of Nepal Himalaya. Journal of Asian Earth Sciences: X, 5, 100061.

Bhandari, B.P., Dhakal, S. and Tsou, C.Y., 2024. Assessing the Prediction Accuracy of Frequency Ratio,Weight of Evidence, Shannon Entropy, and Information Value Methods for Landslide Susceptibility in the Siwalik Hills of Nepal. Sustainability, 16, 2092. https://doi.org/10.3390/su16052092.

Chen, Y. C., Chang, K. T., Wang, S. F., Huang, J. C., Yu, C. K., Tu, J. Y. and Liu, C. C., 2019. Controls of preferential orientation of earthquake and rainfall triggered landslides in Taiwan's orogenic mountain belt. Earth Surface Processes and Landforms, 44(9), 1661-1674. https://doi.org/10.1002/esp.4601.

Chigira, M., Mohamad, Z., Sian, L. C. and Komoo, I., 2011. Landslides in weathered granitic rocks in Japan and Malaysia. Bulletin of the Geological Society of Malaysia, 57, (1–6). https://10.7186/ bgsm2011001.

Dahal R.K., Hasegawa S., Yamanaka M., Dhakal S., Bhandary N.P. and Yatabe R., 2009. Comparative analysis of contributing parameters for rainfall-triggered landslides in the Lesser Himalaya of Nepal. Environmental Geology, 58(3), 567–586. https://doi. org/10.1007/s00254-008-1531-6.

Dahal, R. K., Hasegawa, S., Nonomura, A., Yamanaka, M., Masuda, T. and Nishino, K., 2008. GIS-based weights-of-evidence modelling of rainfall-induced landslides in small catchments for landslide susceptibility mapping. Environmental Geology, 54, 311–324.

Guzzetti, F., Peruccacci, S., Rossi, M. and Stark, C. P., 2008. The rainfall intensity–duration control of shallow landslides and debris flows: an update. Landslides, 5(1), 3-17.

Gyawali P, Aryal Y.M. and Tiwari A., 2021. Landslide Susceptibility Assessment Using Bivariate Statistical Methods: A Case Study of Gulmi District, western Nepal. https://doi.org/10.36297/vw.jei.v3i2.60.

Larsen, I. J., Montgomery, D. R. and Korup, O., 2010. Landslide erosion controlled by hillslope material. Nature Geoscience, 3(4), 247-251.

Pokharel, B. and Thapa, P. B., 2019. Landslide susceptibility in Rasuwa District of central Nepal after the 2015 Gorkha Earthquake. Journal of Nepal Geological Society, 59, 79–88. https://doi.org/10.3126/jngs.v59i0.24992.

Regmi, A. D., Devkota, K. C., Yoshida, K., Pradhan, B., Pourghasemi, H. R., Kumamoto, T. and Akgun, A., 2014. Application of frequency ratio, statistical index, and weights- of-evidence models and their comparison in landslide susceptibility mapping in Central Nepal Himalaya. Arabian Journal of Geosciences, 7(2), 725–742. https://doi.org/10.1007/s12517-012-0807-z

Schmidt, J., Turek, G., Clark, M. P., Uddstrom, M. and Dymond, J. R., 2008. Probabilistic forecasting of shallow, rainfall-triggered landslides using real-time numerical weather predictions, Natural Hazards and Earth System Science, 8, 349–357, https://doi.org/10.5194/nhess-8- 349.

Thapa, D. and Bhandari, B. P., 2019. GIS-Based frequency ratio method for identification of potential landslide susceptible area in the Siwalik zone of Chatara-Barahakshetra section, Nepal. Open Journal of Geology, 9(12): 873.

Wang, S., Zhang, K., van Beek, L. P., Tian, X. and Bogaard, T. A., 2020. Physically-based landslide prediction over a large region: Scaling low resolution hydrological model results for high-resolution slope stability assessment, Environmental Modelling and Software, 124, 104 607, 2020.

Journal of Nepal Hydrogeological Association (JNHA), Vol (1), 79-93 (2024)
ISSN: 3059-9725 (Online)

RESEARCH ARTICLE

Hydrogeological assessment of groundwater resources in Khutti Khola Watershed, Siraha District, Eastern Nepal

Goma Khadka[1], Sumitra Dhungana[1], Manjari Acharya[1], Ram Bahadur Sah[1] and *Kabi Raj Paudyal[1]

[1]Central Department of Geology, Tribhuvan University, Kathmandu, Nepal
**Corresponding author: paudyalkabi1976@gmail.com*

***(Submission Date**: 27 April 2024; **Accepted Date:** 5 September 2024)*

ABSTRACT

The Khutti Khola watershed, located in eastern Nepal, is a region that has been experiencing increasing water scarcity over the past few decades. These regions face water scarcity due to rapid and poorly planned urbanization, fragile geology, overexploitation of existing water resources and ineffective water governance systems. The present study focuses on examining the availability, distribution, and management of groundwater resources in Khutti Khola watershed. It provides insights into the geological features, hydrogeological inventories, water table dynamics of Khutti Khola watershed and a Nature-based Solution (NbS) for groundwater recharge at water scarce areas of Bhabar zone. Hydrogeological assessment was carried out in Terai, Bhabar as well as Chure region within Khutti Khola watershed and the local people from the communities were interviewed for the identification of water scarce areas. The main scarcity was found in places like *Ranaha, Dadatol* and *Simaltoki* in the Bhabar zone. Recommendations for the development of artificial ponds were proposed in those areas as a Nature-based Solution (NbS) and a feasibility study was carried out for identifying the appropriate location for the pond. As such ponds made at the surface of the recharge zone will work as extra pockets to store surface runoff and recharge the area, construction of artificial recharge pond is recommended as sustainable solutions to mitigate water scarcity in the Khutti Khola watershed and similar regions across Nepal, ultimately improving livelihoods and resilience of local communities.

Keywords: ***Khutti Khola watershed, Groundwater resources, Bhabar zone, Nature-based Solution (NbS), Artificial recharge pond***

INTRODUCTION

The people living in Khutti Khola watershed depend on groundwater for both drinking and irrigation purposes. But these regions are at risk of water shortages because of rapid and poorly planned urban growth, along with fragile geology, and ineffective water management systems. In addition to these, the region relies heavily on monsoon rains, which are highly seasonal and unpredictable. Most of the annual rainfall occurs during the monsoon season, leading to a surplus of water for a few months and scarcity during the dry months.

The Bhabhar zone of the Khutti Khola watershed faces significant water unavailability primarily due to its highly porous and thick gravelly substrate. The northern part of the watershed consists of the Siwalik range separated by the Main Frontal Thrust. This zone is also fragile and porous in nature. There is huge accumulation of loose sediments at the base of the Siwalik, called the Bhabar zone, which acts as the recharge zone for the rest of the Terai regions southward (Neupane and Paudyal, 2021; Neupane et al., 2023; Dahal and Paudyal, 2022). Though the

region facilitates groundwater recharge, access to water remains limited in the shallow aquifer because of the deeper water table (Pathak 2016; Luitel et al., 2020) leading to a lack of accessible water for agricultural, domestic, and ecological needs. Groundwater in the Bhabar Zone is accessible during the monsoon season, but the water table recedes significantly during the pre-monsoon period, causing shallow wells to run dry. Lahan municipality and Dhangadimai Municipality of Khutti Khola watershed have already been drilling sub-surface to extract water from deep aquifers and lifting surface water from rivers to meet immediate water supply demands. This may solve the problem of water scarcity in the short-term; however, these solutions are costly, unsustainable in the long term, and vulnerable to climate variability such as damage of the pipeline of the system by flood/landslide.

To address these complex issues, the concept of Nature-based Solutions (NbS) is gaining attention. NbS involves using natural systems or processes to manage water resources, rather than relying solely on conventional infrastructure (UN Water, 2018; UN Environment-DHI, UN Environment and IUCN, 2018). In the context of the Bhabar zone, the identified NbS is the construction of artificial recharge ponds. This approach aims to enhance groundwater storage by allowing rainwater and surface runoff to infiltrate into the aquifer naturally, replenishing groundwater levels. Based on hydrogeological assessment conducted and series of discussion and knowledge exchange among stakeholders, constructing sites for artificial recharge ponds was identified and prioritized as the most appropriate intervention to recharge groundwater in Bhabar zone in the study area.

Study area

The Khutti Khola watershed area is in the Siraha district of Madhesh province, Nepal, spanning between approximately 26° 42' 20" to 26° 55' 0" north latitude and 86° 23' 30" to 86° 31' 10" east longitude. It encompasses parts of Lahan municipality and Dhangadhimai municipality. The watershed exhibits a dendritic and parallel drainage pattern, characterized by major tributaries such as Khutti Khola, Sarre Khola, Ambule Khola, Maini Khola, Maina Khola, Raini Khola, Raydhar Khola, Dalame Khola, Mahajani Khola, and Madhyan Khola. The topography varies from gentle to steep in the northern section, gradually transitioning to flat plains in the southern section.

Methodology

This study encompassed a comprehensive approach involving literature review, field investigations, data compilation, and analysis. Topographic maps (Risku, Dhangadhimai, Lahan and Kadarbona of sheet no: 2686 02 B, 2686 02 D, 2686 06 B and 2686 07 A which covers overall Khutti Khola watershed were used for the preparation of location map, geological map, hydrogeological inventory and water level maps in GIS. Field investigation was carried out to collect detailed information on geology and hydrogeological condition of the area. Geological map from the Department of Mines and Geology (DMG 1984), Government of Nepal has been used as reference for geological survey in the field. Hydrogeological inventory of wells and springs within the Khutti Khola watershed was conducted during fieldwork. Information on water scarcity areas was gathered through social surveys in local communities (Figure 3). A feasibility study was undertaken to identify suitable locations for constructing artificial recharge ponds. The design and location of ponds within the watershed were determined considering three important factors: runoff collection, drainage channels and safe disposal of excess water. The national guideline provided by Department of Local Infrastructure Development and Agriculture Roads (DoLIDAR) was considered for recommending pond types (DoLIDAR, 2013).

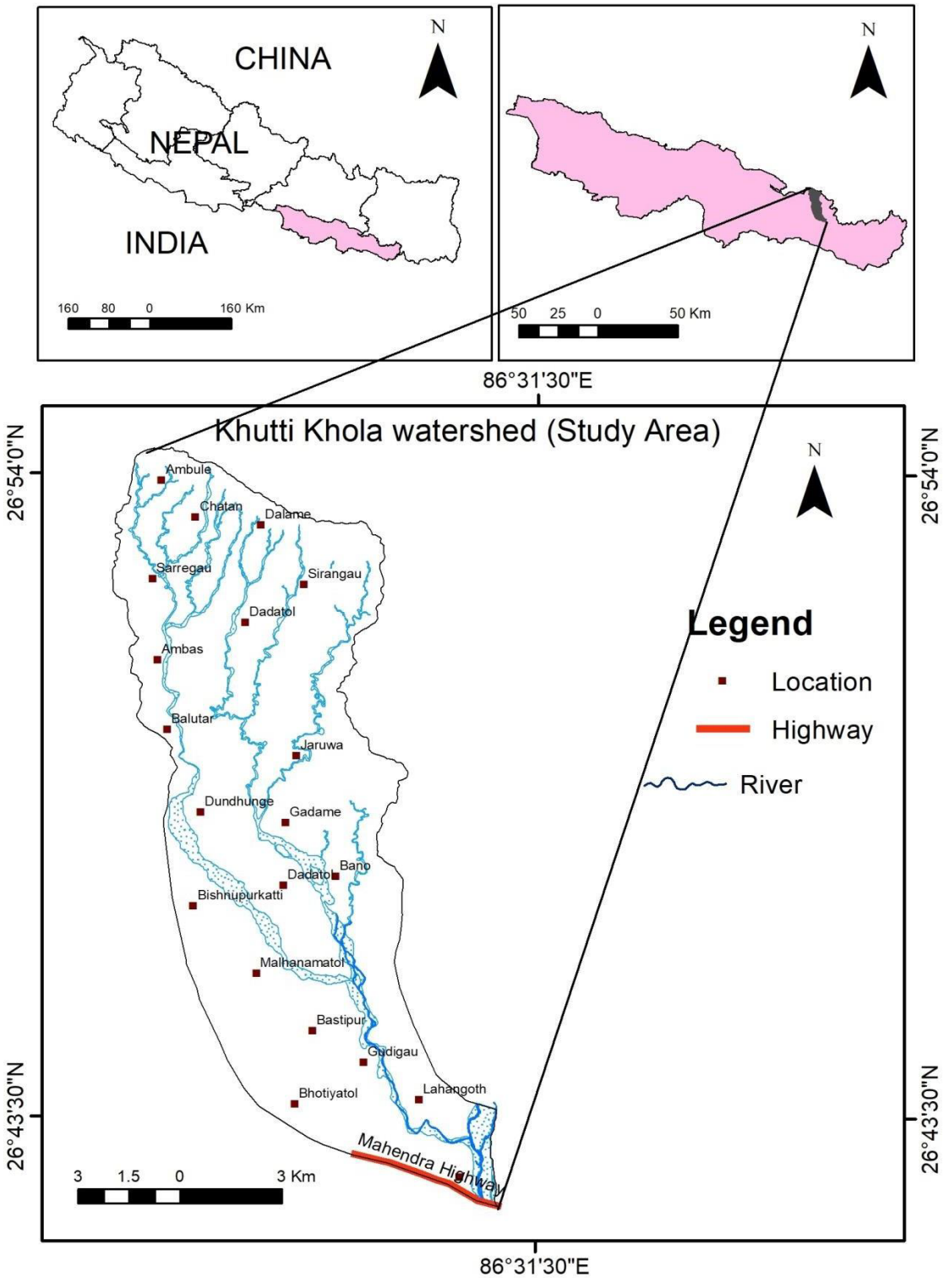

Fig. 1: Location map of the study area

Results

Geology

A detailed geological map of the area at a scale of 1:25000 has been prepared from the data collected during the field study (Figure 2). The study area is geologically diverse, comprising two major geological units: the Sub-Himalaya and the Terai Plain. It encompasses the Terai plain to the south and the Siwalik Group/ Sub-Himalaya/Chure Region succession to the north, separated by the Main Frontal Thrust (MFT). The Siwalik Group includes Lower Siwalik, Middle Siwalik (further divided into Middle Siwalik 1 and Middle Siwalik 2), and Upper Siwalik. The Terai plain is also divided into the Bhabar Zone and the Middle Terai in the studied section. Boundaries between these geological units have been delineated based on evidence such as lithological characteristics, structural features, and geomorphological indicators.

The Upper Siwalik comprises a thick-bedded conglomerate with loose sandstone and mudstone. Poorly sorted, clast-supported, less compacted conglomerate in the lower part of the Upper Siwalik is followed by poorly sorted, matrix-supported conglomerate bed towards stratigraphic up-section. Middle Siwalik comprises inter bedding of pale yellow to dark grey, fine- to coarse grained, thin-to thick-bedded sandstone, and pale yellow to ash grey, thinly bedded mudstone. The Middle Siwalik is further subdivided into the Middle Siwalik 1 and the Middle Siwalik 2. The Middle Siwalik 1 consists of greenish grey to light yellow mudstone and pale yellow, fine- to medium-grained, salt and pepper appearance sandstone in the lower portion. The proportion of sandstone increases in the upper portion. The Middle Siwalik 2 unit consists of thick-bedded, medium-to coarse-grained, salt and pepper appearance sandstone with thin-bedded pebbly sandstone at the lower portion. The proportion of pebbly sandstone increases toward the upper portion. The Lower Siwalik consists of purple, light yellow, ash to greenish grey variegated mudstone, black shale, and ash grey, fine-medium-grained sandstone. The spheroidal weathering in the mudstone bed is common.

The Terai plain is subdivided into the Bhabar zone and the Middle Terai. The Terai plain consists of boulders, gravel, silt, and clay of Quaternary alluvium deposits. The Bhabar zone lies immediately south of the Main Frontal Thrust at the foothill of the Chure. The Bhabar zone comprises rounded to sub-rounded gravel, cobble, pebble and coarse-grained sand. The Middle Terai mainly comprised of coarse to fine-grained sand, silt, and clay. The Recent Riverbed Deposits cover some parts of the study area along the river course which includes boulders, cobbles, pebbles, sand, silt, and clay.

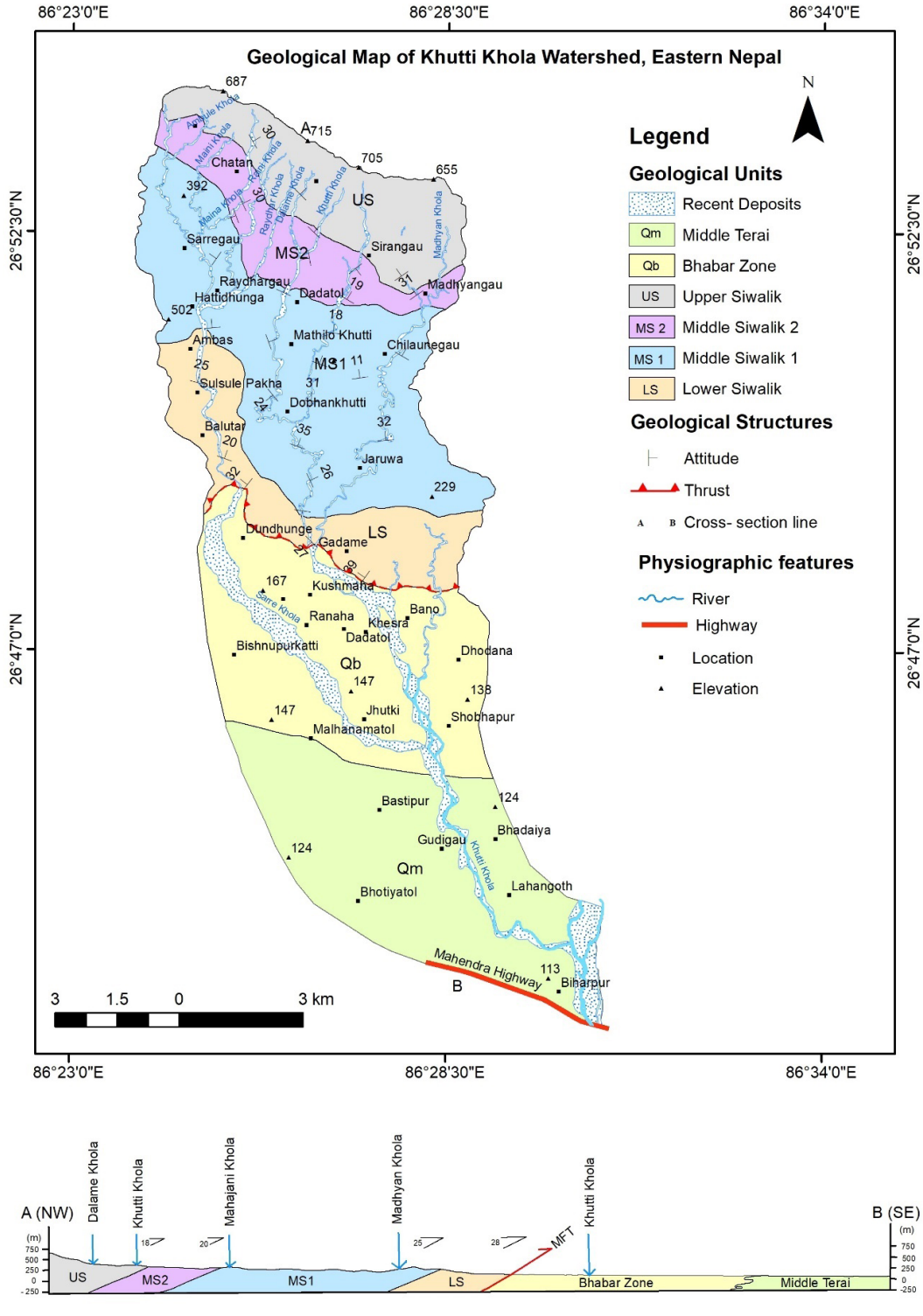

Fig. 2: Geological map and cross-section (through line A-B) of the Khutti Khola watershed area.

Hydrogeology

Hydrogeological study was carried out in the Siwalik region, Bhabar zone and the Middle Terai for finding availability and distribution of groundwater resources in the watershed. The information about shallow tube wells, deep tube wells, and springs was collected from the field and is listed in Tables 1 and 2. Some photographs from the field during hydrogeological inventory are shown in Figure 4 whereas Figure 5 depicts the hydrogeological inventory map.

Well inventory

The local people constructed dug wells, hand pump and deep tube well for the drinking and household purposes in the study area. Well inventory of the Khutti Khola watershed was done to find the availability of the water, static water level, drilling depth and depth of aquifer zone. The deep tube well data was collected from the Groundwater Irrigation Development Division (GWIDD) office, Lahan. The deep tube well data includes GPS coordinates, lithology data, elevation, and static water level. In the Siwalik zone, dug wells are constructed mostly on the bank of the river which is of shallow depth. The number of dug wells and hand pumps are large, but the number of deep tube wells is less in the Bhabar zone. Both hand pumps and deep tube wells can be seen in the Middle Terai. The quality of tube well water is predominantly satisfactory across most of the surveyed areas. This conclusion is based on the data collected by interviewing local people, which shows that most regions have access to water that meets acceptable quality standards for drinking which is within the concentration limits of Nepal Drinking Water Quality Standards (NDQS, 2005) and has no side effects and is used for all purposes including agriculture.

Table 1: Inventory of shallow and deep tubewell within Khutti Khola watershed.

Well Type	Well. No.	X	Y	Place	Elevation (m)	Total depth (m)	Static water level (m bgl)
Hand pump	T1	449520.3	2954360.1	Raghunathpur	110	13.7	1.5
Hand pump	T2	444607.4	2960456.4	Malanhma	126	18.2	14.8
Hand pump	T3	445954.6	2958684.8	Bastipur	118	45.7	9.1
Hand pump	T4	448320.5	2958766.2	Bhadaiya	132	8.5	5.2
Hand pump	T8	446043.8	2958266.3	Ragunathpur	120	15.2	4.8
Hand pump	T12	447619.9	2962838.1	Dhodana	131	30.5	15.0
Hand pump	T15	448194.8	2961472.2	Birnagar	127	9.1	1.2
Hand pump	T16	448380.0	2958537.4	Bhadaiya	125	8.5	5.2
Hand pump	T17	447743.4	2961495.3	Shobapur	119	6.1	1.2
Hand pump	T18	445461.7	2963307.0	Dadatol	136	16.8	15.2
Hand pump	T19	448448.3	2957832.3	Asanha	108	38.7	30.5
Hand pump	T23	449151.7	2957956.2	Magartol, Bhadaiya	120	34.1	30.5
Hand pump	T25	448781.7	2959000.4	Bishnupur	110	29.0	25.0
Hand pump	T26	447899.9	2957852.9	Gudigau	120	24.4	22.0
Dug well	W1	446510.9	2962109.1	Khesra (Magartol)	157	14.4	12.6
Dug well	W2	445867.2	2963362.8	Dadatol	161	19.8	14.4

Dug well	W3	445402.4	2963393.7	Dadatol	168	11.1	7.2
Dug well	W4	445360.3	2963694.3	Dadatol	163	30.6	26.1
Dug well	W5	445591.7	2963228.9	Motidadatol	166	36.0	28.0
Dug well	W6	442599.2	2966487.5	Bhotetar	201	5.4	3.6
Dug well	W8	442768.8	2965669.4	Dundunge	203	5.5	4.5
Dug well	W10	443184.0	2964244.8	Bishnupurkatti	186	12.6	9.0
Dug well	W11	441780.2	2969815.7	Ambas	256	18.0	8.1
Dug well	W12	442027.9	2969066.3	Ambas	251	8.0	5.7
Dug well	W13	441841.9	2971080.2	Hattidhunga, Dhangadhimai	277	3.6	2.7
Dug well	W16	444545.0	2969692.0	Mahajani	265	3.0	2.3
Dug well	W17	446485.4	2969761.5	Chilaunegau	264	2.8	2.5
Dug well	W18	444238.2	2963358.2	Ranaha	172	12.6	11.7
Dug well	W19	444521.3	2963119.0	Ranaha	165	52.5	37.5
Dug well	W20	444851.4	2962942.3	Ranaha	164	14.0	12.0
Dug well	W22	444360.6	2963790.1	Simaltoki	170	15.3	9.9
Dug well	W23	443029.0	2962366.9	Bishnupur-12	170	27.0	15.3
Dug well	W24	443458.7	2962001.6	Bishnupurkatti	169	12.6	9.6
Dug well	W26	443270.0	2961064.1	Raitol	163	13.0	11.7
Dug well	W27	443191.0	2960737.9	Raitol	160	14.5	7.2
Dug well	W28	444263.7	2960213.2	Premtol	155	15.0	13.5
Dug well	W31	446643.1	2970171.2	Chilaunegau	243	2.8	2.5
Dug well	W32	444402.7	2965229.8	Ahale	164	5.4	2.7
Dug well	W36	444084.2	2963668.8	Simaltoki	145	10.4	9.6
Dug well	W37	443861.6	2963805.8	Simaltoki	147	15.3	9.9
Dug well	W39	443131.4	2961694.6	Bishnupurkatti	136	15.0	14.0
Deep tubewell	DTW-1	445291.8	445291.8	Khapanitol	132	78.0	13.0
Deep tubewell	DTW-2	444461.3	444461.3	Malhnmatol, Govindapur	130	157.0	15.0
Deep tubewell	DTW-3	445995.1	445995.1	Govindapur	150	104.0	25.0
Deep tubewell	DTW-4	448211.5	448211.5	Bhadaiya-1	136	112.0	14.0
Deep tubewell	DTW-5	448330.6	448330.6	Bhadaiya	135	101.0	15.0
Deep tubewell	DTW-6	446652.2	446652.2	Bastipur	131	126.0	14.0
Deep tubewell	DTW-7	446109.1	446109.1	Bastipur-12	130	129.0	15.0
Deep tubewell	DTW-8	442510.4	442510.4	Bishnupur-11	146	95.0	12.0

Spring inventory

The maximum resident of the Siwalik (Chure) depends on the spring's water for drinking and other household purposes. Spring inventory was carried out in Siwalik to check the availability of the water. The study was done in Magh/Falgun months, a dry season in Nepal. Almost all the observed springs are perennial. The various types of spring observed are springs from riverbed, springs from colluvium, contact springs and seepage.

Springs from riverbed

The riverbed spring is found near the *Chilaunegau*. The riverbed containing sand, gravel and boulders provide the origin of spring water. The upper part of the stream was found dry. The *Chilaunegau* lies in the Middle Siwalik near to the Madhyan Khola. The whole of *Chilaunegau* depends on this riverbed aquifer for drinking and other domestic purposes.

Springs from colluvium

The maximum springs observed in the study area are colluvium originated springs. The colluvium spring is observed in *Ryadhargau, Sarregau, Bhibare and Bhalutar*. *Ryadhargau* and *Sarregau* lies in the upper part of Lower Middle Siwalik. *Bhalutar* and *Amiletar* lies in the Lower Siwalik.

Contact springs

The contact spring flows between mudstone and brown siltstone inter bedded within light grey, medium grained sandstone bed. It is observed near Lower Middle Siwalik near the *Mahajani* village. Another contact spring can be seen near the *Bhalutar* in the Lower Siwalik. It is observed between pale yellow, fine – grained sandstone and greenish mudstone bed.

Seepage springs

Seepage is seen in the contact of the fine-grained compacted sandstone and medium grained sandstone bed. It is observed on the left bank of the Khutti Khola about 1.5 km upstream from confluence of the Khutti Khola and the Madhyan Khola. It lies in the Lower Middle Siwalik.

Table 2: Spring inventory data within Khutti Khola watershed.

S.N.	X	Y	Type	Discharge	Location
A1	441516.2	2972135.0	Spring from riverbed	Perennial	Mainamaini Dobhan
A2	441953.2	2971910.2	Spring from colluvium	Perennial	Sarregau
A3	441644.6	2971807.9	Spring from riverbed	Perennial	Sarregau
A4	441713.3	2968580.7	Spring from colluvium	Perennial	Bihibare
A5	441973.6	2968756.1	Seepage	Seasonal	Sulsulepakha
A6	444391.2	2965339.7	Spring from colluvium	Perennial	Ahale
A7	447012.8	2970546.7	Spring from colluvium	Perennial	Madhyangaun
A8	441454.6	2971370.0	Spring from colluvium	Perennial	Raydhargau
A9	441947.2	2967754.9	Spring from colluvium	Seasonal	Bhalutar
A9	444649.1	2969654.4	Contact Spring	Perennial	Mahajani
A10	444601.5	2966720.0	Seepage	Seasonal	Khutti Khola
A11	442405.8	2967854.3	Contact spring	Perennial	Bhalutar

Fig. 3: Interviewing local people from the Khutti Khola watershed.

Fig. 4: Some photographs of wells and springs from the Khutti Khola watershed.

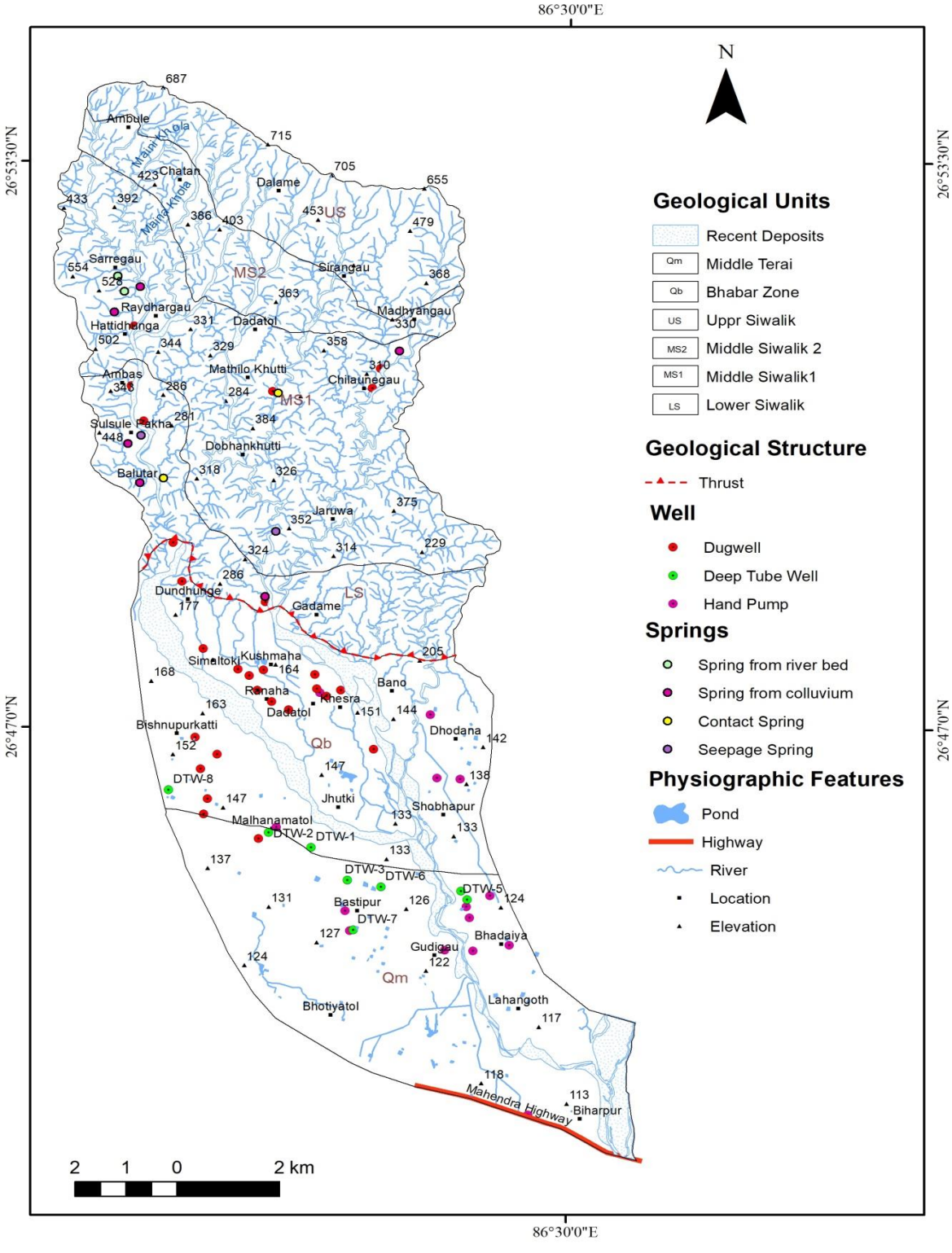

Fig. 5: Hydrogeological inventory map of the Khutti Khola watershed.

Depth of water level

Both drilling depth and static water level depth are measured during field visits. Based on the static water level of the shallow well, a water level map is prepared (Figure 6). The water level can be divided into 5 categories in the interval of 8 m bgl. The water level of the dug well in the villages named *Chilaunegau*, *Ryadhargau*, *Bhalutar* and *Mathillokhutti*, ranges between 1 m bgl and 8 m bgl. Wells are situated along the riverbanks in the Siwalik region, leading to a shallow static water level. In the Terai plain, the water level is at an intermediate level. Meanwhile, the water level in the Bhabar zone fluctuates depending on the location. In *Malhanmatol*, *Bishnupurkatti*, *Kushmaha*, *Gadame*, *Khesra* and *Dhodana villages*, the water level ranges from 8 m bgl to 16 m bgl. The water level of the *Ranaha* and *Dadatol* is from 24 m bgl to 32 m bgl. But in the *Shobapur* water level is at shallow depth. In the Middle Terai, the water table is found at a relatively shallow depth. The deep-water level lies around *Bhadaiya* and the *Gudigau* village.

Information about the subsurface of the area can be obtained from the litholog of the deep tube-well data available from the GWIDD office, Lahan (Figure 7). The deep tube-well drilled in the *Khapani* (DTW-1) was 78 m depth and static water level depth was 13 m. It consists of 28 m cobble and pebble, 11 m pebble and gravel, 34 m clay mixed with gravel and 5 m coarse - grained sand in the top layer. The litholog indicates that it lies in the Bhabar zone. The tube-well drilled at the *Govindapur* (DTW-3) was 104 m and *Bhadaiya* (DTW-4) was 112 m. DTW-3 consists of the thick layer of coarse-to medium - sand, a very thick layer of clay and thin layer of gravel. DTW-4 comprises of a very thick layer of clay with thick layer of sand and very thin layer of gravel. The contrast results are seen in the DTW-3 and DTW-4. In the DTW-3 and DTW-4 there is a thin layer of gravel and thick layer of sand, silt, and clay. Both tube-well litholog represent the sediments of the Middle Terai.

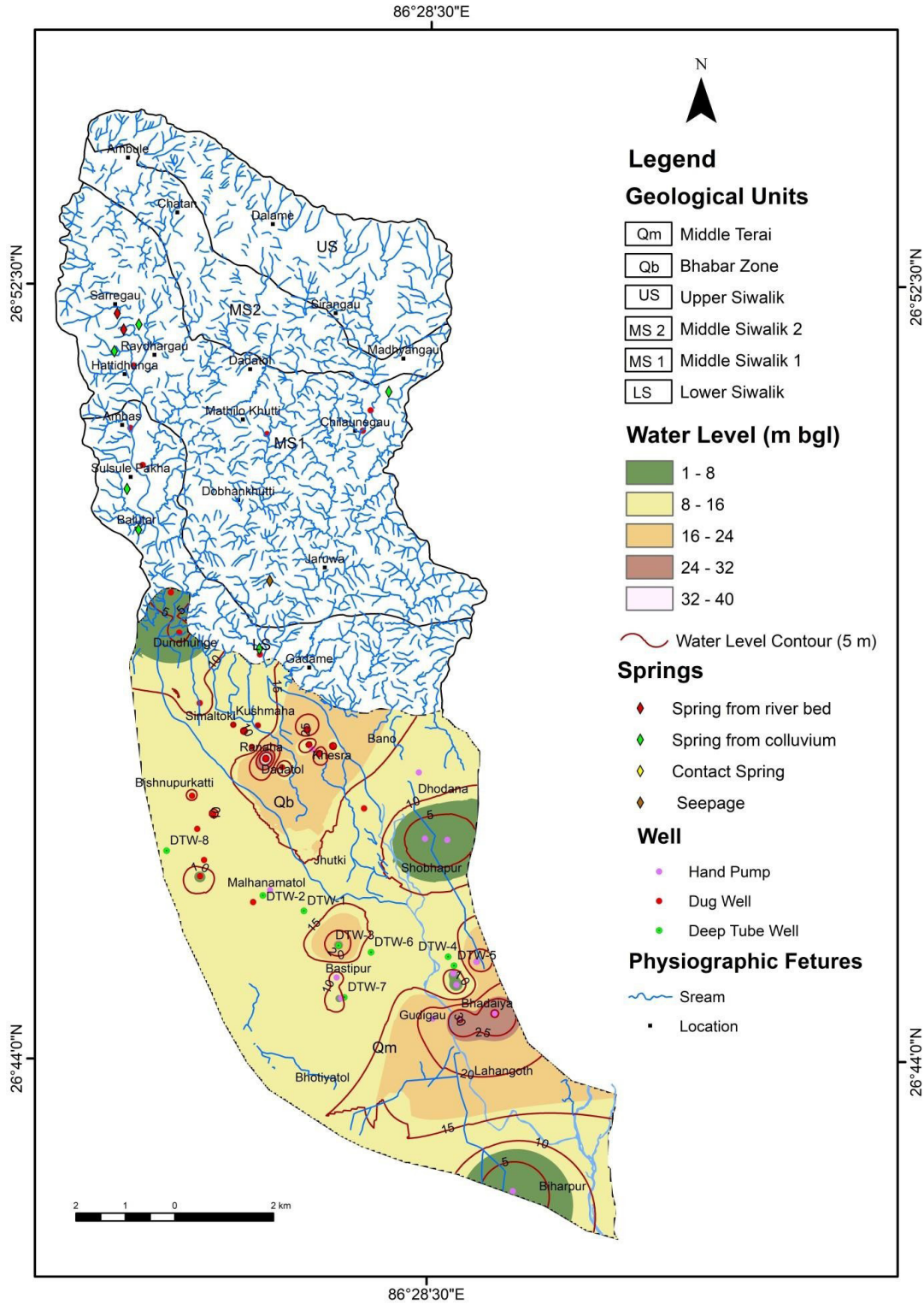

Fig. 6: Shallow water level map of the Khutti Khola watershed.

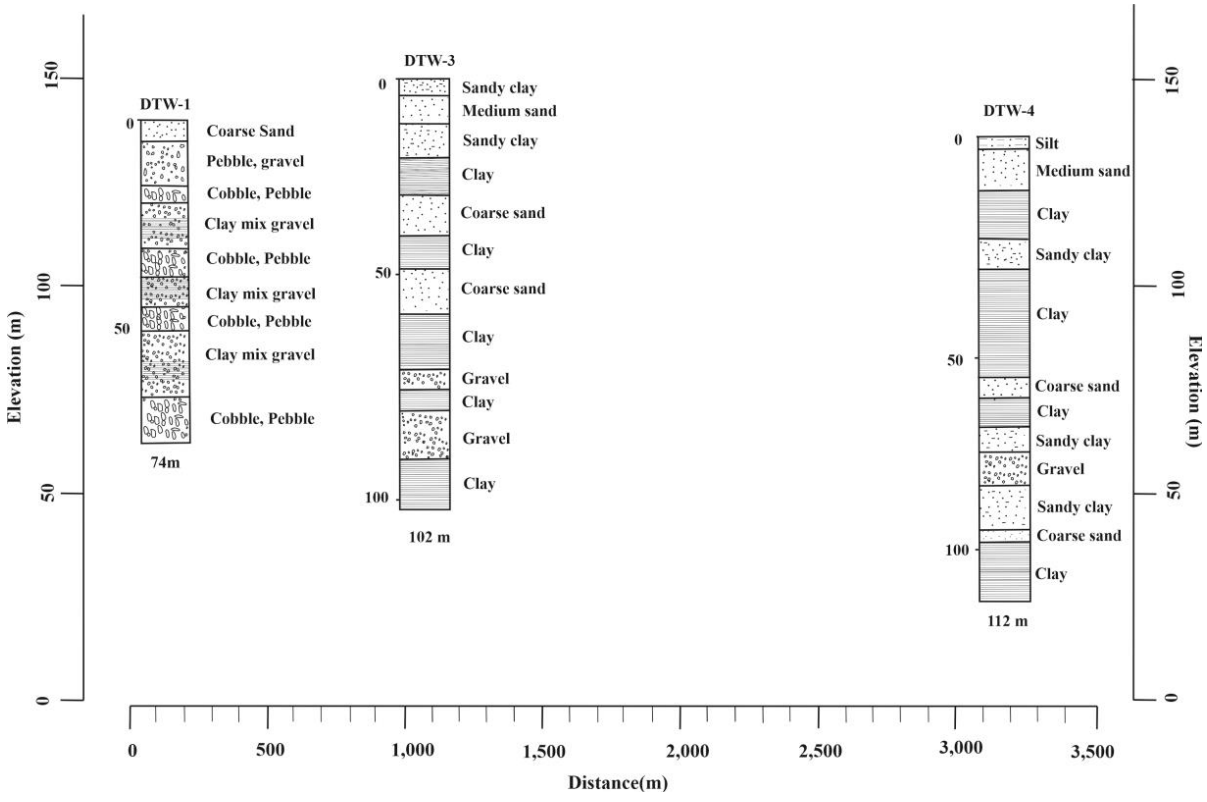

Fig. 7: Lithology of deep tube well from the study area.

Discussions and Conclusions

In the study area, Bhabar zone is still facing water scarcity problem. The Bhabar comprises of loose admixture of the cobble, pebble and coarse sand which are highly permeable and have less porosity. Many deep wells are constructed in the Bhabar to solve the water scarcity problem. But *Dadatol*, *Ranaha and Simaltoki* still have water scarcity problem in the dry season.

Addressing water scarcity is critical for ensuring the long-term sustainability and well-being of communities in the Khutti Khola watershed and similar regions. One of the most effective and sustainable Natural based Solution (NbS) methods to combat water scarcity is the implementation of artificial recharge ponds (Shrestha et al. 2021; Aryal et al., 2022). Additionally, use of water from the riverbed aquifers could be another alternative to harness the water in the region (Paudyal et al., 2023). However, in the present study, the possibilities of riverbed aquifers are not fully considered. A recharged pond is proposed at *Ranaha, Dadatol* and Simaltoki (Table 3) which is expected to solve the water scarcity problem of the communities from the *Ranaha, Dadatol* and *Simaltoki* tole. It lies in Bhabar zone which is a suitable place for recharging groundwater. The main purpose of ponds is to recharge groundwater and maintain water level in all seasons. The locations were chosen based on several criteria, communities demand including their ability to collect runoff, their status as public land, and their position in the bhabar zone, where there is no impermeable clay layer. This ensures that runoff and rainfall can easily infiltrate into the soil.

Table 3: GPS location of proposed recharge pond

S.N.	Northing	Easting	Spot Height	Place Name
1	444381	2963235	163	Ranaha
2	445145.5	2963357	165	Dadatol
3	443946.9	2963475	167	Simaltoki

Conclusions

The assessment of groundwater resources of the Khutti Khola watershed identified the availability of groundwater through well and spring inventories, revealing varying water levels across different zones. The Bhabhar zone struggles with water accessibility because of its highly porous substrate and deep-water table. Current engineering solutions like deep aquifer drilling and surface water lifting are costly and unsustainable in the long term. A promising sustainable solution is the implementation of Nature-based Solutions (NbS), specifically artificial recharge ponds, which enhance groundwater storage by allowing rainwater and surface runoff to infiltrate naturally. This helped in providing water for longer period and thus enhanced percolation rate boosting the replenishment of the underlying aquifers and hence increasing the well yield at shallow depth. The proposed recharged ponds at Ranaha, Dadatol, and Simaltoki are strategically located in the Bhabar zone, which provides favorable conditions for groundwater recharge. The ground conditions are ideal due to the absence of impermeable clay layers and characterized by its highly porous and thick gravelly substrate allowing for efficient infiltration of runoff and rainfall. Hence, artificial ponds are recommended in the Bhabar zone which will help the communities to combat water scarcity during dry seasons.

Acknowledgment

The authors would like to thank the Central Department of Geology, Tribhuvan University, Nepal, and the President Chure Terai Madhesh Conservation Development Board for providing research facilities and financial support as a part of government to government (G-to-G) research project entitled " Aquifer mapping and sensitivity analysis of watershed systems of Chure region" between these two governmental organizations of Nepal Authors would like to extend their thanks to the reviewers who provided valuable suggestions and feedback in the draft manuscript.

Author contribu`tion

All the authors have made significant contributions to the development of this research article. First, Dr. Kabi Raj Paudyal and Ms. Sumitra Dhungana made the study concept and design. Ms. Goma Khadka accompanied the fieldwork with Sumitra Dhungana for two weeks and contributed a lot to field data collection. Dr. Kabi Raj Paudyal and Dr. Ram Bahadur Shah took verification traverses in the field with the team members. Ms. Manjari Acharya assisted in compiling and analyzing the field data. Ms. Goma Khadka also provided technical support to digitize the maps. The initial draft of the manuscript was written by Goma Khadka and all authors contributed to making the draft form of the manuscript into the final version. Finally, all the authors have contributed to making corrections as per the suggestion of reviewers.

Data availability

The data that support the findings of this study are available from the corresponding author, upon reasonable request.

Conflict of interest

The authors declare no competing interests.

References

Aryal, Y. M., Poudel, P., Ansari, K., and Paudyal, K. R. (2023). Application of Geospatial Techniques for Artificial Recharge to Groundwater in Ratu Khola Watershed, Central Nepal. Journal of Institute of Science and Technology, 28(1), 1–10. https://doi.org/10.3126/jist.v28i1.47459

Dahal, A., and Paudyal, K.R. (2022). Mapping of Geological Sensitive Areas along the Budhi Khola Watershed, Sunsari/Morang Districts, Eastern Nepal Himalaya. Journal of Development Innovations, © 2022 Karma Quest International, Canada. Link: www.karmaquest.org/journal (ISSN: 2371-9540), Vol. 6, No. 1, 44-68.

DMG (1984). Geological Map of eastern Nepal, Scale 1:250,000. Department of Mines and Geology, Kathmandu, Nepal.

GoN (2013). Recharge Ponds Handbook for WASH Programme. Department of Local Infrastructure Development and Agricultural Roads (DoLIDAR), Ministry of Federal Affairs and Local Development, Government of Nepal, Kathmandu.

Luitel, S., Pathak, D., and Shrestha, S. R. (2020). Hydrogeological Assessment of Siraha. District Nepal, Journal of Hydrogeology and Hydrologic Engineering, v. 9, 1–6. 10.37532/jhhe.2020.9(1).188

NDWQS (2005). Ministry of Physical Planning and Works, Government of Nepal. National Drinking Water Quality Standards and Directives (NDWQS), p. 21.

Neupane, A., Paudyal, K. R., Devkota, K. C., and Dhungana, P. (2023). Landslide susceptibility analysis using frequency ratio and weight of evidence approaches along the Lakhandehi Khola watershed in the Sarlahi District, southern Nepal. Geographical Journal of Nepal, 16(01), 73–96. https://doi.org/10.3126/gjn.v 16i01.53486

Neupane, A., and Paudyal, K. R. (2021). Lithological Control on Landslide in the Siwalik Section of the Lakhandehi Khola Watershed of Sarlahi District, South-Eastern Nepal. Journal of Development Innovations, © 2022 Karma Quest International, Canada. Link: www.karmaquest.org/journal (ISSN: 2371-9540), Vol. 5, No. 2, 44-65.

Pathak, D. (2016). Water Availability and Hydrogeological Condition in the Siwalik Foothill of East Nepal, Nepal Journal of Science and Technology, v. 17, 36–37. https://doi.org/10.3126/njst.v17i1.25061

Paudyal, K. R., Sah, R. B., Paudel, P. N., Acharya, P. C., Sayami, M., Khadka, G., Thapa, A., and Paudayal, K. N. (2023). Water Management in Hariwan Municipality of Nepal: Groundwater Harvesting from Riverbeds and Aquifers. Bulletin of Department of Geology, Tribhuvan University, Kathmandu, Nepal, vol. 24, 2023, 1-14. https://doi.org/10.3126/bdg.v24i.68372

Shrestha S, Devkota K, Dahal N, Neupane K.R. (2021). Application of recharge ponds for water management: Explaining from nature-based solution perspective. Dhulikhel's Journey Towards Water Security, pp.142-163.

UN Environment-DHI., UN Environment and IUCN (2018). Nature-based solutions for water management: A Primer U.S. Environmental Protection Agency, 2003. Protecting water quality from urban runoff. EPA 841-F-03-003. U.S. Environmental Protection Agency, Washington, DC, USA.

UN Water (2018). UN World Water Development Report, Nature-based Solutions for Water.

Un.org (2022). The human right to water sanitation: https://www.un.org/waterforlifedecade/pdf/human_right_to_water_and_sanitation_media_brief.pdf.

Journal of Nepal Hydrogeological Association (JNHA), Vol (1), 94 -106 (2024)
ISSN: 3059-9725 (Online)

RESEARCH ARTICLE

GIS-Based analysis of landslide susceptibility in Madi Watershed: Nepal

***Ramjee Prasad Pokharel[1] and Mishan Gurung[1]**
[1]Department of Geography, Prithvi Narayan Campus, Tribhuvan University, Nepal
**Corresponding author: ramjeepp@gmail.com*
***(Submission Date**: 2 July 2024; **Accepted Date:** 29 August 2024)*

ABSTRACT

Landslides are known as the most calamitous natural hazard in Nepal, posing significant threats to human lives, infrastructure, and natural resources. The main objective of this study is to use the Weighted Overlay Method (WOM) in ArcGIS software to generate a map of landslide susceptibility in the study area. Landslide susceptibility assessment is essential to recognize the high-risks areas, which in turn will help solidify land-utilization planning decisions, risk minimization, and disaster prevention measures. The WOM is produced using raster-based Geographic Information System (GIS) employing characteristics such as aspect, curvature, elevation, geology, NDVI (Normalized difference vegetation index), rainfall, distance from rivers, and slope. The analysis of the obtained results shows that slope, geology and rainfall have the greatest influence on landslide occurrence, particularly in the northern region. The study area was classified into four classes of vulnerability zones based on the analytical results. The results showed that increasing elevation, precipitation, non-vegetative land and slope influence the frequency and magnitude of landslides. Consequently, 0.003 percent of total area of watershed were classified as "Low Susceptibility" to landslides, whereas the "Very High Susceptibility" has coverage of 3.447 percent. Similarly, "Moderate Susceptibility" covers 25.703% of the total area and "High Susceptibility" covers 70.847% of the watershed's total area. The areas of high and moderate risk mainly consist of hilly terrain, due to steep slopes and gravity. The region of moderate vulnerability has primarily located in mountainous regions, attributable to hilly vegetation and cloudy weather conditions. In general, aspect with Southeast to Southwest part was more vulnerable to landslides along with increased rainfall and elevation factors with slope degree heightened the area's vulnerability."

Key Words: ***Landslide, Madi watershed, susceptibility, vulnerability, weighted overlay***

INTRODUCTION

The term 'landslide' is typically described as "the descending movement of a mass of rock, debris, or earth under the influence of gravity, with or without water in solid or liquid form." Landslides refer to the gravitational-induced movement of debris, rocks, soil, and earth (Cruden and Varnes, 1996). A landslide can consist of rock, soil, or both, are classified depending on the material and its movement. A slide can be made up of rock or soil or a combination of both. When it is fine it is termed as earth and when it is a little large it is referred to as debris. The manner or mode of motion, such as fall, topple, slide, spread, or flow, describes how the material advances. Such words as "rockfall" and "debris flow" refer to landslides because they incorporate both the material and the movement. A complicated failure involving multiple types of movement, such as a rockslide-debris flow, can also result from a landslide (Highland and Bobrowsky, 2008; Cutter et al., 2013). Landslides occur in a variety of environments, characterized by either

steep or gentle slope gradients from mountain ranges to coastal cliffs or even underwater. Even regarding the process of landsliding, knowledge of what controls this process and how these controls are interrelated, remains chiefly unknown as it is therefore evident that geographical location influences those agents that cause natural landslides (Regmi et al., 2010; Ghimire, 2011; Lin et al., 2013; Wang et al., 2015; Petley et al., 2007). Additionally contributing to the occurrence of landslides, one can include such human initiated actions as construction of roads, dams and other similar infrastructural projects. Another significant cause of landslides is also disturbances by mankind through constructing roads or dams and any other man-made project (Erskine, 1973; Hunt et al., 1993; Arbanas and Arbanas, 2015).

Nepal is situated in a seismically very active zone of the earth where the Indian plate is thrusting beneath the Eurasian plate (Chaulagain et al., 2015). This has weakened the slopes, reduced the slope stability threshold, and caused numerous landslides (Dahlquist and West, 2019). The varied geographical features, intricate topography, and geomorphology, as well as the presence of active seismic faults, recent geological formations, and fluctuating climatic patterns attributed to landslide's susceptibility in Nepal (Petley et al., 2007; Bhandary et al., 2013; K. C. et al., 2021). Landslides pose a significant threat to human lives, infrastructure, and natural resources in Nepal, making it one of the most calamitous natural hazards in the country. More than 80% of Nepal's population is prone to natural hazards such as floods, landslides, windstorms, hailstorms, fires, earthquakes, and glacial lake outburst floods (Ministry of Home Affairs [MoHA], 2017). Over the course of the past ten years (2011-2020), a total of 2121 landslide incidents were reported, in addition, resulting the tragic loss of 1206 individuals (K. C. et al., 2023). According to Nepal Disaster Risk Reduction Portal, the landslides exhibit a gradual increase from May to July, reaching their peak, before subsiding in September coinciding with the monsoon season which takes place from June to September.

Landslide susceptibility mapping identifies the probability of landslides in a zone, which in turn will help solidify land-use planning decisions, risk management, and disaster prevention measures. According to landslide susceptibility mapping theory, new landslides will likely occur in areas with geo-environmental conditions similar to those where previous landslides occurred (Guzzetti et al., 2012). The acquired data were analyzed using the Weighted Overlay Method (WOM), which can model potential regions for landslides. These methods play an important role in producing landslide susceptibility maps, as several previous works have demonstrated the potential of WOM.

Landslides has threatened the communities and ecosystems in the regions of Madi watershed, influenced by unstable geology, steep terrain, and erratic rainfall, as exemplified by the event of 3rd August 2010, which had blocked the river in Naune village, Kaski, endangering the people (Khanal et al., 2013). The existing susceptibility map lacks continuation and updates, further, addressing these gaps by applying Weighted Overlay Method (WOM) in ArcGIS, the study aims to generate a landslide susceptibility map of Madi watershed.

The primary objective of this study is to use (Weighted Overlay Method) WOM in ArcGIS software to create a map of the susceptibility of landslides in the study area. The Weighted Overlay Method (WOM), which is produced using raster-based GIS (Goodchild, 2011) employing characteristics such as aspect, curvature, elevation, NDVI, rainfall, distance from river and slope, will be utilized in developing the landslide susceptibility map.

Study area

The figure illustrated as Fig. 1 depicts the watershed of the Madi River, which is the study area, covering

an estimated area of 1123 sq.km. This region falls under the jurisdiction of three districts, viz., Kaski, Lamjung, and Tanahun, located in the Gandaki Province. Eventually, this stream converges with other tributaries to form the Gandaki River basin, which is the second-largest river basin in Nepal. The coordinates for the study area are 84°0'0" E to 84°20'0" E longitude and 28°0'0" N to 28°30'0" N latitude, with the elevation ranging from 303 meters to 7943 meters above sea level. The area encompasses three main geological formations: Lesser Himalayan meta-sediments, Higher Himalayan crystalline rocks, and Tibetan sedimentary Tethys sediments.). The Madi Watershed of south western part of Nepal has high vulnerability to environment degradation due to complication in geology, increased slope of the area and excessive monsoon precipitation (Khanal and Watanabe, 2008,). Likewise, upper part of the area has slope gradient which is highly steep and amount of rainfall is higher comparatively (Gurung, 2013). The name "Madi" is a portmanteau of the words “Ma,” which means 'mother,' and “di,” which means 'water' in the Magar language. Kapuche Lake, recognized as Nepal's lowest elevated glacier lake, is located at an altitude of 2546 meters above sea level. This lake serves as the origin of the Madi River.

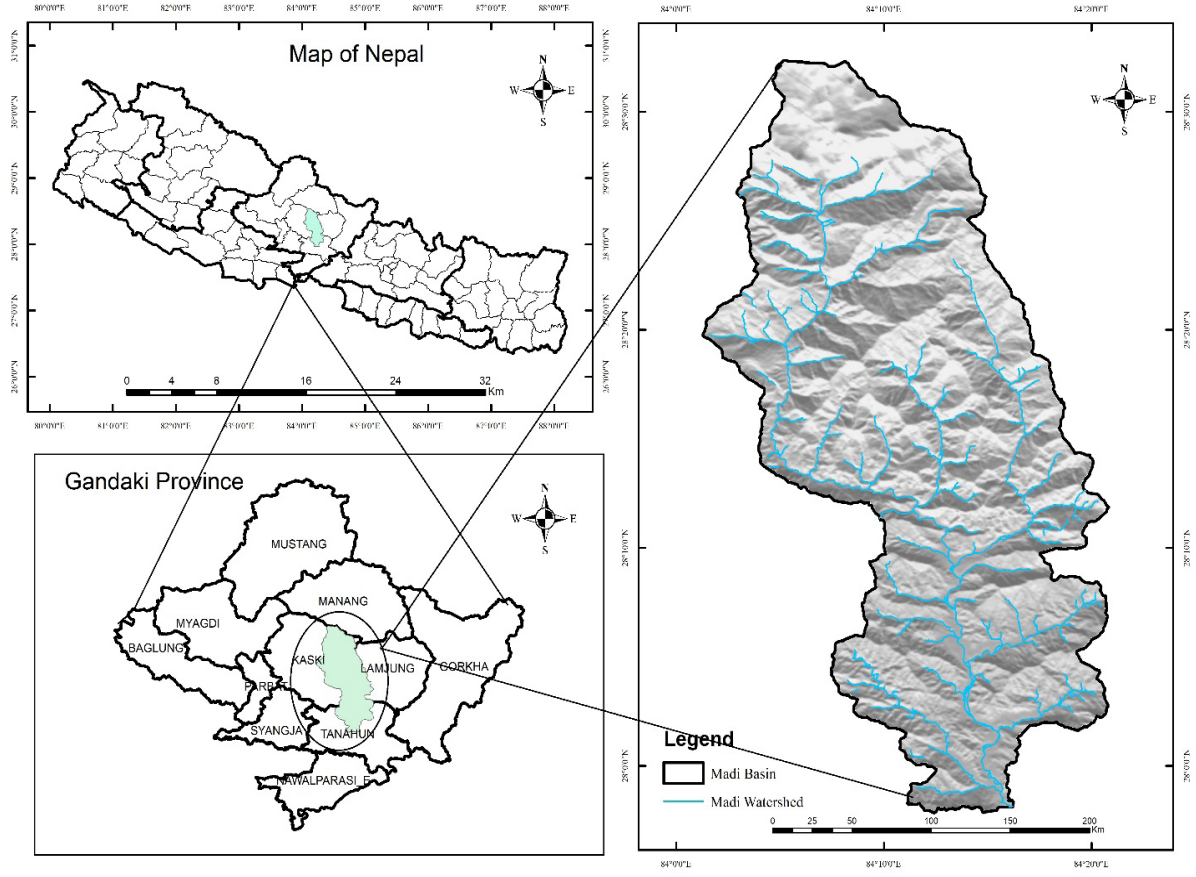

Fig. 1: Location map of the study area

METHODOLOGY

The Weighted Overlay Method (WOM) is a widely used method for combining different layers into a single output layer, where the method involves assigning a weight to each layer according to its relative significance in determining landslide susceptibility (Jamil et al., 2022). This study follows following research design:

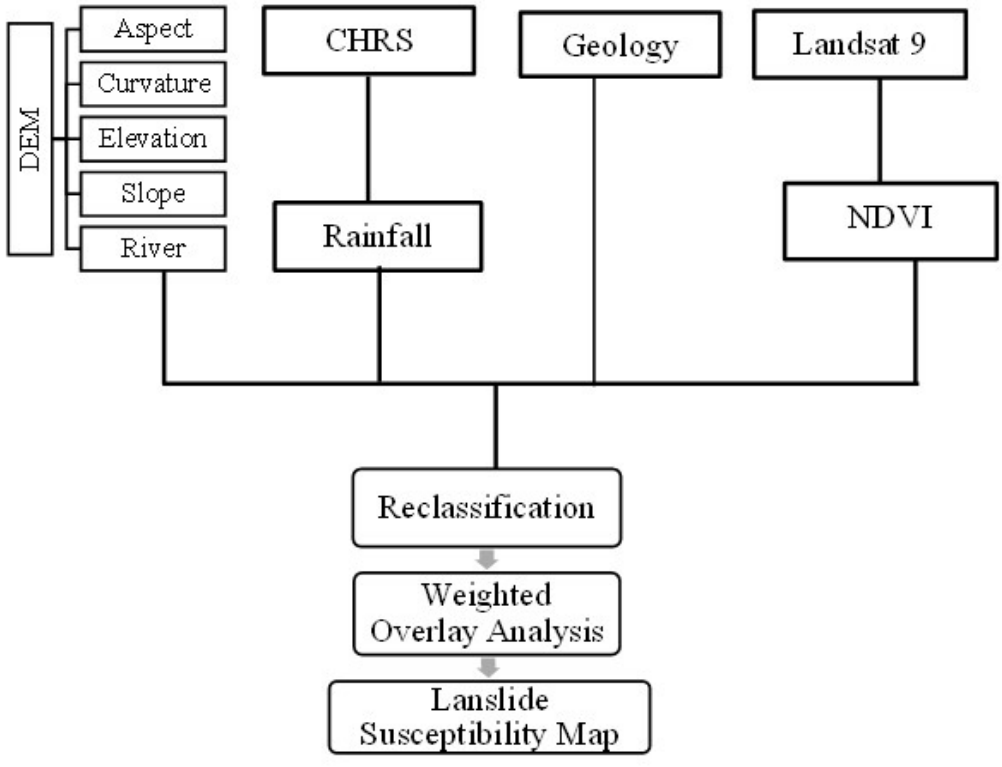

Fig. 2: Research design

WOM combines various environmental factors for the landslide susceptibility analysis as each factor is allocated an appropriate weight so as to detect vulnerable areas (Shit et al., 2016). It was combined with utilization of remote sensing and geographic information system (GIS) techniques to create the map of the Madi watershed's landslide susceptibility. A Digital Elevation Data (DEM) and Landsat 9 of resolution 30m were extracted from Earth Explorer (earthexplorer.usgs.gov). Additional data on rainfall was sourced from CHRS Data Portal. To determine the likelihood of landslides in each area, the information with data on aspect, curvature, elevation, geology, NDVI, rainfall, distance from rivers, and slope were overlaid. When integrating each of these different types of data in the ArcGIS Spatial Analyst tool, it was able to build up a holistic perspective of the area's likelihood of landslide occurrence.

Table 1: Open-source spatial dataset used in study

S.N.	Data	Resolution	Source
1	DEM and Landsat 9	30m	Earth Explorer (earthexplorer.usgs.gov)
2	Rainfall	0.25°*0.25°	CHRS Data Portal (uci.edu)
	Geology		U.S. Geological Survey (Wandrey & Law, 1998)
3	Geology		U.S. Geological Survey (Wandrey and Law, 1998)

The Weightage were assigned manually in terms of influencing factors under the expert opinion and literature's related to landslide susceptibility. In addition, the entries for scale value were done in terms of suitability; 1 being not suitable followed by 2 less suitable, 3 being moderate, 4 for suitable and 5 highly suitable and more. Rainfall is a key trigger for likelihood of a landslides by decreasing shear strength and increasing pore, especially in regions with steeper slope (Crozier, 2010b). That's why, rain and slope were identified as significant factors for landslide susceptibility with the weighted of 15 and 30 percent, respectively. Geology is the second most crucial factor assigned 20 percent as sedimentary rocks are comparatively softer and vulnerable to weathering and can contain clay or shale and will slide over each other when wet (What Are Sedimentary Rocks?) (U.S. Geological Survey, 2016). Also, it is necessary to note that some metamorphic rocks may contain weak plane that causes them to slide in the given circumstances. Aspect is the also most crucial factor assigned 10 percent. It is important to note that NDVI and elevation are assigned a weight of 5 percent each and curvature 10 percent. In the case of curvature, concave curvature (negative values) indicates areas of concentration where water flows across the surface of the earth to increase water accumulation. This can lead to a situation where the volume of water in the soil becomes higher, which serves as a catalyst for landslides (Zhou et al., 2002). Generally, some factor like aspect (10%) which is direction of slope face; where Southeast to Southwest part is more vulnerable to landslides as conditions like exposure of the sun that causes drying and subsequent cracking of the soil hence releases a lot of strength and cohesion (Pareta and Pareta, 2012). Therefore, the scale value of five has been assigned to the aspect for category of 144.78376 to 209.89107 degree. The weightage for river was given five percent.

Table 2: Weightage distribution for parameters (Weightage of each sub-class of landslide conditioning factor using expert opinion)

Parameters	Class	Field Value	Scale Value (weightage)
Aspect (10 %)	-1 to 74.014945 (N- E to NE)	1	2
	74.014945 to 144.78376 (E – NE to SE)	2	4
	144.78376 to 209.89107 (SE to SW)	3	5
	209.89107 to 280.659886 (SW to W- NW)	4	3
	280.659886 to 359.920959 (W-NW to N)	5	1

Parameters	Class	Field Value	Scale Value (weightage)
Curvature (10%)	-6.224893 to -0.957676 (Highly Concave)	1	5
	-0.957676 to -0.25202 (Concave)	2	4
	-0.25202 to 0.264621 (Flat)	3	3
	0.264621 to 0.982878 (Convex)	4	2
	0.982878 to 6.552519 (Highly Convex)	5	1
Elevation (m) (5%)	304	1	1
	2196	2	2
	4089	3	3
	5981	4	4
	7873	5	5
Geology (20%)	Tertiary Igneous Rock	1	3
	Jurassic Metamorphic & Sedimentary Rock	2	4
	Others	3	1
	Undivided Precambrian Rock	4	2
NDVI (5%)	-0.133167 to 0.013554 (non-vegetation)	1	5
	0.013554 to 0.090907 (Low Vegetation)	2	4
	0.090907 to 0.153757 (Moderate Vegetation)	3	3
	0.153757 to 0.20452 (High Vegetation)	4	2
	0.20452 to 0.419659 (Very High Vegetation)	5	1
Rainfall (mm) (15%)	829 – 923	1	1
	924 – 1021	2	2
	1022 – 1124	3	3
	1125 – 1218	4	4
	1219 – 1413	5	5
River (5%)	500	1	5
	900	2	4
	1700	3	3
	5500	4	2
	7000+	5	1
Slope(degree) (30%)	0 – 13	1	1
	14 – 22	2	2
	23 – 30	3	3
	31 – 40	4	4
	41 – 60	5	5

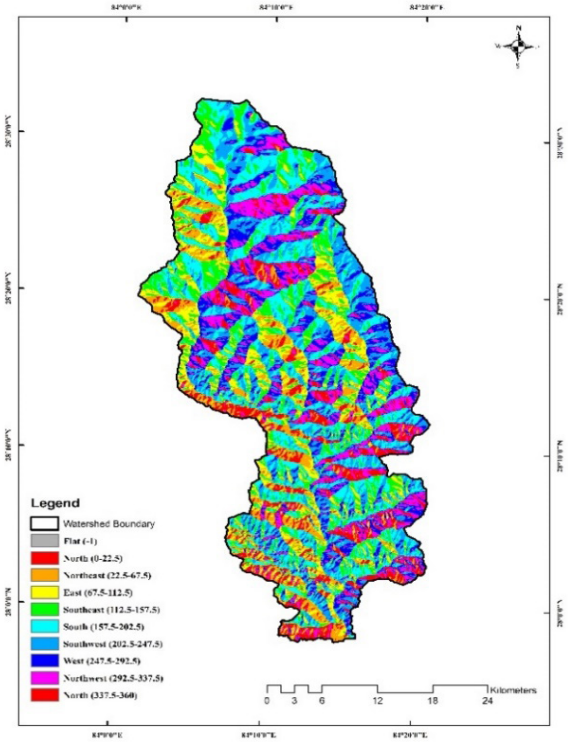

Fig. 3: Aspect map of Madi watershed

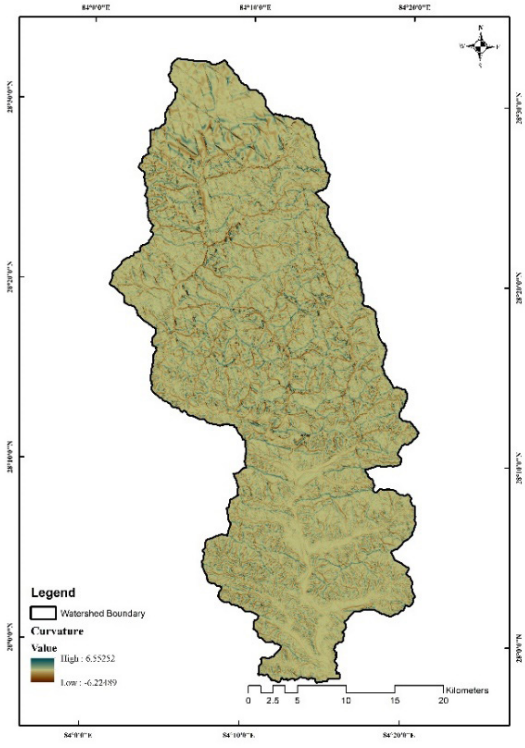

Fig. 4: Curvature Map of Madi watershed

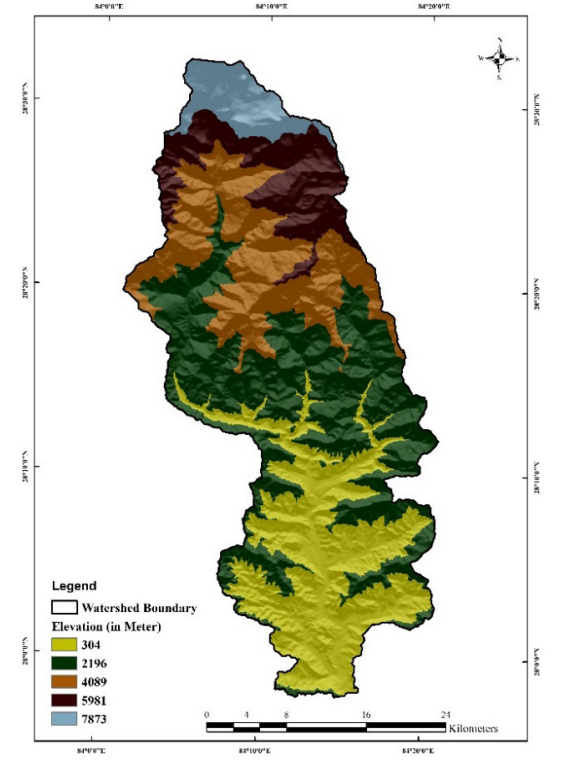

Fig. 5: Elevation Map of Madi watershed.

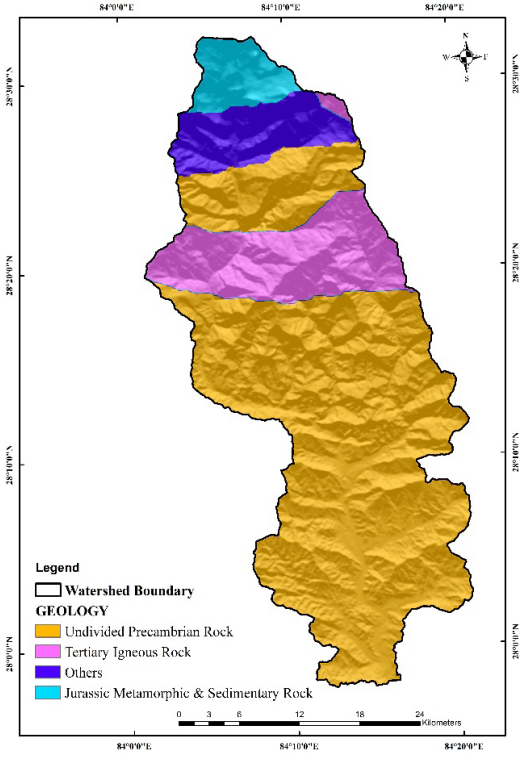

Fig. 6: Geology Map of Madi watershed.

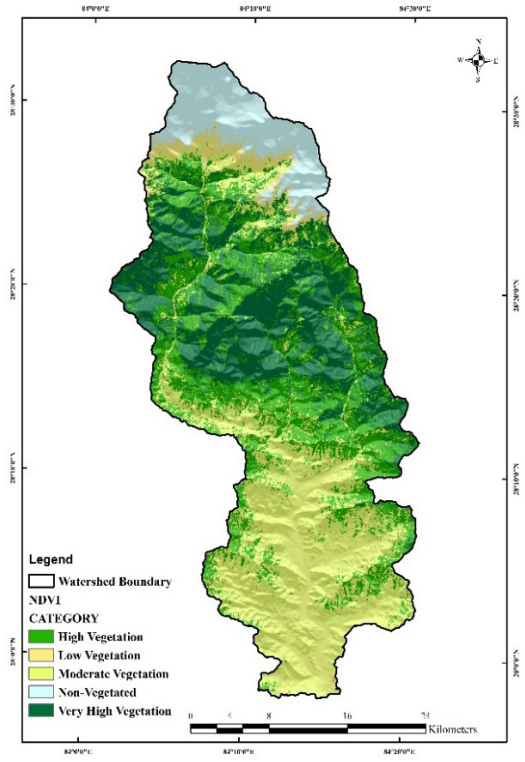

Fig. 7: NDVI Map of Madi watershed.

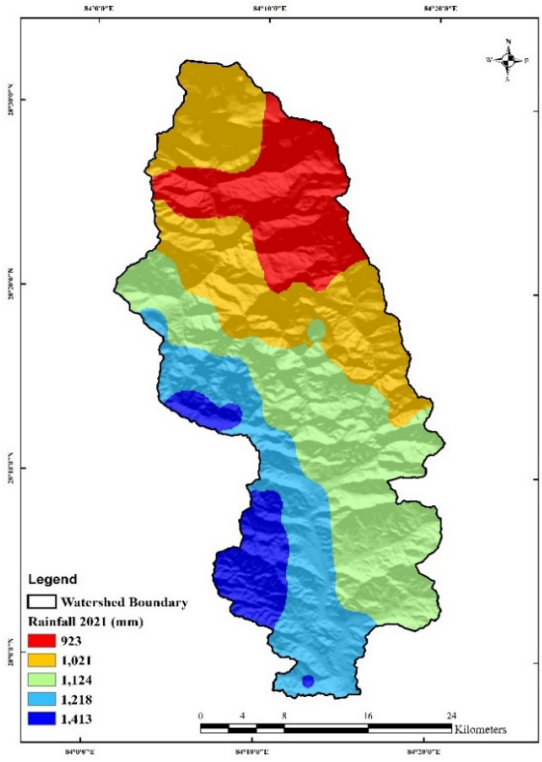

Fig. 8: Rainfall Map of Madi watershed.

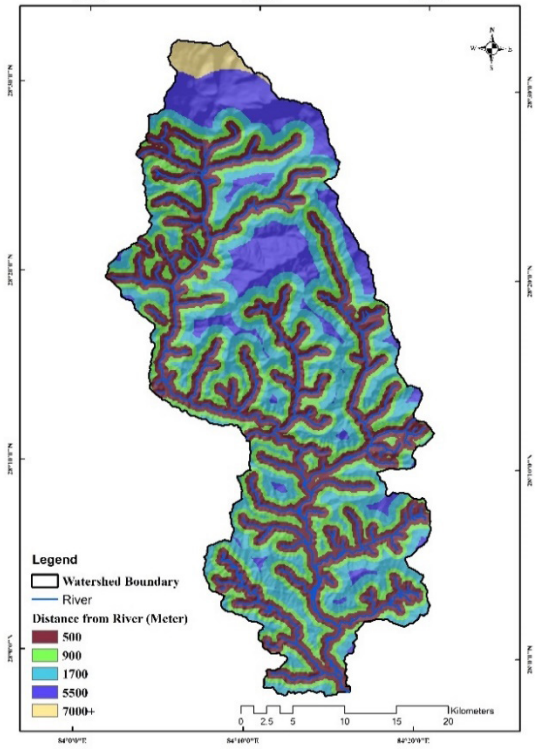

Fig. 9: River Map of Madi watershed.

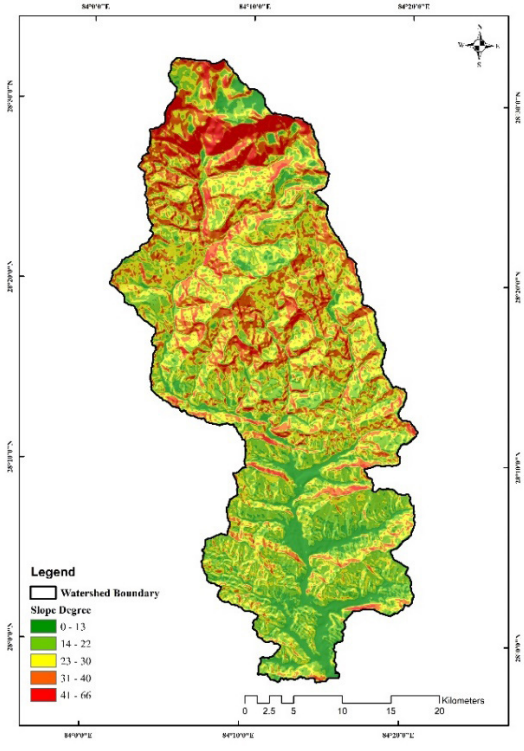

Fig. 10: Slope Map of Madi watershed.

RESULT AND DISCUSSION

For this study, all the thematic maps of the study area were classified with respect to seven criteria using the Weighted Overlay Method (WOM) in ArcGIS 10. 4 assigning weights for each parameter manually. The Table 3 and Fig. 9, represents the landslide susceptibility of Madi watershed.

Table 3: Classes of Landslide Susceptibility

S.N.	Susceptibility Classes	Area (sq.km)	Landslide %
1	Low Susceptibility	0.037	0.003
2	Moderate Susceptibility	288.645	25.703
3	High Susceptibility	795.617	70.847
4	Very High Susceptibility	38.701	3.447
	Total	1123	100

The classes range from "Low Susceptibility" to "Very High Susceptibility". The largest region of watershed comes under 'High Susceptibility' class with 795.617 square kilometers coverage, which accounts for 70.847% of the total area. From the distribution, it indicates that almost three-quarters of the watershed area represents the high susceptibility to landslides. Followed by "Moderate Susceptibility" class that comprises 288.645 square kilometers (25.703% of total area), depicting a substantial portion of watershed moderately risk of experiencing landslides. At the same time, "Very High Susceptibility" category covers 38.701 square kilometers, accounts for 3.447% of overall area of the watershed, indicating areas with a decreased landslide risk when compared to first two categories, but higher risk of landslide among all susceptibility class. On the other hand, "Low Susceptibility" class are relatively smaller in coverage as shown in the map (Fig. 11) below, occupying just 0.037 square kilometers (0.003%). The Fig. 11 highlight that a minimal portion of the region falls under extreme prone in susceptibility spectrum. Distribution of this risk reveals that the majority of the region is with moderate to high risks while there is very little area with either very low or very high risk of landslides.

While very highly susceptibility zones comprise a smaller percentage, they require intensive approaches to eliminate tendencies towards landslides and reduce the impacts of the phenomenon. However, the low susceptibility areas are relatively static but should be kept this way to maintain their motionless nature as the potential damages they could cause can be enormous and could potentially turn into devastating zones in the future. Overall, the area's general landslide risk varies from low to high; therefore, implementation of proper planning of land use and monitoring is crucial. The susceptibility map can be an essential instrument for local officials and urban planners to pinpoint high-risk zones and determine which mitigation strategies should take precedence. Additionally, it aids in the development of land use regulations and emergency response plans aimed at minimizing the threat of landslides.

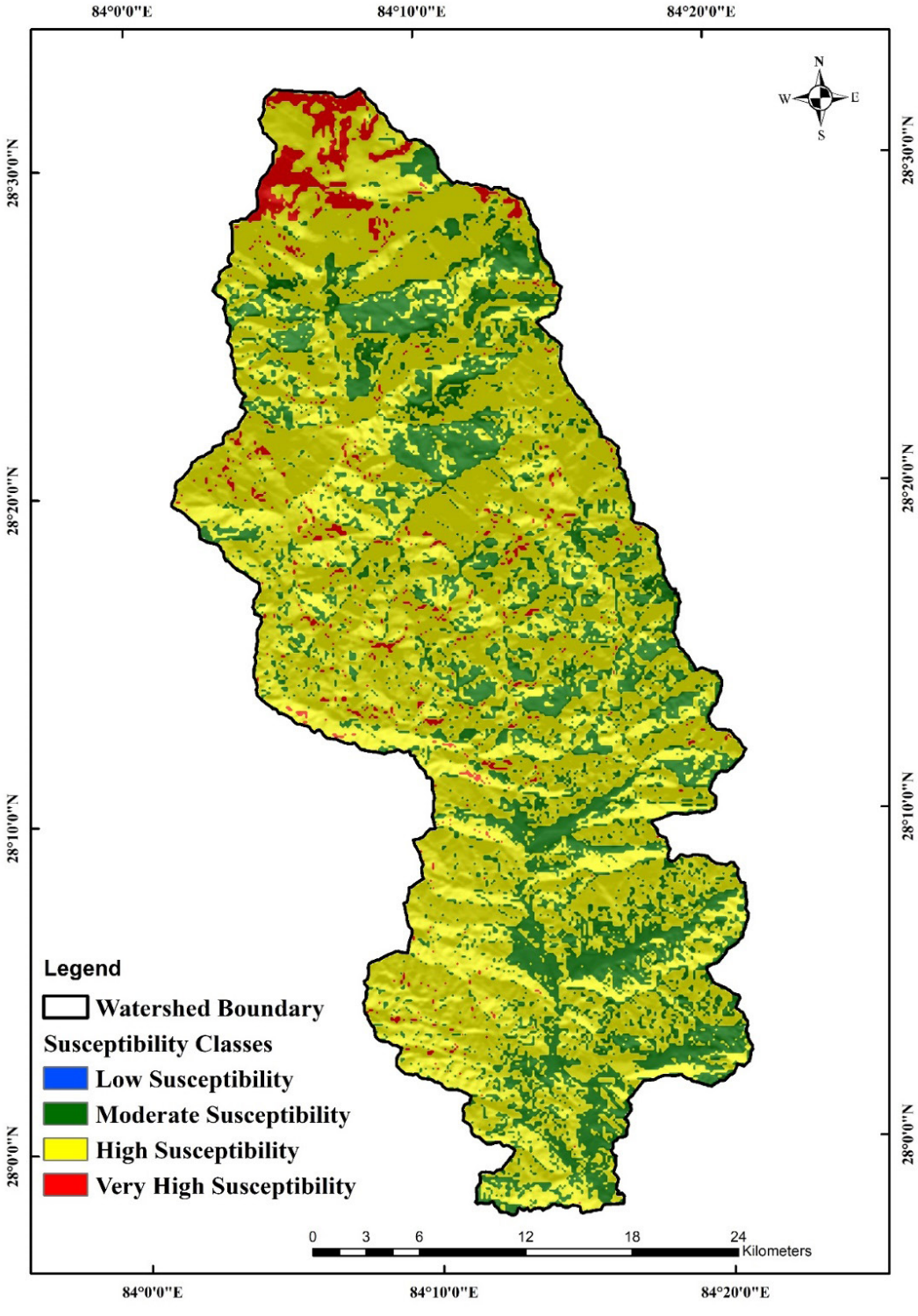

Fig. 11: Landslide susceptibility map derived from weighted overlay method

CONCLUSION

In conclusion, this study demonstrates the effectiveness of the Weighted Overlay Method in creating a map of the Madi watershed's landslide susceptibility. The analysis of landslide susceptibility in the study area indicates a significant prevalence of high-risk zones; it can be stated that most of the area belongs to high and moderate susceptible regions and combinedly make up more than 95% of the total area of the Madi watershed. That is why, it is possible to conclude that the quantity of the territory which contains a high risk of landslides constitutes important portion of the territory need to be undertaken the measures that will help in preventing the risk of landslide. Furthermore, the" Very High Susceptibility" areas are constrained to a small percentage of the total geographic area, which is approximate 3.447%, it requires intensive and strong preventive measures due to its highest sensitivity to landslide hazards. Although the "Low Susceptibility" areas has received little coverage in this paper, it also requires high concern because of their sensitivity and influence on surrounding areas. The level of detail thus enables the planners in the fields of land-use planning, development of infrastructure and planning of disaster preparedness measures.

Based on the study findings, we conclude that the landslide susceptibility map needs to be frequently revised with the existing environment as well as the climatic conditions undergoes constant change. The integration of this data provides a comprehensive assessment of landslide risk by integrating various conditioning factors, which helps with urban planning and disaster preparedness efforts, for the reason that has revealed several areas that are highly susceptible to landslides, which could have disastrous repercussions for those residing there. The areas of high and moderate landslide risk mainly consist of hilly terrain, where steep slopes and gravity can cause landslides. Mapping landslide susceptibility in mountainous regions is usually difficult due to poor access, dense vegetation, and cloudy weather conditions. Based on the obtained results, it is evident that slope, higher elevated region, precipitation and non-vegetative zone greatly influence landslide occurrence. Mostly, regions with high precipitation, slope instability and non-vegetative region, especially in the northern region land having exposure to sun are in the vulnerable zone. Close proximity to rivers in these zones could lead to landslides that might block rivers and create debris dams, which could burst and produce floods affecting anthropogenic activities. More importantly, the zones that are identified as high landslide susceptibility doesn't mean that landslide will occur any soon, it is indication of more favorable to landslides. Furthermore, in mitigating risk of landslides, it becomes necessary to have modern forms of monitoring and warning system in zones that are moderately to highly vulnerable. Moreover, the land-use policies should encourage the proper use of the land and restrict approval of risky activities. Landslide awareness, sustainable construction, and civil engineering procedures including help using retaining walls and effective drainage techniques need to be taught to the people of the community. Additionally, new research aimed at refining existing susceptibility maps, coordinated actions of scientific institutions and governmental bodies, and cooperation with the inhabitants will improve the efficiency of disaster management and actions.

As this study is based on secondary data and it hasn't been verified with the historical landslide inventory so, there need to be conducting additional investigations for more accuracy. There are also need of exploring different approaches to weighting the various variables used in the analysis. While the Weighted Overlay Method is useful, other techniques such as the Analytical Hierarchy Process (AHP) might be more appropriate depending on the data or terrain characteristics. Future projects can enhance the precision and reliability of their findings by considering alternative approaches.

REFERENCES

Arbanas, S. M. and Arbanas, Z., 2015. Landslides: A guide to researching landslide phenomena and processes, In Guarina-Medimurec, N., eds., Handbook of Research on Advancements in Environmental Engineering, Chapter 17, 474-510. doi:10.4018/978-1-4666-7336-6

Bhandary, N. P., Yatabe, R., Dahal, R. K., Hasegawa, S. and Inagaki, H., 2013. Areal distribution of large-scale landslides along highway corridors in central Nepal. Georisk, 7(1), 1–20. doi.org/10.1080/17499518.2012.743377.

Chaulagain, H., Rodrigues, H., Silva, V., Spacone, E. and Varum, H., 2015. Seismic risk assessment and hazard mapping in Nepal. Natural Hazards, 78(1), 583-602. https://doi.org/10.1007/s11069-015-1734-6.

Crozier, M., 2010b. Deciphering the effect of climate change on landslide activity: A review. Geomorphology, 124(3–4), 260–267. doi.org/10.1016/j.geomorph.2010.04.009

Cruden, D. M. and Varnes, D. J., 1996. Landslide types and processes. In Landslide Investigation and Mitigation. Special Report 247. https://www.researchgate.net/publication/209802944

Cutter, S. L., Ash, K. D. and Emrich, C. T., 2013. The geographies of community disaster resilience. Global Environmental Change, 23(6), 1571-1582.

Dahlquist, M. P. and West, A. J., 2019. Initiation and runout of post-seismic debris flows: Insights from the 2015 Gorkha earthquake. Geophysical Research Letters, 46(16), 9658-9668. https://doi.org/10.1029/2019GL083548.

Erskine, C.F., 1973. Landslides in the vicinity of the Fort Randall Reservoir, South Dakota; A study of some fundamental causes of landslides in the Pierre Shale along the Missouri River trench. U.S. Department of the Interior, Geological Survey Professional Paper 675.

Ghimire, M., 2011. Landslide Occurrence and Its Relation with Terrain Factors in the Siwalik Hills, Nepal: Case Study of Susceptibility Assessment in Three Basins. Natural Hazards, 56, 299-320. https://doi.org/10.1007/s11069-010-9569-7.

Goodchild, M. F., 2011. Geographic information systems and science: Today and tomorrow. Annals of GIS, 17(1), 3-9.

Gurung, S. B., 2013. Landslide susceptibility analysis of Madi watershed, Nepal. ResearchGate. https://www.researchgate.net/publication/315662384.

Guzzetti, F., Mondini, A. C., Cardinali, M., Fiorucci, F., Santangelo, M. and Chang, K. T., 2012. Landslide inventory maps: New tools for an old problem. Earth-Science Reviews, 112(1-2), 42-66.

Highland, L. M. and Bobrowsky, P., 2008. The landslide handbook—A guide to understanding landslides. U.S. Geological Survey Circular 1325.

Hunt, R. E., Miller, S. M. and Bump, V. L., 1993. The Forest City Landslide. International Conference on Case Histories in Geotechnical Engineering. 60. https://scholarsmine.mst.edu/icchge/3icchge/3icchge-session01/60.

Jamil, R. M., Fadzil, F. N., Nawawi, S. A., Nor, A. N. M., Sulaiman, N., Sulaiman, N. and Ibrahim, N., 2022. Landslide susceptibility mapping using Geographic Information System (GIS) in Kuala Balah, Jeli, Kelantan. IOP Conference Series: Earth and Environmental Science, 1102(1), 012048. doi:10.1088/1755-1315/1102/1/012048.

K. C. R., Aryal, M., Dahal, B. M. and Sharma, K., 2021. Spatial and temporal analysis of landslides during last decade in Nepal. Conference Paper October 2021. ResearchGate. https://www.researchgate.net/publication/358987469

K. C, R., Sharma, K., Dahal, B. K., Aryal, M. and Subedi, M., 2023. Study of the spatial distribution and the temporal trend of landslide disasters that occurred in the Nepal Himalayas

from 2011 to 2020. Environmental Earth Sciences, 83(1). https://doi.org/10.1007/s12665-023-11347-7.

Khanal, N. R., Koirala, A., Gurung, S. B., Kumar, U., Rijal, R., Sigdel, S., Acharya, C. and Yadav, U. P., 2013. Madi River, Nepal: Landslide dam outburst flood risk management. ICIMOD.

Khanal, N. R. and Watanabe, T., 2008. Landslide and debris flow in the Himalayas: A case study of the Madi Watershed in Nepal. Himalayan Journal of Sciences, 2(4), 180–181.

DOI: 10.3126/hjs.v2i4.864.

Lin, C. W., Tseng, C. M., Tseng, Y. H., Fei, L. Y., Hsieh, Y. C. and Tarolli, P., 2013. Recognition of large-scale deep-seated landslides in forest areas of Taiwan using high resolution topography. Journal of Asian Earth Sciences, 62, 389-400.

Ministry of Home Affairs, 2017. Nepal disaster report: The road to Sendai. http://drrportal.gov.np/uploads/document/1321.pdf.

Mitchell, T. M., Smith, S. A., Anders, M. H., Di Toro, G., Nielsen, S., Cavallo, A. and Beard, A. D., 2015. Catastrophic emplacement of giant landslides aided by thermal decomposition: Heart Mountain, Wyoming. Earth and Planetary Science Letters, 411, 199-207.

Nepal Disaster Risk Reduction Portal, (n.d.). http://www.drrportal.gov.np.

Nguyen, P., Shearer, E. J., Tran, H., Ombadi, M., Hayatbini, N., Palacios, T., Huynh, P., Braithwaite, D., Updegraff, G., Hsu, K., Kuligowski, B., Logan, W. S. and Sorooshian, S., 2019b. The CHRS Data Portal, an easily accessible public repository for PERSIANN global satellite precipitation data. Scientific Data, 6(1). https://doi.org/10.1038/sdata.2018.296.

Pareta, K. and Pareta, U., 2012. Landslide Modeling and Susceptibility Mapping of Giri River Watershed, Himachal Pradesh (India), International Journal of Science and Technology 1(2) 91-104. https://www.researchgate.net/publication/225284445.

Petley, D. N., Hearn, G. J., Hart, A., Rosser, N. J., Dunning, S. A., Oven, K. and Mitchell, W. A., 2007. Trends in landslide occurrence in Nepal. Natural Hazards, 43(1), 23–44. https://doi.org/10.1007/s11069-006-9100-3.

Regmi, N.R., Giardino, J.R. and Vishnu, D., 2010. Mapping landslide hazards in western Nepal: Comparing qualitative and quantitative approaches. Environmental and Engineering Geoscience, 16(2), 127-142. doi.10.2113/gseegeosci.16.2.127.

Sharma, P. and Joshi, S., 2016. Urban growth and its impact on the vulnerability of Pokhara City, Nepal. Land Use Policy, 58, 25-38.

Shit, P. K., Bhunia, G. S. and Maiti, R., 2016. Potential landslide susceptibility mapping using weighted overlay model (WOM). Modeling Earth Systems and Environment, 2(1). https://doi.org/10.1007/s40808-016-0078-x.

Wandrey, C. J. and Law, B. E., 1998. Maps showing geology, oil and gas fields and geologic provinces of South Asia. U.S. Geological Survey Open File Report/Open-file Report. https://doi.org/10.3133/ofr97470c.

Wang, G., Li, T., Xing, X. and Zou, Y., 2015. Research on loess flow-slides induced by rainfall in July 2013 in Yan'an NW China. Environmental Earth Sciences, 73, 7933-7944.

What are sedimentary rocks? U.S. Geological Survey. (2016, July 20). https://www.usgs.gov/faqs/what-are-sedimentary-rocks.

Zhou, C., Lee, C., Li, J. and Xu, Z., 2002. On the spatial relationship between landslides and causative factors on Lantau Island, Hong Kong. Geomorphology, 43(3–4), 197–207. https://doi.org/10.1016/s0169-555x(01)00130-1.

Journal of Nepal Hydrogeological Association (JNHA), Vol (1), 107-134 (2024)
ISSN: 3059-9725 (Online)

RESEARCH ARTICLE

Assessment of the 2021 debris flow and flood related loss and damage in Melamchi Watershed of Central Nepal

***Subash Duwadi[1], Danda Pani Adhikari[1], Megh Raj Dhital[2] and Nawaraj Parajuli[3]**

[1]Department of Environmental Sciences, Tri-Chandra Multiple Campus, Tribhuvan University, Kathmandu, Nepal

[2]Department of Geology, Tri-Chandra Multiple Campus, Tribhuvan University, Nepal

[3]Department of Geology, Prithvi Narayan Campus, Pokhara, Nepal

**Corresponding author's email: subash.duwadi@trc.tu.edu.np*

***(Submission Date**: 22 July 2024; **Accepted Date:** 1 September 2024)*

ABSTRACT

Nepal, characterized by its youthful mountain ranges, predominantly features mountainous terrain that is geologically fragile and at high risk for prone to geodisasters. Factors such as steep slopes, intense summer rainfall, riverbank erosion, landslide and earthquake contribute to these disasters leading to a significant loss of life and property. This study aims to elucidate the 2021 debris flow and flood-related loss and damage and its impact on local livelihoods in the Melamchi Municipality and Helambu Rural Municipality of Sindhupalchok district. Data were collected through both qualitative and quantitative techniques by using household surveys, focus group discussions, key informant interviews, and field observations were carried out. The sample size was determined by using the Arkon and Colton formula. Disruption of infrastructure, extensive sediment deposition and damage across affected areas, significant erosion, river widening, landscape transformation, temporary river blockage, changes in river morphology, formation of new river channels, and the destruction of agricultural lands were observed in satellite imagery and aerial photographs and they were verified in the field. The event heavily impacted Melamchi Bazaar, claiming over 25 lives and causing substantial damage to the Melamchi Water Supply Project and the Melamchi settlement. The survey revealed that 56% of the respondents lost their agricultural land, 28% lost non-agricultural income sources, 11% lost their employment, and a few others lost other income sources. The total estimated loss of the event was USD 436 million in Melamchi and USD 62 million in Helambu Rural Municipality, including the loss and damage of houses, land, crops, and livestock. Flood and landslides are common phenomena in the Nepal Himalaya and the 2021 Melamchi event was unprecedented in terms of the loss and damage. The result of this study can help policy makers and managers with better planning to minimize the impacts of loss and damage of the geodisaster in the future.

Keywords: ***Disaster, Flood, Landslides, Melamchi Watershed, Sediment***

INTRODUCTION

Nepal lies in the central part of the Himalayas and it has young mountains and fragile geological conditions. The country is susceptible to a range of natural hazards, including landslide, debris flow, avalanche, flood glacial lake outburst flood (GLOFs), and earthquake. Factors such as the presence of fragile, fragmented rock, substantial soil and debris covering steep and rugged landscapes, climatic fluctuations, monsoons rain, and frequent seismic activity contribute to the country's vulnerability to natural disasters. Many anthropogenic causes, such as deforestation, rapid encroachments on natural habitats, and land use changes heighten the already existing hazard levels. To effectively create secure urban and mountain environments, it is essential to understand the relationship between geological

and geomorphological factors along with climatic changes.

The Des Inventar and Building Information Platform against Disaster (BIPAD) websites, which catalog past disasters, reveal an increase in the frequency of disasters in Nepal in recent years. Ice avalanches entering a lake can often create a surge wave that breaches the unconsolidated terminal moraine dam (Emmer and Cochachin, 2013; Chen et al., 2017). Other potential trigger mechanisms include displacement waves from rock falls, moraine failure due to dam settlements and/or piping, the degradation of an ice-cored moraine, seismic activity, or the rapid input of water from extreme events or from an outburst flood from a glacial lake located upstream (Rounce et al., 2017a). Twenty-four known GLOF events have been recorded in Nepal, the majority occurring since the 1960s (ICIMOD, 2011). At least five additional GLOFs or glacier-related floods have been reported since then: the Koshi River flood of May 5, 2012 (Kargel et al., 2013), the Langmoche Lake flood of April 25, 2015 (Byers et al., 2017), the Lhotse glacier outburst floods of 2015 and 2016 (Rounce et al., 2017b), Imja Tsho GLOF of Imja valley, Everest region June 2016 (Lala et al., 2018), Tsho Rolpa GLOF of Rolwaling valley (Reynolds, 1999).

Since the 1980s, a number of field-based studies concerned with the causes and impacts of contemporary GLOFs have been conducted in Nepal (Vuichard and Zimmermann, 1987; Cenderelli and Wohl, 2001; Lamsal et al., 2015; Byers et al., 2017). Nearly all have taken place years to decades after the events, and there is often uncertainty as to the actual flood-triggering mechanisms involved (Lamsal et al., 2015). Debris had dammed the floodwaters directly above the village of Barun Bazaar, displacing ten families from their homes, destroying fields, and threatening to impact at least eighty families living within the immediate area if the dam suddenly failed (Shakya, 2017). The lake also threatened downstream villages, including Phaksinda, Diding, Chetabesi, Lumningtar, and other riverside communities in the Bhojpur and Dhankuta districts (My Republica, 2017). Flood devastation in Melamchi is not only because of rains (Mandel, 2021). Experts believe that the land, already weakened by earthquakes, can cause landslides with even a moderate amount of rainfall due to water seepage from the surface. Experts in geology, seismology and hydrology often discuss the impacts of the earthquake on land stability and the increase risk of landslides following seismic events. These experts includes researchers and professionals from organizations such as the United States Geological Survey (USGS), the British Geological Survey (BGS), and academic institutions with the strong geology departments.

According to the Department of Hydrology and Meteorology (DHM), the Melamchi and Indrawati basins experienced rainfall from June 9, 2021. The highest hourly precipitation on June 10 was 22 mm, increasing to 37 mm per hour by June 11. On June 14 and 15, a maximum hourly rainfall of 10 mm was recorded. Sermathang recorded more than 100 mm of daily rainfall on June 11. Over a six-day period, the station received more than 200 mm of rainfall. The intense rainfall and rapid snowmelt led to the erosion of glacial deposits in the headwaters of the Pemdan Khola, Yangri River, and Larche River. A landslide dam formed and subsequently collapsed in Bhemathan near Langtang National Park. A past landslide also formed a natural dam near the confluence between Pemdan Khola and Melamchi Khola on the Melamchi Watershed. This natural dam temporarily blocked the Melamchi River, causing an outburst flood that destroyed settlements, bridges, and roads downstream. The situation was further intensified by heavy rainfall runoff, snowmelt, possible glacial lake outburst, and moraine erosion in the Pemdan Khola region. A second flood event occurred on August 1, 2021, possibly due to heavy rainfall and erosion of the sediment deposited as a result of the first Landslide Dam Outburst Flood (LDOF) event (World Bank, 2021).

The massive downpour, coupled with rapid snowmelt from June 15, led to the erosion of glacial deposits in the far upstream of the Melamchi watershed. This phenomenon caused the formation of a landslide dam and its eventual collapse in Bhemathan. The flood event caused at least 17 casualties and damaged more than 540 houses and critical infrastructure, including bridges and roads. Recovery from the economic impacts may take several years. The effects and impacts of the floods include water depth and residence time, flow velocity, erosive capacity, sediment transport and deposition, and other associated geological phenomena (Andres et al., 2009). Increased temperature will result in an increase in saturation vapor pressure, thereby increasing atmospheric moisture and causing increased rainfall (Allen and Ingram, 2002; Dankers and Feyen, 2008). An increase in the frequency and intensity of rainfall events indicates a higher risk of flooding in the river (Duan et al., 2017).

The frequency and magnitude of floods are also affected by gradual land use change, which may exacerbate the situation (Mallakpour and Villarini, 2015). Floods are complex natural hazards that can cause massive socio-economic damage (Asgharpour and Ajdari, 2011). Increasing frequency and intensity of hydrological extremes pose threats to human life, the economy, infrastructure, and the environment of riverside catchment areas (Maghsood et al., 2018). Among the major disasters in the past decade are the Seti flood in 2012, the Jure landslide dam in 2014, the Gorkha earthquake in 2015, the GLOF in Bhote Koshi in 2016, the Barun Khola flood in 2017, the Terai floods in 2017, the tornado in the Bara-Parsa district in 2019, and the landslide and debris flow in Sindhupalchowk in 2020 (Gurung et al., 2015; Miyake et al., 2017; Geest, 2018; Byers et al., 2019; Shrestha et al., 2019; Liu et al., 2020; Yagi et al., 2021). Nepal faces flood hazards very often (NDRRMA, 2021). Nepal's Disaster Report of 2019 stated that floods and landslides are very common in Nepal and caused 213 fatalities in 2017 and 2018, responsible for national economic losses of over 11 million USD annually.

The Himalayas have steep elevation changes over short distances (Duncan et al., 2003), making landslides and avalanches highly susceptible in the upstream area (Dhital et al., 2021), with debris and slurry sediments (Adhikari et al., 2005). Floods have become one of the most serious natural disasters (Sarhadi et al., 2012; Duan et al., 2022). The nature of floods has become more cascading and widening in dimension over the years, causing significant damage (Gautam et al., 2021; Maharjan et al., 2021). The damage due to floods continues to rise. Due to heavy precipitation in the Tistung area of Makawanpur district (>500 mm in 24 hours), inundation of agricultural land and destruction of more than 67 irrigation schemes occurred (Adhikari et al., 2023). The same flood turned into a devastating debris flow event in some steep terrains, resulting in more than 60 lives lost and 52 houses damaged (Dhital, 2003). In 2021, flood events in the Melamchi River originated from heavy rainfall in the upper catchment area, which contains permafrost in the deglaciated valley. On June 14-15, 2021, heavy rainfall intensified the erosion process, possibly leading to the erosion of the end moraine dam of Pemdan Lake (at 4700 m) and the subsequent emptying of the lake. This resulted in a flash flood in Pemdan Khola, depositing large amounts of boulders, gravel, and sand in the Bhemathan area, an old landslide dam that became filled with sediment and debris. The flood also mixed the trees of Bhemathan with the debris flow of Pemdan Khola, blocking the old landslide area and causing floodwater with debris to flow as overtopping flow through the old landslide dam. Then, on August 1, 2021, heavy rainfall caused the overtopping water flow at the Bhemathan area to abruptly erode the old landslide dam, triggering a massive flash flood downstream, eroding old glacial deposits and river channel deposits along a stretch of over 4 km of the river.

Recent research by Shrestha et al. (2021) and Dahal et al. (2022) reveals that the 2021 Melamchi Flood was due to the combined effects of changing temperature, which breached the Pemdan glacial lake, creating a series of landslides and erosion in the Melamchi River basin. The outburst of the Pemdan Glacier Lake is equally important in the upstream area of the Melamchi River basin, destroying the natural dam near the Bhemathan area, which later supported erosion (Dahal et al., 2022). The study reveals that 228,309 m^3 of sediment loss and 16,925,260 m^3 of deposition occurred in the Bhemathang area (Dahal, 2021; NDRRMA/ World Bank, 2021). A volume of 88,454,507 m^3 of sediment was moved during the events (Dahal et al., 2022). The flood events in the Melamchi watershed on June 15, 2021, and July 31, 2021, were the combined effects of high-intensity rainfall, GLOFs, rainfall-induced landslides, and LDOFs in the upstream area of the watershed (ICIMOD, 2021; NDRRMA, 2021; Pandey et al., 2021). The flooding caused damage to 252 households in Helambu and 287 households in Melamchi Municipality. It also damaged many access roads and foot-trails to several settlements. The disaster resulted in 5 human casualties and 20 people missing. Furthermore, the flood debris destroyed the road network, bridges, transmission lines, the intake structure of the Melamchi water supply project, and agricultural land along its path. Additionally, the debris caused sedimentation over 10 m high in the downstream area (NDRRMA, 2021; Takamatsu et al., 2022).

STUDY AREA

The study area, which is part of the Indrawati River basin, is shown in Fig. 1. It lies within the subtropical to alpine climatic zone of the Himalayan range, spanning three central hill districts of Nepal: Sindhupalchok, Kabhrepalanchok, and Kathmandu. The basin's catchment area totals 1240 km2 with natural forest covering nearly 40% of it. Presently, less than 3% of the total basin area is utilized for farming. The study encompasses an 18 km distance, including the Helambu Rural Municipality and Melamchi Municipality, with elevations ranging from 712 to 5,747 meters above sea level. Our study mainly focuses on the areas highly impacted by the flood event of 2021, which include Timbu, Halde, Kiul, Chanaute, Gyalthum, Taramarang and Melamchi Bazaar in the Melamchi Municipality (Fig. 2). The population density of the basin was approximately 175/km^2 in 1998. The average annual rainfall in the basin ranges from 3,874 mm at higher-elevations (Sarmathang) to about 1,128 mm at Dolalghat in the lower elevation zone, with an average annual potential evapotranspiration of around 954 mm (WECS/IWMI, 2000). The average relative humidity is about 70%, varying from 60% in the dry season to 90% in the rainy season. Daily average sunshine is 6.2 hours per day, with variations from 3.3 hours per day in July to 8.1 hours per day in April. Major tributaries of the Indrawati River basin include Larke Khola, Yangri Khola, Melamchi Khola, Jhyangri Khola, Chaa Khola, Handi Khola, and Mahadev Khola. The Melamchi, Handi, and Mahadev River basins are significant sub-basins in the Indrawati river system in terms of water use practices.

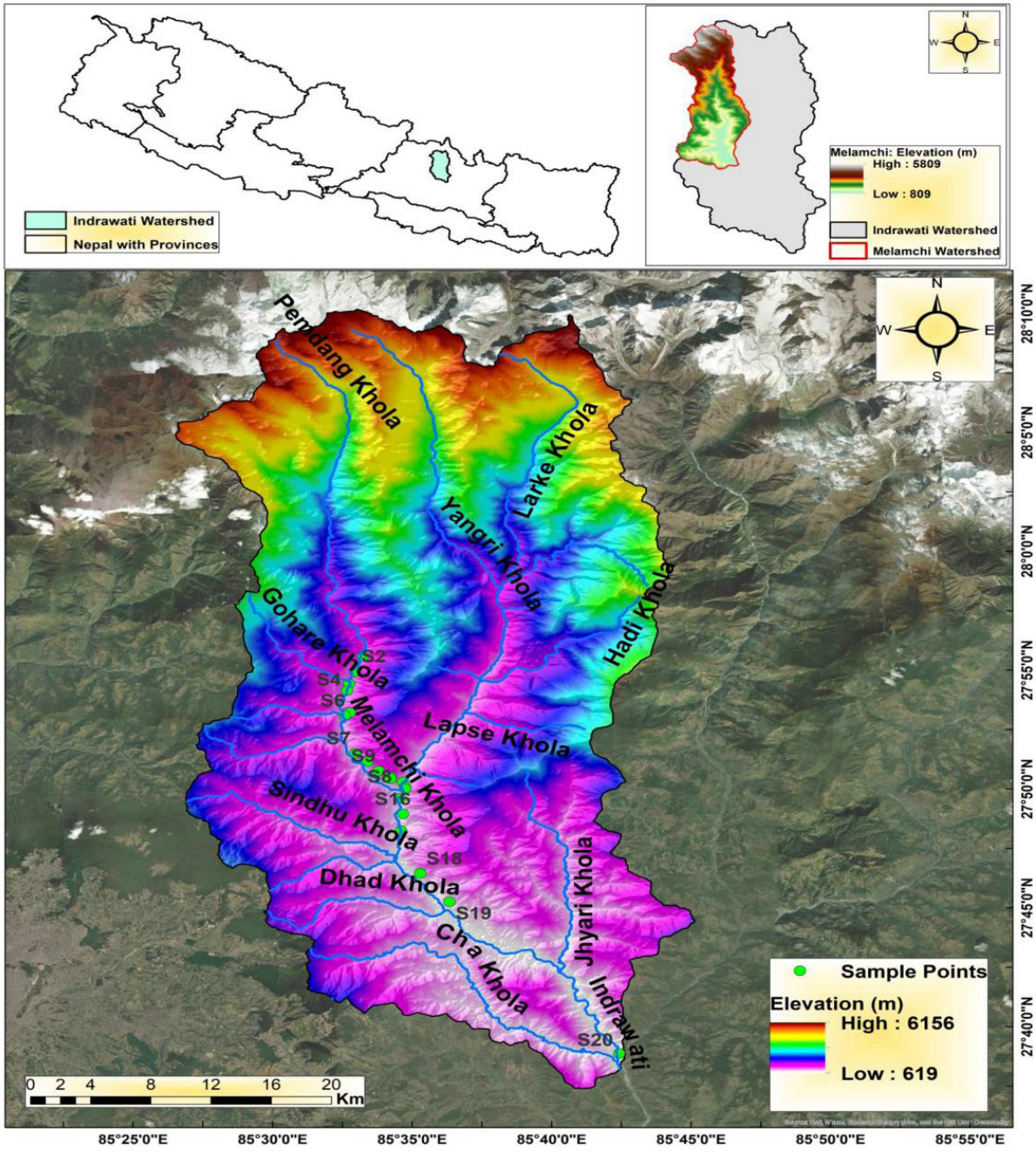

Fig. 1: Digital Elevation Model of the Study area (Melamchi- Indrawoti River basin) indicating 20 different sampling sites

MELAMCHI FLOOD

The Melamchi flood is a cascading hydrological hazard (multiple hazards co-occurring) caused by intense rainfall continuously occurring in the upstream area, which creates significant damage to the downstream regions. Climatic and anthropogenic factors are also associated with these devastating debris flow events (Maharjan et al., 2021; Takamatsu et al., 2022; Talchabhadel et al., 2023). The Melamchi flood is not solely due to rain; various other factors contribute to these events (Mandal, 2021). Thapa et al. (2022) have found that the greatest losses from the devastating flood were in the agricultural sector, which was reduced by 90.48%. According to the Department of Mines and Geology (DMG) and the National Disaster Risk Reduction and Management Authority (NDRRMA), numerous landslides occurred in the section (upstream and downstream regions of Bhemathang). The Pemdang Khola deposited 16,925,260 m^3 of sediments and debris in the initial period, with active scouring and unstable boulders being other significant issues. Among the various causes, soil slides, cloud bursts, and steep glacier moraines were major contributors to the disaster (Baskota et al., 2021). The flood resulted in the loss of many lives and significant damage to property, residential buildings, bridges, and other infrastructure. Localized rainfall triggered debris flow events, as the debris had already accumulated in the upstream area due to the fragile geological formation. The event was characterized as a cascading effect of the 2015 Gorkha earthquake. Sediments were transported over a 30 km stretch, with a high transport rate of soft sediments, and riverbed was elevated by up to 15 m in most locations (Pandey et al., 2021).

On June 9, 2021, the DHM recorded heavy rainfall, with the highest rate of 37 mm/hr occurred on June 11. This was a major factor contributing to the disaster. Fig. 3 shows the amount of rainfall received by each station from June 12 to 16, 2021, with the Shermathang station receiving only 200 mm of rainfall over the six days. Studies reveal that the landslide dam formed in the Bhemathang area was swept away and collapsed due to heavy rainfall in the upstream area, combined with snowmelt erosion in the Yangri River, Larche River, and Pemdang River. This landslide disrupted the natural flow of the Melamchi River, creating a natural dam that later burst, destroying infrastructure, settlements, bridges, and roads downstream. Other factors, such as possible glacial lake outbursts, heavy rainfall runoff, and erosion in the Pemdang River area, contributed to these events. This resulted in riverbank failures, damaged infrastructure, and landslides, leading to another devastating flood event on August 1, 2021, exacerbated by the previous events (Maharjan et al., 2021; Takamatsu, 2022; Adhikari et al., 2023). The high recorded temperatures and precipitation in June 2021 simultaneously caused glacier lake melting and heavy rainfall in the upper part of the catchment area, which later helped destabilize the steep portions of the Bhemathang area, where debris had already accumulated. Intense continuous rainfall and erosional action in the upper part resulted in a huge landslide in the Melamchi Ghyang downstream. The natural dam created by the landslide blocked the river, but the dam was later breached, causing another devastating flood event. This heavily eroded the riverbanks and led to significant deposition in the downstream area. Continuous rainfall was a supporting factor for all these cascading hydrological events and numerous landslides (Fig. 3).

Breaching and blocking of the river upstream can lead to significant disasters especially in mountainous regions like the Himalayas such events often result from a combination of climatic factors and geological activities (ICIMOD, 2021). Heavily deposited and transported materials from upstream caused significant losses and damage to livestock, property, and infrastructure in Melamchi town and damaged or destroyed riverbeds (Talchabhadel et al., 2023). Land and infrastructure near the Melamchi River corridor collapsed due to increased sediment

load (Joshi et al., 2023). The Melamchi flood resulted in 23 people missing, 1 fatality, 6 injuries and 539 households damage (Adhikari et al., 2023). The flood damaged and destroyed bridges (trails and suspension), headworks of the MWSP, trout, pig, and poultry farms, and buildings were washed away, swept away, or buried with sediments (Pandey et al., 2021; Gautam et al., 2022; Dahal et al., 2023). According to the National Aeronautics and Space Administration (NASA), in the Melamchi and Helambu areas, the highest precipitation (168 mm) occurred on June 15, 2021, while the highest daily maximum temperature (20.73°C) was observed on June 9, 2021. The significant rise in temperature possibly contributed to glacier melting, creating the disaster (Source: NASA, POWER Data Access Viewer).

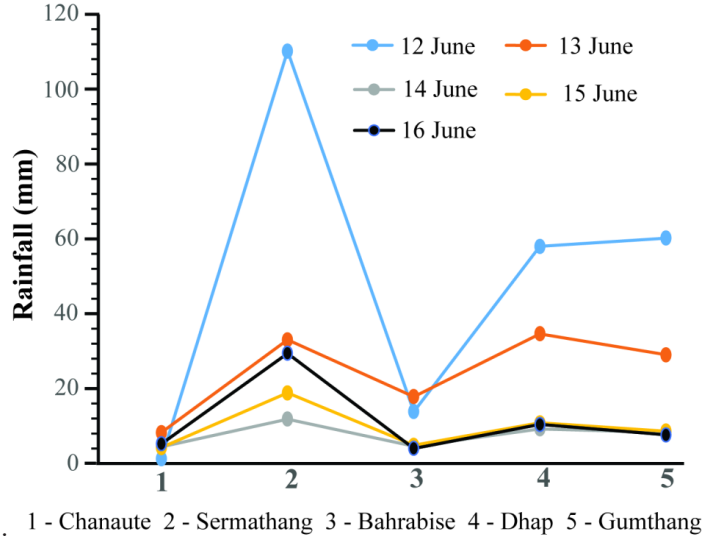

Fig. 2: Rainfall in Sindupalchowk district during June 12-16, 2021.

MATERIALS AND METHODS

For primary data, field visits were conducted in the most affected areas of the Melamchi Municipality and Helambhu Rural Municipality. For event detailing, data from residents and proxy information were used. Similarly, the catchment features of the area were studied with the help of a topographical map (Table 1). Questionnaire surveys, focus group discussions, and key informant interviews were employed. A consultation workshops, as well as informal interviews and case analyses of the events, were also conducted. Both qualitative (case analysis) and quantitative (for the total valuation of economic losses) approaches for data collection were applied. A total of 539 households were considered as survey populations (Adhikari et al., 2023). The populations were surveyed equally from upstream to downstream regions by considering low, middle, and highly affected areas due to the Melamchi Flood. The sample size for the survey was determined using the (Arkin and Colton, 1963). The sample size (n) for the questionnarie survey was determined by using the following formula given by (Arkin and Colton, 1963) at a 95% confidence level.

$$\text{Sample Size}(n) = N * Z^2 * P (1- P) / N * d^2 + Z^2 * P (1-P)$$

Where,

N = Total number of the affected households

Z = Value of standard variate at 95% confidence level (1.96)

P = Estimated population proportion (0.05)

d = Error limit of 5% (0.05)

Hence, the sample size (n) = 70

Table 1: Types of data used in this study

Data Type	Year	Source
Topographical Map	2021	Survey Department, Nepal
Google Earth Image	2023	Google Earth
SRTM- DEM	30 m	USGS/ Nasa Earth Data
Local level boundary	2021	Survey Department
Ancillary data	CBS 2021	CBS, Kathmandu
Field Survey	2023	Sindupalchowk District

For the secondary approaches, historical events were studied from the Bipad portal (https://bipadportal.gov.np/) as well as from situational analysis and site visits after the debris flow. Data on the losses and damages during the Melamchi Flood were collected, along with ancillary data on casualties, causes, and implications from various sources. Satellite images (before and after), Google Earth images, and digital elevation models of the study area were also analyzed. The fieldwork encompassed local household surveys, site investigations, and the collection of losses and damage data records with photographs of each Global Positioning System (GPS) location. Kobo Collector, OpenStreetMap, SRTM- DEM, Nasa Earth data and mobile phones were used during the field days. Additionally, various analyses and reviews of the events were performed. Secondary data collection involved reviewing articles, books, journals, and publications. Maps were analyzed and presented using remote sensing and Q GIS tools and techniques.

RESULTS

The overall flood-impacted area includes household settlements from upstream to downstream along the river courses, especially from the origin of the glacial lake outburst flood to Dolalghat. The disaster area along the Melamchi River comprises locations such as area affected by glacial lake drainage and snow cover, Bhremanthang, Melamcheegaun, Ribarna, Dana, Otero, Nakote, Chanaute, Thapagaun, Helambhu, Melamchi Bazaar, Thadkol, Jogitar, Dolalghat. These regions are categorized based on previous snow cover, heavy rainfall, snowmelt, erosion, and sediment deposition. In this study, we focused on the most severely impacted areas within Helambu Rural Municipality and Melamchi Municipality (Fig. 2). The study includes the roadways from the headworks to Ambathan, Timbu, Halde, Nakote, Sankathali, Kiul (Chiple Dhunga), Ganeshi, Chanaute, Gyalthum, Taramarang, Melamchi Bazaar, Sipaghat, Eklebesi, Maghitar, and Dolalghat. Specifically, sampling was conducted in the major affected areas of Timbu, Halde, Kiul, Chanaute, Gyalthum, Taramarang, and Melamchi Bazaar.For the analysis, the region from Timbu to Melamchi Bazaar, termed as the Melamchi River corridor, which was divided into three segments: upper, middle and lower. The upper and middle sections span from Timbu to Gyalthum, whereas the lower section stretches from Taramarang to Melamchi Bazaar.

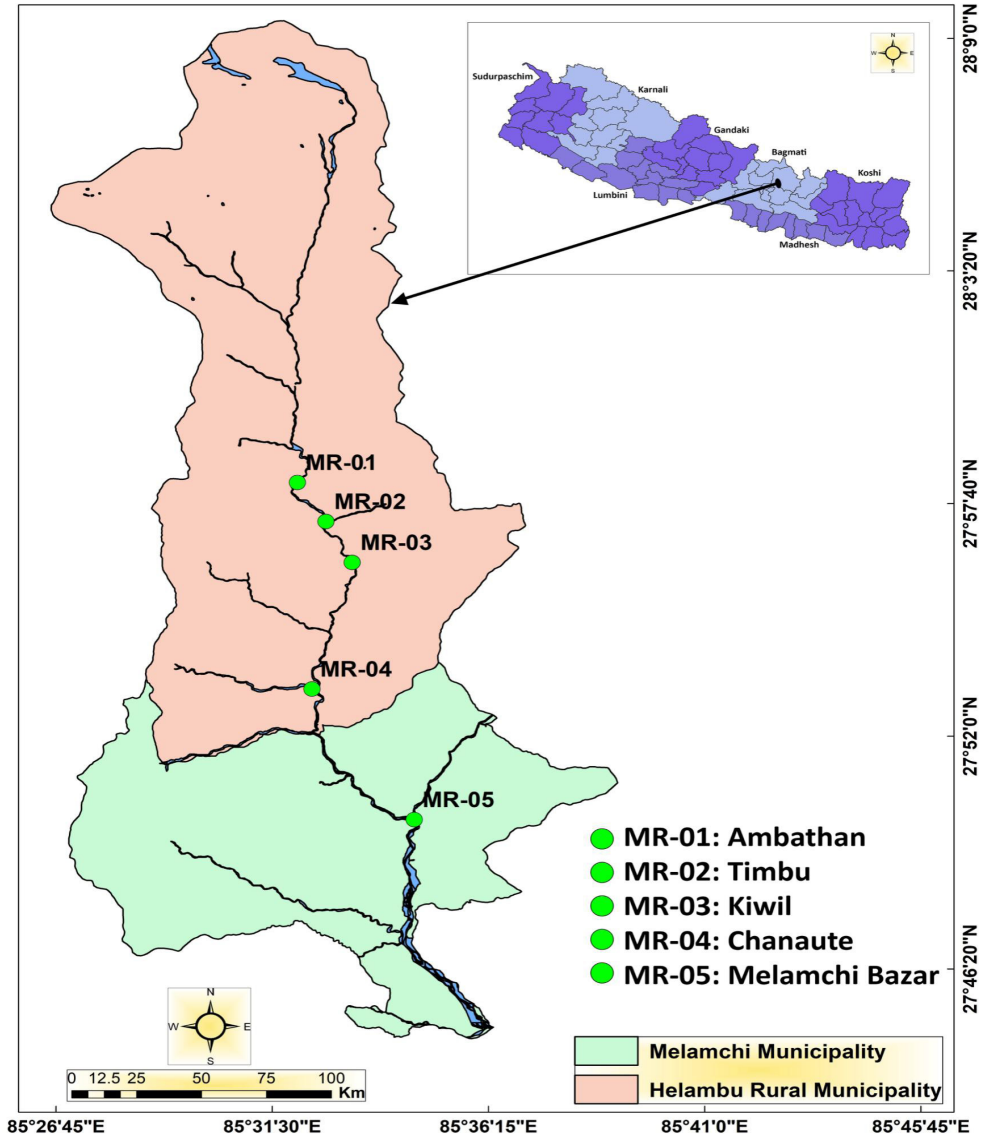

Fig. 3: Location of major affected areas in the Melamchi river Basin

Life and property along the Melamchi River corridor were heavily affected during the 15 June 2021 flood. The event lasted for about 10 hours and caused enormous loss of lives and property, including domesticated livestock and poultry, land, and physical infrastructures. At least 350 residential buildings, half a dozen bridges, and many more infrastructures were affected by the devastating debris flow events (Tables 2 and 3). The disaster caused by the Melamchi flood resulted in 5 human casualties and 20 persons missing. As a consequence, the devastating flood destroyed road access, bridge, transmission lines, schools, irrigation, FM station and heavily impacted the Melamchi Water Supply Project (MWSP). Sedimentation in the downstream area is another serious issue. The survey data revealed that among the total respondents 2.8% of the respondents were missing their family members

who had gone outside for work. Some respondents reported injuries to their family members. Mental health problems were a serious issue during the flood events, affecting people in the both municipalities.

Most respondents raised concerns about clean drinking water, malaria, and dengue during the flood events in both municipalities. About 58% of people living in the Helambu area faced problems with inaccessible roads due to the flood. They were unable to go to schools or health posts for checkups. In contrast, in Melamchi Municipality, only 4% of respondents mentioned this issue. Most respondents from both municipalities (43% in Melamchi and 55% in Helambu) discussed the cultural and religious values of their ethnicity, expressing distress over the destruction of temples, churches, cremation sites, stupas, and prayer buildings. Additionally, 55% of respondents in Melamchi and 49% in Helambu agreed on the issues relating to biodiversity loss, such as the invasion of new weeds, loss of wild animals and birds from their localities, water degradation, drying of water sources, increased temperatures, reduced beauty and aesthetic values, and decreased fish diversity. Lastly, 55% of respondents from both municipalities reported considering migration due to the loss of houses, agricultural lands, lack of jobs, and other factors.

Table 2: Losses and Damaged data (Source: Melamchi Municipality and Field Survey, 2023)

Information	Number	Remarks
Houses Partially Damaged by flood	78	
Vulnerable Houses After Flood	123	
Vulnerable Houses After Flood	123	
Plots fully damaged by flood	3082 Ropani	1882 Private 1200 Public
Fully damaged business	250	Different Patterns of Businesses
Partially damaged but highly Vulnerable public infrastructure	10	
Fully damaged public infrastructure	31	
Lost livestock	120	
Fully damaged sheds of livestock	50	

Table 3: Other losses and Damaged in Melamchi Municipality, Source: Melamchi Municipality and Field Survey 2023

Infrastructure	Ward No	No.	Remarks
Motorable bridge	11	2	Fully Damaged
Suspension bridge	11 6	3 3	Fully Damaged (2) and one highly vulnerable Highly vulnerable
Lift water supply system	11 10 and 11	1 1	Fully damaged Fully damaged
House	11 6	18 1	Fully damaged (17) and one Highly vulnerable Highly vulnerable
Melamchi city park	10	1	Fully damaged
Bus Park	11	1	Fully damaged
Road	11 10 10	1 1 1	Partially damaged (Melamchi to Helambhu Road) Partially Damaged but Highly vulnerable (Indrawati Corridor Road) Partially Damaged but Highly Vulnerable (Sikharpur-Bhiotang Road)
Agricultural land	13	1	Partially damaged (community-based agricultural land)
School	6	1	Fully Damaged (3) and temaining are highly vulnerable (Terse M.V Talamarang)
Irrigation canal	10 11 7 9 and 10	1 1 3 1	Fully Damaged (Khaharekhola Irrigation) Partially Damaged (Nuhar Khola Irrigation) Fully Damaged (Sungure, Amare Thulobagar, Soldunga Irrigation) Fully Damaged
Church	10	1	Fully Damaged (Located in Simlebesi)
Electric power lines and poles	10 and 11	1	Fully damaged
Funeral house	6 10	2 1	Fully Damaged (Talamarang and Nuhankhola) Fully Damaged (located at Rampur)

Additionally, Melamchi Bajaar was severely impacted by the flash flood, which originated from two upper tributaries. This flood caused five deaths, 20 people went missing and resulted in significant loss to the Melamchi Water Supply Project. Information on the total population, number of houses, and the affected houses in the Helambu and Melamchi Municipalities were obtained from the census of 2021 and field survey. There were 4,589 houses with 8,907 males and 8,816 females in the Helambu rural municipality, and 10,811 houses with 20,073 males and 21,097 females in the Melamchi municipality. The total number of affected or damaged houses in the Helambu Rural Municipality was 252, while in Melamchi it was 287.

Stratification was done based on the spatial distribution, meaning that each sampling area was taken as a stratum. The stratified random sampling method was used to determine the household survey of three sections of the affected river corridors: Upper, Middle, and Lower. As mentioned already, Timbu to Gyalthum represented the Upper and Middle sections, whereas Taramarang to Melamchi Bazaar represented the Lower sections. The sample size of the households to be surveyed was determined as $n/N \times 69$, where n is the sample of affected households of the selected study sites and N is the total number of affected households in the entire study sites (Table 4).

Table 4: Number of Sampled households in Study sites, Source (Field Survey 2023)

Study Sites	Helambhu	Melamchi	Total
No. of total households	252	287	539
No. of samples	33 (47%)	37 (53%)	70 (100%)

The total surveyed respondents from Helambu Rural Municipality and Melamchi Municipality represented 47% and 53%, respectively. The majority of the respondents were aged between 40-60 years. Among the respondents, 55% were men and 45% women. Most of the respondents depended on agriculture, and some were self-employed. A few were entrepreneurs engaged in the fishing business and trout farming. However, it is important to mention that all these businesses collapsed after the flooding events in Melamchi. The Melamchi flood destroyed many infrastructures, schools, agriculture, tourism, businesses, and many other sectors. A total of six bridges (Motorable bridge, bailey bridge, suspension bridge, Pedestrain bridge, Arch bridge and Truss Bridge) were damaged during the flood events in the Melamchi area. Since trout farming and tourism were the main sources of revenue generation, the flood events caused most of these businesses to collapse, leading to unemployment. According to Melamchi Municipality data, there was a loss of USD 417,840,665.03 in houses, USD 17,845,821.75 in land, and USD 91,230.66 in livestock, with a total loss of USD 435,777,717.44. In Helambu Rural Municipality, the losses were USD 4,084,343 in houses, USD 16,188 in livestock, and USD 19,844,170 for crop loss, ensuring a total loss of USD 61,772,407 in Helambu Municipality (Parajuli et al., 2023) (Table 5). These documents also proved relevant to the household survey data. The majority of the respondents from both municipalities reported losses of agricultural land, houses, and livestock.

Table 5: Economic Valuation of Assets loss of survey respondents (Source, Parajuli et al., 2023)

Information	losses	Cost (NRs)	Cost (USD)
Total house loss	63	21,10, 05,013	1,603,638
Total land loss	16.714 hectares	43,47,13,250	3, 303, 821
Total livestock loss	Hen, Goat, Pig, Buffalo Ox, Cow	27,45,500	20,866
Total crop loss		22, 70, 197	17, 253
Total loss		65,14,08,960	4, 945, 578

The survey data revealed that 95% of the respondents felt insecure about their income as a result of the flood. Among them, 56% had lost their agricultural income, 28% lost their non-agricultural income sources, 11% lost their employment, and a few lost income-generating sources such as tourism. While surveying, some people also complained about the loss and damage to Water Mills (Ghatta) and irrigation canals. They added that this has also impacted their daily routines. Nevertheless, some respondents were facing depression and anxiety issues after the flood events. They also mentioned problems they are currently experiencing with cremation due to the high deposition of debris on the riverside of Melamchi. Both municipalities were unaware of the non-economic loss and damage in the area, which need to be revealed as soon as possible.

While conducting the analysis of the sample taken from the left bank of the Melamchi Khola near the head works area close to the dam. The followings results were revealed. The sample is from the high flood level debris flow deposits shows the sieve analysis curve for a sample with the following composition. Gravel 41.42%, Sand 57.65% and Silt and Clay 0.93%. Gravel: represented by the steep initial portion of the curve up to about 2 mm, indicating that 41.42% of the sample is gravel. Sand: The curve rises significantly between 0.075 mm and 2 mm, showing that 57.65% of the sample consists of sand. Silt and Clay: The smallest portion of the sample, represented by the smallest particle sizes (0.075 mm and smaller), with only 0.93% passing the sieve. The curve illustrates the cumulative percentage of the particles passing through sieves of decreasing sizes. The points on the curve are marked with percentages, indicating the cumulative passing at specific sieve sizes. This curve is typical for moderately graded soils with a mix of different particle sizes, where sand is the predominant fraction, followed by gravel, and very little silt and clay. (Fig. 4 a and b)

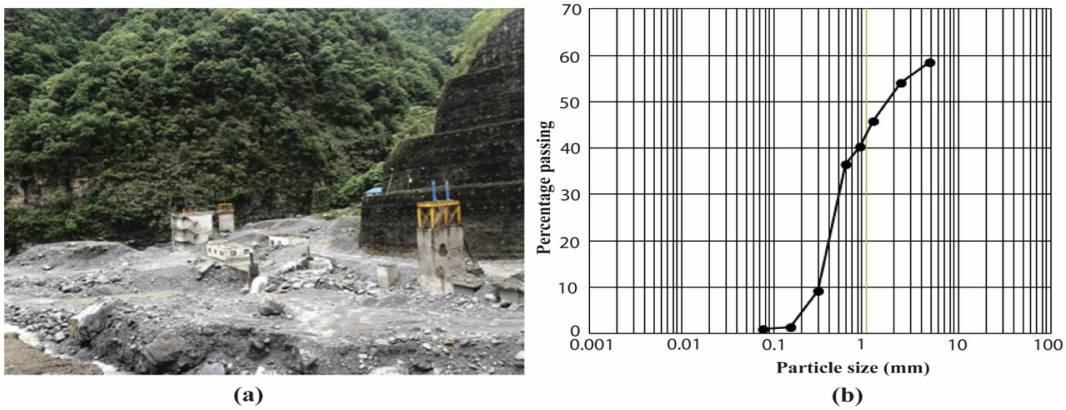

Fig. 4: (a) Flood impacted Melamchi head works area, (b) Particle size distribution of sediment sample (Sample No. 2) collected at the head work area.

This is the analysis of the sample taken from the right bank of the Melamchi river at two previous fishponds buried sites by the debris flow of Melamchi. The materials were fine (granule to silt and clay) with some light grey quartzite boulders. The figure shows the sieve analysis curve for a sample with the following composition. Gravel 18.17%, Sand 75.65% and Silt and Clay 6.18%. The soil represented by this curve is poorly graded. It shows the significant portion of the particles within a specific size range and a lack of the intermediate size. This typically implies that the soil might not have the desirable properties for the certain engineering applications as it lacks a good mix of the particle's sizes. (Fig. 5 a and b).through sieves of decreasing sizes. The points on the curve are marked with percentages, indicating the cumulative passing at specific sieve sizes. This curve is typical for moderately graded soils with a mix of different particle sizes, where sand is the predominant fraction, followed by gravel, and very little silt and clay. **(Fig. 4a and b)**

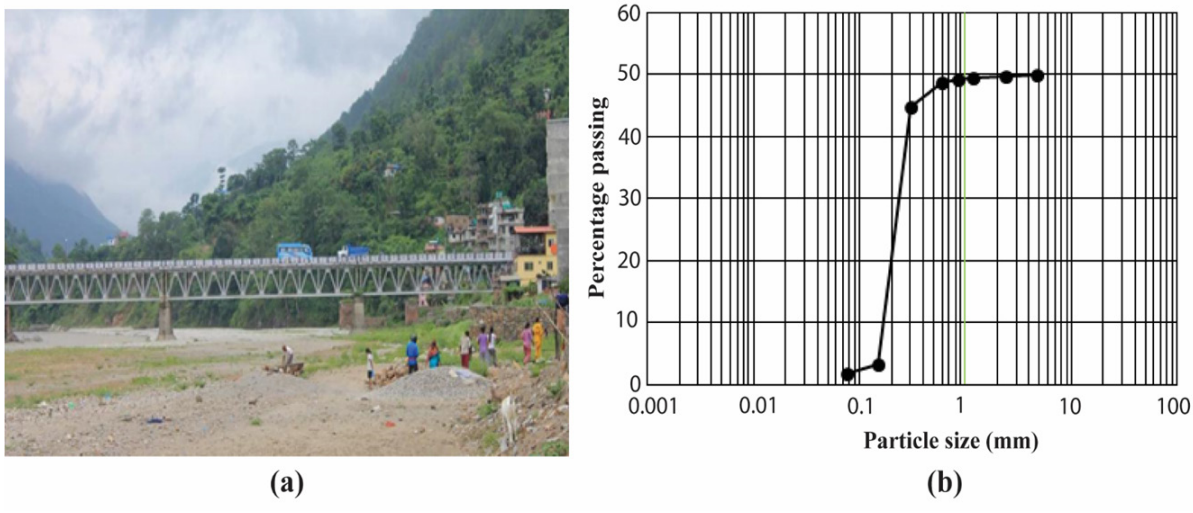

Fig. 5: (a) Fish Pond buried site at the Right Bank of Melamchi River above danuwar gaun, (b) Particle size distribution of sediment sample (Sample No. 20) collected at the fish pond buried site above danuwar gaun.

This is the analysis of the sample which was taken from the right bank of the Indrawoti river, at Dolalghat. The sample was appeared as a grey silty sand. The figure shows the sieve analysis curve for a sample with the following composition. Gravel 0.12% Sand 96.52% and Silt and Clay 3.36%. In this case, given the steepness of the curve around the fine particle sizes and the flattening at larger sizes, the soil appears to be poorly graded with a high concentration of the fine particles (Fig. 6 a and b)

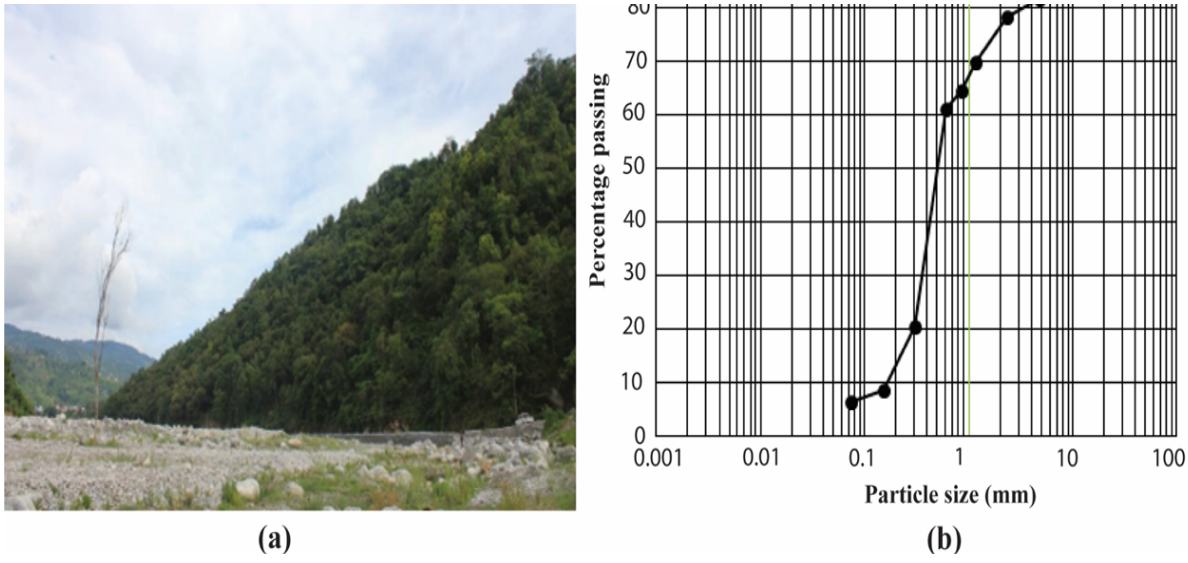

Fig. 6: (a) Flood deposit at the Dolalghat bridge, the southernmost part of the study area, (b) Particle size distribution of sediment sample collected at the Dolalghat bridge site.

Based on the field observations, interviews and surveys, the following sequences of the losses and damages were recorded along the study alignment with the specific GPS coordinates. The Melamchi Water Supply Project (MWSP) headworks area was totally damaged due to the flash flood. A huge amount of the debris flow was deposited along the site, creating high flood debris flow deposits (Fig. 7a). A few landslides were also observed near the site (Fig. 7b). Roads from the headworks to Ambathan had about 4 m of the debris flow deposits (Fig. 7c). Debris flow remanents from Timbu (Fig. 7d). Cut heights of the banks of the tributary brought much debris and partially dammed the Melamchi River (Fig. 7e). A high flood of about 5 meters from the bridge slab washed out one bridge along Ambathan road (Fig. 7f). Few houses (4-5) were buried in Halde, with debris covering the ground floor. Multiple debris flow damming was observed from Nakote to Sankathali. Electric poles were also destroyed. Here is the detailed explanation of the debris flow and the loss and damage due to the Melamchi flood.

Fig. 7: Debris flow, landslide and flood related observations between the headworks and Ambanthan, (a) Deposits seen at the road section, (b) Landslide of colluvial soil on weathered gneiss, (c) Debris flow cliff (4m), (d) Debris flow remanent at Timbu, (e) Cut height of debris at the bank of tributary, (f) Ambathan road washed out bridge.

At Kiul (Chiple Dhunga), one house was buried up to the ceiling of the ground floor at coordinates 03-57-521 E, 30-88-717 N, with an elevation of 1097 m (Fig. 8f). About 6 destroyed houses were recorded at Ganeshi, with a road ~5 meters above the cut bank also damaged. The area was unclear, and the other houses were on the river bed; boulders ranged in size from 5 cm to 1.5 to 2 m, mostly of banded gneiss. Altogether, 22 houses were buried, among them one floor was buried about 10 feet (Fig. 8d). At 03-56-868 E, 30-87-774 N, with an elevation of 1056 m, most buildings were buried up to 2 floors (~7 meters). Most houses are abandoned, and Chanaute now appears as a ghost town. Boulders' sizes range from 5 cm to 1 m, mostly of dark grey banded gneiss and quartzite, with a buried depth of about 10 meters.

Fig. 8: Debris flow, houses damaged and buried between Ambathan and Ganeshi (a) Boulder of the flood erosion at Ambathan, (b) Inverse grading of the debris flow deposits south of Halde, (c) Road on the boulder bar at Kiul, (d) Destroyed houses at Ganeshi, (e) Houses partially buried by debris flow at Halde, (f) Damaged house at Kiul.

A remanent of the bailey bridge (Rato Pul) brought down from Chanaute was left at 03-56-891 E, 30-85-510 N (elevation, 972 m) on the left bank of the Melamchi River, opposite side of the landslide at Gyalthum. There were rocks in the landslide: dark grey to grey, thin-bonded parallel laminated quartzite alternating with garnet (5 mm) schist. The disaster occurred on the 16th of Saun, at night from 11:00 PM to 12:00 AM. The depth of the deposit was 10-12 m. The flow continued for four days at a velocity of 1-2 m/minute (Fig. 9a). At 03-56-589 E, 30-85-298 N, with an elevation of 964 m, at the Melamchi Khola bar, southwest of Gyalthum, a matrix of gravel and liquefied masses was moving slowly for four days at a rate of 50-60 m/hour or 1-2 m/min, creating high dynamic viscosity with a boiling mass of debris. The debris flow must be matrix-supported sandy silt or sandy silty clay (Fig. 9b). At 03-57-175 E, 30-82-354 N, with an elevation of 905 m, at Thulo Khet on the right bank of the Melamchi River, collapsed buildings of pink color, which was a single-storeyed building (Fig. 9c). At 03-57-878 E, 30-81-686 N, with an elevation of 880 m, it is at the right bank of the Melamchi River at about 100 m long and 50 m wide bar. The bar has banded gneiss and dark grey quartzite. Boulders sizes were 5cm to 1.5 m of different variations i.e boulders to matrix (Fig. 9d).

At 03-58-532 E, 30-80-976 N, Debris flow at 858 m on the Melamchi River's right bank buried two fish ponds with fine material like granule to silt and clay having some light grey quartzite boulders (Fig. 5a). At 03-59-239 E, 30-80-485 N, with an elevation of 841 m, destroyed buildings of Danuwar Gaun were seen, buried up to 4 m, the ceiling of ground floor (Fig. 9e). At 03-59-219 E, 30-80-356 N, Granule sand and silt deposits on the right bank of the Melamchi River formed a crudely stratified 3-meter-high bar near a damaged bridge abutment at 838 m elevation (Fig. 9f)

.

Fig. 9: Damaged bridge, houses, sand bar observed between Gyalthum and Danuwar gaun. (a) landslide opposite Gyalthum with baily bridge, (b) Melamchi khola bar SW of Gylthum, (c) Collapsed building at left bank of Melamchi river at Thulokhet, (d) Sand bar on top of boulder, (e) Destroyed building of Danuwar Gaun (f) Fine particles deposietd on 3m high bar near damaged bridge abutment.

At 03-59-947 E, 30-80-080 N, the Melamchi River Resort at 818 m elevation was buried by debris flow up to 6 meters, covering the ground floor and half of the first floor (Fig. 10a). At 03-60-078 E, 30-79-706N, and 823 m elevation in southern Melamchi, debris flow buried hotel houses up to 3.5 storeys (13 meters deep), leaving a flood mark on green-blue buildings. The debris was mostly silty sand (Fig. 10b). At 03-60-094 E, 30- 79- 557 N and 818 m elevation on the Indrawati River's left bank, a 15-meter-thick sediment deposit buried a two-story house. The debris flow height exceeded 2 meters, forming a flat area about 600 m long and 150 m wide near a new Bailey bridge construction site (Fig. 10c).

At 03- 59-774 E, 30- 78- 821 N having 806 m elevation on the right bank of a gully near the Armed Police Force, debris flow deposits composed mainly of crudely stratified sand and silt were observed. The thickness of the deposits was about 6 m. According to the respondents, the debris flow took place on the 1st of Asar at 5 PM, and the deposition occurred from 1:00 AM that night and continued almost the whole day on the 2nd of Asar. On the 1st of Asar, there was also flooding from the Indrawoti River, which washed out the fine and light materials. The flooding of the Indrawoti started at 5 PM on the 1st of Asar and continued through the night. The floods subsided in the Indrawoti River, but the debris flow continued in the Melamchi River. Since the power of the Indrawoti weakened, the debris flow churning by the Indrawoti and the removal was not possible, leading to sediment deposition. The deposition began at the lower reach and built up upstream. The deposition progressed from downstream to upstream. The pebbles were all angular and composed of gneiss and dark grey quartzite (Fig. 10d). At 03-59-931 E, 30-77-604 N, with an elevation of 782 m, on the left bank of the Indrawoti River near a suspension bridge. The matrix was mainly composed of angular granules and sand with silty sand. Boulders made up approximately 20%, ranging in size from 5 cm to 1 m.

At 03-59-795 E, 30-76-300 N, with an elevation of 763 m, on the right bank of the Indrawoti River about 500 m upstream from a bridge at Bahune Pati, a crudely stratified sand bed approximately 2 m thick was observed (Fig. 10e). At 03-60-888

E, 30-72-966 N, with an elevation of 732 m near Sipaghat at Eklebesi, Maghitar, on the right bank of the Indrawati River, a light brown sand bar about 30 cm thick was observed (Fig. 10f). At 03-62-589 E, 30-70-751 N, with an elevation of 709 m, at the east end of Sipaghat near a temple and bridge, there was observed an alluvial fan of the Dhad Khola, which was formed by the floodplain deposits of the 2021 Melamchi flood. Similarly, last but not least, at 03-72-463 E, 30-58-846 N, with an elevation of 630 m, on the right bank of the Indrawoti River at the confluence of the Cha Khola, in Dolalghat, the flood covered the ground floor ceiling of the house. The sediments were mainly grey silty sand, and a flood mark was also observed on the Dolalghat bridge (Fig. 6a)

Fig. 10: Buried houses, flood mark, debris flow deposits, sand bar observed below Danuwar gaun and Dolalghat. (a) Buried Melamchi river resort, (b) High flood mark on green blue buildings, (c) Houses buried on two floors on Melamchi bazzar, (d) Debris flow deposits at the transverse from Melamchi to Dolalghat area, (e) Deposits of Crudely stratified sand bed at Bahunepati, (f) 30 cm thick sand bar near Sipaghat at Eklebesi, Magitar

RESULTS AND DISCUSSIONS

This research is entirely based on field observations and aims to validate the collected information with data from the various sources, including field data, satellite images, and aerial photographs. The results show drastic changes in particle size distribution from upstream to downstream, as well as the loss and damage caused by the Melamchi flood. For the purpose of identification of clast sizes in both source and sample or in debris deposits: Block (coarse > 8 m, medium = 8-4 m, fine = 4-2 m); Boulder (coarse = 2-1 m, fine = 1-0.256 m); Cobble (256-64 mm); Pebble (64-4 mm); Gravel (4-2 mm); Sand (2-0.0625 mm); and Mud (< 0.0625 mm) scales were used. Additionally, for particle size distribution, the following scale was also used: Gravel > 2 mm, Sand (2-0.63 mm), Silt (0.63-0.004 mm), and Clay (< 0.004 mm). To determine the particle size distribution of debris flow events from the Melamchi headworks area to Dolalghat, a total of 31 collected samples of debris/soil were used and analyzed. Near the headworks area, close to the dam site, there was a significant proportion of sand followed by gravel, silt, and clay, indicating well-graded soils with a mix of different particle sizes. At the Ambathan road, results revealed that the majority of particles in the sample were fine to medium-sized with a well-graded distribution. Similarly, the sample from Halde showed that most particles were fine to medium-sized with a well-graded distribution. In Kiul, the particle size distribution displayed a range of particle sizes with a steady increase in the percentage passing as particle size increased, with the majority of sample particles larger than 0.35 mm and smaller than 2 mm. The median size was 1.2 mm, providing a central measure of particle size distribution. The sample from Ganeshi indicated a high percentage of fine particles, especially below 0.1 mm. The majority of the sample's particles were larger than 0.02 mm and smaller than 0.13 mm, with a median particle size of 0.09 mm in Chanaute. The landslide opposite Gylthum indicated a well-graded sample, with particle size distributed across a range rather than concentrated at a specific size. The sample from Thulo Khet predominantly comprised medium-sized particles between 0.1 mm and 1 mm, forming a well-graded sample with a mixture of fine to coarse particles. The sample from Danuwar Gaun indicated 20% gravel (> 4.57 mm), 50% sand (0.075 mm to 4.75 mm) with a significant rise between 0.1 mm and 1 mm, 10% silt (0.002 mm to 0.075 mm), and 0% clay (< 0.002 mm). The sample taken from the Melamchi River Resort indicated a particle size distribution curve with a significant amount of fine particles and a rapid increase in percentage passing around 0.1 mm and 1 mm. The sample from the left bank of the Indrawoti Khola at the new Bailey bridge construction site represented a well-graded soil sample with a broad range of particle sizes. Lastely the sample from the right bank of the Indrawoti river at Dolalghat area having the composition of very less amount of silt and clay nearly 0.12%, Sand 97.87% and gravel is about 0.18%. Studies reveal that the highest amount of sediment accumulation in the study area occurs during the pre- monsoon and monsoon seasons. The particle size and accumulation of debris vary in different regions due to river velocity. Thoroughly considering the above results the upper section of the sample consists of poorly graded materials having sediments size 0.1 mm to more or less > 7mm. However, in the downstream area the sediment size ranging from 0.09 mm to > 2 mm. Most of the sediment passing zone was Chanaute and Melamchi bazaar area. Due to the conjugal point of the Indrawoti and the Melamchi river in Melamchi bazaar area most sediment were passed and the river is more erosive on that zone. Due to the erosive nature of the river in the upper part huge sediments were carried out and supported the huge loss and the damage in the lower areas.

For the purpose of identification of the loss and damage on-site field visit, focus group discussions, key informant interviews, and a few alternating workshops were conducted. Land Use Land Cover (LULC) maps from before and after the flood events were also studied. Satellite images were

observed. Key informants, multiple household surveys, and case analyses were also carried out in the field. According to all survey data, interviews, and technical workshops, we concluded that the devastating flood was not solely due to rain but rather resulted from multiple factors which having a multiple cascading effect. The Melamchi flood resulted from the significant cumulative impacts of a devastating flood event. The timing of the flood was also a major factor in the extent of loss and damage downstream. Communities downstream were alerted by those upstream, which significantly helped to reduce the loss and damage, allowing people to move to safer areas. Based on the responses of the informants and the data from the Department of Hydrology and Meteorology, there was a maximum amount of rainfall during those days in that area. This included earlier snowfall, temperature fluctuations, and a rapid rate of snow melting. Intense continuous rainfall in the upper area contributed to extreme rainfall and erosion towards the higher elevations. The upper part mechanism significantly destabilized the lower part of the sediments in Bhemathang. Extreme rainfall events and erosion activities in the upper reach resulted in huge landslides in the Melamchi Ghyang area downstream. The dam that had already blocked the river was later breached, causing devastating flood events. These events heavily eroded the river banks and led to significant deposition in the downstream area.

Climate change has impacted river discharge (Hock et al., 2019). The risk of floods is very high in Nepal among South Asian regions (UNEP, 2009). Sediment deposition in the Melamchi Valley was measured at 23.24 million m^3 (Chen et al., 2023). During the first event, a discharge of 2,893 m^3/s was recorded, and during the second event, it was 1,105 m^3/s at Melamchi Bazaar. The peak discharge at Nakote during the second event was 285 m^3/s. The daily average discharge at Bhemathang was 357 m^3/s during the first event and 76 m^3/s during the second event. The daily average erosivity was also high during both events. Sediment passing was high in the Chanaute and Melamchi river segments (Baniya et al., 2023). The estimated total loss was approximately USD 436 million for the Melamchi Municipality and USD 62 million for the Helambhu Rural Municiplaity (Parajuli et al., 2023).

These factors all contributed to significant loss and damage in the Melamchi area during the flood events, particularly in the middle section of the river basin. Our study has documented that the area from Timbu to Gyalthum was severely affected due to the presence of soft, weathered rocks, as well as thrusts and faults in this zone. Weak geology and a steep gradient also contributed to the issue. Moreover, the loss and damage below Melamchi Bazaar were exacerbated by an increase in river velocity at the confluence point by mixing of the two rivers and also the mixing of sediment carried by the Indrawoti River. The sediment deposition rate is also very high in the downstream area from the Melamchi confluence, which supports these facts. During the field observation, the study also attempted to correlate the downstream loss and damage with the upstream-to-downstream sediment transport phenomena, yielding satisfactory results. Moreover, the areas where large amounts of coarse sediments or debris accumulated experienced significant damage, whereas the zones where sand, silt, and clay settled caused less damage but buried much of the infrastructure. Beyond these observations, respondents revealed that there was a loss of economic assets, non-economic assets, cultural, archaeological, and aesthetic values in the damaged area. Sleeplessness due to fear of floods, gender-specific impacts, water-borne diseases, educational impacts, and psychological impacts were other forms of loss and damage experienced during the flood event.

CONCLUSIONS

Sindhupalchowk district is a zone with fragile geological conditions, characterized by numerous faults and thrusts. The area is highly susceptible to earthquakes and other natural disasters such

as floods and landslides. Due to its weak geology, rugged topography, and dynamic geological settings, the region has faced numerous challenges over the years. The community experienced a devastating earthquake in 2015 B.S. and, as it was gradually recovering, an unprecedented flood in 2021 further exacerbated the difficulties in the Melamchi area. Since 2011, the municipality has experienced rapid population growth, with an annual rate of 5.2%. This growth has made the area a central hub for many businesses and services. However, the region's fate took a drastic turn after the June 2021 flood, resulting in significant loss of life and extensive damage to infrastructure. Despite the area's consistent vulnerability to various disasters—such as earthquakes, floods, landslides, fires, lightning, glacier melt, and glacial lake outbursts—several studies have facilitated a better understanding of these hazards and laid the groundwork for developing risk mitigation plans in the Melamchi watershed. It is evident that the impacts of climate change have further compounded the challenges, as seen in the significant loss of life and severe damage to homes and infrastructure. Considering various contributing factors, there is evidence that intense, continuous rainfall, steep slopes, steep river gradients, landslide dam bursts in upstream areas, fragile geological conditions, increasing temperatures, rugged topography, and frequent seismic activities likely contributed to these disasters. Cloudbursts, steep glacial slides, soil movements, and their cumulative downstream impacts were also significant contributors to the scale of the disasters. There is an urgent need for a geo-engineering investigation to collect all relevant information about the potential hazards in the area. This recommended detailed study can form the basis for mitigating and rehabilitating vulnerable areas and proposing potential locations for mitigation structures, ultimately benefiting the livelihoods of people in the region. The focus should be on prioritizing houses, roads, and infrastructure while also addressing the hardships faced by families impacted by the disaster events. It is essential to clear all debris and sediments from the area immediately and to plan for three levels of mitigation approaches: slope stabilization, resilient intake design, and river engineering works. Additionally, installing more meteorological stations near the sites and preparing for the installation and regular monitoring of early warning systems is crucial.

ACKNOWLEDGEMENTS

The authors are grateful to the staff of the Department of Geology, Tri Chandra College, Nepal, for their support during the material analysis process in the lab. We are also very thankful to Mr. Madhav Adhikari and Mr. Ramesh Kathariya, MSc Environmental Science graduates from CDES, TU for their support and cooperation during map preparation and Mr. Sujan Dulal from the Melamchi Municipality for providing the data. This paper is part of the Ph.D. research work of the first author, Subash Duwadi, who is currently working as a faculty member in the Department of Environmental Sciences, Tri-Chandra Multiple Campus

REFERENCE

Adhikari, T. R., Baniya, B., Tang, Q., Talchabhadel, R., Gouli, M. R., Budhathoki, B. R. and Awasthi, R. P., 2023. Evaluation of post extreme floods in high mountain region: A case study of the Melamchi flood 2021 at the Koshi River Basin in Nepal. Natural Hazards Research, 3, 437-446.

Adhikari, D. P. and Koshimizu, S., 2005. Debris flow disaster at Larcha, upper Bhotekoshi Valley, central Nepal. The Island Arc, 14(4), 410-423.

Allen, M. R. and Ingram, W. J., 2002. Constraints on future changes in climate and the hydrologic cycle. Nature, 419(6903), 224-232.

Andres, N., Sattar, A. M. and Zhang, K., 2009. The effects and impacts of the floods include water depth and residence time, flow velocity, erosive

capacity, sediment transport and deposition, and other associated geological phenomena. Natural Hazards Review, 10(4), 173-178.

Arkin, H. and Colton, R. R., 1963. Tables for statisticians. Barnes and Noble. Inc., New York, 19637.

Asgharpour, S. E. and Ajdari, B., 2011. Seasonal flood in Iran, a case study Ghotour Chai Basin watershed. Procedia - Social and Behavioral Sciences, 19, 556-566.

Baniya, B., Tang, Q. H., Neupane, B., Xu, X. M., He, L., Adhikari, T. R. and Dhital, Y. P., 2023. Rainfall erosivity and sediment dynamics in the Himalaya catchment during the Melamchi flood in Nepal. Journal of Mountain Science, 20(10), 2993-3009.

Baskota, S., Shrestha, A. B. and Ghimire, S., 2021. The Pemdang Khola deposited 16,925,260 m^3 of sediments and debris in the initial period, with active scouring and unstable boulders being other significant issues. Among the various causes, soil slides, cloud bursts, and steep glacier moraines were major contributors to the disaster. Natural Hazards, 1-19.

Byers, A., Byers, E., McKinney, D. and Rounce, D., 2017. Study on the impacts of earthquake 2015 on potentially dangerous glacial lakes in Nepal. Himalaya, 37(1), 26-41.

Byers, A. C., Rounce, D. R., Shugar, D. H., Lala, J. M., Byers, E. A. and Regmi, D., 2019. An induced glacial lake outburst flood due to rockfall, Upper Barun Valley, Nepal. Landslides, 16(3), 533-549. https://doi.org/10.1007/s10346-018-1079-9

Bhattarai, M., Pant, D., Mishra, V. S., Devkota, H., Pun, S., Kayastha, R. N. and Molden, D., 2002. Integrated development and management of water resources for productive and equitable use in the Indrawati River Basin, Nepal (41). IWMI.

Cenderelli, D. and Wohl, E., 2001. Estimation of the peak discharge of glacial-lake floods and normal climatic floods in the Mount Everest region, Nepal. Geomorphology, 40(1-2), 57-90. https://doi.org/10.1016/S0169-555X(01)00037-X

Chen, H., Zhang, W. C., Deng, C., Nie, N. and Yi, L., 2017. Volunteered geographic information for disaster management with application to earthquake disaster databank & sharing platform. IOP Conference Series: Earth and Environmental Science, 57, 012015. https://doi.org/10.1088/1755-1315/57/1/012015.

Chen, C. M., Hollingsworth, J., Clark, M., Zekkos, D., Chamlagain, D., Bista, S. and West, A. J., 2023. The 2021 Melamchi Flood: A massive erosional cascade in the Himalayan mountains of Central Nepal.

Christensen, J. H., Hewitson, B., Busuioc, A., Chen, A., Gao, X., Held, I. and Whetton, P., 2007. Regional climate projections. In Climate Change 2007: The Physical Science Basis. Contribution of Working Group I to the Fourth Assessment Report of the Intergovernmental Panel on Climate Change (Chapter 11).

Dahal, R. K., Upreti, S., Timilsina, M., Basnet, G., Sapkota, G., Kafle, K.R., Shrestha, H.K., Niraula, R., Upadhaya, M., Dahal, A., Dhakal, O.P., Malla, A.B. and Maharjan, K., 2022. Flood Risk Assessment and Build Back Better in the Aftermath of 2021 Flood at Melamchi Municipality, Geotech Solutions International.,Nepal.

Dahal, V., Shakya, N. M. and Bhandari, R., 2022. Melamchi Flood 2021 is due to the combined effects of changing temperature, which breached the Pemdan glacial lake, creating a series of landslides and erosion in the Melamchi River basin.

Dahal, T. P., Dangol, S., Nepali, P. B. and Shrestha, R., 2023. Restoration of Land Parcels using Land Consolidation & Readjustment: A Case of Resilience after Flood Disaster. Journal on Geoinformatics, Nepal, 47-56.

Dhital, M. R., Shrestha, S. and Bhandari, R., 2021. making landslides and avalanches highly susceptible in the upstream area.

Dhital, M. R., Sunuwar, S. C. and Shrestha, R., 2002. Geology and structure of the Sundarijal–Melamchi area, central Nepal. In Proceedings of the Third Nepal Geological Congress.

Dhital, M. R., 2003. Causes and consequences of the 1993 debris flows and landslides in the Kulekhani watershed, central Nepal. In D. Rickenmann & C.-L. Chen (Eds.), Proceedings of the Third International Conference on Debris-Flow Hazards Mitigation: Mechanics, Prediction, and Assessment (Vol. 2, pp. 931-942). Millpress, Rotterdam, Netherlands.

Dottori, F., Martina, M. l. and Figueiredo, R., 2016. A simple methodology for flood susceptibility and vulnerability analysis in complex flood scenarios. Journal of Flood Risk Management, 11(S1), S633-S645. https://doi.org/10.1111/jfr3.12234

Dankers, R. and Feyen, L., 2008. Impact of climate change on flood hazards in Europe: An assessment based on high-resolution climate simulations. Journal of Geophysical Research: Atmospheres, 113(D16), D19105. https://doi.org/10.1029/2007JD009719

Duan, J. G., Bai, Y., Dominguez, F., Rivera, E. and Meixner, T., 2017. Framework for incorporating climate change on the flood magnitude and frequency analysis in the upper Santa Cruz River. Journal of Hydrology, 549, 194-207.

Duan, L., Liu, C., Xu, H., Pan, H., Liu, H., Yan, X. and Lu, H., 2022. Susceptibility assessment of flash floods: A bibliometrics analysis and review. Remote Sensing, 14(21), 5432.

Duncan, C., Masek, J. and Fielding, E., 2003. How steep are the Himalaya? Characteristics and implications of along-strike topographic variations. Geology, 31(1), 75-78.

Emmer, A. and Cochachin, A., 2013. Moraine-dammed Lake failures and their causes and mechanisms in the Cordillera Blanca, North American Cordillera and Himalaya. Acta Universitatis Carolinae Geographica, 48(1), 5-15.

Gautam, D., Shrestha, S. and Bhandari, R., 2021. The nature of floods has become more cascading and widening in dimension over the years, causing significant damage.

Gautam, D., Adhikari, R., Gautam, S., Pandey, V.S., Thapa, V.R., Lamichhane, S., Talchabhadel, R., Thapa, S., Niraula, S., Aryal, K. R., Lamsal, P., Bastola, S., Sah, S.K., Subedi, S.K., Puri, B., Kandel, B., Sapkota, P. and Rupakheti, R., 2022. Unzipping flood vulnerability and functionality loss: tale of struggle for existence of riparian buildings, Natural Hazards. https://doi.org/10.1007/s11069-022-05433-5

Geck, J., Hock, R., Loso, M. G., Ostman, J. and Dial, R., 2021. Modeling the impacts of climate change on mass balance and discharge of Eklutna Glacier, Alaska, 1985–2019. Journal of Glaciology, 67(265), 909-920.

Geest, K. V. D., 2018. Loss and damage by landslides in Sindhupalchok District, Nepal: Comparing income groups with implications for compensation and relief. International Journal of Disaster Risk Science, 9(2), 157-166. https://doi.org/10.1007/s13753-018-0178-5

Gurung, D. R., Maharjan, S. B., Khanal, N. R., Joshi, G. and Murthy, M. S. R., 2015. Seti River flash flood: DRR interventions and technical analysis. In R. Dangal & D. Paudel (Eds.), Nepal Disaster Report 2015.

ICIMOD, 2011. Glacial lakes and GLOF events in Nepal. International Centre for Integrated Mountain Development (ICIMOD), Kathmandu.

ICIMOD, 2021. The Melamchi flood disaster: Cascading hazard and the need for multihazard risk management. International Centre for Integrated Mountain Development (ICIMOD), Kathmandu.

Joshi, I., Chaudhary, R. K. and Diwakar, K. C., 2021. Engineering Perspective of Melamchi Disaster and Mitigation Methods. Zenodo, 1-4.

Kargel, J. S., Paudel, L., Leonard, G., Regmi, D., Joshi, S., Poudel, K. and Fort, M., 2013. Human impacts and causes of the Seti River (Nepal) disaster of 2012. Paper prepared for Glacial Flooding and Disaster Risk Management Knowledge Exchange and Field Training Workshop, Huaraz, Peru, 11–24 July 2013. USAID and The Mountain Institute.

Kirschbaum, D., Watson, C. S., Rounce, D. R., Shugar, D. H., Kargel, J. S., Haritashya, U. K. and Jo, M. (2019). The state of remote sensing capabilities of cascading hazards over High Mountain Asia. Frontiers in Earth science, 7, 197.

Lala, J. M., 2018. Modeling and risk assessment of glacial lake outburst floods (GLOFs): A case study of Imja Tsho in the Nepal Himalayas (Doctoral dissertation).

Lamsal, D., Sawagaki, T., Watanabe, T., Byers, A. C., and McKinney, D. C., 2015. An assessment of conditions before and after the 1998 Tam Pokhari outburst in the Nepal Himalaya and an evaluation of the future outburst hazard. Hydrological Processes, 30(4), 676-691. https://doi.org/10.1002/hyp.10636

Liu, M., Chen, N., Zhang, Y. and Deng, M., 2020. Glacial lake inventory and lake outburst flood/debris flow hazard assessment after the Gorkha Earthquake in the Bhote Koshi Basin. Water, 12(2), 464. https://doi.org/10.3390/w12020464

Maghsood, H., Gholami, V. and Shahabi, H., 2018. Increasing frequency and intensity of hydrological extremes pose threats to human life, the economy, infrastructure, and the environment of riverside catchment areas. Journal of Hydrology, 566, 1000-1009.

Maharjan, S., Shrestha, S. and Bhandari, R., 2021. The nature of floods has become more cascading and widening in dimension over the years, causing significant damage.

Maharjan, S., Shrestha, S. and Bhandari, R., 2021. The Melamchi flood is a cascading hydrological hazard (multiple hazards co-occurring) caused by intense rainfall continuously occurring in the upstream area, which creates significant damage to the downstream regions. Climatic and anthropogenic factors are also associated with these devastating debris flow events. Natural Hazards and Earth System Sciences, 21(4), 1133-1147.

Mallakpour, I. and Villarini, G., 2015. The frequency and magnitude of floods are also affected by gradual land use change, which may exacerbate the situation. Water Resources Research, 51(11), 8579-8592.

Mandal, S., 2021. The Melamchi flood is not solely due to rain; various other factors contribute to these events. International Journal of Disaster Risk Reduction, 60, 102316.

Miyake, H., Sapkota, S.N., Upreti, B.N., Bollinger, L., Kobayashi, T. and Takendra, H., 2017. The 2015 Gorkha, Nepal, earthquake and\ Himalayan studies: First results. Earth Planets Space. 69, 12. https://doi.org/10.1186/s40623-016-0597-8

My Republica, 2017. Flood debris blocks confluence of Arun and Barun rivers. http:// www.myrepublica.com/news/18603/?categoryId=81.Accessed 21 April 2017.

NASA, (n.d.). POWER Data Access Viewer. NASA Langley Research Center. Retrieved [date], from https://power.larc.nasa.gov/data-access-viewer/

NDRRMA, 2021. A Field Report on Investigation of Cause of Disaster and Future Risk around Melamchi- Bhemathang area, Sindhupalchok, Melamchi Disaster Preliminary field investigation Report, DMG, NDRRMA, 2021.

NDRRMA/World Bank, 2021. Arial Image Acquisition Using Drone Flights of Melamchi Helambu and Panchpokhari Area (Indrawati and Melamchi Watershed) of Sindupalchowk District by Consultant Trimex IT Infrastructure and Service Pvt. Ltd, 2021.

Pandey, B., Shakya, N. M. and Maharjan, S., 2021. The flood resulted in the loss of many lives and significant damage to property, residential buildings, bridges, and other infrastructure. Localized rainfall triggered debris flow events, as the debris had already accumulated in the upstream area due to the fragile geological formation. The event was characterized as a cascading effect of the 2015 Gorkha earthquake. Sediments were transported over a 30 km stretch, with a high transport rate of soft sediments, and riverbed was elevated by up to 15 m in most locations. Natural Hazards and Earth System Sciences, 21(3), 781-796.

Parajuli, B. P., Baskota, P., Singh, P. M., Sharma, P., Shrestha, Y. and Chettri, R. P. 2023. Locally-led Assessment of Loss and Damage Finance in Nepal: A Case of Melamchi Flood 2021. Kathmandu: Prakriti Resources Centre.

Peacock, G. L., Byrd, D., Wilkins, M., Robson, B. A., Harrison, S. and Hough, R., 2021. The impacts of the 2015 Gorkha earthquake on glacial lakes in Nepal. Geophysical Research Letters, 48(12), e2021GL093334. https://doi.org/10.1029/2021GL093334

Rana, B., Shrestha, A. B., Reynolds, J. M., Aryal, R., Pokhrel, A. P. and Budhathoki, K. P., 2000. Hazard assessment of the Tsho Roipa Glacier Lake and ongoing remediation measures. Journal of Nepal Geological Society, 22, 563-570.

Reynolds, J. M., 1999. Glacial hazard assessment at Tsho Rolpa, Rolwaling, Central Nepal. Quarterly Journal of Engineering Geology and Hydrogeology, 32(3), 209-214.

Rounce, D. R., Byers, A. C., Byers, E. A. and McKinney, D. C., 2017. Brief communication: Observations of a glacier outburst flood from Lhotse Glacier, Everest area, Nepal. The Cryosphere, 11(1), 443-449.

Sarhadi, A., Behzad, M. and Mohammad, H. 2012. Floods have become one of the most serious natural disasters. International Journal of Environmental Research and Public Health, 9(12), 4487-4505.

Shakya, D. and Sabha, S., 2017. Arun Displaced Urge Government for Relief-National-The Kathmandu Post. Kathmandu: Kathmandu Post.

Takamatsu, N., Khanal, N. R. and Dahal, V., 2022. Impact of the 2021 Melamchi Flood on infrastructure and agriculture in the downstream area. Journal of Disaster Research, 17(4), 582-596.

Shrestha, B. R., 2019. An assessment of disaster loss and damage in Nepal. The Geographic Base, 6, 42-51.

Shrestha, S., Bhandari, R. and Maharjan, S., 2021. Melamchi Flood 2021 is due to the combined effects of changing temperature, which breached the Pemdan glacial lake, creating a series of landslides and erosion in the Melamchi River basin.

Talchabhadel, R., Shrestha, B. and Sharma, A., 2023. Heavily deposited and transported materials from upstream caused significant losses and damage to livestock, property, and infrastructure in Melamchi town and damaged or destroyed riverbeds. Natural Hazards, 1-15

Thapa, N. and Prasai, R., 2022. Impacts of floods in land use land cover change: A case study of Indrawati and Melamchi River, Melamchi and Indrawati municipality, Nepal. SSRN Electronic Journal. https://doi. org/10.2139/ssrn, 4104357(3), 59-70.

Vuichard, D. and Zimmermann, M., 1987. The 1985 catastrophic drainage of a moraine-dammed lake, Khumbu Himal, Nepal: cause and consequences. Mountain Research and Development, 91-110.

Yagi, H., Sato, G., Sato, H. P., Higaki, D., Dangol, V. and Amatya, S. C., 2021. Slope Deformation caused Jure Landslide 2014 Along Sun Koshi in Lesser Nepal Himalaya and Effect of Gorkha Earthquake 2015. Understanding and Reducing Landslide Disaster Risk: Volume 5 Catastrophic Landslides and Frontiers of Landslide Science 5th, 65-7

Guidelines for Authors

General Information

The **Journal of Nepal Hydrogeological Association (JNHA)** is the annual publication of the Nepal Hydrogeological Association. This peer-reviewed journal is dedicated to disseminating original research across a broad spectrum of topics within hydrogeology, groundwater studies, hydrology, and glaciology. Additionally, it welcomes contributions from related fields such as engineering, environmental science, climate change, natural hazards, geotechnical engineering, remote sensing, natural resources, laws, and regulations connected to water issues. Research not related to water in any form will not be considered for publication.

The journal places a special emphasis on research centered on the Himalayan region but also welcomes studies from other parts of the world. It aims to publish scholarly articles that are based on extensive fieldwork, experimental results, theoretical analysis, numerical modeling, and innovative ideas.

Key guidelines for submissions include:

- Manuscripts should not exceed 30 printed pages, inclusive of figures and tables.
- All submissions undergo a rigorous review process.
- Authors may suggest three potential reviewers, providing their names and email addresses to assist the editato the Journal of Nepal Hydrogeological Association (JNHA), authors affirm that the work is original, has not been published elsewhere in any form, and is not under consideration by another publication. Authors must also agree to transfer copyright to the Nepal Hydrogeological Association upon acceptance.

Correspondence and manuscript submissions should be directed to:

Editor-in-Chief: Nepal Hydrogeological Association (For duration: 2024-2026 address to Dr. Kabi Raj Paudyal, Central Department of Geology, Phone: +977-9851036129, Personal Email: paudyalkabi1976@gmail.com). Formal Email:editorial@nha.org.np and **Website**: http://www.nha.org.np.

Manuscript Preparation

Authors are required to submit an electronic copy of their manuscripts, formatted according to journal specifications, in 'MS Word' on A4 size paper (297 x 210 mm). Manuscripts should be written in clear and concise English, avoiding complex sentences and unnecessary jargon.

Organization of Manuscript:

1. **Title:** It should be formatted in 14-point Times New Roman (TNR) type. Only capitalize the initial letters of words that are necessary, such as proper nouns or acronyms. Avoid capitalizing the first letter of each word unless required by standard conventions. Ensure that the title accurately reflects the content and focus of your research work.
2. **Author Names and Affiliations:** Following the title, list the full names and affiliations of all authors in 12-point Times New Roman (TNR) type. For multiple authors, provide the affiliation for each author, which should include the full address, country, and email address. Indicate the corresponding author.
3. **Abstract**: The abstract should be preceded by the heading "ABSTRACT" in all caps. The abstract itself should be less than 300 words, formatted in 12-point Times New Roman (TNR) type, aligned with the left margin. It should provide a concise and objective summary of the paper, presenting the information and results clearly and briefly. Include the overall scope of the research, emphasize new information, and state the main conclusions drawn from the study. Citation of literature in the abstract is discouraged.
4. **Keywords:** Include fewer than seven keywords, each starting with an initial capital letter. These keywords should effectively represent the main topics and themes of your paper.
5. **Introduction**: Provide background information, location and state the objectives of the research. Study of relevant literatures, previous works, research gaps or research questions or justification of the study can be included in this section.
6. **Methodology**: Detail the methods and procedures used in the study.
7. **Main Body**: Include data, results, and interpretations.
8. **Discussions**: Analyze and discuss the findings.
9. **Conclusions**: Summarize the main points and findings of the research.
10. **Acknowledgments**: Recognize contributions and funding sources.
11. **References**: List all references cited in the manuscript.

Illustrations

All figures (drawings, photographs, charts, etc.) and tables must be submitted as high-quality JPG images with a resolution of 300 dpi. Ensure that figures and tables are prepared in print-ready form. Figures should be clear, page-size-friendly, and utilize distinct lines, font sizes (8 to 10-point), and patterns (either black and white or color). Place type labels or scales directly on the photographs rather than on a separate overlay or in the caption. Use graphic scales instead of verbal scales on illustrations.

Tables should use 8 to 10-point Times New Roman (TNR) plain type. Use only three border lines: one above the heading, one below the heading, and one at the bottom of the table. The overall size of the table should be compatible with the journal's page size, fitting at one of the various stops (quarter, half, or full page). A4 is the standard size of the journal layout.

Style

Authors are responsible for ensuring that their manuscripts use approved geological and other scientific terminology correctly and are free of grammar and spelling errors. Consistency in capitalization, spelling, abbreviations, and dates must be checked thoroughly. Figure and table captions should be formatted in 10-point Times New Roman (TNR) bold type. Examples are as follows: **Fig. 1: Drainage map of the study area/ Table 1: Analysis of water chemistry.**

Acknowledgment

In the acknowledgment section, authors should mention any grant support, organizations, and individuals who have significantly contributed to the research.

References

Ensure that every reference cited in the main body of the manuscript is also included in the reference list, and vice versa. All references mentioned in the text, figures, captions, and tables must be listed in the reference section. Consistency and accuracy in citations are essential to maintain the integrity of the manuscript.

In-Text Citations

- **Single Author**: Use the author's surname and the year of publication, e.g., (Sharma, 2020) or Pradhan (2021).
- **Two Authors**: Include both authors' surnames and the year of publication, e.g., Paudyal and Paudel (2013) or (Paudyal and Paudel, 2013).
- **Three or More Authors**: Use the first author's surname followed by "et al." and the year of publication, e.g., (Carosi et al., 2015) or Carosi et al. (2015).

References: The authors are organized in alphabetical and chronological order, every author separated by comma “,”. References by the same author, published in the same year should be distinguished using suffixes: 2020a, 2020b, 2020c. All author names are set in small letters. Publication/journal names are given in full title/name. Volume numbers are printed in bold and issue numbers are given in parenthesis followed by a comma and page numbers. Examples:

Author, A. 1998. Title of paper. Full name of journal, 31 (2) 200-215.

Author, B., Author, C. and Author, D. 1990. Title of paper. Full name of journal, 35, 33-46.

Author, A. 1999. Title of book. Name of Publisher, place of publication, 303p.

Author, A. 1999. Title of contribution. In: Editor, A. (ed.), Title of book. Name of Publisher, place of publication,200p.

Author, A., Author, B. 1990. Title of contribution. In: Editor, A. & Editor, B. (eds.), Title of book. Name of Publisher, place of publication,150p.

Cover Photographs: High-quality photographs (TIFF file on min 400 resolution) related to the submitted manuscript is welcome for use on the cover page. However, it is not compulsory to use the cover photos.

Publication time: Currently the time between initial submission and publication of regular articles is about 1 year. Articles accepted for publication are generally published in order of submission. Exceptions can be made for papers of high scientific significance. The schedule of publication is 1st week of September. However, the first volume may be shifted for some month due to the processes of ISSN number, and other official processes.

Reprints: PDF files of published articles will be provided free of cost to authors.

If any queries, contact the editorial board at editorial@nha.org.np

CONTENT